THE GENERATION AND AMPLIFICATION OF NANOSECOND PULSES OF 10 μm RADIATION

THEODOSIOS STAMATAKIS

Royal Holloway College

This thesis is submitted in partial fulfilment of the requirements for the degree of Doctor of Philosophy in the University of London

September, 1977

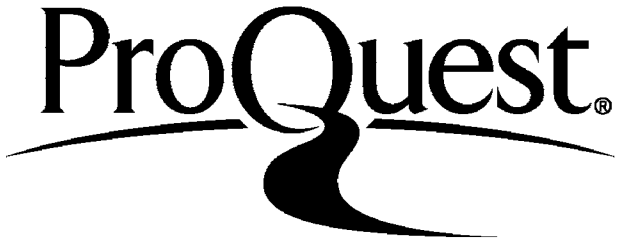

TO MY PARENTS

CHRISTODOULOS AND MARIA

We shall not cease from exploration
And the end of all our exploring
Will be to arrive where we started
And know the place for the first time.

T.S. Eliot

CONTENTS

CONTENTS

(continued)

CONTENTS
(continued)

Page

CHAPTER VI

CHAPTER VII

APPENDICES

ACKNOWLEDGEMENTS

I should first like to record my appreciation of all the help given to me by the late Dr V.I. Little, whose enthusiasm for and genial interest in my work sustained it at every stage.

My gratitude is also extended to Professor D.W.O. Heddle for ably continuing the supervision of my research and for gently urging me through the labour of actually writing my thesis.

I am much indebted to Culham Laboratory at which this work was entirely carried out — under an agreement between Royal Holloway College and U K A E A — and especially to Drs T.K. Allen and I.J. Spalding who enabled me to make the fullest possible use of the extensive facilities offered by the Laboratory.

My particular thanks are due to Dr A.C. Selden who has — from the start — unstintingly given me the benefit of his experience and who has followed the progress of my work with the most meticulous concern.

My work at Culham Laboratory has also profited from many useful discussions with various members of the Laser Group — in particular, Drs A.C. Walker and J.M. Green.

I am grateful to Royal Holloway College for the financial award which has assisted me over the last two years of my research and, finally, my thanks are due to Ina Godwin for her assiduous typing of the manuscript.

ABSTRACT

The generation of single CO_2 laser pulses, having sub-nanosecond rise and fall time, is described. The duration of these pulses is controlled in the range 0.83 to 100 ns and their peak power is of the order of 1 MW. For the generation of these pulses, a double-discharge TEA CO_2 laser has been used, in conjunction with an electro-optical shutter.

A telescopic CO_2 laser amplifier has been employed to amplify the nanosecond pulses to 1 GW power levels. The design and operational characteristics of this device are presented and the effective elimination of associated problems is discussed. The effect of organic vapour additives on the performance of this oscillator-amplifier system is investigated.

Experimental evidence is presented indicating an increased efficiency in the amplification of multi-line — as opposed to single line — nanosecond pulses. A novel method for single longitudinal mode operation of pulsed TEA CO_2 lasers — incorporating the use of two unstable coupled resonators — has been developed. The powers thereby achieved are in excess of 30 MW.

PREFACE

The possibility of achieving laser-induced fusion has stimulated world-wide investigation and has motivated the development of high power lasers capable of meeting the requirements imposed by this unconventional approach to controlled thermonuclear energy. Although this approach had been mooted soon after the advent of lasers[1,2], the essential idea of using laser radiation to compress as well as to heat the thermonuclear fuel, was not declassified until 1972[3]. This has made the laser-fusion concept highly attractive since the laser energy requirements are drastically reduced for strongly compressed pellets to well within the immediate future capabilities of the rapidly advancing laser technology.

Theoretical predictions indicate that multi-kilojoule pulses of nanosecond or shorter duration are implicit in the accomplishment of laser-fusion. The short pulse length is required for the sufficiently rapid heating of the thermonuclear fuel (a small pellet of deuterium and tritium) to fusion-ignition temperatures (10^8 K) before significant expansion and cooling take place. This process, known as 'inertially confined laser fusion', circumvents some of the magnetohydrodynamic instability and anomalous diffusion problems of the conventional magnetic confinement systems.

A laser has yet to be developed which features the high efficiency, high repetition rate and short wavelength capable of emitting multi-kilojoule subnanosecond pulses which are appropriate to laser-fusion. Existing laser systems capable of meeting the energy and pulse duration requirements (i.e. the neodumium-glass, the iodine and the carbon dioxide) are handicapped by low efficiency, low repetition rate or long wavelength.

The neodumium-glass laser is currently regarded as the best system for gauging the feasibility of laser-fusion. The most recent experimental results of the Los Alamos Scientific Laboratory, on the other hand, have given rise to increased optimism about the suitability of the CO_2 laser for commercially-viable fusion. These results indicate a much more efficient coupling of the laser radiation and the thermonuclear pellets than had been anticipated[4]. The CO_2 laser offers the advantage of a replaceable active medium — which, in turn permits a high repetition rate — a good optical quality and, at pressures of several atmospheres, is capable of a relatively high efficiency in amplifying multi-frequency short laser pulses.

The purpose of the work reported in this thesis is to develop a TEA CO_2 laser system capable of the reliable generation and efficient amplification of nanosecond pulses and to gain an understanding of the physical processes involved in the optimization of such a system.

With this latter objective in mind, the first chapter outlines some of the essential background — with particular emphasis given to the excitation and relaxation processes involved in achieving population inversion — and concludes with a résumé of the principal recent research conducted in the field of nanosecond CO_2 laser pulse generation.

The second chapter describes the design and performance of the two CO_2 laser modules used throughout this work: the Double-Discharge and Double Rogowski modules. In particular, there are sections devoted to: the merits of stable and unstable resonators used in conjunction with these modules; the effect of single transverse mode operation on self-mode locking; energy and power measurements; and the effect of organic additives on the laser-performance. The potentialities of one of the modules (Double Discharge) as a laser amplifier, have also been investigated by measuring the small signal gain — and the effect upon it of the gas composition and the electrical input energy — and the saturation energy density for 70 ns pulses.

Chapter III comprises a detailed analysis of the design and operation of an electro-optical shutter which, used together with a CO_2 laser, generates pulses of variable duration and sub-nanosecond rise time. A full investigation is presented both of the effects of the crystal quality and of the variation of the spark-gap parameters (voltage, gap length and gas pressure) on the shutter's performance. The choice of gas filling and electrode material is also discussed. In addition, this chapter includes a section on the formation of wedge-fringes by optical components.

The fourth chapter discusses the gain saturation measurements of nanosecond pulses and the resultant pulse broadening. The design and performance of an efficient type of amplifier — a telescopic amplifier — are analysed. The problems, namely the elimination of parasitic and self-oscillation, which had to be surmounted, before this amplifier could operate successfully, are also dealt with.

Chapter V concentrates upon the generation and amplification of multi-line nanosecond pulses. Experimental evidence is presented which confirms the theoretically-predicted increased efficiency, and reduced pulse-distortion

resulting from the amplification of multi-line — as opposed to single-line — pulses.

In Chapter VI, a novel method for single longitudinal mode operation of the CO_2 laser is described, based on the coupling of two unstable resonators which share the active medium. A simple interpretation of the single longitudinal mode operation of this three-mirror resonator is proposed. In addition to single-mode operation of the P(20) line in the 10.4 μm band, some observations are also reported of the simultaneous generation of two or three adjacent rotational transitions, each on a single longitudinal mode. The applications of this device, capable of generating peak powers in the range 30 to 100 MW, are discussed.

The final chapter presents a résumé and assessment of the results achieved in the course of this research. The limitations of the system are outlined and possible improvements to it are suggested. The principal modifications, dictated by the findings of this research, which have been taken into consideration in the current construction at Culham Laboratory of an enlarged CO_2 laser system, with a potential 200-400 GW power output, are reviewed at the end of this chapter.

CHAPTER I

CO_2 LASER PHYSICS AND SHORT PULSE LASER TECHNOLOGY

1.1 INTRODUCTION

The astounding increase in power of the pulsed CO_2 laser, from its first negligible output of a fraction of a watt in 1964[5] to its present impressive capability of several hundred gigawatt[6], is the result of massive investigation, documented in a correspondingly remarkable proliferation of published papers which defy enumeration here. A comprehensive account of this published work can be found in a number of articles, e.g. references (7-10), among which the excellent review by WOOD[10], with its plethora of experimental and analytical information is pre-eminent.

Before attempting to review in brief the most recent research concerning the generation of short CO_2 laser pulses — which is the principal theme of this thesis — it would seem appropriate to summarize here the CO_2 infrared spectra and molecular structure as well as the various excitation and relaxation processes involved in the production of population inversion, and the subsequent laser action in the 10 μm region. This general background will also help to elucidate some of the topics explored in the following chapters.

1.2 CO_2 INFRARED SPECTRA AND MOLECULAR STRUCTURE

1.2.1 Vibrational Energy Levels of CO_2

The CO_2 molecule is a linear symmetric molecule (point group $D_{\infty h}$) whose structure and vibrational-rotational spectrum have been thoroughly investigated[11-13]. As a result of its linearity, the CO_2 molecule possesses $3N-5=4$ normal modes of vibration (where $N=3$ is the number of nuclei in the molecule) which are illustrated in Fig.1.1.

In the symmetric stretching mode $\nu_1 = 1388.2\ cm^{-1}$ the oxygen atoms vibrate along the molecular axis symmetrically with respect to the

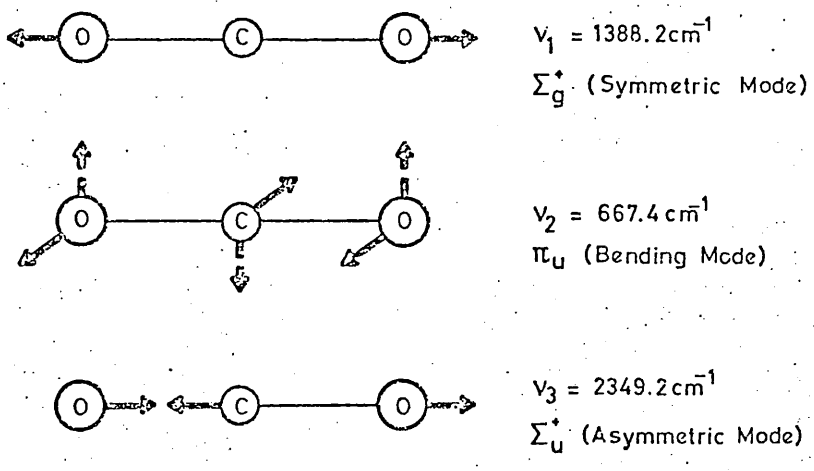

Fig.1.1
Normal modes of vibration of the CO_2 molecule

stationary carbon. There is an infinite number of ways whereby the CO_2 molecule can vibrate perpendicularly to the molecular axis with the same frequency $\nu_2 = 667.4\ cm^{-1}$. In these vibrations all the atoms describe ellipses, in general, which are perpendicular to the molecular axis and which give rise to a vibrational angular momentum about the axis. However, any such vibration can be regarded as a superposition — with an appropriate phase difference — of the two mutually perpendicular degenerate bending modes ν_{2a}, ν_{2b}. In the asymmetric stretching mode $\nu_3 = 2349.2\ cm^{-1}$ the oxygen atoms always move in the same direction along the axis and in opposition to the carbon. Both the asymmetric and the bending modes involve a change in the dipole movement of the molecule and consequently are strongly infrared-active by contrast with the symmetric mode which — causing no such change — appears only in the Raman spectrum (infrared-inactive).

Any arbitrary vibrational state of the molecule can be described by the number of excited quanta in each normal mode using the notation $(\eta_1\ \eta_2^{\ell}\ \eta_3)$ where η_1, η_2, η_3, are the quantum numbers of the symmetric stretching, the double degenerate bending and the asymmetric stretching modes respectively. The superscript ℓ denotes the vibrational angular momentum of the molecule.

In the CO_2 molecule, the vibrational levels 10^00 and 020 (which consists of the sublevels 02^00, 02^20) have nearly the same energy, resulting in the perturbation of both these levels, as first discussed by FERMI[14]

and denoted by the term Fermi resonance. Perturbations of this type occur only between levels with the same value of ℓ [2, p.216] and, as a result, the two levels $10^{\circ}0$ and $02^{\circ}0$ repel each other and appear in positions different from those expected. In addition, a strong mixing of the eigenfunctions of the two levels occurs and the resulting levels are mixtures of the two states. Thus the designations $10^{\circ}0$ and $02^{\circ}0$ can no longer unambiguously represent these levels. A more accurate designation proposed by AMAT and PIMBERT[15] is $[10^{\circ}0, 02^{\circ}0]_I$ and $[10^{\circ}0, 02^{\circ}0]_{II}$ for the levels lying at 1388.2 cm^{-1} and 1285.4 cm^{-1} respectively. Contrary to the traditional assignment, the level at 1285.4 cm^{-1} is associated with the symmetric stretching mode and that at 1388.2 cm^{-1} with the bending mode. A number of investigators[16-18] have confirmed the new assignments and the nomenclature proposed in [15] will be applied throughout this thesis.

1.2.2 Rotational Energy Levels

A series of rotational sublevels — designated by the rotational quantum number $J = 0,1,2,\ldots$ — is superimposed on each vibrational level. In a non-degenerate vibrational level, the rotational energy of each sublevel is given by[12, p.14]:

$$\frac{E_r}{hc} = BJ(J+1) - D^2J(J+1)^2 + \text{---} \qquad \ldots (1.1)$$

where B is the rotational constant ($B_{00^{\circ}1} = 0.38714$ cm^{-1} [19]) and $D = \frac{4B^2}{\nu_1^2}$ is the centrifugal distortion constant ($D_{00^{\circ}1} = 1.3303 \times 10^{-7}$ cm^{-1} [19]).

The population N_J of a given rotational level in thermal equilibrium is given, to a good approximation, by [20, p.125]

$$N_J = \frac{2N(2J+1)\,hc\,B}{\kappa T}\, e^{-BJ(J+1)\,hc/\kappa T} \qquad \ldots (1.2)$$

where N is the population of the vibrational level as a whole, κ is the Boltzmann constant, and T the absolute temperature.

The quantum number of the rotational level with the maximum population can be found from the above relation to be the nearest allowed integer

to the value

$$J_{max} = \sqrt{\frac{KT}{2hcB}} - \frac{1}{2} \,. \qquad \ldots (1.3)$$

1.2.3 *Vibrational-Rotational Spectra*

An energy diagram of low-lying vibrational levels of the CO_2 molecule is shown in Fig.1.2. Vibrational-rotational transitions between these levels are determined according to the following selection rules: (21)

$$\Delta\ell = 0 \quad |\Delta\eta_2| : \text{even} \quad |\Delta\eta_3| : \text{odd} \quad \Delta J = \pm 1$$

or

$$|\Delta\ell| = 1 \quad |\Delta\eta_2| : \text{odd} \quad |\Delta\eta_3| : \text{even} \quad \Delta J = 0, \pm 1 \qquad \ldots (1.4)$$

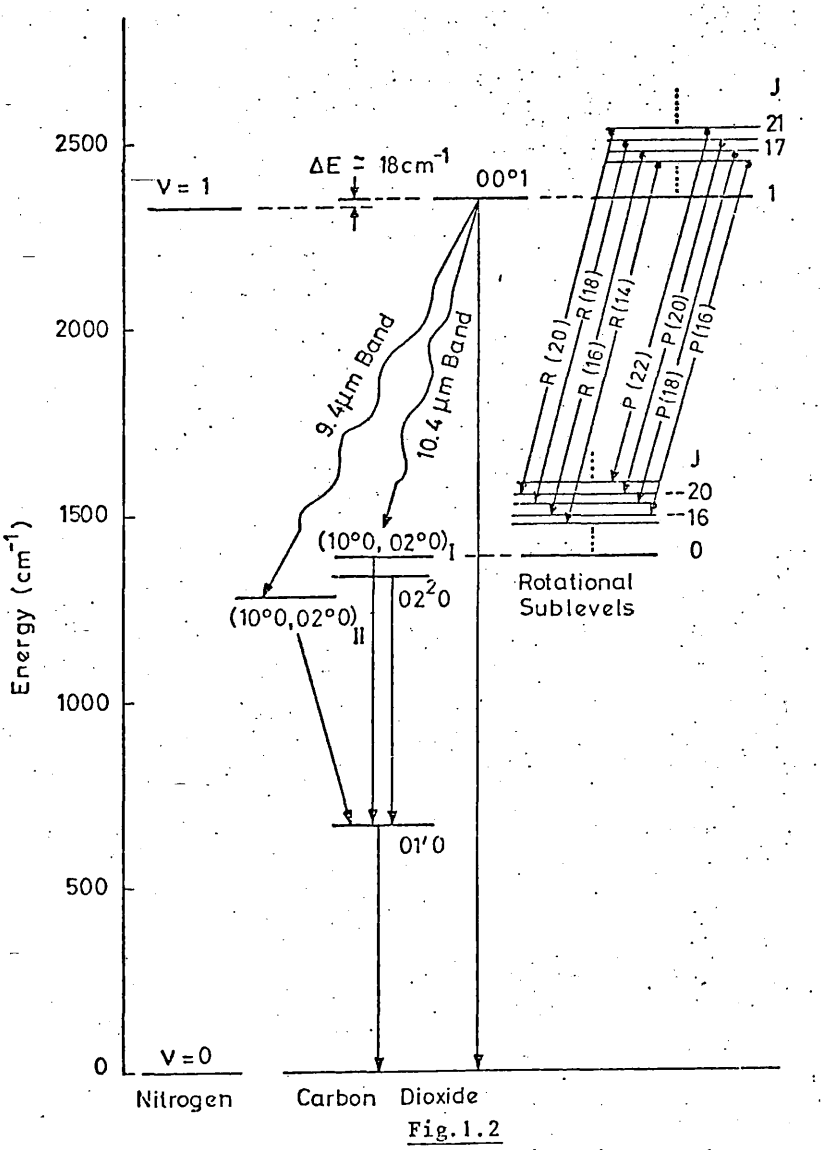

Fig.1.2

Partial energy diagram of the vibrational and rotational levels relevant to 10 μm CO_2 laser emission

These transitions give rise to the vibration-rotation infrared bands, defined as groups of all possible rotational transitions for a particular vibrational transition. The strongest and one of the most significant CO_2 laser bands is the 10.4 μm band corresponding to the $00°1 \rightarrow [10°0, 02°0]_I$ transition. Oscillation on 66 lines has been obtained in the wavelength range 10.026 - 11.189 μm [22] from both the $P(\Delta J = -1)$ and R branches $(\Delta J = 1)$ of this band, some of which are shown in Fig.1.2. Individual lines are denoted P(J) or R(J) where J is the rotational quantum number of the lower laser level. Lines with only even J appear in the 10.4 μm band as a result of the absence of rotational levels with odd J in the lower laser level caused by the zero values of nuclear spin and the symmetry of the normal isotopic species $^{12}C\,^{16}O_2$ [12, p.382].

1.3 UPPER LASER LEVEL EXCITATION

The 00°1 vibrational level of CO_2 is excited mainly by two processes, namely: inelastic collisions with low-energy electrons [23-25]; and resonant energy transfer from the first vibrationally-excited level of nitrogen (U = 1) to ground state CO_2 molecules [26-27].

1.3.1 Direct Vibrational Excitation

The low-lying vibrational levels of CO_2 can be excited directly by inelastic collisions with low energy electrons. This process may be expressed as:

$$e^- + CO_2 \rightleftarrows CO_2^* + e^- \quad \ldots (1.5)$$

where CO_2^* denotes a vibrational excited species.

The probability of excitation of the 00°1 level was found by BONESS and SCHULZ [23] to be substantially greater than that of 10°0 and 02°0. ANDRICK et al [24] however, have shown that the 01^10 is also strongly excited. The cross section for excitation of the 00°1 and 01^10 levels is 1.5×10^{-16} cm^2 and 3×10^{-16} cm^2 respectively [30].

Although the vibrational excitation by electron impact was attributed originally to the formation of a negatively-charged compound state with an estimated lifetime of 10^{-15} s [23], it is now generally accepted (see references 24,25,28,30,(9,p.143)) that for electrons with energy less than 3 eV the excitation proceeds directly without the CO_2^- formation. The levels excited by this process are the 00^01 and 01^10, while the 10^00 (as well as the 01^10) is excited by electrons in the range 3-5 eV through the CO_2 compound state formation.

The excitation of the vibrational levels of nitrogen by slow electrons is also attributed to the formation of a short-lived negatively charged compound[28,29] through the process:

$$N_2 + e^- \rightarrow N_2^- \rightarrow N_2^* + e^- \qquad \ldots (1.6)$$

SCHULZ[29] has measured the total, as well as the partial, cross section for the excitation of the first eight vibrational levels of N_2. For electron energies near 2 eV the cross section for the $v=1$ level is 1.5×10^{-16} cm^2 while the total cross section attains a maximum value of $\sim 3 \times 10^{-16}$ cm^2 at electron energies of 2.3 eV. Radiative decay of the N_2 levels is precluded by selection rules since N_2 is a homonuclear diatomic molecule with no permanent dipole moment[20]. Combined with the large cross sections, this enables the generation of a substantial population of N_2^*.

The relative populations of the various vibrational levels of N_2 and CO_2 in a discharge are influenced by the ratio of the electric field E to the total density of the neutrals N. Using the above cross sections, NIGHAN[30] has calculated the fraction of the electron power transferred to each of these levels as a function of E/N for $CO_2 - N_2 - He$ mixtures typical of steady-state laser discharges. These calculations are, however, applicable also to high-pressure pulsed CO_2 lasers since the electron-neutral collision occurs on a time scale much faster than that of the discharge pulse[31]. According to these calculations, the values of

$\frac{E}{N} = 2 \times 10^{-16}$ V cm^2 result in a maximum power transfer in both the CO_2 (00°1) and N_2 (U = 1 - 8) levels, while for $E/N > 4 \times 10^{-16}$ V cm^2 a considerable fraction of the electrical energy is transferred to the CO_2 (01^{1}0) thus reducing the laser efficiency. It is therefore evident that CO_2 laser systems such as the electron-beam controlled type in which the ratio E/N can be adjusted for maximum excitation of the coupled CO_2 (00°1) - N_2 (U = 1) levels are potentially more efficient. Such systems are also most suitable for the amplification of ns pulses since — as will be seen later — in this time-scale the energy stored in the N_2 is not available and therefore, the value of E/N needs to be adjusted for the maximum direct electron excitation of the upper laser level. The ratio of E/N for the two laser modules used in this research — Double-Discharge and Double-Rogowski — (see Chapter II), could attain values in the range $3.4 - 4.9 \times 10^{-16}$ V cm^2 and $5.1 - 7 \times 10^{-16}$ V cm^2 respectively.

1.3.2 *Resonant Energy Transfer*

The first vibrationally excited level of N_2 (U = 1) lying 2329,66 cm^{-1} above the ground state is in near coincidence with the 00°1 of CO_2 (see Fig.1.2). The consequence of this small energy difference between the two levels (ΔE = 18 cm^{-1}) is a very rapid and efficient selective excitation of the CO_2 (00°1) level involving vibrational energy transfer from N_2 to CO_2 (00°0) by means of the process:

$$CO_2(00°0) + N_2(U=1) \underset{K_e'}{\overset{K_e}{\rightleftharpoons}} CO_2(00°1) + N_2(U=0) - 18\ cm^{-1} \quad \ldots (1.7)$$

This reaction proceeds mainly in the forward direction since only the CO_2 molecule can decay radiatively. The forward and reverse rate constants for the process are $K_e = 1.9 \times 10^4$ torr^{-1} s^{-1} and $K_e' = 106$ torr^{-1} s^{-1} respectively[32].

1.4 RELAXATION PROCESSES

The amplification of 10 μm radiation by the vibrationally excited CO_2 molecules is significantly affected by the various processes which result in their de-excitation. The basic relaxation processes which — in conjunction with the stimulated emission — govern the population densities of the upper and lower laser levels are discussed in this section.

1.4.1 Radiative Relaxation

The probability of the spontaneous relaxation of a CO_2 molecule from an excited to a lower energy level is expressed by the Einstein coefficient A_{ul}. A number of theoretically deduced and experimentally determined values of the Einstein coefficient have been reported for the transitions indicated in Fig.1.2 [33-38]. The $00°1 \rightarrow 00°0$ transition is radiatively trapped and, as a result, the coefficient for the individual lines of this transition was found to be of the order of $10\ s^{-1}$ [33]. The A_{ul} coefficient for all the other transitions, ranges between 0.2 and $2\ s^{-1}$. Even though the contribution of spontaneous emission in the relaxation of the CO_2 molecules is not significant because of their very small radiative relaxation rates, it is of great value to ascertain accurately the A_{ul} coefficient for the laser transitions since important laser parameters such as small signal gain and saturation intensity depend upon the value of A_{ul}. BIRYUKOV et al[39] after critically analysing the reported experimental data, recommend the value $A_{ul} = 0.187\ s^{-1}$ for the P(20) line of the $00°1 - [10°0, 02°0]_I$ transition.

1.4.2 Upper Laser Level Relaxation

The relaxation of the upper laser level by collisions with various molecules or atoms has been extensively investigated[32,40-42](9,pp.156-9). The vibrational energy stored in this level can be transferred to a number of $(\eta_1\ \eta_2^{\ell}\ 0)$ levels by means of the process:

$$CO_2(00°1) + M \xrightarrow{K_1} CO_2(\eta_1\ \eta_2^{\ell}\ 0) + M + E_{trans.} \qquad \ldots (1.8)$$

where the collision partner M is any gas molecule or atom in the laser discharge. The probability of such a vibration-vibration (v-v) energy transfer is higher for the $(\eta_1\, \eta_2^{\ell}\, 0)$ levels closest to $00^{\circ}1$[32]. Consequently, direct conversion of the entire vibrational energy of the upper laser level into translational energy is precluded.

The reported values of the relaxation rate constants for this process are in fairly good agreement with each other. The mean values of the constants, relevant to a $CO_2 : N_2 : He$ laser, reported in references (9, p.157)(32,43-49) at 300°K are :

$K_{1(M=CO_2)} = 351 \pm 33$, $K_{1(M=N_2)} = 122 \pm 20$ and $K_{1(M=He)} = 80 \pm 9$ all in units of $torr^{-1}\, s^{-1}$.

Thus the expected relaxation rate constant of the upper vibrational laser level for the gas mixture principally used throughout the subsequent experiments ($CO_2 : N_2 : He$, $1 : \frac{1}{6} : 2$) is:

$$K_1 = \frac{1}{3.17}\left(K_{1(M=CO_2)} + \frac{1}{6}\, K_{1(M=N_2)} + 2K_{1(M=He)}\right) = 168\ torr^{-1}\, s^{-1} \qquad \ldots (1.9)$$

CHEO[50] and REID et al[44,51] have shown that the rise and fall times of the optical gain coefficient in a CO_2 laser amplifier correspond to the effective lifetimes of the lower and upper vibrational laser levels respectively. As will be shown in section 2.5.2, analysis of the gain waveforms of the TEA CO_2 laser amplifier employed in this research, indicates a relaxation rate constant $K_1 = \frac{1}{\tau_1 P} = 160\ torr^{-1}\, s^{-1}$ for the $00^{\circ}1$ level which is in excellent agreement with the expected value.

1.4.3 Lower Laser Level Relaxation

It is generally accepted[8,9,52] that the relaxation of the lower vibrational laser level $[10^{\circ}0,\ 02^{\circ}0]_I$ or $[10^{\circ}0,\ 02^{\circ}0]_{II}$ into the bending mode (01^10) is very rapid ($\sim 10^5\ torr^{-1}\, s^{-1}$) and, as a result, it is effectively controlled by the relaxation of the bending mode which can be written as:

$$CO_2(01^10) + M \xrightarrow{K_2} CO_2(00^{\circ}0) + M + 667\ cm^{-1}. \qquad \ldots (1.10)$$

This reaction has been widely studied and there is a plethora of experimental data for CO_2 and He as collision partners, as opposed to the sparsity of recent data concerning the effect of N_2 on this relaxation process. By averaging out the results reported in references (40,42,53-56) the following values and their deviation from the mean have been derived:

$$K_{2(M=CO_2)} = 206 \pm 12 \text{ torr}^{-1} \text{ s}^{-1}, \quad K_{2(M=N_2)} = 100 \text{ torr}^{-1} \text{ s}^{-1}$$

and

$$K_{2(M=He)} = (3.86 \pm 0.4) \times 10^3 \text{ torr}^{-1} \text{ s}^{-1} \quad \ldots (1.11)$$

The relaxation rate constant expected from these values for the gas mixture $CO_2 : N_2 : He$, $1 : \frac{1}{6} : 2$ is $= 2.3 \times 10^3 \text{ torr}^{-1} \text{ s}^{-1}$. Analysis of small signal gain waveforms (section 2.5.2) — based on the assumption that the effective lifetime of the lower laser level corresponds to the rise-time of the gain pulse — indicated a value of

$$K_2 = \frac{1}{\tau_2 P} = 1.1 \times 10^3 \text{ torr}^{-1} \text{ s}^{-1}$$

for this gas mixture. The agreement between these two values is satisfactory.

The exact value of the rate at which the two levels in Fermi resonance exchange energy as well as the rates at which they decay to the (01^10) level is still the subject of some uncertainty[57,58]. Relaxation of the lower vibrational laser level could enhance the amplification of laser pulses provided that its lifetime does not exceed their duration. However, this relaxation cannot affect the amplification of nanosecond laser pulses, at atmospheric pressure, since even the fastest reported rate constants[59]

$$K_{3(M=CO_2)} = (3 \pm 1) \times 10^5, \quad K_{3(M=N_2)} = (3 \pm 1) \times 10^5$$

and

$$K_{3(M=He)} = (0.8 \pm 0.3) \times 10^5 \text{ torr}^{-1} \text{ s}^{-1}$$

for the process:

$$CO_2[10°0, 02°0]_I + \underset{\longleftarrow}{\overset{K_3}{\longrightarrow}} CO_2[10°0, 02°0]_{II} + M + 102.8 \text{ cm}^{-1} \quad \ldots (1.12)$$

cannot credit a nanosecond lifetime of the lower laser levels. For this reason the amplification-efficiency of such pulses is substantially curtailed.

1.4.4 *Rotational Relaxation*

The efficiency with which the optical energy stored in a CO_2 laser amplifier can be extracted by a nanosecond pulse is principally governed by the rotational relaxation within the vibrational laser levels. Since optical energy can be extracted only from CO_2 molecules whose rotational quantum numbers correspond to the spectral content of the incoming laser pulse, the total energy stored in the $00^\circ1$ level is extractable only after its transfer, via collision, into the rotational levels which interact directly with this pulse. Measurements of the rotational relaxation rate constant K_R have been reported by CRAFER et al[60], CHEO and ABRAMS[61] and JACOBS et al[62]. Jacobs et al have determined the following rate constants K_R, for this process by monitoring the repopulation of the $00^\circ1$ ($J = 19$) rotational-vibrational level, perturbed by a saturating ~ 2 ns single line pulse:

$$K_{R(CO_2-CO_2)} = 1.3 \pm 0.2,\ K_{R(CO_2-N_2)} = 1.2 \pm 0.2,\ K_{R(CO_2-He)} = 0.6 \pm 0.1$$

all in units of $10^7\ \text{torr}^{-1}\ \text{s}^{-1}$. Thus the expected value of the rotational relaxation time t_R for the mixture $CO_2 : N_2 : He$, $1 : \frac{1}{6} : 2$ at atmospheric pressure is 0.154 ns. It will become apparent in Chapter V that, as a result of this finite value of t_R, a single line pulse of 1 ns duration can extract no more than 20% of the optical energy stored in the $00^\circ1$ vibrational level. This situation can be improved, however, as was suggested by CRAFER et al[60] and later by FELDMAN[63] and SCHAPPERT[64] by using multi-line pulses and/or by operating the laser amplifier at higher than atmospheric pressures. A more detailed discussion of this aspect as well as experimental evidence supporting the validity of this argument are presented in Chapter V.

1.5 CO_2 NANOSECOND PULSE LASER TECHNOLOGY

1.5.1 Mode-Locking

The selection of a single pulse from the output pulse train of a mode-locked oscillator has been the most widely used method for generating nanosecond CO_2 laser pulses.

Active mode-locking of a TEA CO_2 laser using an intracavity acousto-optic loss modulator was first reported by WOOD et al[65] and later by FIGUEIRA et al[66], RICHARDSON[67] and SAKANE[68].

Passive mode-locking using hot CO_2 (350°C) as a saturable absorber has been reported by GIBSON et al[69], while NURMIKKO et al[70], FORTIN et al[71] and DYER and JAMES[72] have obtained mode-locking using SF_6, diluted in He, as the saturable absorber. The suitability of p-type Germanium as a fast relaxing passive mode-locking element for CO_2 lasers has been demonstrated by GIBSON et al[73]. This material saturates at an intensity of about 10 MW/cm^2 [74] and its use has resulted in 500 ps pulses from an atmospheric pressure oscillator. Using this method, FELDMAN and FIGUEIRA[75] have generated 400 ps pulses at 600 torr, while WALKER and ALCOCK[76,77] have obtained pulses in the 75-150 ps range from a high pressure (10-15 atm.) CO_2 laser.

Lastly, BELANGER and BOIVIN[78] and ALCOCK et al[79,80] have generated trains of ns pulses by injecting

(a) a single nanosecond CO_2 laser pulse;
(b) a low energy train of such pulses; and
(c) a short pulse switched out of a CW laser,

respectively, into a 'slave' oscillator. This injection mode-locking method has the advantage that it can be applied to large aperture TEA CO_2 lasers.

Discussion of the spontaneous self-mode-locking tendency, associated with TEA CO_2 laser oscillators emitting a single transverse mode, will be found in the next chapter (section 2.5.4).

1.5.2 *Mode Selection*

The advantage of using a single longitudinal mode rather than a mode-locked oscillator for the generation of ns CO_2 laser pulses is discussed in Chapter VI. Single longitudinal mode operation has been achieved by NURMIKKO et al[70] — and subsequently by others[72,81] — through the insertion of an SF_6 cell in grating-tuned resonators.

Mode selection using interferometric techniques has been reported by WEISS and GOLDBERG[82] and HAMMOND et al[83].

GONDHALEKAR et al[84] and GIRARD[85] have achieved single longitudinal mode operation by inserting a CW, low-pressure CO_2 discharge section into a TEA CO_2 resonator in what has been designated the Hybrid CO_2 laser. The CW section superimposes a narrow peak in the pressure-broadened gain curve of the TEA laser. This extra gain causes the laser oscillation to build up in a single longitudinal mode, lying in the narrow frequency range of the CW gain curve. A variation of this method was recently reported by LOY and RONALD[86] which substituted a low pressure pulsed section for the CW section.

The injection of the output of an independent CW oscillator into the laser resonator has also allowed mode selection control[87,88] provided the two cavities are mode-matched.

One final method[89] for achieving single longitudinal mode operation of TEA CO_2 lasers, based on the coupling of two unstable resonators sharing the active medium, is fully discussed in Chapter VI.

1.5.3 *Generation of Single Nanosecond CO_2 Laser Pulses*

The most common approach to the generation of short laser pulses relies upon the use of a fast electro-optical switch. By means of this method the short pulse is generated either (a) by gating out a segment of the pulse emitted by a single longitudinal mode oscillator, or (b) by

selecting a single pulse from the train of pulses generated by a mode-locked oscillator.

HILL et al[81] have reported the generation of pulses of variable duration (2 - 100 ns), 0.05 MW, by gating the single longitudinal mode output of a TEA CO_2 laser. RICHARDSON[90] has recorded ~600 ps, 5 mJ multi-line pulses using a U V photo-preionized CO_2 laser, while FIGUEIRA and SUTPHIN[91] have obtained the generation of two-band 1 ns, 0.5 mJ pulses. The development of a full-wave CdTe electro-optical shutter at Los Alamos has enabled the production of a 400 ps multi-line pulse[6].

DAVIS et al[92] have produced 1.3 ns, 1 MW pulses from an actively mode-locked TEA CO_2 laser, with extinction ratio of 900, using a GaAs Pockels cell. RHEAULT et al[93] have generated 1.8 ns, 2 mJ pulses, with extinction ratio of 300, which were amplified by four 1 m-long, double-discharge modules to 3.5 J. LITTLE et al[94] using a single-stage telescopic amplifier have achieved 0.83 ns, 1 J pulses with an extinction ratio of up to 3400 (section 3.6). FIGUEIRA et al[66], using a Brewster angle acousto-optic modulator, have generated 1.2 ns, 1 mJ pulses with the high extinction ratio of 5.4×10^4. PAN et al[95] have amplified a multi-line 1.3 ns, 2 mJ pulse, with extinction ratio of 1.5×10^4, to 10 J by passing it three times through a 1.8 m long amplifier. STARK et al[96] reported pulse-energies of 20 J in 1.5 ns, using three large-volume electron-beam controlled amplifiers. VALKYRIE, the short pulse CO_2 laser system at the Lawrence Livermore Laboratory[97], has delivered a multi-line 1.5 ns, 25 J pulse. The extinction ratio of the amplified pulse was found to be 2×10^3, which was three orders of magnitude smaller than that of the input pulse. CHAMPAGNE et al[98], using a chain of eight laser modules, have amplified a multi-line 1.2 ns, 2 mJ pulse to 50 J. MATOBA et al[99] have recorded a 3 ns, 200 J pulse using a nine-module chain of amplifiers. Lastly, the Single-Beam System at LASL[6], comprised of a mode-locked, UV-ionized oscillator; a double electro-optical

switch, with extinction ratio of 4.5×10^5, and four 1 m-long, electron-beam controlled amplifiers has delivered 250 J in 1 ns.

Another - potentially important - method of generating nanosecond pulses has been reported by YABLONOVITCH and GOLDHAR[100] by means of which pulses shorter than 50 ps have been recorded[101,102]. In this method, termed Free Induction Decay, a long single longitudinal mode laser pulse is abruptly terminated by optical breakdown and is subsequently passed through a CO_2 cell acting as a narrow band resonant absorber. The sharp termination of the input pulse causes the absorber to transmit a short pulse while the primary pulse is heavily attenuated.

Finally, ALCOCK et al[103] have demonstrated a technique whereby $\sim$2 ns CO_2 laser pulses were produced by reflection from free carriers induced in a polycrystalline Ge plate by a $\sim$2 ns ruby laser.

CHAPTER II

ANALYSIS AND OPTIMIZATION OF TEA CO_2 LASER PERFORMANCE

2.1 INTRODUCTION

Two different transversely-excited atmospheric pressure (TEA), CO_2 laser modules have been employed throughout the course of this study and, for that reason, they merit particular attention. The first module was a Double-Discharge type with electrode configuration similar to the one first described by DUMANCHIN et al[104] and with electrical driving circuit similar to that reported by PAN et al[105]. This device was in existence at Culham prior to the undertaking of this work but was modified to improve its efficacy for the present study and it is the improved version which is shown in Fig.2.1. The second module, similar to the one first developed by LAMBERTON and PEARSON[106,107] was constructed and assembled entirely in the course of this work (Fig.2.2). Although this is also a Double-Discharge system, in order to distinguish it from the first, it will be referred to as the Double-Rogowski — on account of its electrode shape. A comprehensive analysis of both modules as well as a discussion of their individual and comparative performances is presented here.

2.2 DESCRIPTION OF THE DOUBLE-DISCHARGE MODULE

2.2.1 Electrode Structure

The cathode comprised 158 parallel blades — 6.3 mm apart, 70 mm wide, 0.6 mm thick and 2.7 mm deep — milled from an aluminium base. In between the blades were glass-insulated, trigger electrodes (see Fig.2.3) consisting of 5.4 mm in diameter capillary glass tubes containing 0.3 mm in diameter nichrome central wires. These wires were so arranged as to lie on the same level as the edges of the aluminium blades. The glass tubes were sealed at one end and all the wires emerging from the open end were attached to a $2 \times 2 \times 100$ cm^3 copper bar which in turn was connected to the anode through a

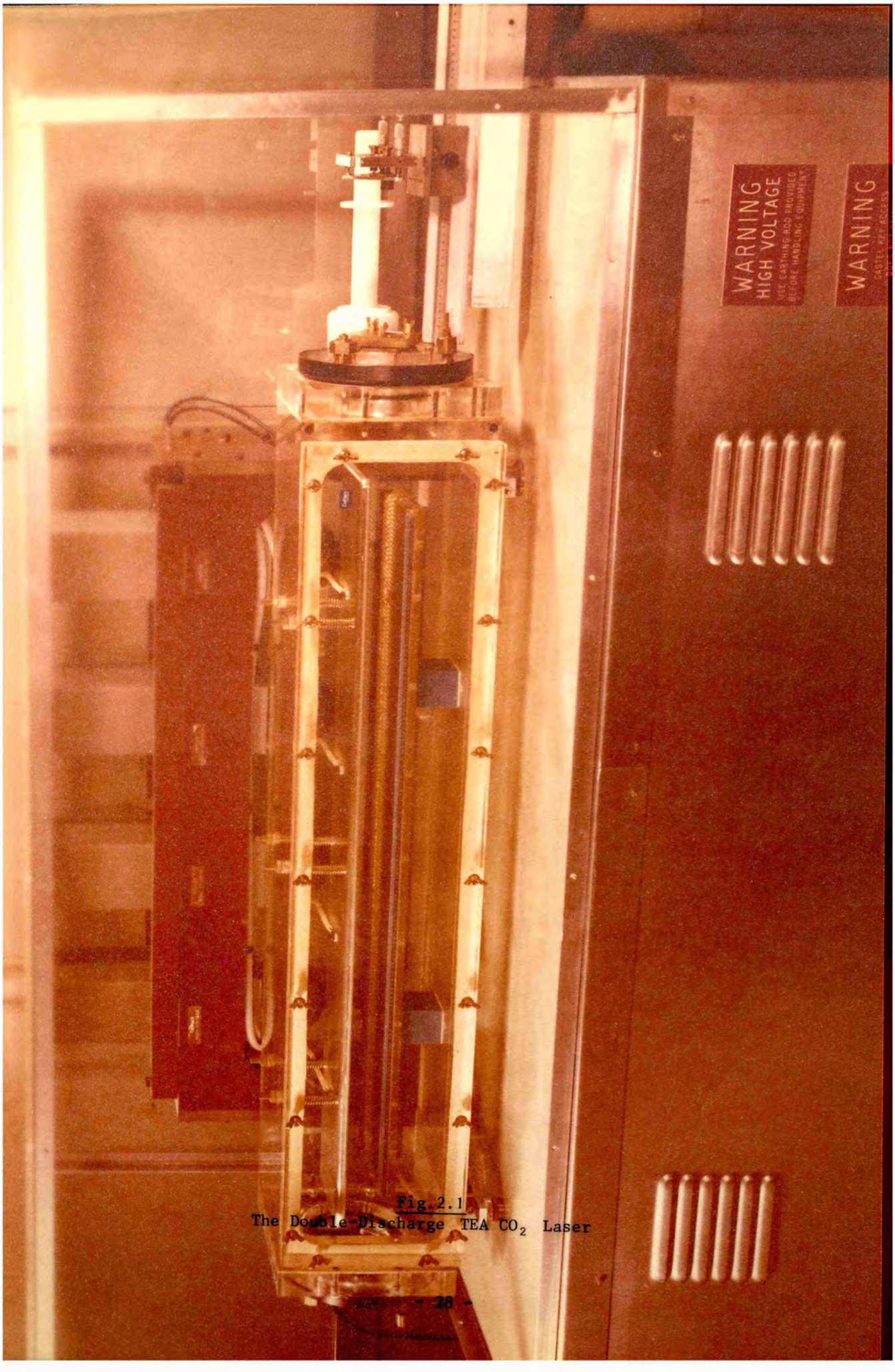

Fig.2.1
The Double-Discharge TEA CO_2 Laser

WARNING
HIGH VOLTAGE
USE EARTHING ROD PROVIDED
BEFORE HANDLING EQUIPMENT
WARNING

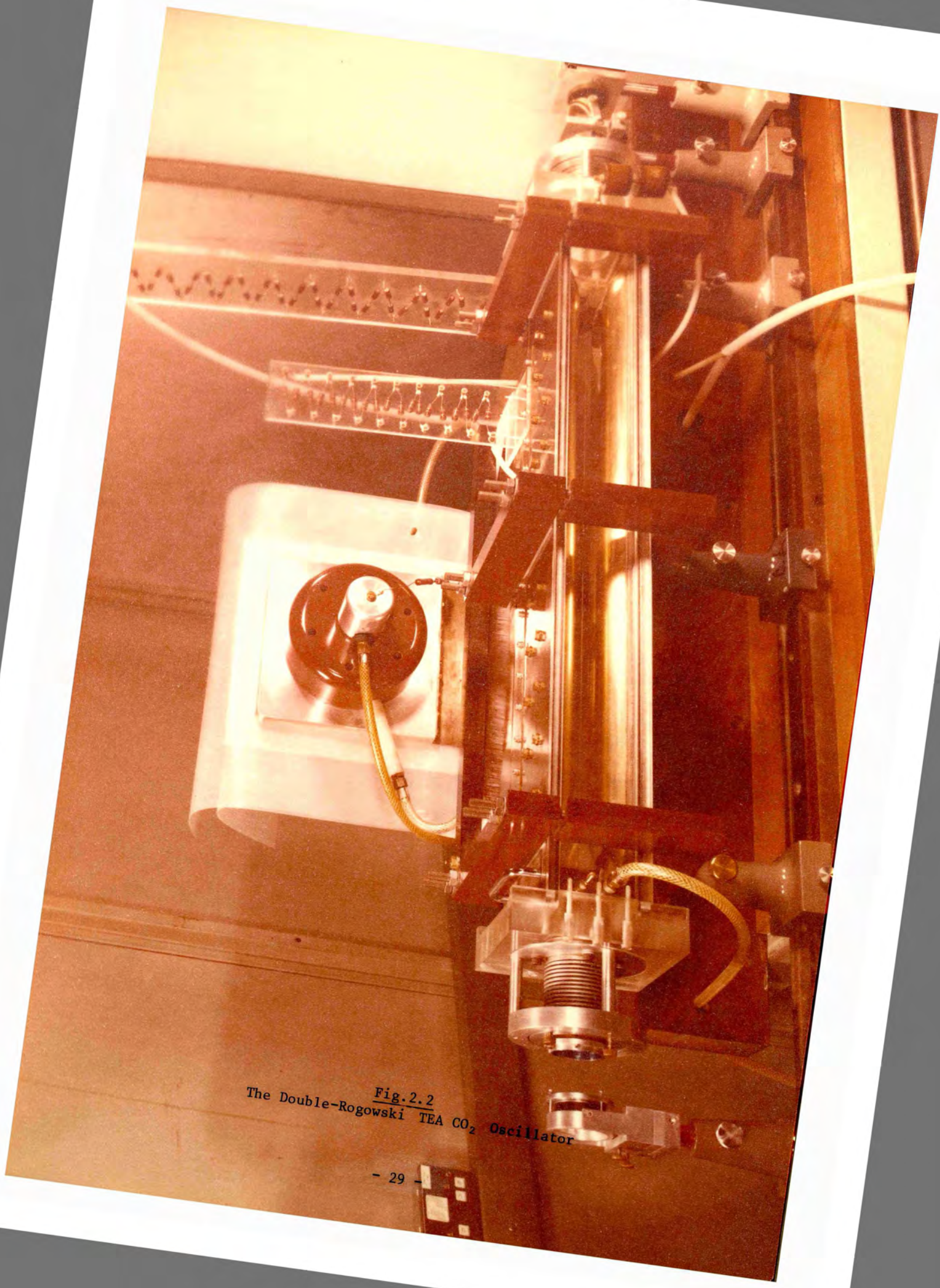

Fig.2.2
The Double-Rogowski TEA CO_2 Oscillator

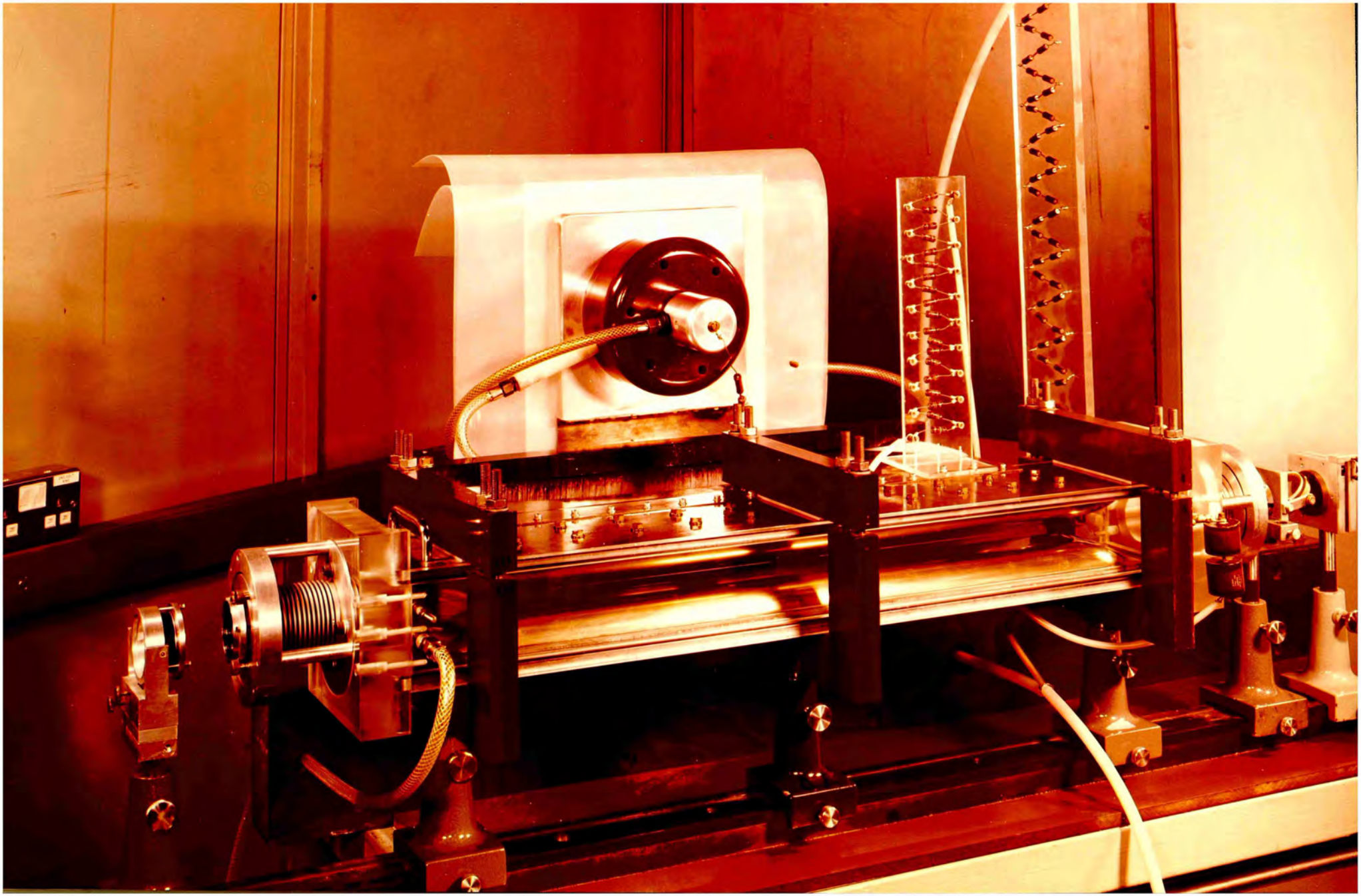

CAUTION
Colour prints fade in strong sunlight

CMP 76-1843c

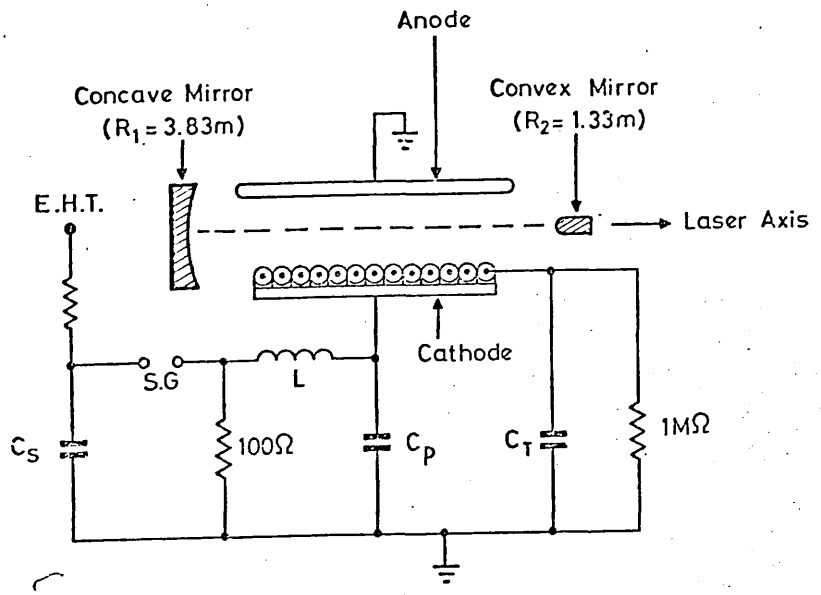

Fig.2.3
Schematic diagram of the double-discharge laser and electrical pulsing circuit

1200 pF coupling capacitor C_t. The anode was a $110 \times 15 \times 1.5$ cm^3 flat aluminium plate with smooth edges to prohibit field concentrations. The electrodes were enclosed in an air-tight perspex box.

2.2.2 *Gas Supply*

The three gases — helium, carbon dioxide and nitrogen — were supplied in separate cylinders each of which was connected to its respective gas flow meter. Having passed through the flow meters, the individual gases were mixed before entering the laser box. Each flow-rate could be independently controlled and the flow-rate of the gas mixture as a whole could be varied from 1 to 8 litres per minute to meet the gas replacement requirement, depending on the frequency of firing which ranged from 1 to 6 pulses per minute. This repetition rate was limited by the capability of the charging supply but since this was found to be adequate for the nature of the experiments undertaken, no attempt was made to improve the rate.

2.2.3 *Electrical Pulse Circuitry and Glow Discharge Mechanism*

The electrical driving circuit is depicted schematically in Fig.2.3. The low inductance storage capacitor $C_s = 0.2\,\mu$F was charged by a high voltage d.c. power supply consisting mainly of a 5 kVA transformer which delivered a

voltage of up to 60 kV via a rectifying assembly of 17 LC 180 HV diodes. The circuit was switched with a nitrogen-filled spark gap of Culham design, operating at pressures between 2500 and 2800 torr.

The second low inductance capacitor $C_p = 0.1\ \mu F$ together with the inductor $L = 9\ \mu H$ formed the pulse-shaping network. When the spark gap was triggered, the electrical energy stored in the capacitor C_s was fed into the pulse-shaping network. The voltage, developed across the capacitor and consequently across the inter-electrode spacing, is expressed as a function of time by[108,109]:

$$V(t) = \frac{V_o C_s}{C_s + C_p}\left[1 - \cos\left(\frac{C_s + C_p}{L\,C_s\,C_p}\right)^{\frac{1}{2}} t\right] \qquad \ldots (2.1)$$

This voltage attains its peak value $V_{max} = \frac{2\,V_o\,C_s}{C_s + C_p} = 1.33\,V_o$ at the time $t = \pi\sqrt{\frac{L\,C_s\,C_p}{C_s + C_p}} = 2.43\ \mu s$ after the closing of the spark gap. During this slowly-rising high voltage pulse, the electric field between the cathode and the trigger wires was sufficiently high - due to the proximity of the trigger wires to the cathode plates — to initiate a corona discharge between these two electrodes. The electron layer, as well as the ultra-violet radiation[110,111] produced by the corona discharge, created the necessary pre-ionization in the inter-electrode gas for the initiation of the glow discharge between the anode and the cathode. Fig.2.4(a) shows a typical current pulse shape of the main discharge displayed on a 454 Tektronix oscilloscope using a Rogowski coil encircling the anode-to-earth leads. Glow discharges at atmospheric pressure were obtained for various gas-mixtures and electrical input energies between 185 and 370 Joules.

This module has been used for three purposes in the course of this research:

(a) as a 180 megawatt peak power CO_2 laser using an unstable resonator emitting a single-transverse but multi-longitudinal mode;

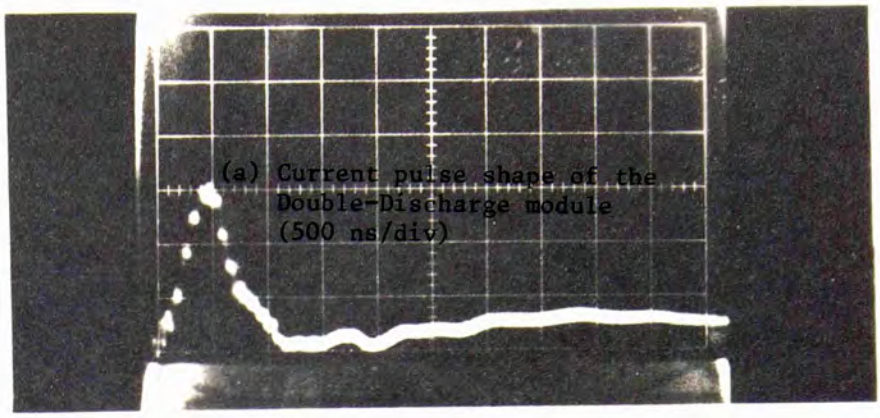

(a) Current pulse shape of the Double-Discharge module (500 ns/div)

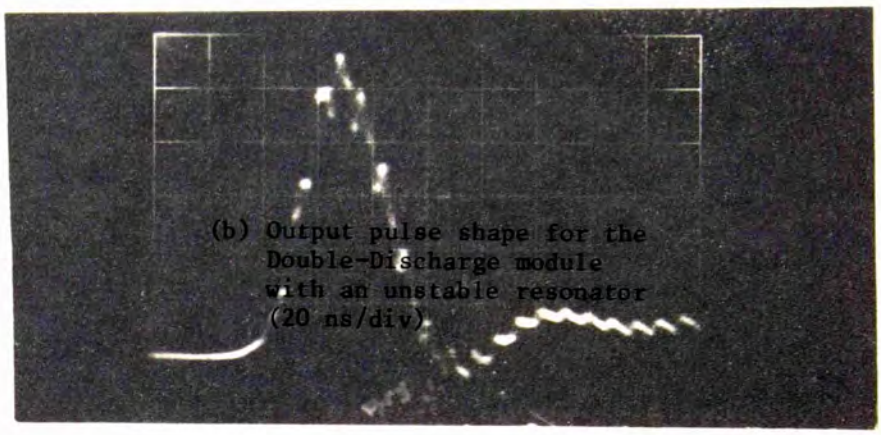

(b) Output pulse shape for the Double-Discharge module with an unstable resonator (20 ns/div)

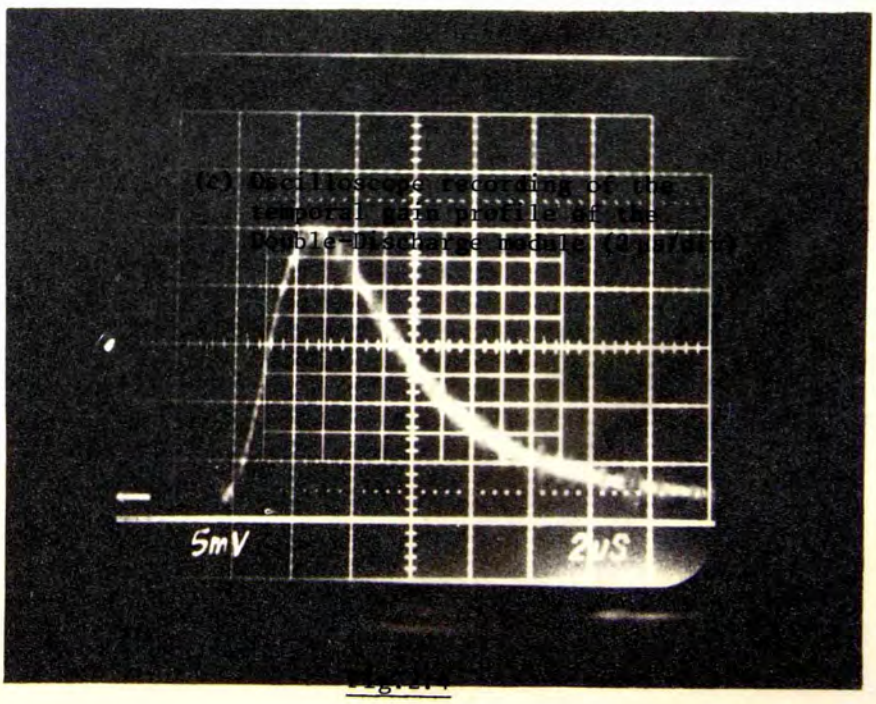

(c) Oscilloscope recording of the temporal gain profile of the Double-Discharge module (2 μs/div)

Fig. 3.1

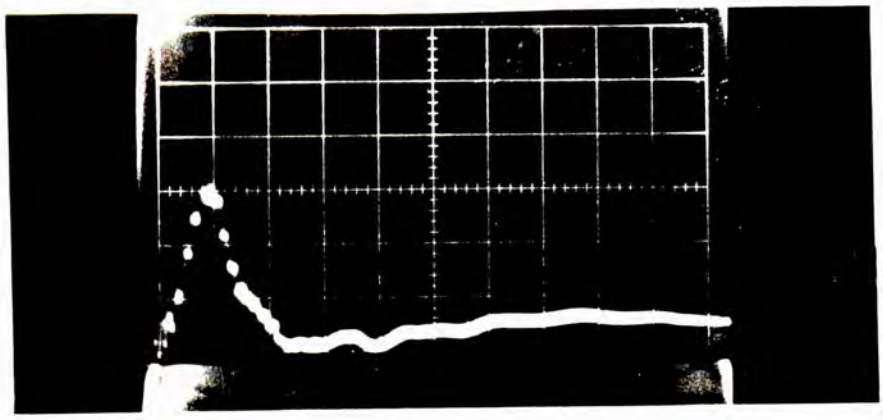

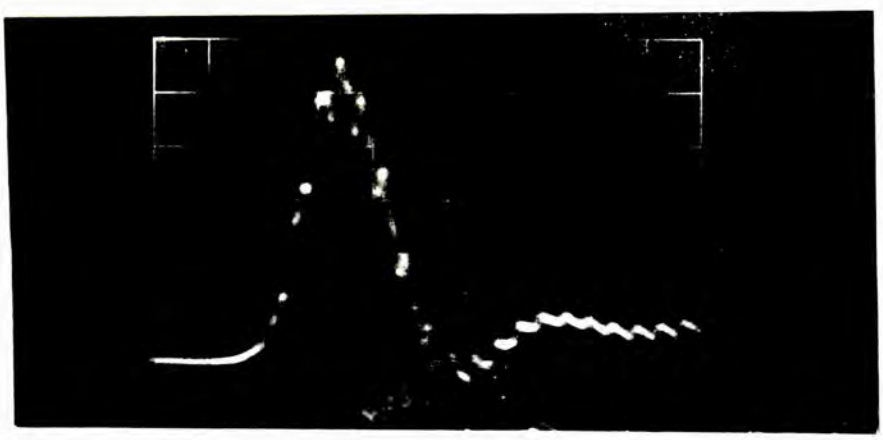

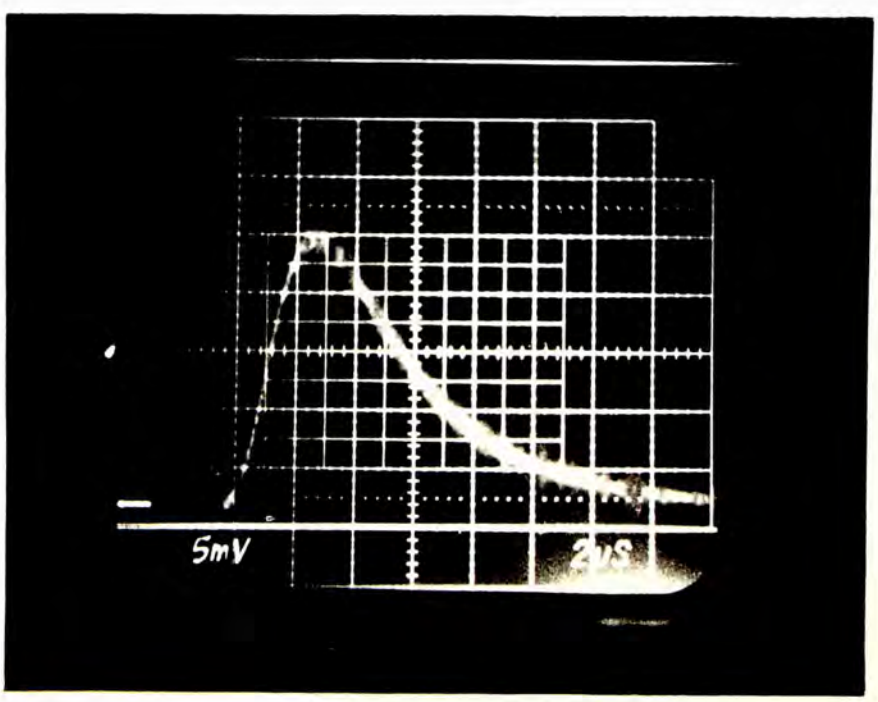
5mV
2μS

(b) as a single-transverse, single-longitudinal mode CO_2 laser with 30 megawatt peak power using two coupled, unstable resonators[89] which is discussed in detail in Chapter VI; and

(c) as a telescopic amplifier emitting 1 GW, 1 ns CO_2 laser pulses[94] which is described fully in Chapter IV.

2.3 PERFORMANCE OF THE DOUBLE-DISCHARGE OSCILLATOR

2.3.1 Optical Cavity: Unstable Resonator

In many laser applications, a beam with divergence as near to the diffraction limit as possible is highly desirable. In stable resonators, however, the emitted beam has diffraction-limited divergence only when an intra-cavity aperture is used to suppress oscillation in all but the lowest order transverse mode. The exact required diameter of such an aperture is a function of the resonator parameters and the laser wave-length[113] but it is generally less than 1 cm^2 in the case of a CO_2 laser. This implies that for the Double-Discharge module which has a 25 cm^2 cross-section, the volume of the lowest order transverse mode is less than 4% of the volume of the active medium, and consequently no more than 4% of the available optical energy can be extracted by a single transverse mode when a stable resonator is used. By contrast, the use of a telescopic resonator does ensure oscillation in the lowest order transverse mode filling the entire cross-section of the active medium. This significant advantage of unstable, over stable, resonators accounts for their increased recognition and use with CO_2 lasers[72,94,114-118]. DATSKEVICH et al[115], using an unstable resonator, have obtained 7.5 kJ single transverse mode CO_2 laser pulses. The properties of unstable resonators are fully analysed and presented in two review papers by SIEGMAN[119] and ANAN'EV[120].

Accordingly, an unstable confocal resonator belonging to the positive branch (telescopic resonator) was used in conjunction with this module was to extract the optical energy stored in the active medium. The radius of curvature of the concave and convex mirrors was $R_1 = 3.83$ m, $R_2 = -1.33$ m respectively.

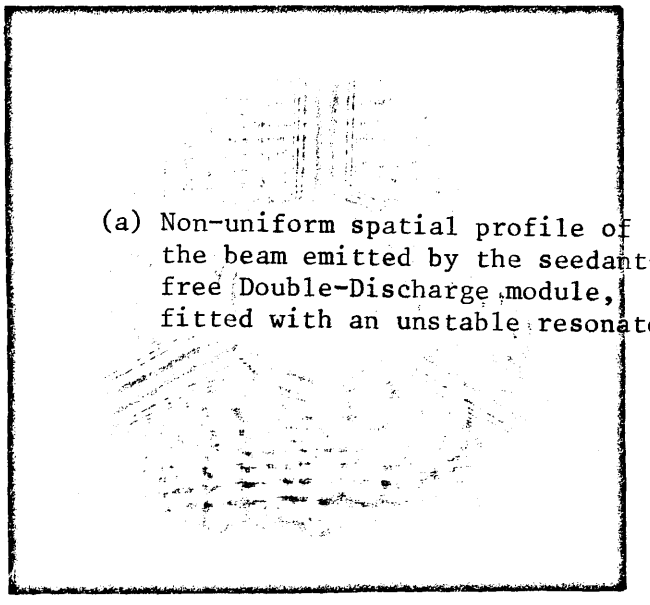

(a) Non-uniform spatial profile of the beam emitted by the seedant-free Double-Discharge module, fitted with an unstable resonator

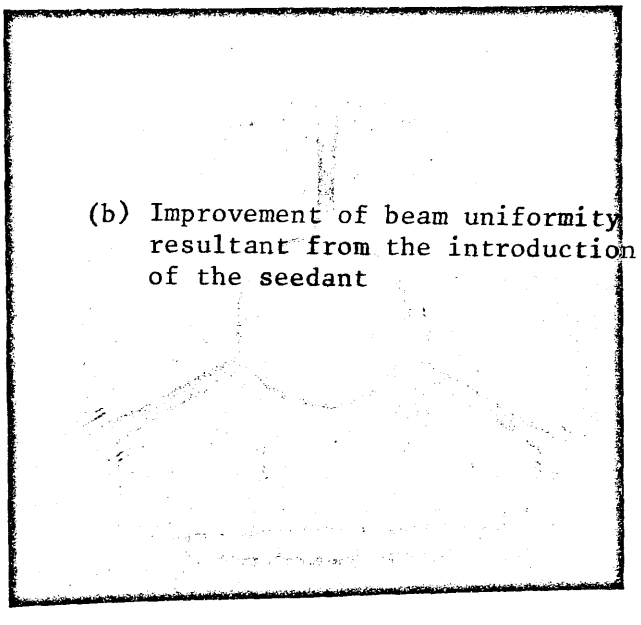

(b) Improvement of beam uniformity resultant from the introduction of the seedant

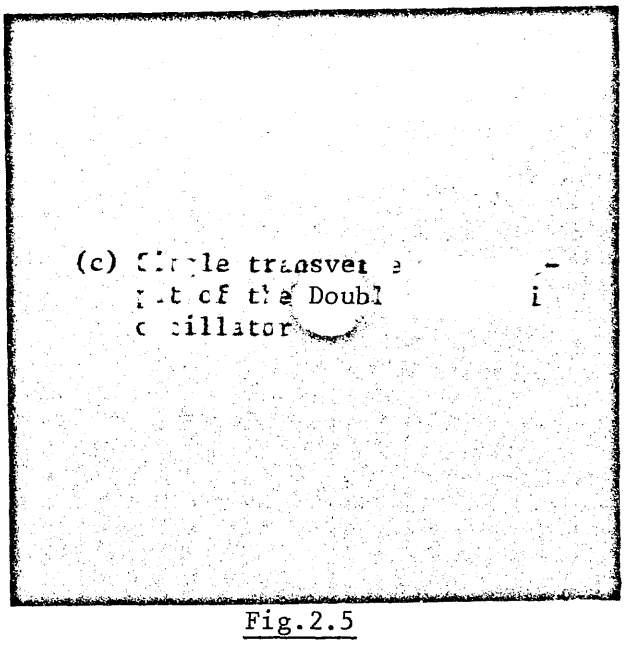

(c) Circle transverse [illegible] of the Double [illegible] oscillator

Fig.2.5

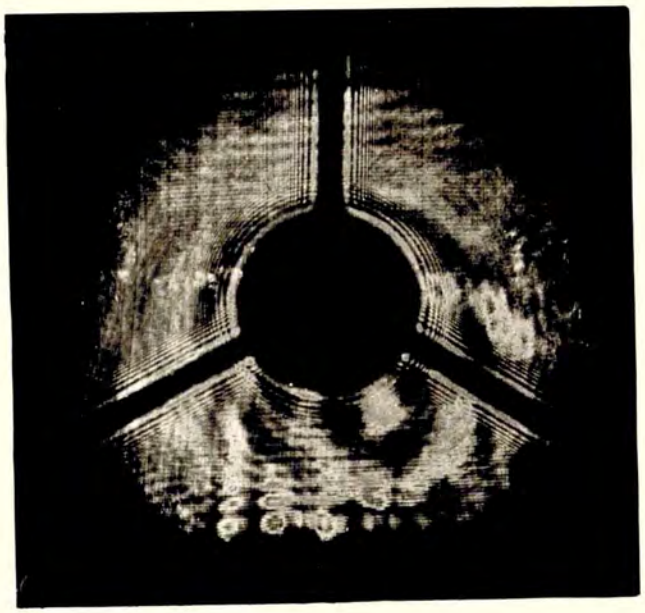

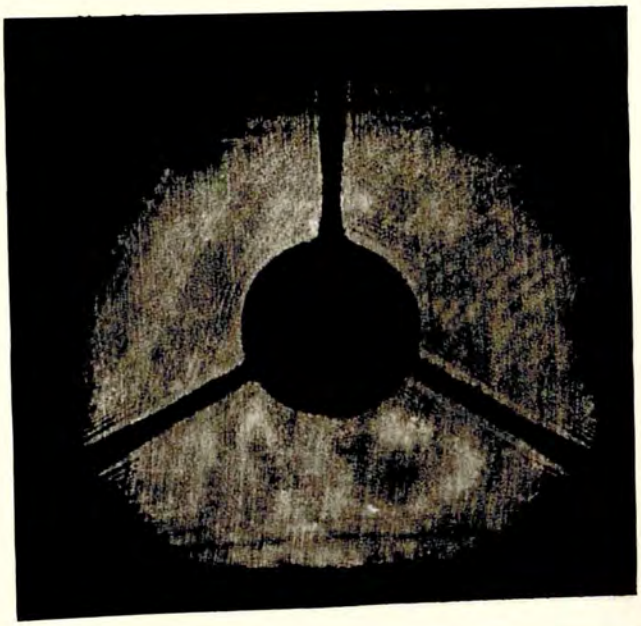

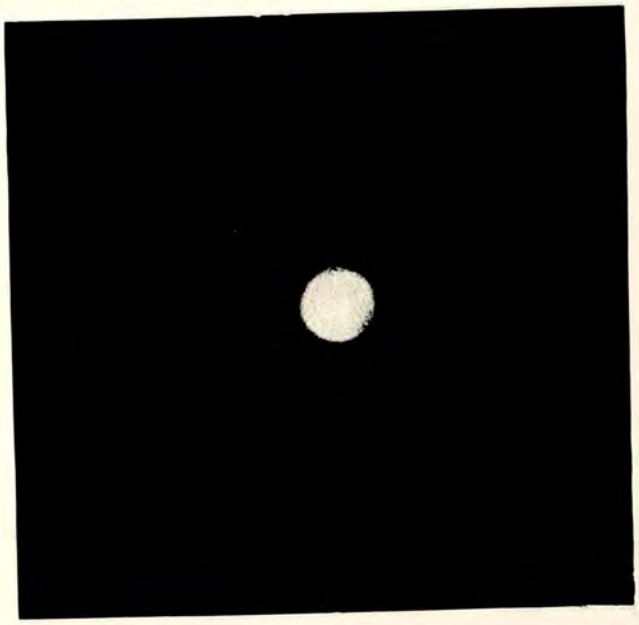

The cavity length was determined by the convocality condition

$$L = \frac{R_1 - |R_2|}{2} = 1.25\,\text{m}.$$

The magnification of this unstable resonator, i.e. $M = R_1/|R_2| = 2.875$, determined the fractional output coupling, $\delta = 1 - \frac{1}{M^2} = 0.88$, in the cavity. The cross-section of the output beam — just after the exit window — was an annulus with a central dark disc 17 mm in diameter equal to the diameter of the convex mirror (Fig.2.5). The shadow of the 'spider' supporting the convex mirror, as is shown in Figs.2.5(a), 2.5(b), can be easily eliminated by using an annular coupling mirror in front of the convex mirror and at 45° to the resonator axis, as was proposed by KRUPKE and SOOY[114].

2.3.2 *Energy Measurements*

The energy of the emitted pulse was measured using a pyro-electric joule meter (Gen-Tec, Model ED-500). The pulse shape was recorded and the peak power was measured using a calibrated germanium photon drag detector[112]. In Fig.2.6, the output pulse energy is plotted against the electrical excitation energy. It can be seen that the laser energy continued to increase linearly with the electrical up to the limit of the power supply. The $CO_2 : N_2 :$ He mixture was maintained at 1:1:6, and the flowing rate was 8 ℓ/min. The efficiency of this laser, defined as the ratio of the laser beam energy to the electrical energy stored in the capacitor C_{st} is also plotted in Fig.2.6. The temporal profile of the laser pulse (see Fig.2.4(b)) comprises a 40 ns (FMHW) spike followed by a 1 μs low power 'tail'. The first spike which was found to occur 500-600 ns after the peak of the discharge current is caused by the gain-switching process[121]. The long tail results from the re-establishment of the population inversion achieved by repumping the upper laser level by collisions with the vibrationally-excited N_2 molecules. The energy contained in the first spike was estimated to be ~40% of the total.

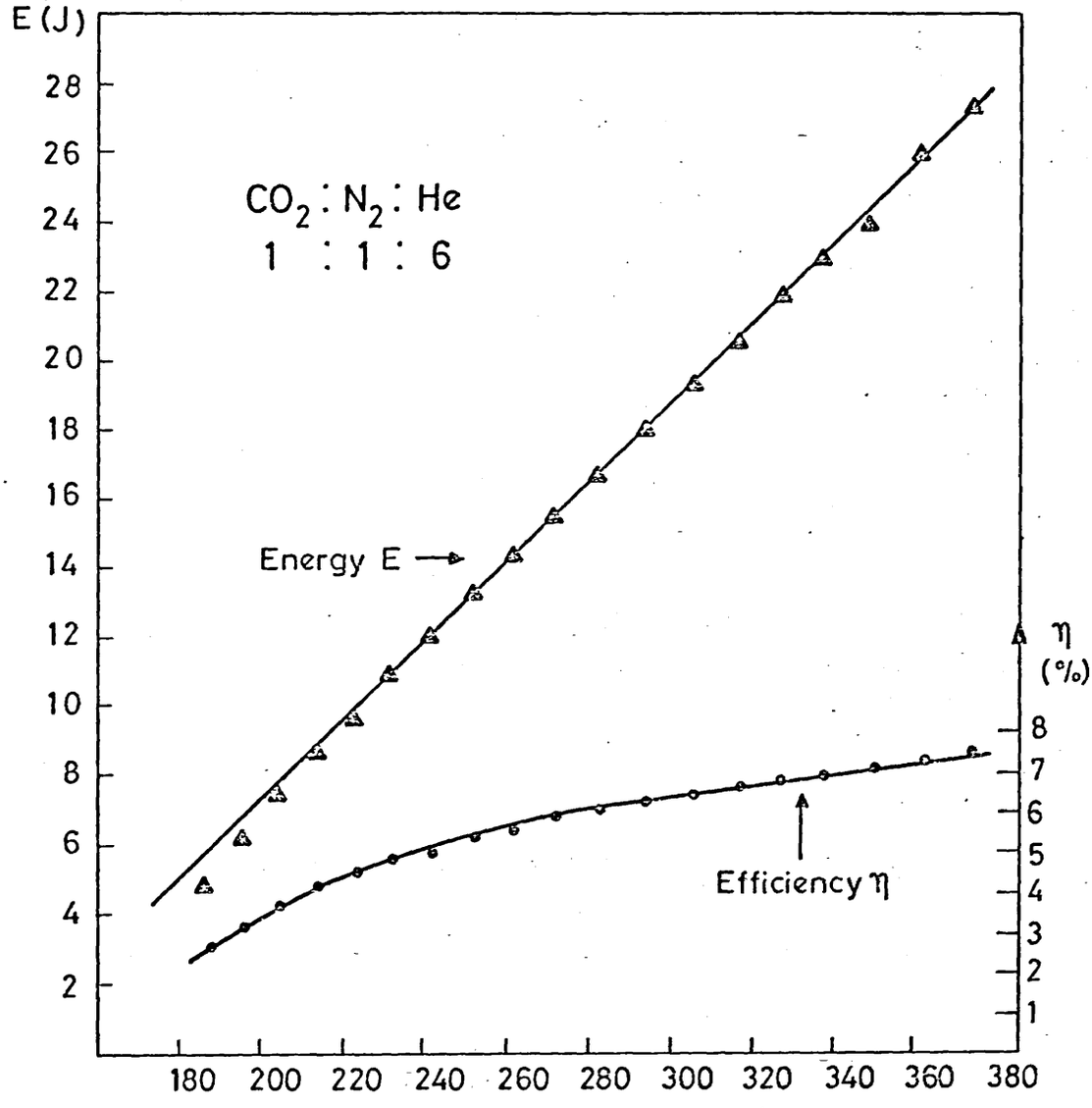

Fig.2.6
Optical energy output and efficiency of the Double-Discharge module as a function of the electrical input energy

2.4 DESCRIPTION OF THE DOUBLE-ROGOWSKI MODULE

2.4.1 *Electrode Structure and Electrical Pulse Circuitry*

The second module used was a Double-Rogowski CO_2 laser[106,107]. Two identical Rogowski-profiled brass electrodes 70 cm long and 2.5 cm apart and two tungsten trigger wires running parallel to these electrodes, but laterally displaced, comprises the electrode configuration (Fig.2.7). The tungsten wires were 0.3 mm in diameter and were connected to the cathode through two 250 pF coupling capacitors at one end of each wire. The storage capacitor was a 0.1 μF fast discharge low inductance capacitor charged via a 50 MΩ current-limiting resistor by a 1 mA Brandenburg power supply (type MR 50/RA). The pressurised spark-gap was again of Culham design. Low inductance connection was ensured by using a parallel plate transmission line made of copper sheet 3 mm thick. The total length of the sheet was 70 cm and the width at the ends connected to the capacitor and spark gap was 30 cm and at the ends connected to the electrodes 70 cm.

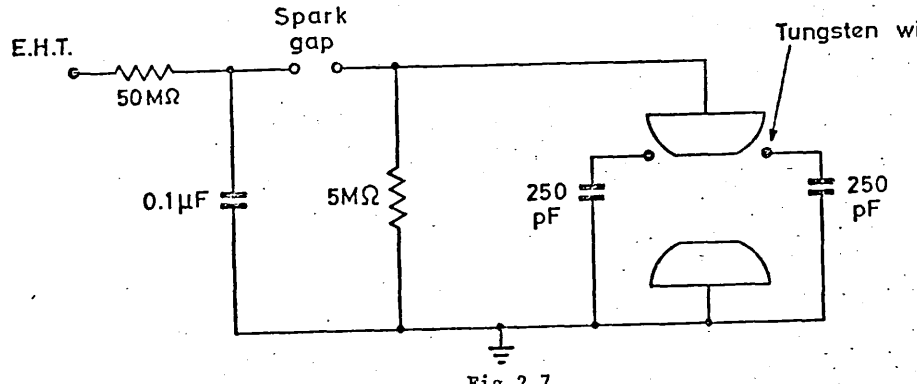

Fig.2.7
Schematic diagram of the excitation circuit of the Double-Rogowski oscillator

2.4.2 *Glow Discharge Mechanism*

When the spark gap was triggered and an ~45 kV voltage pulse was applied to the main electrodes, field emission from the tungsten wires resulted in a sheet discharge along the entire length of the wires and between them and the anode[10,106,107]. The energy dissipated in the discharge was limited by the small values of the coupling capacitors. A glow discharge was initiated between the main electrodes as a result of the ultra-violet

radiation generated by the sheet discharge. This ultra-violet radiation is thought to result from the 584 Å helium resonance line[107].

2.4.3 *Gas Supply*

The same gas supply serviced the Double-Rogowski as the Double-Discharge module, thus obviating the need for the provision of a second gas supply. Having traversed the Double-Discharge device, the gas was fed into the second module with no detrimental effect on its performance.

2.4.4 *Stable Optical Resonator - Single Transverse Mode*

The Double-Rogowski module was constructed for use with an electro-optical shutter (which will be described in the next chapter) to generate nano-second pulses. Because the electro-optical crystal in this shutter had a 1×1 cm^2 cross-section, any larger cross-section in the laser beam would be superfluous. Furthermore the low optical damage of the electro-optical material (< 1 J/cm^2) prohibits the use of an inverted telescope to reduce the beam cross-section. Therefore the advantage offered by an unstable resonator (discussed in section 2.3.1) i.e. of providing large volume single transverse mode, could not be exploited here. For these reasons, a stable resonator, consisting of an $R = 10$ m radius of curvature gold-coated copper mirror (reflectivity 99%) and a germanium flat with an anti-reflection coating on one face (reflectivity 36%) were used. The length of the resonator was $L = 1.35$ m. The waist of the lowest order transverse mode for such a resonator is at the plane mirror and the beam radius ω_0 (or spot-size) at this point is given by[122]

$$\omega_0 = \left(\frac{\lambda}{\pi}\right)^{\frac{1}{2}} \left[L(R-L)\right]^{\frac{1}{4}} = 3.4\,\text{mm} . \qquad \ldots (2.2)$$

In order to restrict oscillation in the lowest order transverse mode an adjustable circular aperture was inserted in the cavity near the plane mirror. It is well-known[113,123] that oscillation in all but the lowest order transverse mode should be suppressed for aperture diameters of smaller

than 3.5 ω_0 (i.e. $d < 12$ mm in the present case). With a 12 mm diameter aperture, however, the divergence of the emitted beam was found to be more than twice the theoretically predicted, thus indicating that the laser was oscillating in more than one transverse mode. By reducing the aperture diameter to 8 mm the far field half-angle divergence attained its minimum value which was measured to be 1 mrad. This figure compares favourably with $\theta = 1.27 \frac{\lambda}{d} = 0.84$ mrad which is the theoretical value for the lowest transverse mode of the same cross-section[124]. Fig.2.5(c) shows a typical burn pattern of a single transverse mode taken on a developed polaroid film 30 cm away from the exit mirror.

2.4.5 Self-Mode-Locking

When the temporal profile of the emitted single transverse mode laser pulse is displayed on a fast oscilloscope, such as the Tektronix 7904 (rise time 0.8 ns) using a Ge photon drag detector (rise time 0.6 ns) a periodic amplitude modulation of up to 100% can be observed (Fig.2.8(a)). The duration of the individual pulses in this self-mode-locked pulse train is typically 2 ns (FWHM) (Fig.2.8(b)), but their shape was not reproducible from shot to shot, reflecting the fact that no mode-locking element was present in the cavity. Similar self-mode-locking has also been observed by a number of other investigators[125-129]. The theory of self-mode-locking has been the subject of numerous papers (130 and cited references) and all that need be emphasized here is that unless oscillation in a single transverse mode is accomplished, the depth of modulation is decreased to less than 50% and, when the mode-limiting aperture is removed, the pulse shape is irregular with random mode beating (Fig.2.8(c)). It was also found that the presence of a polarizing KCl plate in the cavity enhanced the depth of modulation which was, on average, between 90% and 100%. The 9 ns spacing between the individual pulses equals the calculated 2L/c round trip cavity transit time.

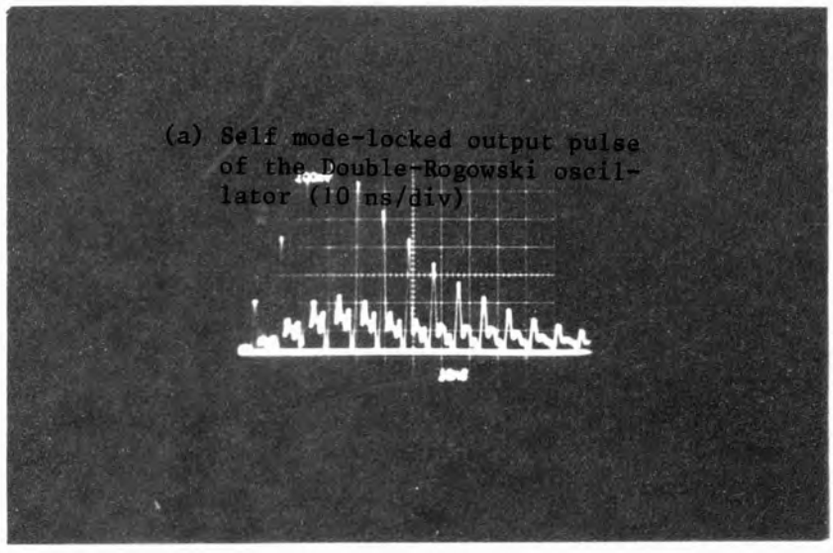
(a) Self mode-locked output pulse of the Double-Rogowski oscillator (10 ns/div)

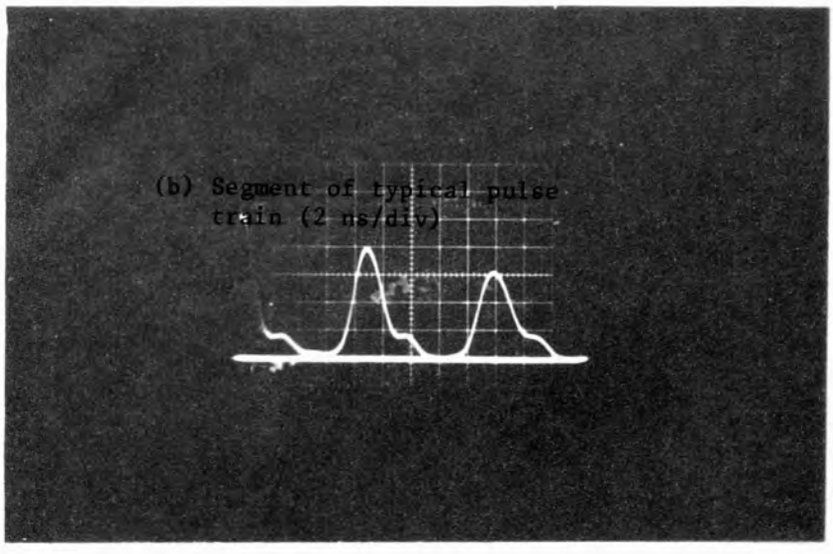
(b) Segment of typical pulse train (2 ns/div)

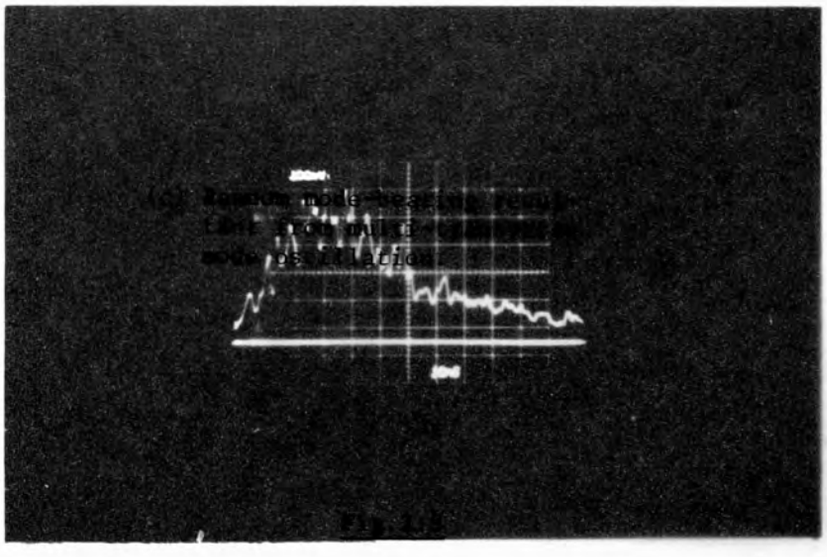

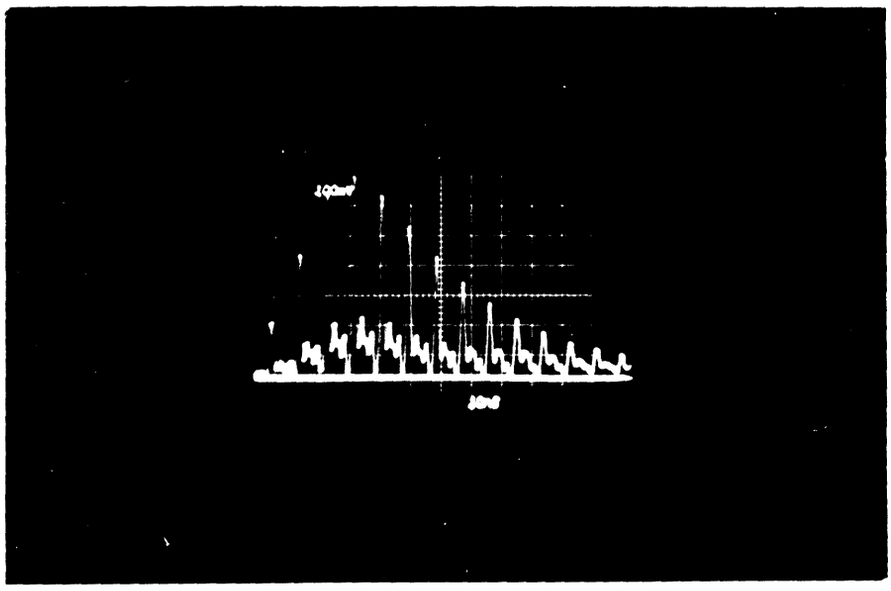

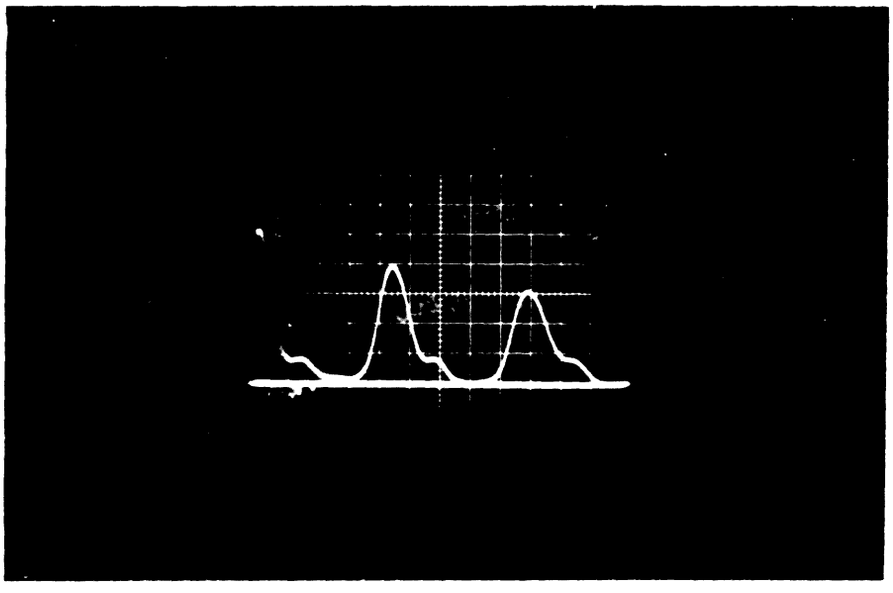

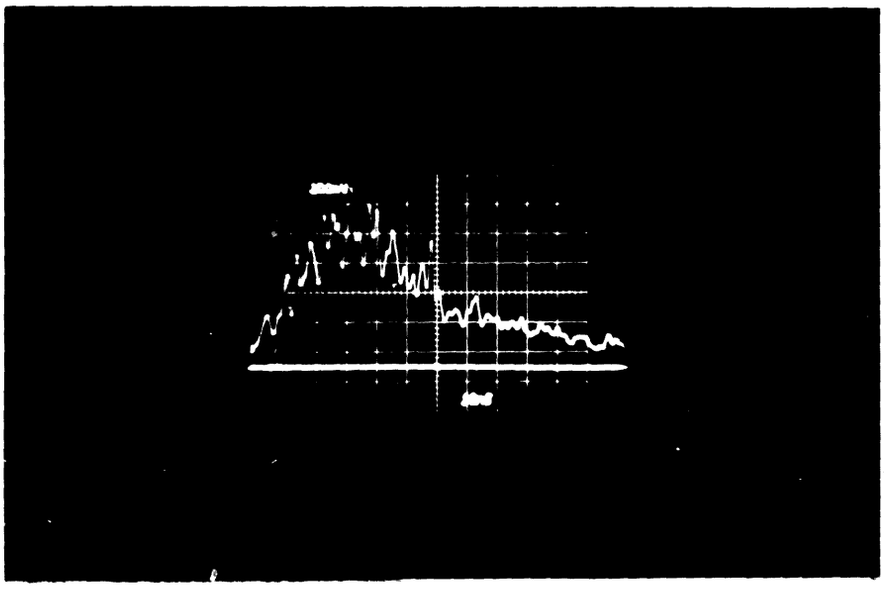

2.4.6 *Degree of Polarization*

As will become apparent in the next chapter, a linearly polarized beam with a high degree of polarization, P, is required for the generation of nanosecond pulses with low background. It will also be shown that a partially polarized output pulse of the double-Rogowski oscillator can be readily converted into a highly-polarized beam. In order to increase the conversion efficiency (defined as the ratio of the intensity of the linearly-polarized beam to the total intensity of the emitted pulse) a KCl plate was inserted into the resonator to polarize the output pulse. The degree of polarization of this pulse was measured using the arrangement shown in Fig. 2.9. It can be easily shown that

$$P = \left| \frac{E_1 - R_\perp E_2}{E_1 + R_\perp E_2} \right|$$

where E_1, E_2 are the energies measured by the two joule meters and $R_\perp$ is the reflectivity of the Ge plate for radiation linearly polarized in a direction perpendicular to the plane of incidence. The measured value of P was P = 80% ± 8%. The energy of the emitted pulse was in no way adversely affected by the presence of the KCl plate. As a result of introducing this polarizing plate, the efficiency of the conversion was increased by 80% and this promoted an equivalent increase in the intensity of the generated nanosecond pulses.

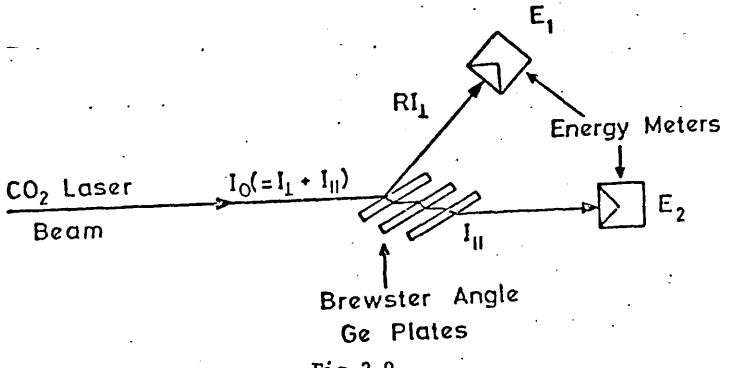

Fig.2.9
Experimental arrangement for measuring the degree of polarization of a laser pulse

2.4.7 *Energy and Power Measurements. Effect of Gas Composition*

The total pulse shape of this module — typical of a gain-switched laser — comprised a main spike followed by a 'tail', which was also characteristic of the Double-Discharge device. The duration of the tail following the initial 70 ns pulse was found to be dependent on the ratio of the partial pressures P_{N_2} and P_{CO_2} of the N_2 and CO_2 in the gas mixture. For a ratio $P_{N_2}/P_{CO_2} = 3$ the duration of the tail was $\sim 3\,\mu s$ (Fig.2.10(a). Energy and power measurements of such a pulse revealed that the initial pulse contained no more than 12% of the energy of the total pulse. For a ratio $P_{N_2}/P_{CO_2} = \frac{1}{3}$ the duration of the tail was reduced to $\sim 1\,\mu s$ (Fig. 2.10(b)). The pulse had no tail at all for ratios $P_{N_2}/P_{CO_2} \leq \frac{1}{8}$ (Fig.2.10(c). The peak power as well as the energy of the emitted pulse was found to be largely dependent on the gas mixture.

A series of simultaneous measurements of both the energy and the peak power of the emitted pulse are plotted against the ratio $\frac{P_{N_2}}{P_{N_2} + P_{CO_2}}$ in Fig.2.11. In the course of these measurements, the partial pressure of the helium was kept constant at $P_{He} = 456$ torr. It can be seen from these graphs that the energy of the laser pulse increases monotonically with the nitrogen concentration up to $P_{N_2} = 230$ torr where arc formation in the discharge drastically reduces the energy output. The peak power of the pulse, on the other hand, originally increases with the values of $\frac{P_{N_2}}{P_{CO_2} + P_{N_2}}$ and attains a maximum value when $\frac{P_{N_2}}{P_{CO_2} + P_{N_2}} = 0.14$ (i.e. $P_{N_2} = 43$ torr, $P_{CO_2} =$ 260 torr). Further increase in P_{N_2} results in an almost linear decrease of the peak power.

For the generation of nanosecond pulses, it is desirable that the oscillator should emit pulses with the maximum obtainable peak power while the energy of the pulse should be kept as low as possible to avoid optical damage (see section 3.7). Furthermore, as will be seen later, the small

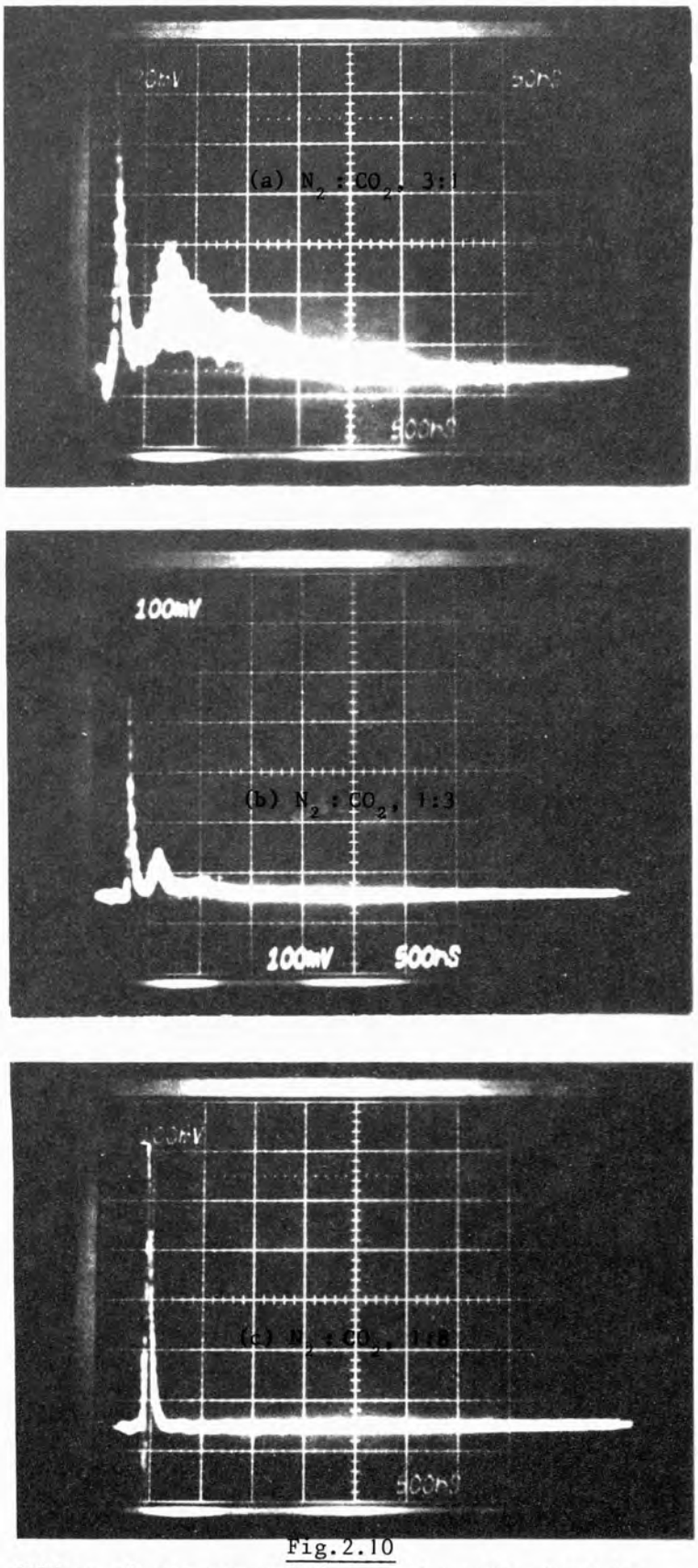

Fig.2.10
Effect of gas composition on the pulse duration

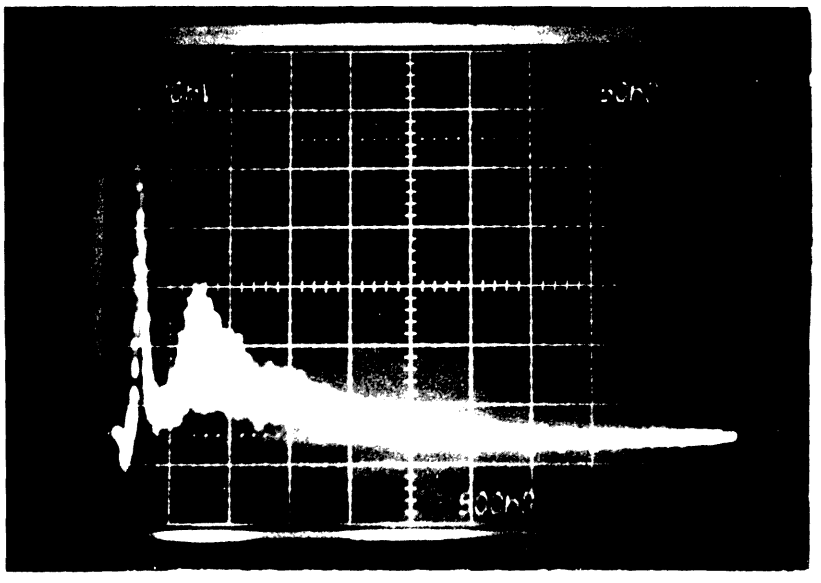

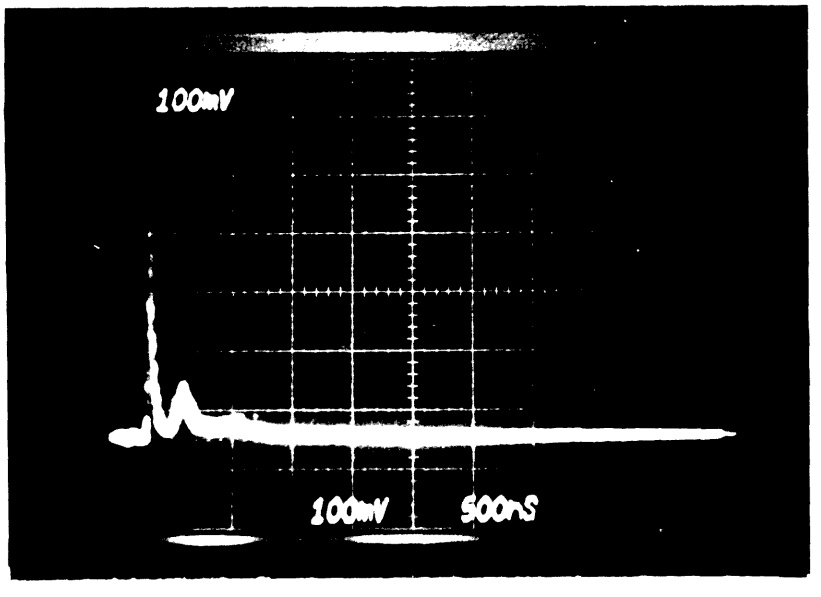
100mV
100mV
500nS

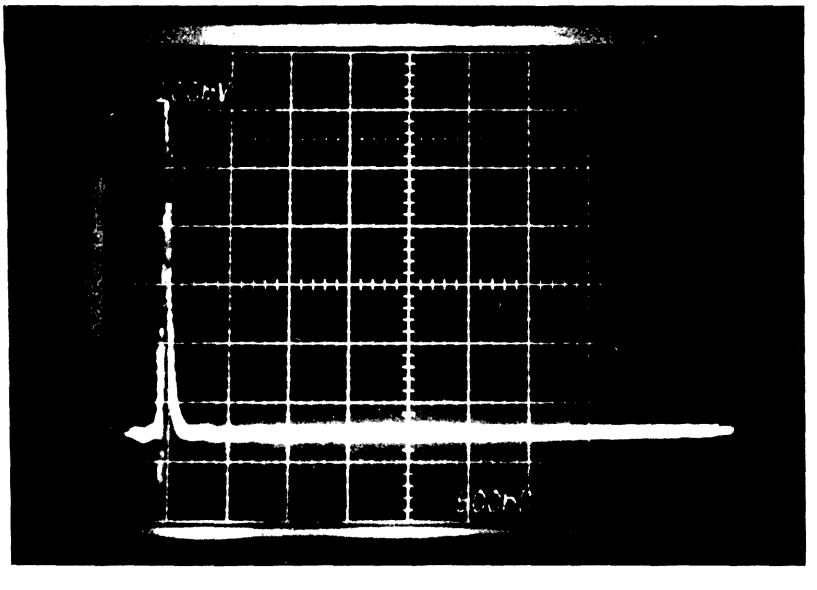

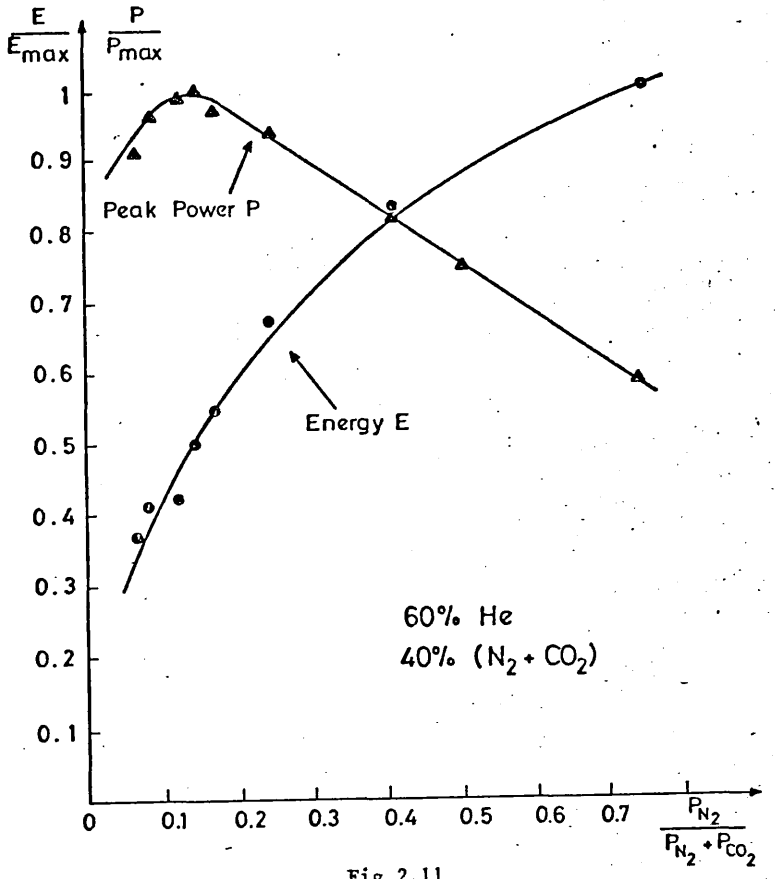

Fig.2.11
Effect of gas composition on the energy and peak power of the emitted pulse

signal gain in the Double-Discharge module was maximised for gas mixtures having the same composition. For these three reasons the ratio of $\frac{P_{N_2}}{P_{CO_2}} = \frac{1}{6}$ will be, in general, maintained throughout this study.

The mean peak power of the emitted pulse in ten consecutive shots was found to be $(9.8 \pm 0.5)\,MW/cm^2$, while the energy was $(290 \pm 10)\,mJ/cm^2$. The shape of these graphs was not affected by the amount of helium in the discharge (which varied within the range 315 - 700 torr) although — as might be expected — both the peak power and the energy were reduced at higher helium concentrations.

2.4.8 *Effect of Organic Additives on the CO_2 Laser Performance*

It has been so far ascertained that in order to maximise the peak power output of the pulse emitted from the Double-Rogowski module, a laser gas mixture should be used with:

(a) an appropriately chosen ratio in the molar fractions of the two molecular gases (i.e. $P_{N_2}/P_{CO_2} = 0.14$); and

(b) a low helium concentration.

However, when the helium concentration is reduced, at any given excitation energy input, formation of localized bright arcs drastically reduces the intensity of the emitted pulse. The minimum helium concentration for which reliable and arc-free glow discharges could be readily obtained was 60% for the Double-Rogowski module and 72% for the Double-Discharge module for excitation energies of 88 J and 290 J respectively. This arc formation is attributable to insufficient pre-ionization density[131] which occurs as a result of the reduction in the helium concentration[132].

LEVINE and JAVAN[133] demonstrated that the ultra-violet radiation emitted from xenon flashlamps could produce sufficient ionization to sustain a glow discharge when the laser gas mixture was seeded with an organic vapour of low ionization-potential (~ 7.5 eV). Consequently an enhancement in the pre-ionization density would be expected to follow the introduction of such a substance in the gas mixture of the two laser modules under discussion, as a result of a more efficient use of the ultra-violet radiation produced by the auxiliary discharges. This expectation was substantiated when small quantities (0.2 torr) of organic vapour such as triethylamine, $(C_2H_5)_3N$ or tripropylamine, $(C_3H_7)_3N$, having an ionization-potential of 7.5 eV and 7.23 eV respectively, allowed lower helium concentrations to be used in arc-free glow discharges. The new lower limits in the helium content were 45% and 60% for the Double-Rogowski and Double-Discharge modules respectively. As a result of this increase in the concentration of the

molecular gas ($N_2 + CO_2$) an ~30% increase in both the peak power and the energy of the two modules was established.

A further beneficial effect was observed on the Double-Discharge module which normally suffers from a spatially non-uniform laser output. The 'hot spots' in the lower part of the output beam shown in the 'burn-pattern' (Fig.2.5(a)) taken on a developed polaroid film, are eliminated when 0.5 torr of the seedant is introduced to the laser gas (Fig.2.5(b)). This indicates a gain uniformity in the whole volume of the active medium. The effect of the ultra-violet radiation created by the corona discharge on the preionization density has been overlooked in many publications concerning this type of laser[10,134-137]. MAZURENKO and RUBINOV[138], however, have recently shown that a significant amount of soft ultra-violet radiation is created and is particularly instrumental in establishing the pre-ionization of the laser gas. It is therefore reasonable to interpret the observed uniformity as the results of the photo-ionization of the seedant gas which is distributed evenly in the laser gas.

The amount of seedant which was introduced in the laser gas was controlled by bubbling a variable fraction of nitrogen through a vessel containing liquid triethylamine or tripropylamine. The partial pressure, P_s (in torr) of the seedant was accurately calculated by measuring the volume V (in cm^3) of the liquid which was vapourized in a time t (in min). It can be shown that $P_s = \frac{68V\rho}{t\,FM}$ where ρ is the density of the seedant in the liquid phase (gr/cm^3), M is its molecular weight and F is the total flow rate (ℓ/min) of the laser gas.

The beneficial effect of various organic vapours has also been experienced in the laser performance of Double-Rogowski modules as has been reported by REITS and OLBERTZ[139,140] and NAKATSUKA and KUBO[141]. Similarly, BYCHKOV et al[111] have reported an improvement in the output parameters and the discharge homogeneity of a Double-Discharge module.

2.5 CHARACTERISTICS OF THE DOUBLE-DISCHARGE MODULE AS A CO_2 LASER AMPLIFIER

The potential of the Double-Discharge module, as a CO_2 laser amplifier was investigated and the subsequent findings are presented in this section. The effects of the gas mixture composition and of the density of the electrical input energy upon the value of the small signal gain coefficient were examined. The saturation energy parameter for a 70 ns pulse was also determined.

2.5.1 *Small Signal Gain Measurements*

The small signal gain is an important parameter of the CO_2 laser amplifier for, apart from being a measure of the stored optical energy, its distribution over the various rotational-vibrational lines indirectly discloses information about the values of such quantities as: the rotational temperature: the ratio of the population of the two laser levels: and the absolute densities of these populations[142-146]. In addition, its rise and fall times can be implemented to assess the lifetimes of the lower and upper laser levels.

Figure 2.12 schematically depicts an experimental arrangement used to measure the small signal gain which does not rely upon the use of a CW CO_2 laser normally required for such measurements. The intensity of radiation entering the amplifier was controlled by varying the d.c. voltage applied on a GaAs electro-optical crystal inserted between two crossed polarizers. The first polarizer consisted of a single Ge plate placed at the Brewster angle while the second contained six similarly positioned plates.

With a 10 kV voltage applied to the crystal, the intensity of the radiation entering the amplifier was attenuated by thin polyethylene absorbers to the lowest level ($\sim$ 1 mJ) measurable by the energy meter E_2. The reading of the E_1, found to be 18 times greater, provided an accurate

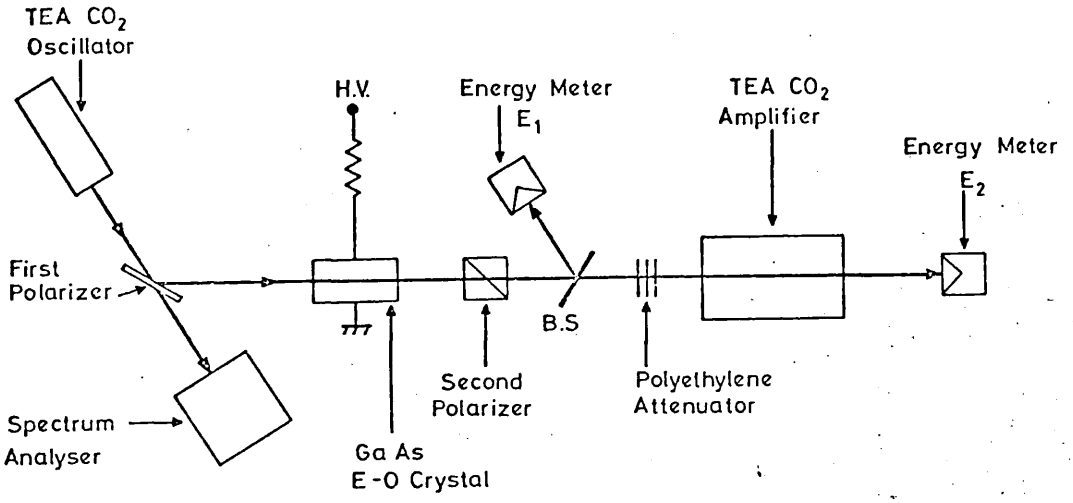

Fig.2.12
Experimental arrangement for measuring small signal gain

measure of the input energy when this was further reduced by decreasing the applied voltage. The input energy measured in this way was sufficiently low (~ 50 μJ) to preclude gain saturation. The small signal gain is thus given by:

$$\alpha_0 = \frac{1}{L_a} \ln\left(\frac{18 E_2}{E_1}\right) \qquad \ldots (2.3)$$

where L_a is the length of the amplifying medium and E_1 and E_2 are the energies measured by the two meters when both oscillator and amplifier were activated. A CO_2 spectrum analyser (Optical Engin. Model 16-A) was used to monitor the wavelength of the emitted pulse.

The time dependence of the small signal gain was examined by varying the delay time between the firing of the amplifier and the oscillator. The measured values of the small signal gain for the P(20) line at the 10.4 μm band were plotted against this delay time in Fig.2.13. As can be seen, the temporal gain profile obtained by this method was found to be in good agreement with the profile achieved using the technique illustrated in Fig.2.14. Adopting this technique[147], a commercial CW CO_2 laser (Apollo-XB) was used to probe the gain of the amplifier. Spectral examination of the output of this laser, using a CO_2 spectrum analyser revealed that the wavelength of the emitted radiation was changing erratically and almost all the

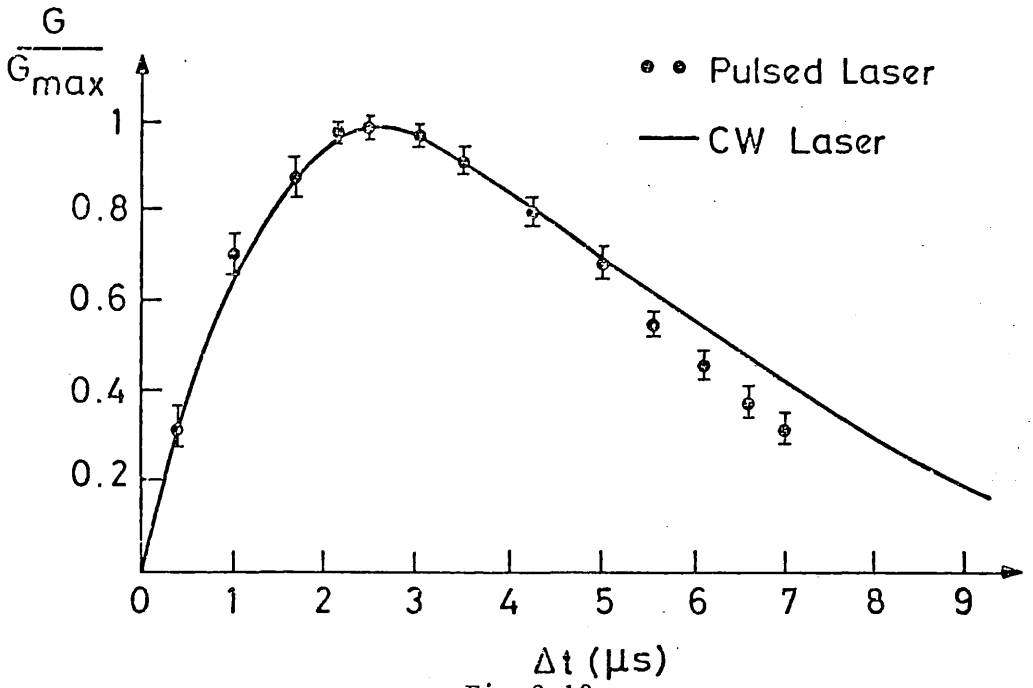

Fig.2.13
Time dependence of the small signal gain

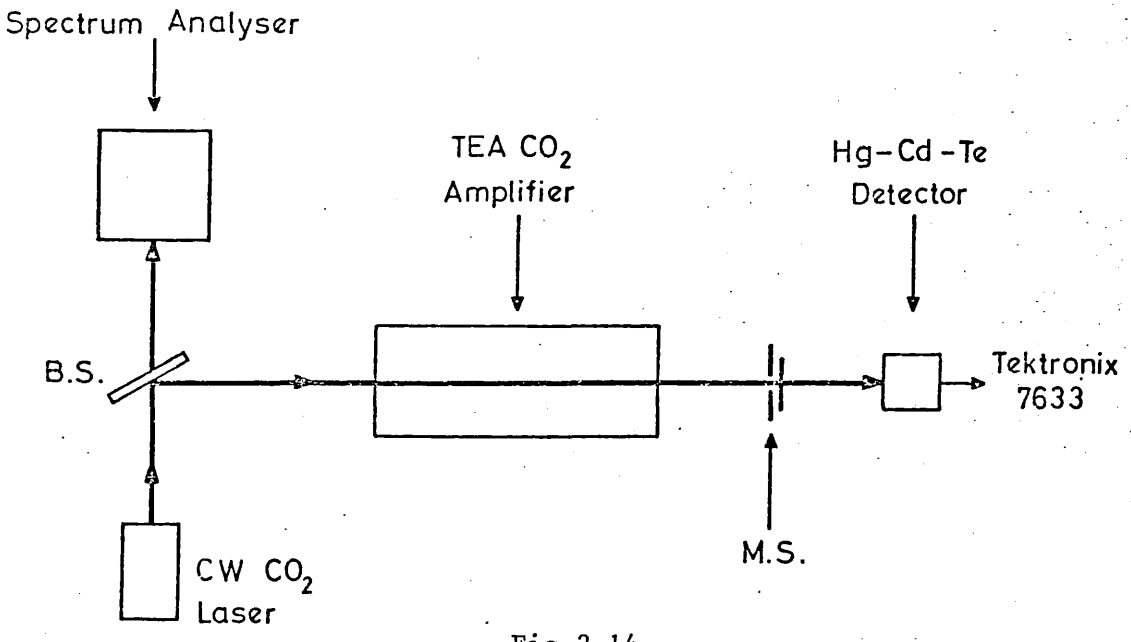

Fig.2.14
Experimental arrangement for small signal gain measurement, using a CW CO_2 laser

rotational-vibrational lines of the 9.4 μm and 10.4 μm bands could be emitted singly or in pairs. This was apparently due to cavity length variation resulting from temperature fluctuations in the laser tube. However, oscillation in any one specific line could be maintained for a period of a few minutes by adjusting the current in the CW laser and the thermostat of its cooling system. The power of the CW beam traversing the amplifier was 0.5 W and its diameter was 3 mm.

A remotely-operated mechanical shutter (M.S.) was arranged to remain open for a period of only 2 ms thus minimizing the detector heating. On opening, this shutter triggered the amplifier discharge circuit.

A typical gain pulse for the P (20) line of the 10.4 μm band, recorded by a liquid-N_2-cooled H_g : Cd : Te detector in conjunction with a Tektronix 7633 oscilloscope, is shown in Fig.2.4(c). The small signal gain, in this case, is simply given by:

$$\alpha_0 = \frac{1}{L_a} \ell n \left(\frac{I}{I_o} \right)$$

where I is the amplitude of the amplified signal and I_o is the d.c. signal level preceding the gain pulse. Although this last technique has the advantage of being direct and simple, the first described method was found to be a useful alternative in the early stages of this study when the CW CO_2 laser was not available. Moreover, it permitted — unlike the CW method — the investigation of the gain saturation.

2.5.2 *Upper and Lower Laser Level Life-Times*

The rise and fall times of the small signal gain pulse, as has been shown by CHEO[50] and REID et al[44,51] correspond to the effective life-times of the lower and upper vibrational laser levels respectively. The temporal profile of the gain coefficient can be described by the expression[44] :

$$\alpha(t) = \alpha_0 \left(e^{-t/\tau_1} - e^{-t/\tau_2} \right) \qquad \ldots (2.4)$$

where τ_1 and τ_2 are the life-times of the upper and lower laser levels.

Although the gain waveform shown in Fig.2.6(c) gives the time dependence of the gain per pass through the amplifier, $g(t) = e^{a(t)L_a}$ it can be readily converted to give the time-dependence of the gain coefficient itself, a(t). A very close fit was obtained between this experimentally-determined gain coefficient and that described by equation (2.4) when $\tau_1 = 8.2\,\mu s$ and $\tau_2 = 1.2\,\mu s$. These values are in good agreement with the expected life-times

$$\left(\tau_1 = \frac{1}{K_1 P} = 7.8\,\mu s, \text{ and } \tau_2 = \frac{1}{K_2 P} = 0.57\,\mu s\right)$$

discussed in Chapter I.

2.5.3 *The Effect of the Gas Composition and Electrical Energy on the Gain*

It was found that the small signal gain was linearly proportional to the electrical excitation energy as shown in Fig.2.15(a). The gas composition was kept constant ($CO_2 : N_2 : He$ $1 : \frac{1}{6} : 2$).

Figure 2.15(b) illustrates the variation of the small signal gain as a function of the ratio $\frac{P_{N_2}}{P_{N_2} + P_{CO_2}}$. It is evident that the same gas composition which maximized the output power of the Double-Rogowski module (Fig.2.11) also maximises the small signal gain of this laser amplifier. The electrical energy density in this case was fixed at 96 J/ℓ and the He concentration was 65%.

2.5.4 *Gain Saturation*

For reliable gain saturation measurements, the small signal gain must be maintained at a constant level. It can be assumed that this requirement is adequately fulfilled if both gas composition and electrical energy density are kept constant. When the polyethylene attenuators were removed, the intensity of the input pulse could be varied in the region 0-50 mJ/cm^2 by adjusting the voltage applied to the crystal from zero to 10 kV. The intensity of the amplified pulse E_o is plotted as a function of the intensity of the input pulse E_i in Fig.2.16.

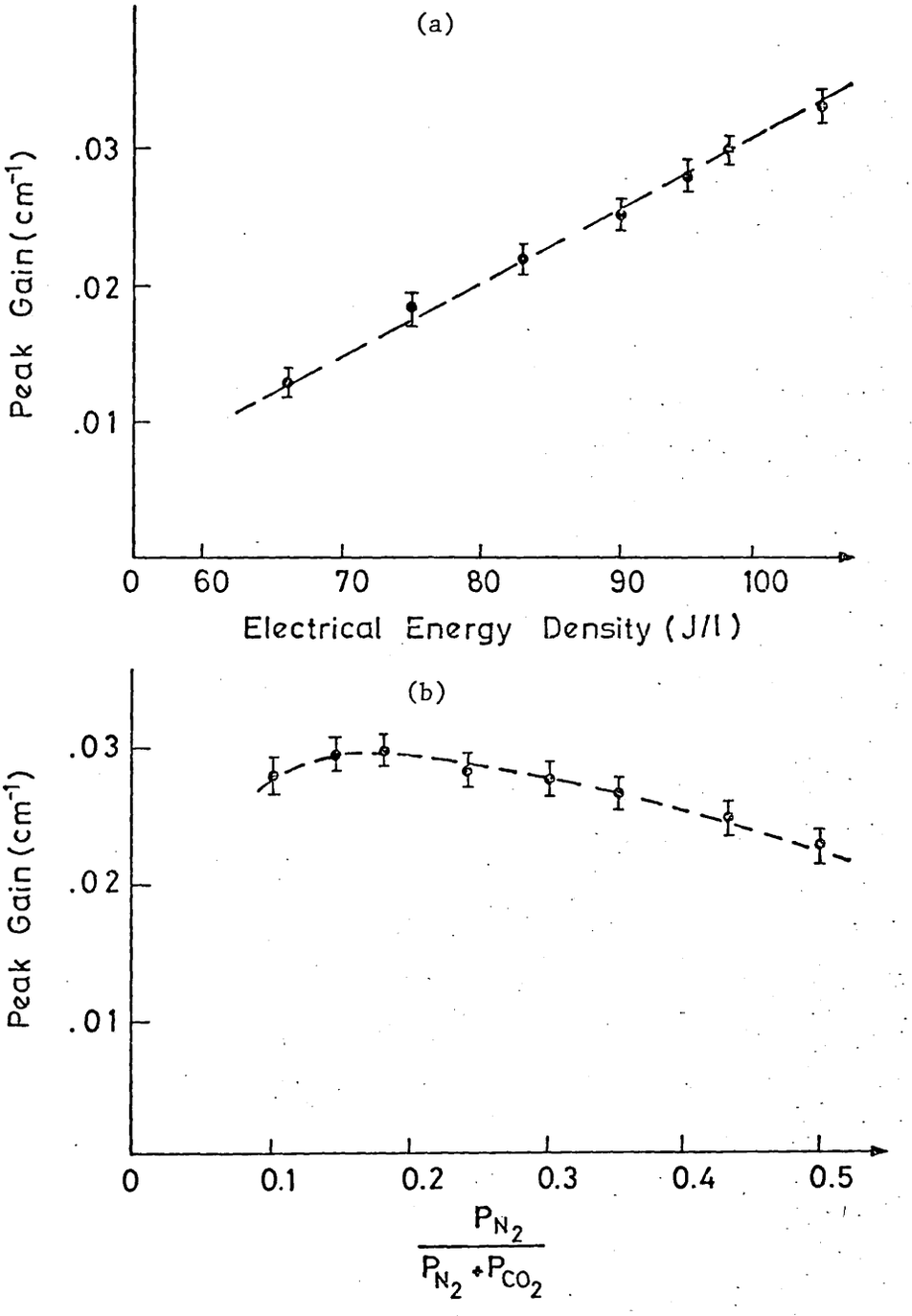

Fig.2.15
Small signal Gain Dependence on:
(a) Electrical Energy Density
(b) Gas Composition

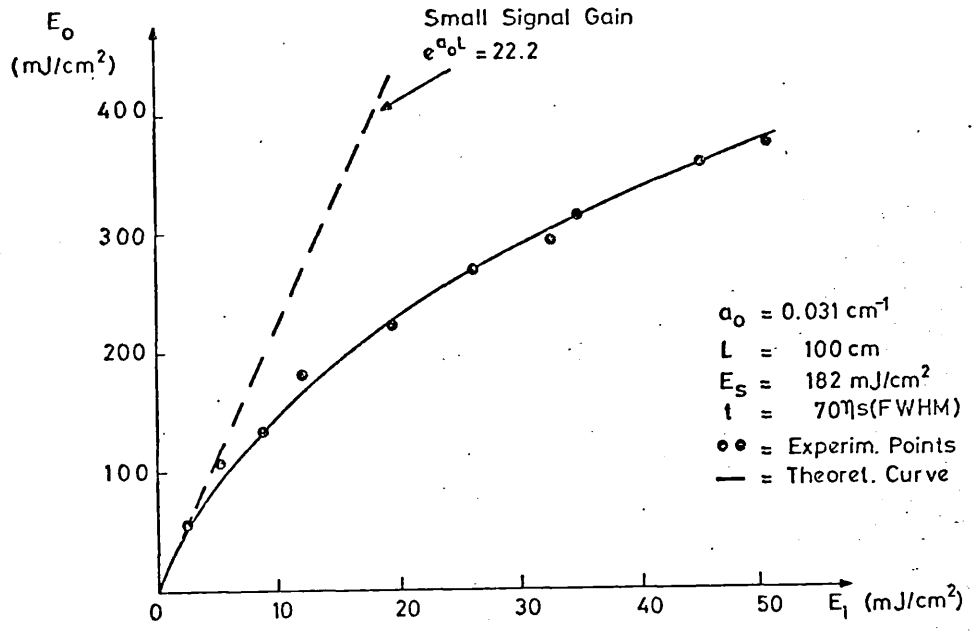

Fig.2.16
Comparison between the experimental and calculated energy extracted by a 70 ns pulse

The solid line represents a theoretical curve calculated from the two-level amplifier equation (equation (5.2)).

In the case of a 70 ns pulse, the CO_2 amplifier can in no way be classified as a two-level system (due to rotational and vibrational repopulation and relaxation of the upper and lower laser levels). However, very good agreement between theory and experiment can still be obtained provided that the appropriate value for the saturation energy density, E_s, is chosen, as is illustrated in Fig.2.16, and has been supported by other investigators[149-152]. This saturation energy parameter is — in the case of a CO_2 amplifier — a function of the pulse duration as well as of the laser gas pressure and composition.

The optimum fit to the experimental points is obtained when the saturation energy density takes the value $E_s = 182\,mJ/cm^2$. It is important to ascertain the E_s because it determines — together with the small signal gain — the potentialities of the laser amplifier; for example, the product: $E_s \alpha_0 = 6\ J/\ell$ gave the maximum optical energy which could be extracted per unit volume by a 70 ns CO_2 laser pulse from the amplifier hitherto investigated.

CHAPTER III

GENERATION OF NANOSECOND PULSES: ELECTRO-OPTICAL SHUTTER

3.1 INTRODUCTION

Nanosecond CO_2 laser pulses were generated using the output of the Double-Rogowski module, described in the previous chapter, in conjunction with an electro-optical shutter. This device comprises an electro-optical crystal, a system of crossed polarizers, a laser-triggered spark gap (LTSG) and a high voltage pulse generator. The time variation of the electric field applied on the crystal is imposed on the laser radiation passing through it, thus enabling the duration of the laser pulse transmitted through the electro-optical shutter to be controlled. The obvious requirements of :

(a) a high degree of synchronization between the laser and the electrical pulse, and

(b) subnanosecond rise time and jitter, are satisfied by the use of the LTSG.

In this chapter all the design considerations for an electro-optical shutter are analysed and the subsequent results presented. These results concern particularly:

(a) the performance of an electro-optical shutter using single crystals of high-resistivity GaAs, suitable for CO_2 laser radiation of 10 μm wavelength;

(b) the experimental assessment of four GaAs crystals, based upon their ability to discriminate against unwanted radiation (extinction ratio); and

(c) the operational characteristics of a pressurised LTSG.

Although this shutter was specially constructed to suit 10 μm radiation, the same design considerations can apply to any electro-optical shutter using crystals which belong (as does GaAs) to the $\bar{4}3m$ crystallographic point group of the cubic system.

3.2 LIGHT TRANSMISSION THROUGH AN ELECTRO-OPTICAL SHUTTER

An electro-optical shutter requires the optical components to be so arranged that no light can be transmitted through the shutter unless an electric field is present. In one such arrangement an electro-optical isotropic crystal is placed between two crossed polarizers (Fig.3.1). This crystal, under the influence of an electric field, becomes anisotropic and the transmission of the system is no longer zero but controlled by the applied electric field.

The transmission of radiation is then given by (see, for example, reference 153, p.696)

$$T = T_0 \sin^2 2\phi \sin^2 \frac{\delta}{2} \qquad \ldots (3.1)$$

where ϕ is the angle between the transmission axis of the first polarizer and one of the privileged directions (see Appendix A), and δ is the phase difference that has been developed between the two linearly polarized waves emerging from the electro-optical crystal. The factor T_0 includes the effects of any reflection, diffraction or absorption loss in the crystal and the polarizers. From equation (3.1) it can be seen that, for a given δ, the maximum transmittance of the electro-optical shutter occurs when $\phi = 45°$. The value of T increases as $\sin^2 \frac{\delta}{2}$, reaching its maximum value $T = T_0$ when $\delta = 180°$.

The performance of an electro-optical switch is often limited because the value of the electric field required for inducing $\delta = 180°$ exceeds that which could be applied to the crystal without the risk of dielectric breakdown. The value of δ, per unit length of the crystal, depends on the amplitude and direction of the electric field as well as on the direction of propagation. It will be shown later, that δ takes a maximum value (for a given field strength) when the field is applied along one particular $(h_1 k_1 \ell_1)$ axis of the crystal and, at the same time, light is propagated along another specific $(h_2 k_2 \ell_2)$ axis. It is therefore essential to ascertain which two

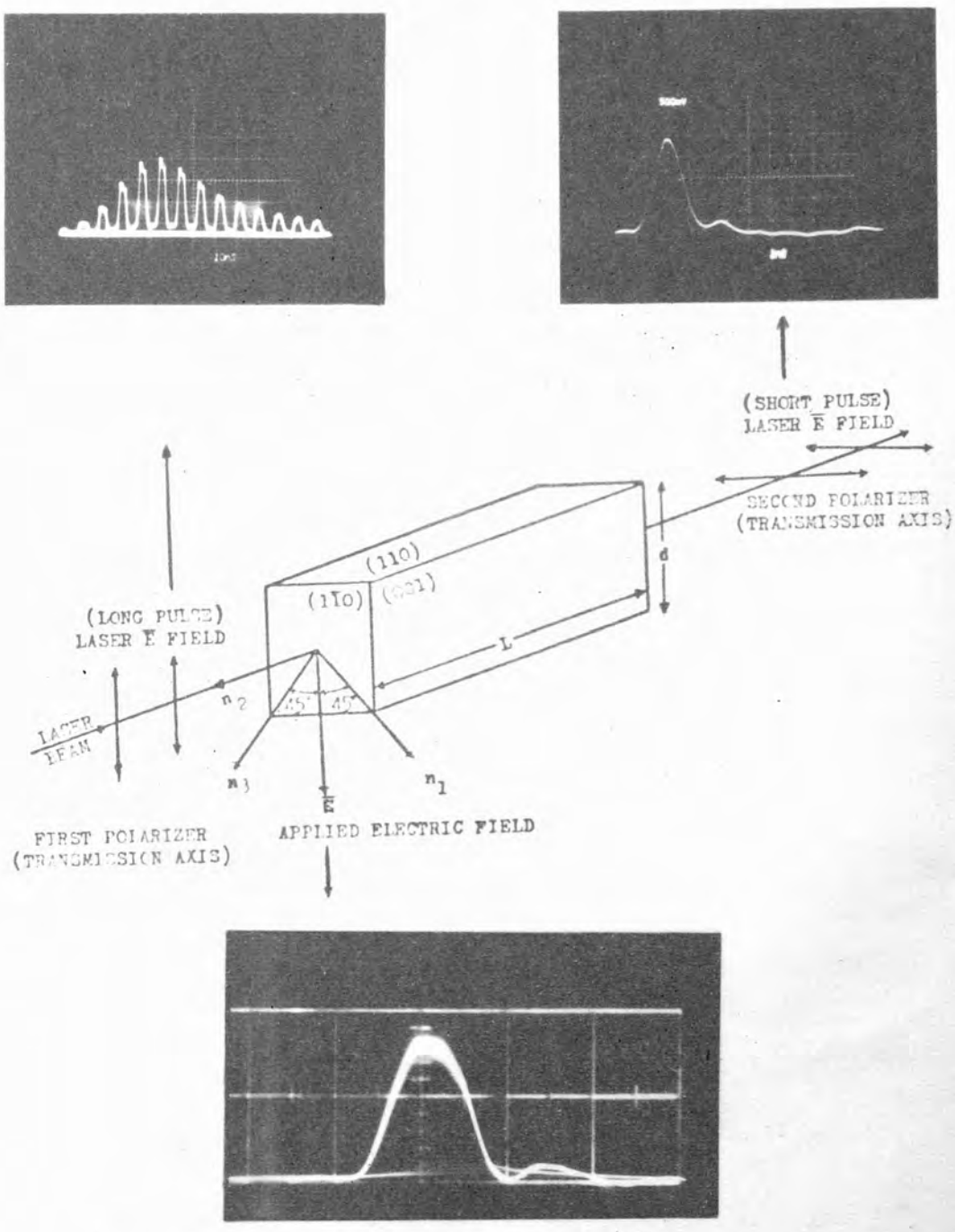

Fig.3.1

Optimum orientation of the GaAs crystal relative to: the polarization of the incident laser pulse (to left 10 ns/div); and the direction of the applied voltage pulse (bottom 2 ns/div). Top right oscillogram shows the generated ns laser pulse (1 ns/div)

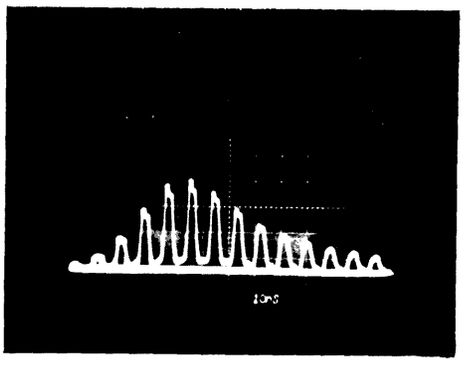

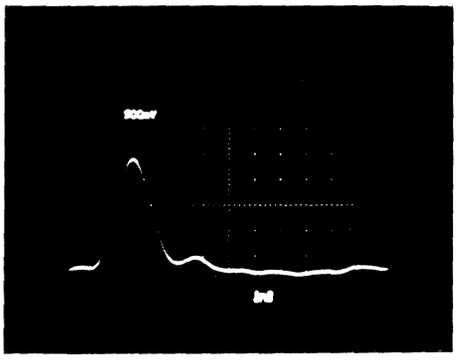

(SHORT PULSE)
LASER $\bar{E}$ FIELD

SECOND POLARIZER
(TRANSMISSION AXIS)

(LONG PULSE)
LASER $\bar{E}$ FIELD

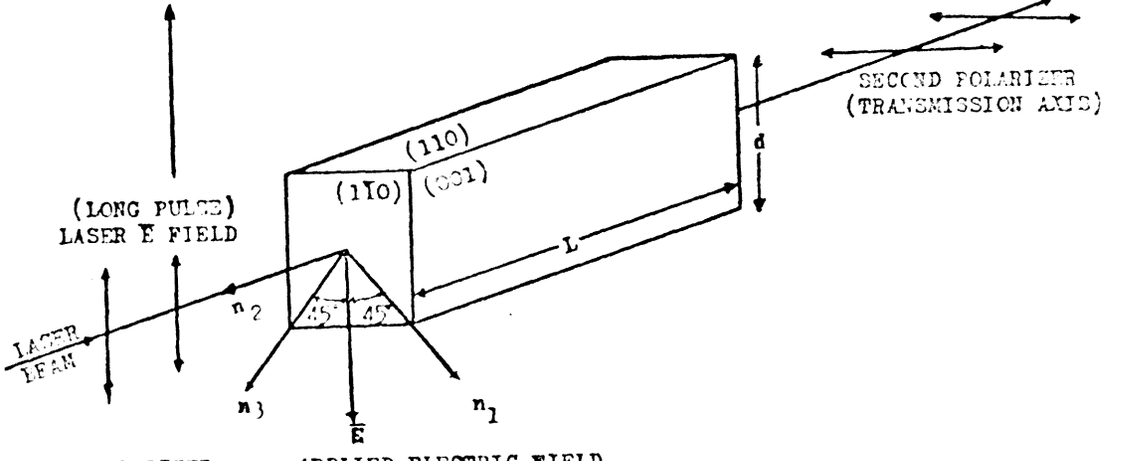

FIRST POLARIZER
(TRANSMISSION AXIS)

APPLIED ELECTRIC FIELD

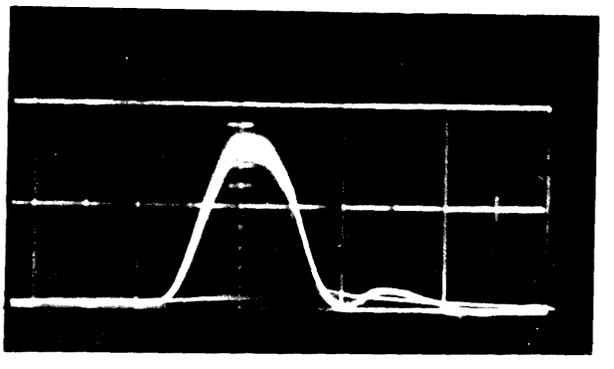

crystallographic axes fulfil this criterion so that an appropriately grown, cut and polished crystal can be used. It is also important to find the corresponding privileged directions so that the crystal can be so located between the two crossed polarizers that $\phi = 45°$.

3.3 INDEX ELLIPSOID

The propagation of light through an anisotropic medium can be illustrated using an ellipsoid. This can be applied to describe any crystal property given by a symmetrical second-rank tensor such as the dielectric tensor $[\varepsilon_{ij}]$. The symmetry of $[\varepsilon_{ij}]$, which is a consequence of Maxwell's equations[153, p.666], reduces the number of components of the tensor from nine to six (since $\varepsilon_{ij} = \varepsilon_{ji}$).

The most general form of the equation of the ellipsoid in Cartesian coordinates is:

$$\sum_{i,j=1}^{3} \frac{x_i x_j}{\varepsilon_{ij}} \equiv \frac{x_1^2}{\varepsilon_1} + \frac{x_2^2}{\varepsilon_2} + \frac{x_3^2}{\varepsilon_3} + 2\frac{x_1 x_2}{\varepsilon_{12}} + 2\frac{x_1 x_3}{\varepsilon_{13}} + 2\frac{x_2 x_3}{\varepsilon_{23}} = 1 \quad \ldots (3.2)$$

However, there is always a system of Cartesian coordinates — the system of principal dielectric axes — in which the above equation takes its simplest form:

$$\frac{x_1^2}{\varepsilon_1} + \frac{x_2^2}{\varepsilon_2} + \frac{x_3^2}{\varepsilon_3} = 1 . \quad \ldots (3.3)$$

The quantities ε_i $(i = 1,2,3)$ are the principal dielectric constants.

Replacing the dielectric constants with the corresponding refractive indices (for a non-magnetic medium $\eta_i = \sqrt{\varepsilon_i}$), equation (3.3) becomes:

$$\frac{x_1^2}{\eta_1^2} + \frac{x_2^2}{\eta_2^2} + \frac{x_3^2}{\eta_3^2} = 1 \quad \ldots (3.4)$$

η_i are the principal refractive indices and henceforth it will be assumed $\eta_1 \geq \eta_2 \geq \eta_3$. This equation represents the index ellipsoid or optical indicatrix. The three mutually perpendicular semi-axes of this ellipsoid are η_1, η_2, η_3. It should be noted that η_i is the refractive index for light linearly polarized — not propagated — along the corresponding semi-axis.

With the aid of the index ellipsoid, the orientation of the privileged directions, as well as the phase velocities of the two linearly polarized electro-magnetic waves permitted to propagate unchanged through the anisotropic medium, can be found. They are determined by the intersection of the index ellipsoid with the plane perpendicular to the direction of propagation passing through its centre. This intersection is, in general, an ellipse. The privileged directions coincide with the principle semi-axes η_a , η_b of this ellipse, and the two phase velocities are

$$U_1 = \frac{c}{\eta_a} \quad , \quad U_2 = \frac{c}{\eta_b} \; . \qquad \ldots (3.5)$$

The phase difference, per unit length of the anisotropic medium, is

$$\delta = 2\pi\nu\left(\frac{1}{U_1} - \frac{1}{U_2}\right) = \frac{2\pi}{\lambda}\,(\eta_a - \eta_b) \; , \qquad \ldots (3.6)$$

where ν, λ are the frequency and the free space wavelength of the radiation. For any arbitrary direction of propagation, $\eta_a - \eta_b \leq \eta_1 - \eta_3$ and therefore δ takes its maximum value when $\eta_a = \eta_1$, $\eta_b = \eta_2$. This condition is obviously only satisfied when light is propagated along the η_2 semi-axis of the index ellipsoid.

3.4 ELECTRO-OPTICAL EFFECT

The values of the six independent components ε_{ij} of the dielectric tensor of certain crystals, and consequently the shape of their index ellipsoid, can change under the influence of an applied electric field $\bar{E} = [E_1 , E_2 , E_3]$ through the electro-optical effect. When this is directly proportional to the applied field, it is known as the linear electro-optical or Pockels effect. This change is given by :

$$\frac{1}{\varepsilon_{ij}} - \left(\frac{1}{\varepsilon_{ij}}\right)_{E=0} = r_{ijk} E_k \qquad \left.\begin{matrix} i \\ j \\ k \end{matrix}\right\} = 1,2,3 \quad \ldots (3.7)$$

The 27 coefficients r_{ijk} are constants of the crystal and constitute the electro-optical tensor. Since $\varepsilon_{ij} = \varepsilon_{ji}$, it follows that $r_{ijk} = r_{jik}$; therefore the symmetry of the dielectric tensor reduces the number of components in the electro-optical tensor from 27 to 18. Furthermore, the presence

of certain symmetry elements in the crystal restricts some of the r_{ijk} components to zero values. This is the result of a general principle of invariance in crystal physics according to which: 'all expressions involving any physical constant of a crystal should be invariant when any symmetry operation of the crystal is applied'(154).

Using equation (3.7), equation (3.2) becomes:

$$\sum \frac{x_i x_j}{\varepsilon_{ij}} + \sum r_{ijk} E_k \; x_i x_j = 1 \; , \qquad \ldots (3.8)$$

which is the general form of the equation of the distorted ellipsoid. Equation (3.8) takes a simpler form if the original ellipsoid is referred to the system of its principal dielectric axes (after the substitution $\eta_i^2 = \varepsilon_i$ has been made):

$$\frac{x_1^2}{\eta_1^2} + \frac{x_2^2}{\eta_2^2} + \frac{x_3^2}{\eta_3^2} + \sum r_{ijk} E_k \; x_i x_j = 1 \qquad \ldots (3.9)$$

For crystals which belong to the $\bar{4}3m$ point group of the cubic system (with $n_1 = n_2 = n_3 = n_0$) the only non-zero electro-optical coefficients are:

$$\left.\begin{aligned} r_{231} &\equiv r_{321} \\ r_{132} &\equiv r_{312} \\ r_{123} &\equiv r_{213} \end{aligned}\right\} = r_{41} \; .$$

The equation of the resulting index ellipsoid (which in the absence of an electric field is a sphere) takes the form:

$$\frac{x_1^2 + x_2^2 + x_3^2}{\eta_0^2} + 2 r_{41}(E_1 x_2 x_3 + E_2 x_3 x_1 + E_3 x_1 x_2) = 1 \; . \qquad \ldots (3.10)$$

Taking the axes (x_1 , x_2 , x_3) of the original co-ordinate system, parallel with the three crystallographic axes $\langle 100 \rangle$, $\langle 010 \rangle$, $\langle 001 \rangle$ respectively, the orientation of a <u>new</u> coordinate system whose axes are parallel with the directions of the principal refractive indices of the distorted index ellipsoid can be found. Equation (3.10) in this new system takes the form:

$$\frac{x_1^2}{\eta_1^2} + \frac{x_2^2}{\eta_2^2} + \frac{x_3^2}{\eta_3^2} = 1 \qquad \ldots (3.11)$$

The values of η_1 , η_2 , η_3 are $\eta_i = \sqrt{1/k_i}$ where the k_i are the three roots of the cubic secular equation(155):

$$\begin{vmatrix} \left(\frac{1}{\eta_0^2}-k\right) & r_{41}E_3 & r_{41}E_2 \\ r_{41}E_3 & \left(\frac{1}{\eta_0^2}-k\right) & r_{41}E_1 \\ r_{41}E_2 & r_{41}E_1 & \left(\frac{1}{\eta_0^2}-k\right) \end{vmatrix} = 0 \qquad \ldots (3.12)$$

3.5 OPTIMUM CRYSTAL ORIENTATION

Using the secular equation, it can be shown that a given electric field induces maximum birefringence, $\Delta\eta = \eta_1 - \eta_3$, when it is applied perpendicularly to any of the (110) (011), (101) planes of the crystal. The components of the electric field $\bar{E}$ in this case are:

$$E_1 = E_2 = \frac{E}{\sqrt{2}}, \quad E_3 = 0 .$$

Substituting these values in equation (3.12) it is found that:

$$\eta_1 = k_1^{-\frac{1}{2}} = \left(\frac{1}{\eta_0^2} - r_{41}E\right)^{-\frac{1}{2}} \simeq \eta_0 + \tfrac{1}{2} r_{41} \eta_0^3 E$$

$$\eta_2 = k_2^{-\frac{1}{2}} = \eta_0 \qquad \ldots (3.13)$$

$$\eta_3 = k_3^{-\frac{1}{2}} = \left(\frac{1}{\eta_0^2} + r_{41}E\right)^{-\frac{1}{2}} \simeq \eta_0 - \tfrac{1}{2} r_{41} \eta_0^3 E .$$

Using the above relations, in a method described by NYE[155], the semi-axes η_1 and η_3 of the index ellipsoid are found to lie on the same plane $(1\bar{1}0)$ as the electric field, and to form angles $\pm 45^0$ with it (see Fig.3.1). The direction of η_2 along which the light should be propagated is consequently perpendicular to the direction of the electric field. This is the great advantage of the cubic over the uniaxial crystals (i.e. the widely-known KDP crystals where the light has to propagate along the directions of the applied field). Firstly, the design of the electro-optical shutter is greatly simplified (with no need for transparent or specially-shaped electrodes) and, secondly, the required field can be reduced by using crystals whose length L is large compared with the dimension along which the field is applied. It is apparent, that in any electro-optical shutter employing a cubic crystal

of the $\bar{4}3m$ point group (i.e. GaAs, CdTe, ZnSe, etc.) the best performance is achieved when the following conditions are satisfied:

(a) The crystal has its faces parallel with the $(1\bar{1}0)$, (110), (001) crystallographic planes.

(b) The field is applied perpendicularly to the $(1\bar{1}0)$ plane.

(c) The laser beam is propagated along the (110) axis with its direction of polarization parallel with (or normal to) the direction of the applied field.

The phase difference which is developed between the two components of the linearly polarized light is then given by:

$$\delta = \frac{2\pi L}{\lambda}(\eta_1 - \eta_3) = \frac{2\pi L}{\lambda d} r_{41} \eta_0^3 V \qquad \ldots (3.14)$$

where $V = Ed$ is the amplitude of the applied voltage. When

$$V_{\frac{1}{2}} = \frac{\lambda d}{2L r_{41} \eta_0^3} \qquad \ldots (3.15)$$

$\delta = 180°$ and the transmittance of the electro-optical shutter reaches its upper limit $T = T_0$. This value of $V_{\frac{1}{2}}$ is the half-wave retardation voltage.

Figure 3.2 shows the Pockels cell used throughout this investigation. The $10 \times 10 \times 50$ mm GaAs crystal is mounted in a way that satisfies the above conditions for optimum orientation. Indium foil inserted between the crystal and the two electrodes ensured that the crystal was firmly held without being stressed; otherwise, in the absence of an electric field, strain birefringence could be induced.

Using equations (3.15) and the values of $\lambda = 10.6\,\mu m$, $r_{41} = 1.4 \times 10^{-10}$ cm V^{-1} $\eta_0 = 3.3$, the half-wave retardation voltage of this Pockels cell is determined as:

$$V_{\frac{1}{2}} = 21.06\,kV\,.$$

3.6 EXTINCTION RATIO

Although in theory there should be no transmission of light through an electro-optical shutter in the absence of an electrical field, in practice there is always a small transmittance arising from optical imperfections

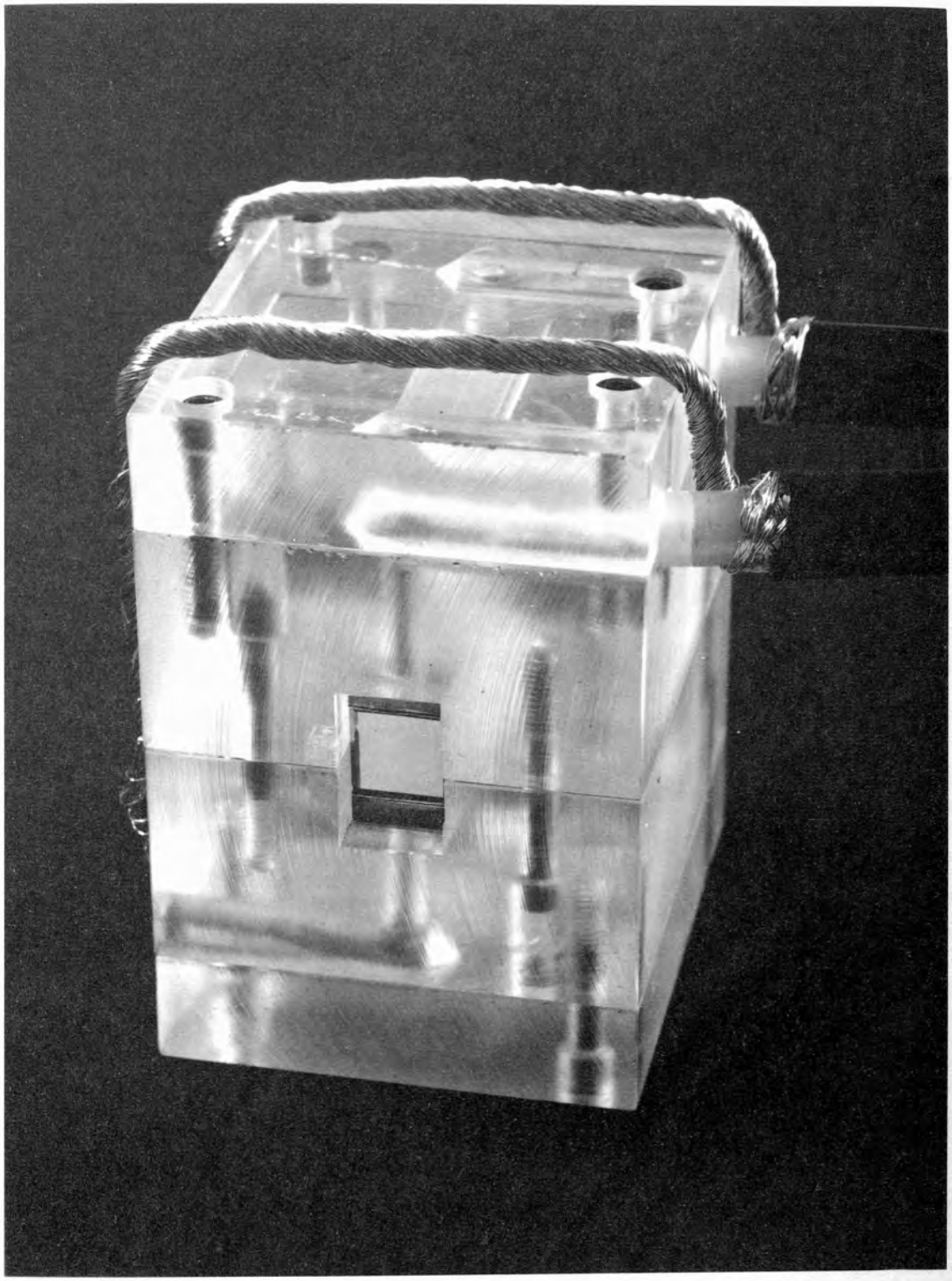

Fig.3.2
GaAs Pockels Cell

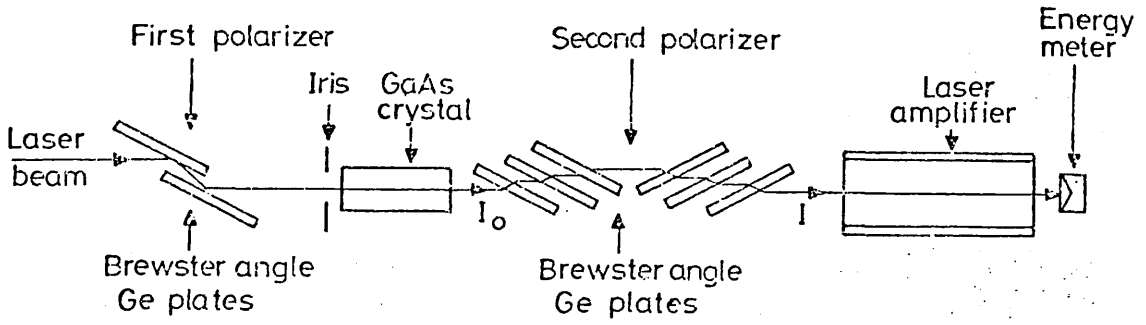

Fig.3.3
Experimental arrangement for measuring the residual birefringence of the GaAs crystal

in the system of polarizers and the electro-optical crystal (residual strain-induced birefringence).

The ratio of the intensity I_0 of the radiation incident on the second polarizer (see Fig.3.3) to the transmitted intensity I when no field is applied, is the extinction ratio of the electro-optical shutter ($E_s = I_0/I$). The value of E_s is an important parameter of the electro-optical shutter employed in a laser system since it determines the signal-to-noise (background) ratio of the transmitted pulse. The presence of this low intensity background creates a serious problem for the amplification of nanosecond pulses because it experiences a high initial gain, with the result that the signal-to-noise ratio continuously decreases as the pulse travels through the amplifying medium. Furthermore, in the case of a chain of amplifiers, that part of the background which is ahead of the short pulse will significantly reduce the energy that the pulse would otherwise extract.

Two factors determine the value of E_s : (a) the extinction ratio, E_p, of the crossed polarizer system itself, (defined as the ratio of the intensity I_0' of the radiation incident on the second polarizer to the transmitted intensity I' with the crystal removed from the system), and (b) the residual strain-induced birefringence in the crystal which reduces the degree of polarization of the laser pulse, thereby increasing the leakage of the unwanted radiation (background). The quantity:

$$E_c = \left(\frac{1}{E_s} - \frac{1}{E_p}\right)^{-1} \qquad \ldots (3.16)$$

represents the extinction ratio of the crystal and gives the upper limit of the extinction ratio of the system as a whole.

Using the Fresnel formulae, the theoretical value of E_p, for the system of polarizers shown in Fig.3.3 is:

$$E_p = \left(\frac{\eta^4 + 1}{2\eta^2}\right)^m \qquad \ldots (3.17)$$

where m is the number of plates which comprise the second polarizer. An experimental arrangement for measuring the values of E_p and E_s is also shown in the same figure.

When the second polarizer and the GaAs crystal were removed, the intensity I'_0 was measured. After the polarizer had been replaced, the very low intensity, I', of the transmitted radiation was amplified by the laser amplifier to bring I' to a measurable level. Taking into account the known gain of the amplifier, the extinction ratio in the case of three, four and five Ge plates, comprising the second polarizer, was found to be:

$$E_{p3} = 560 \ , \ E_{p4} = 4{,}600 \quad \text{and} \quad E_{p5} \geq 10^4 .$$

These values closely agree with the theoretical values deduced from equation (3.17), indicating a very high degree of polarization of the radiation reflected from the first polarizer, and also allowing a value of $E_{p6} > 10^5$ to be estimated when six plates are used.

Replacing the crystal, the extinction ratio E_s of the electro-optical shutter as a whole was similarly measured and, using equation (3.16), the value of E_c was deduced.

Four GaAs crystals were tested and the values of their E_c, with the full cross-section of the crystals exposed to the radiation, were found to be 100, 400, 600, and 3,400 respectively. When the exposed area of the

crystal was reduced by placing an iris symmetrically in front of it, the values of E_c were found to increase. This clearly shows that the quality of the crystal is poorer near the edges and according to FIGUEIRA[156] this is due to strains introduced during the cutting and polishing processes. The same study also noted this large sample-to-sample variation in the quality of the GaAs crystals.

3.7 FORMATION OF WEDGE FRINGES BY OPTICAL COMPONENTS. OPTICAL DAMAGE

The use of optical components made of material with a high refractive index - like Ge or GaAs - as beam splitters, windows, polarizers and electro-optical modulators of the laser beam, often results in the formation of undesirable sharp fringes[157]. Usually these fringes are of equal thickness (straight line wedge fringes) which occur when the two surfaces of the component are inclined. Generally in such components the locus of the points of equal thickness, which represents the edge of the wedge, forms an angle with the geometrical edge of the component, i.e. a rectangular plate. As a result of this, the fringes which are produced on transmission or reflection appear to rotate when the angle of incidence is changed, i.e. the angle between the plane of incidence and the straight line fringes appears to change (Fig.3.4(a)).

In the course of operating the electro-optical shutter under discussion, surface damage occurred to the GaAs crystal. The damage pattern resembled the fringe pattern of the beam reflected by the Ge polarizing plate (Fig.3.4(a), far right). The absence of any damage on the Ge plate is clearly attributable to its higher damage threshold. A feature of interest is that although the incident beam was parallel, only the exit surface of the crystal was damaged, whilst the entrance surface suffered no damage. It has been proposed that this asymmetry between entrance and exit damage thresholds, can be explained by considering FRESNEL reflections

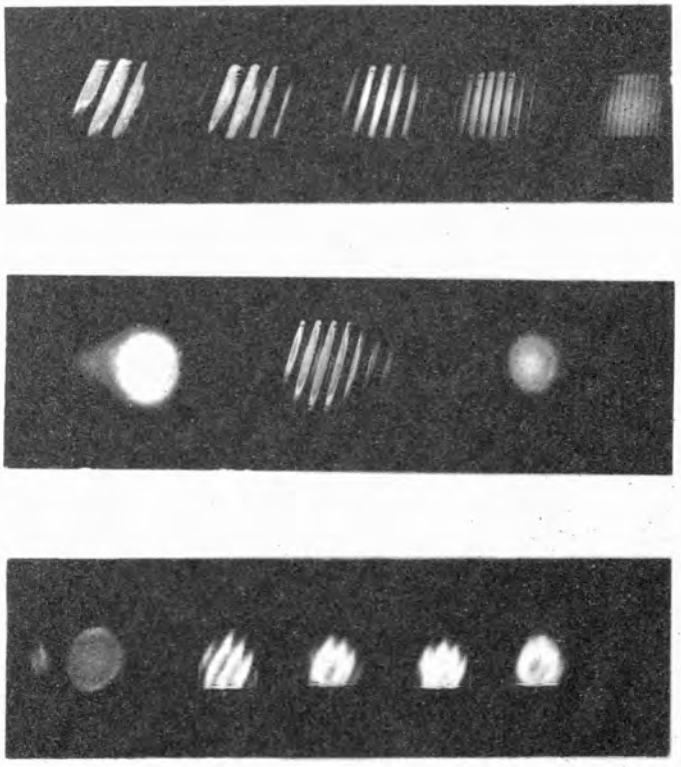

Fig.3.4

Wedge fringes on CO_2 laser components

(a) Rotation of fringes with varying angle of incidence

(b) Effect of back surface finish of Ge plate on fringe visibility: from left to right, incident beam, reflected fringes (both faces polished), and smooth reflected beam with matt back surface;

(c) Effect of applied voltage on fringes produced in GaAs electro-optic crystal-voltage increasing left to right from zero to quarter wave value. Incident beam on far left.

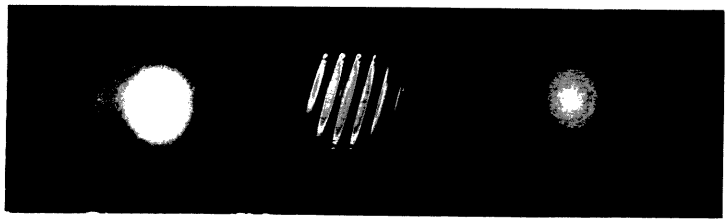

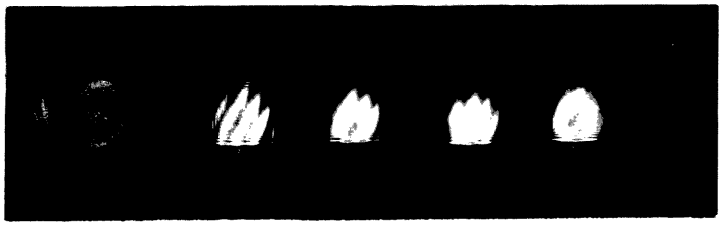

CR74/29

2.4

at the surfaces[158,159]. In the case of GaAs, which has refraction index $\eta = 3.3$, the light intensity inside the crystal at the exit surface is $4\eta^2/(\eta+1)^2 = 2.35$ times greater than the intensity inside the crystal at the entrance surface.

As can be seen from Fig.3.4(c), the wedge fringes formed by the GaAs crystal can be excluded by applying a bias d.c. voltage equal to the quarter wave value. Although this is an impractical solution in the present case since it will induce continuous birefringence, the disappearance of the fringes can be used to measure the quarter wave voltage and the electro-optical coefficient r_{41} of the GaAs. Antireflection coatings on both surfaces of the crystal would seem to be the obvious solution to avoid the fringes although new problems might arise, such as current flow through the coating or an overall lower damage threshold, depending on the coating material. However, the fringes produced by the polarizing Ge plate can be easily excluded by grinding its back surface with a wet emery cloth (Fig. 3.4(b)).

The angle of inclination ϕ of the two faces of the GaAs crystal can be calculated by measuring the fringe spacing d. For normal incidence

$$\phi = \frac{\lambda}{2\eta d} . \qquad \ldots (3.18)$$

The angle $\phi = 8 \times 10^{-4}$ rad, thus ascertained, agreed within 4% with the values deduced from the displacement of the reflected and transmitted beams caused by refraction in the wedge. This is a useful method of measuring small wedge angles on infrared components over relatively long path differences - 50 mm in the present case.

An interesting fine structure in the wedge fringes, formed by the Ge plate at angles of incidence greater than 45°, can be seen in Fig.3.5. The high reflectivity of the Ge plate at such angles of incidence accounts for the appearance of the fine structure. A discussion of these secondary maxima

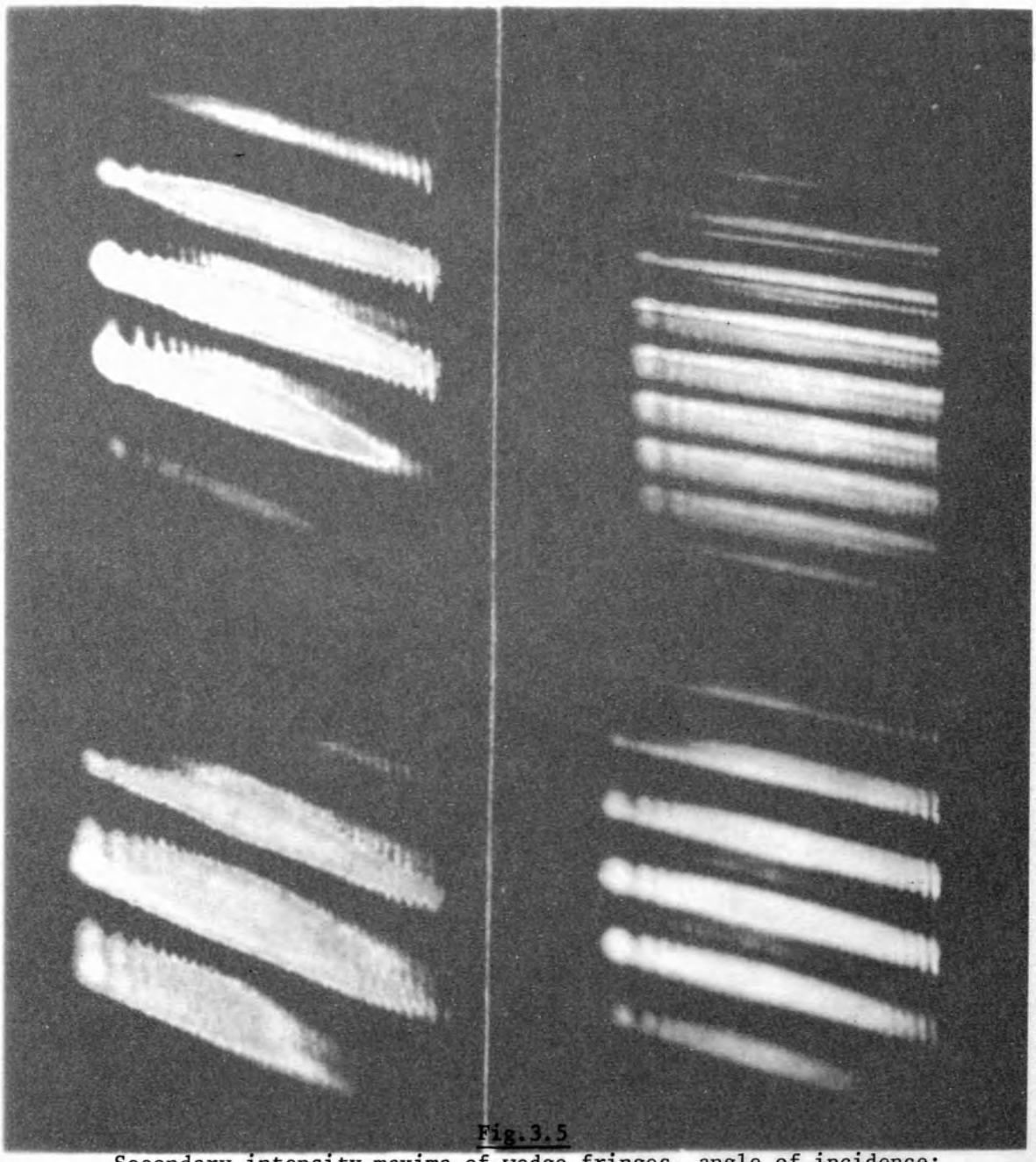

Fig.3.5

Secondary intensity maxima of wedge fringes, angle of incidence:
top left - 30° bottom left - 65°
top right - 15° bottom right - 50°

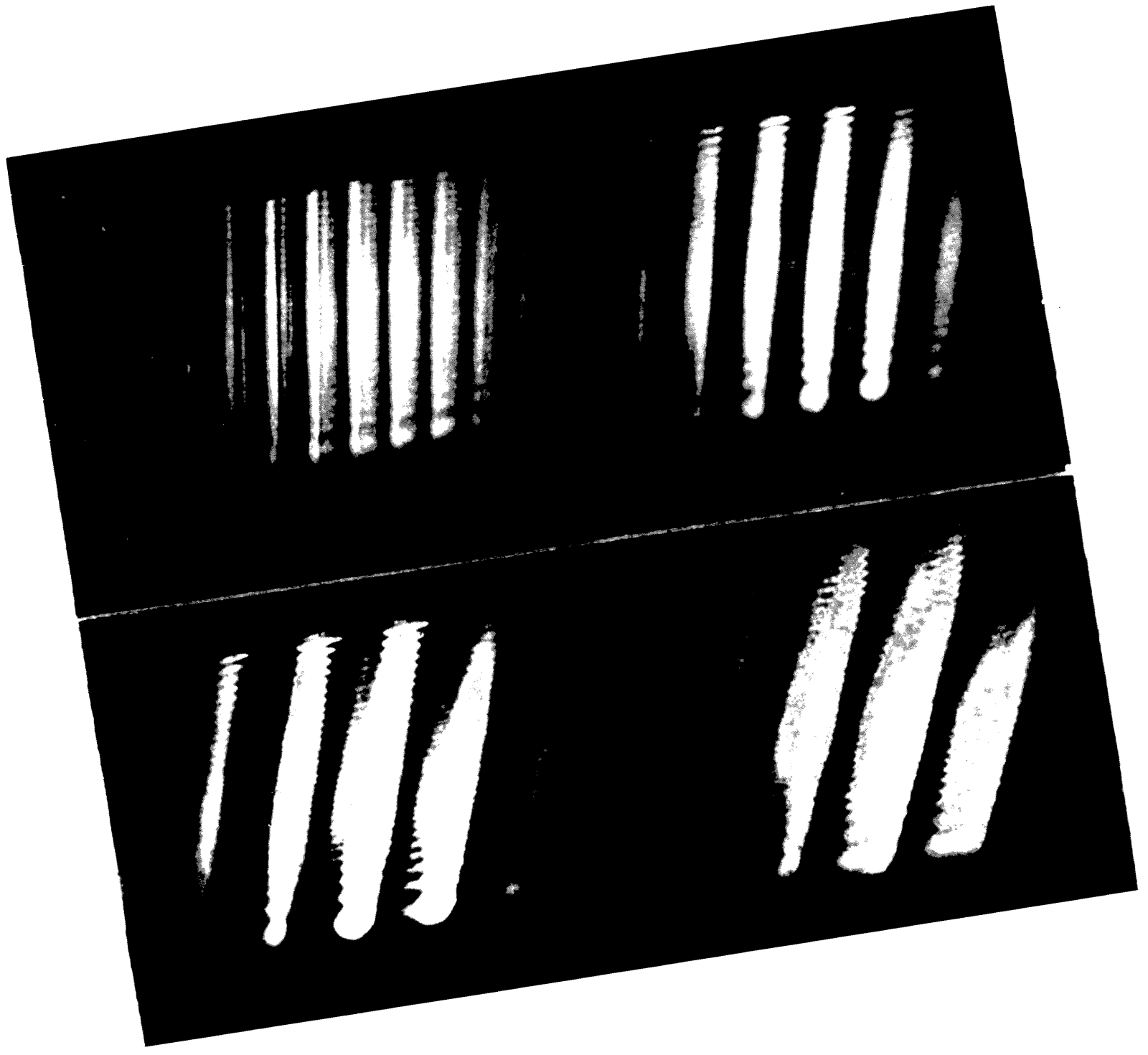

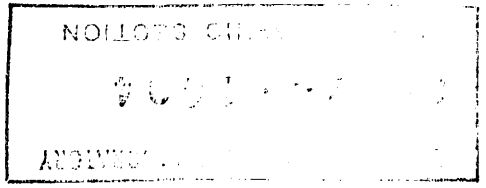

which have been theoretically predicted[160] can be found in reference (153, pp 351-4).

3.8 LASER-TRIGGERED SPARK-GAP

The advantage of the laser-triggered spark-gap over the conventional electrically-triggered switch were widely recognised soon after the first experiments initiating a spark discharge by focussing a laser beam into a d.c. charged spark gap, were reported[161]. These advantages can be itemised as:

(a) the absence of electrical coupling between the triggering device (i.e. the laser) and the high voltage assembly;

(b) the very short delay time (a few nanoseconds) and its sub-nanosecond variation (jitter) from shot-to-shot;

(c) the capability of simultaneously triggering several L T S G's ; and

(d) the very simple, robust and compact structure of the L T S G.

The L T S G is ideal for the generation of short laser pulses. In such an application, the laser pulse itself provides the triggering of the spark gap via a beam-splitter, thus achieving the necessary high degree of synchronisation without the need for a separate triggering device.

Gas-filled spark gaps appear to be preferable to liquid or solid dielectric-filled gaps and have been much more thoroughly investigated[168,175].

The main disadvantage of the liquid dielectric-filled spark gap is that it has a delay time of several microseconds, compared with the nanosecond response of the gas-filled pressurized gap.

Gaps insulated with solid dielectric have the drawback that the dielectric must be replaced after each gap closure since it lacks self-healing properties.

For the gas-filled spark gap, a pressurized gap is preferable to a low or atmospheric pressure spark gap for two reasons:

(a) the time taken for the development of the conduction path is reduced by increasing the pressure for a given value of V/V_{sb} (where V is the charging voltage and V_{sb} the self breakdown voltage of the gap);

(b) by increasing the gap pressure, the gap spacing required to hold off a certain voltage decreases (Paschen's Law) resulting in a faster rise-time of the electrical pulse generated by the gap closure (as will be shown later).

The coaxial structure of the L T S G used (see Fig.3.6) is shown in cross-section in Fig.3.7. The laser beam is directed on the cathode disc via a 2 mm central hole in the anode, using a plane-convex Ge lens as combined window and focusing element. The lens was so chosen that its focal point would lie ~2 mm behind the target electrode. This arrangement, according to BETTIS et al[162], results in the minimum delay time and jitter. The gap spacing is adjusted by means of a 6.67 turns per centimetre thread on the main body of the L T S G, and is effected by rotating the main ring bearing the cathode assembly. Nitrogen, at pressures of up to 7000 torr was used as the insulating gas.

3.9 PULSE GENERATION

A pressurised spark-gap similar to that reported by ALCOCK et al[163] was employed as the switch in a transmission-line pulse generator (Fig.3.8) of a type first described by FLETCHER[164], who used it, as here, to produce multi-kilovolt pulses with a sub-nanosecond risetime.

The distributed capacitance of the high frequency coaxial cable L_1 is charged from a high voltage d.c. power supply through a resistor $R_1 = 10^7\Omega$. The other end of the cable is connected, at point A, to one of the electrodes of a pressurised L T S G. The electrode spacing and gap pressure are such that the self-breakdown voltage V_{sb} of the gap is higher than the potential $V_A = V_o$ to which the cable is charged. The potential on the second electrode of the gap is $V_B = 0$. When the gap is triggered by the laser beam at the time $t_1 = 0$ the potentials at the points A and B are equalised: $V'_A = V'_B$.

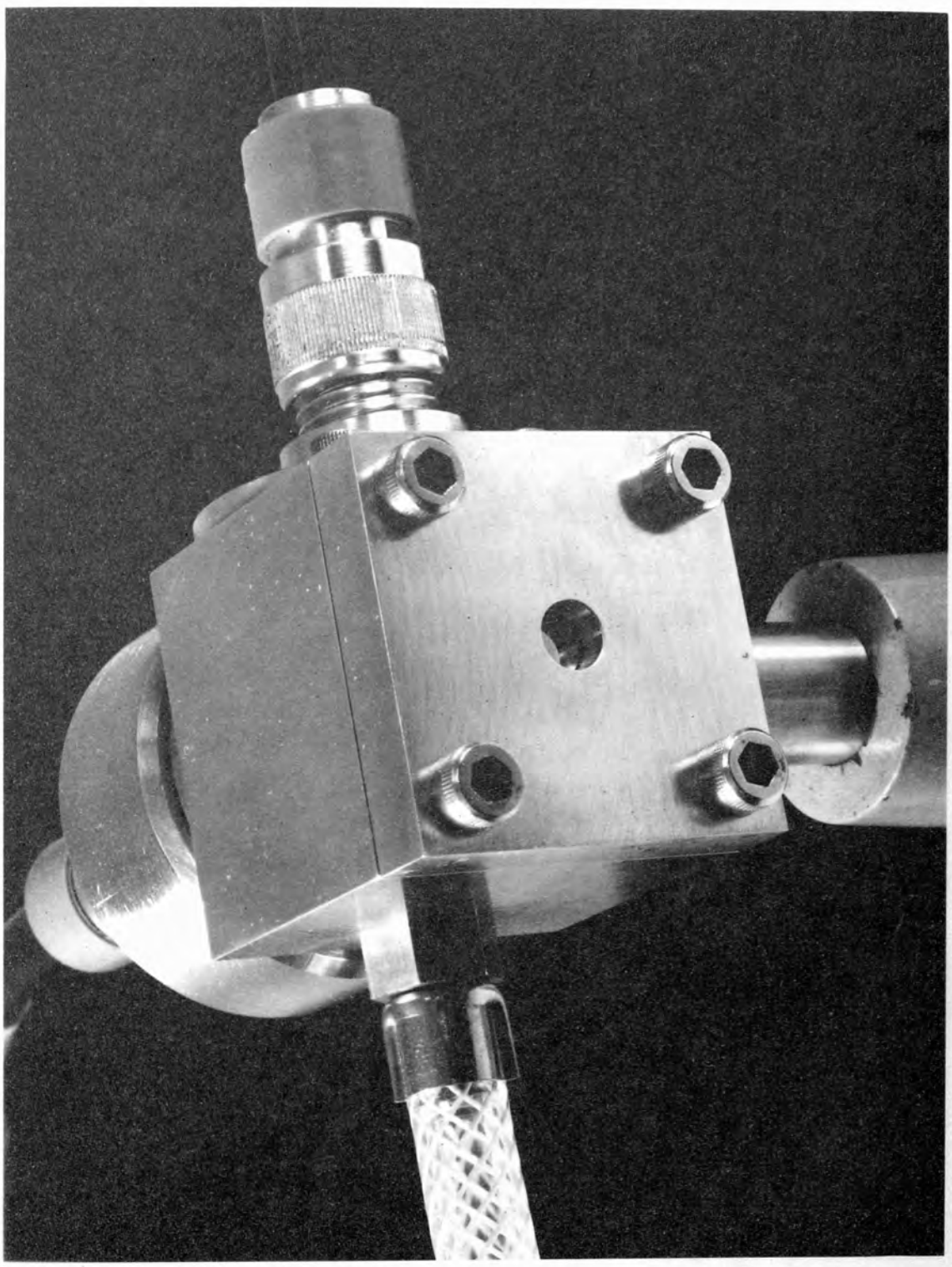

Fig.3.6
High-pressure Laser-triggered Spark Gap

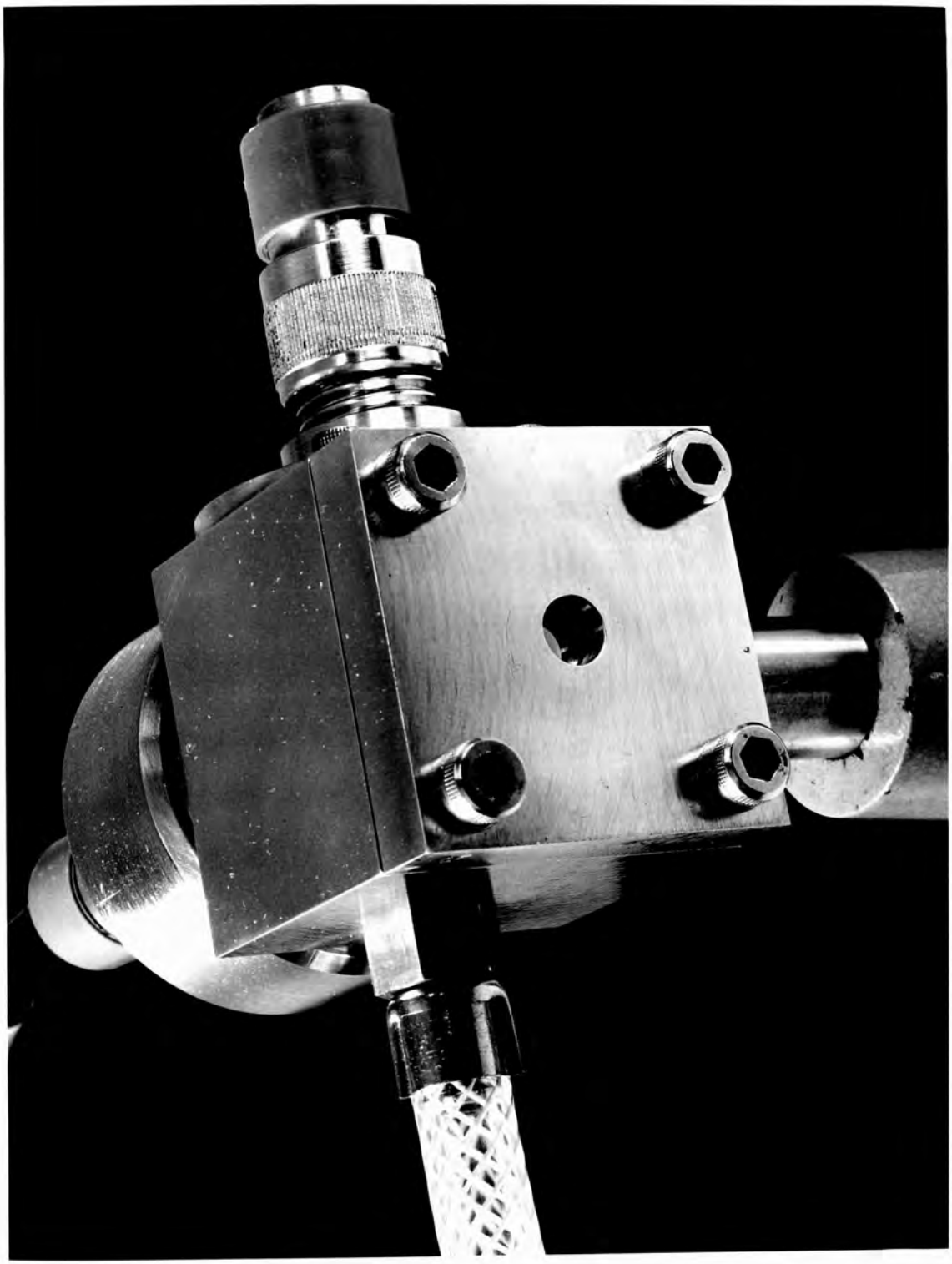

76/157

3.6

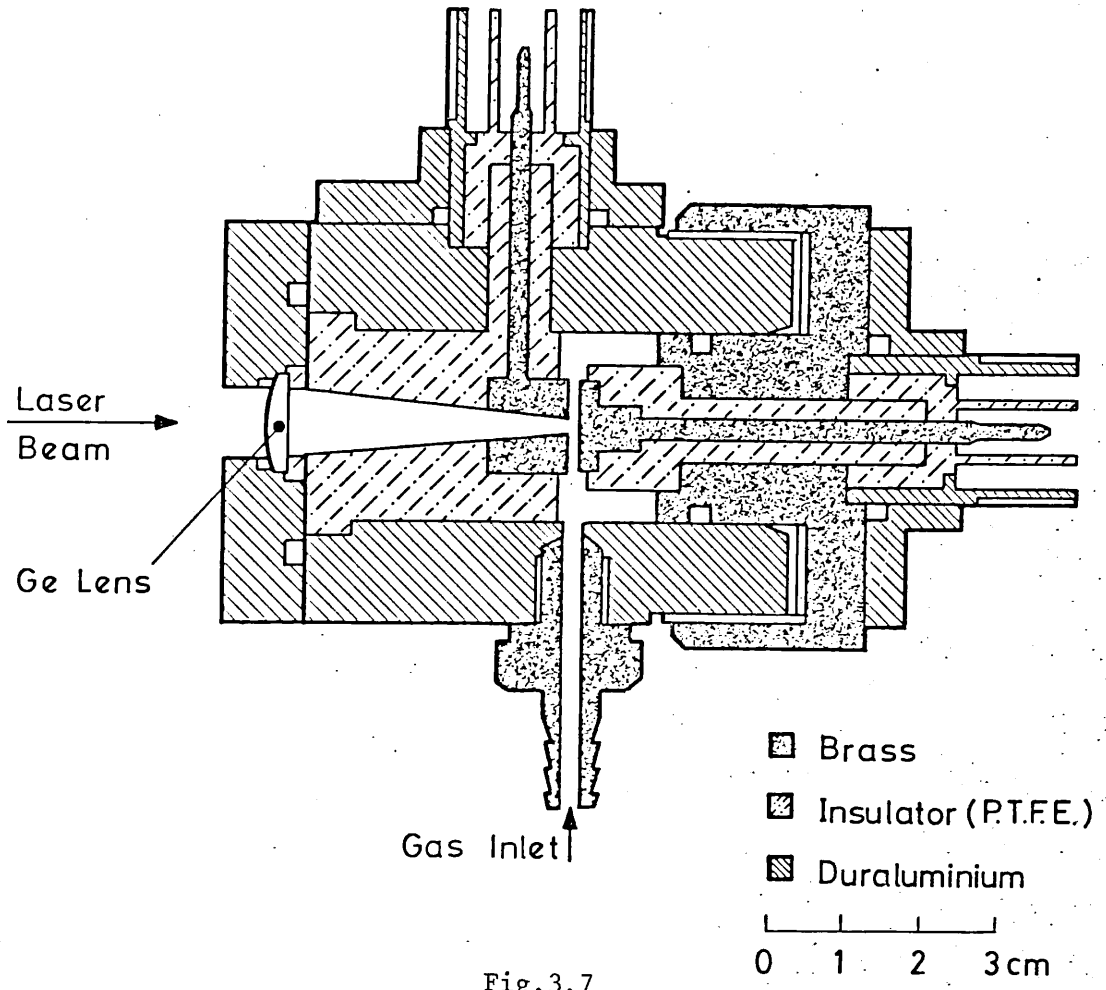

Fig.3.7
Cross-section of the L T S G

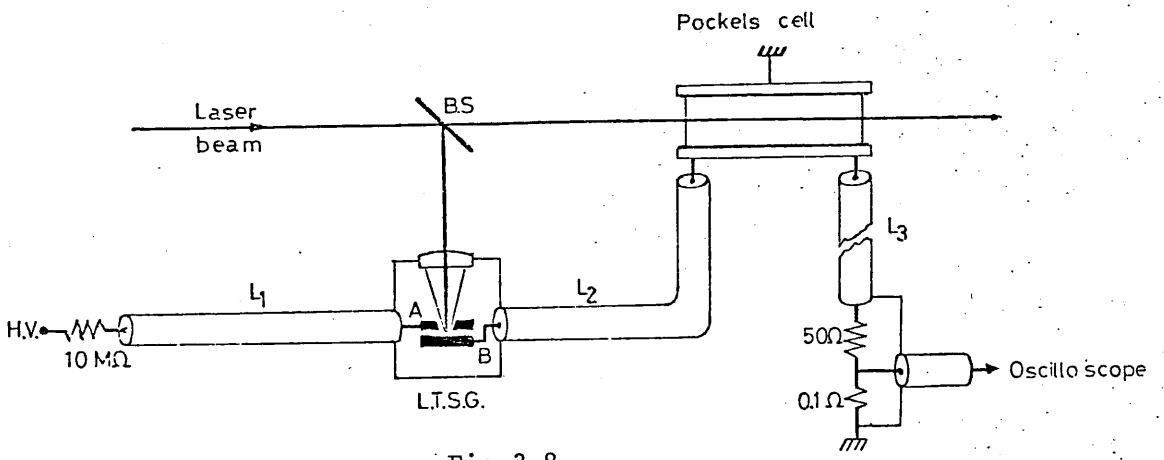

Fig.3.8
Multi-kilovolt transmission-line type
nanosecond pulse generator

Since the potential V_B at the point B was originally zero, the gap closure is equivalent to a short circuit appearing at one end of a charged line[165] and therefore $V'_A = V_A/2 = V_0/2$. Consequently, two similar ramp functions of opposite sign are generated at the switching point. These propagate out in opposite directions along the lines L_1 and L_2 with amplitudes

$$V_1 = \frac{V_0}{2} - V_0 = -\frac{V_0}{2} \quad \text{and} \quad V_2 = \frac{V_0}{2} - V_0 = \frac{V_0}{2}.$$

Both waves travel with the group velocity U of the line which is:

$$U = c/\sqrt{\varepsilon}$$

where c is the velocity of electromagnetic waves in free space, and ε is the relative dielectric constant of the insulating medium between the two conductors of the line. The dielectric in the cables used here was polyethylene, for which $\varepsilon = 2.3$ and therefore $U = 0.66c \simeq 1.98 \times 10^8$ m/s.

The positive amplitude of the wave on the line L_2 imposes a step voltage $V_0/2$ as it travels along it, whereas the negative wave discharges the voltage on the line L_2 to half of its original value as it travels towards the charging resistor R_1 where it arrives at time $t_2 = L_1/U$. Because of the impedance mis-match, it is reflected at this point, and travels back along L_1. The reflection coefficient is given by:

$$\rho = \frac{R_1 - Z_0}{R_1 + Z_0} \qquad \ldots (3.19)$$

where $Z_0 = 50\,\Omega$ is the characteristic impedance of the transmission line. With $R_1 = 10^7\,\Omega \gg Z_0$, the reflection coefficient $\rho = 1$ and the reflected wave remain negative with the same amplitude $(-V_0/2)$. Thus the reflected wave completes the discharge of the line L_1 as it returns to the LTSG, where it arrives at the time $t_3 = 2L_1/U$ and cancels the positive potential $V_0/2$ at B.

Since the positive wave has already been travelling for a similar time $2L_1/U$ before being cancelled by the negative wave, the net result is clearly

the generation of a rectangular pulse of height $V_0/2$ and width $t = 2L_1/U$ on the line L_2, leading to the Pockels cell. A rigorous mathematical treatment of this type of pulse generator can be found in reference (166).

This electrical pulse, having propagated along the line L_2, over the electro-optical crystal and through L_3, arrives at the terminating resistor R_2. With the values of R_2 and R_3 chosen such that $R_2 + R_3 = Z_0$, the pulse will be absorbed because reflectivity $\rho = 0$ for an impedance match (equation (3.19)). Thus there can be no reflection of the pulse to activate the electro-optical crystal further.

The two resistors R_2 and R_3 ($R_3 \ll R_2$) form a voltage divider to attenuate the multi-kilovolt pulse to an amplitude suitable for oscilloscope display. By varying the length of the line L_1 from 0.15 to 10 metres, electrical pulses of duration $\sim$1.5 to 100 nanoseconds are readily achieved. A Tektronix 519 Oscilloscope with a deflection sensitivity of 9.8 V/div and a rise time of 0.29 ns was used to display these pulses (Fig.3.9). Because the duration of the voltage pulse depends solely on the length and the dielectric material of the transmission line L_1, this pulse generator has a remarkable stability usually lacking in generators using active elements.

3.10 MECHANISM OF THE LASER-INDUCED GAP BREAKDOWN

The breakdown mechanism proposed by GUENTHER et al[167] seems more likely to apply to the present case than those suggested by other investigators[168,169] and will be described first. In this mechanism, it is assumed that the electrons generated by focusing the laser on to the target electrode, drift across the gap under the influence of the applied electric field and gain sufficient energy to ionize the gas molecules or atoms by collision. The growth of ionization conforms to the Townsend classical avalanche process according to which the number of electrons N produced after a distance x is :

$$N = N_0 \exp(\alpha x). \qquad \ldots (3.20)$$

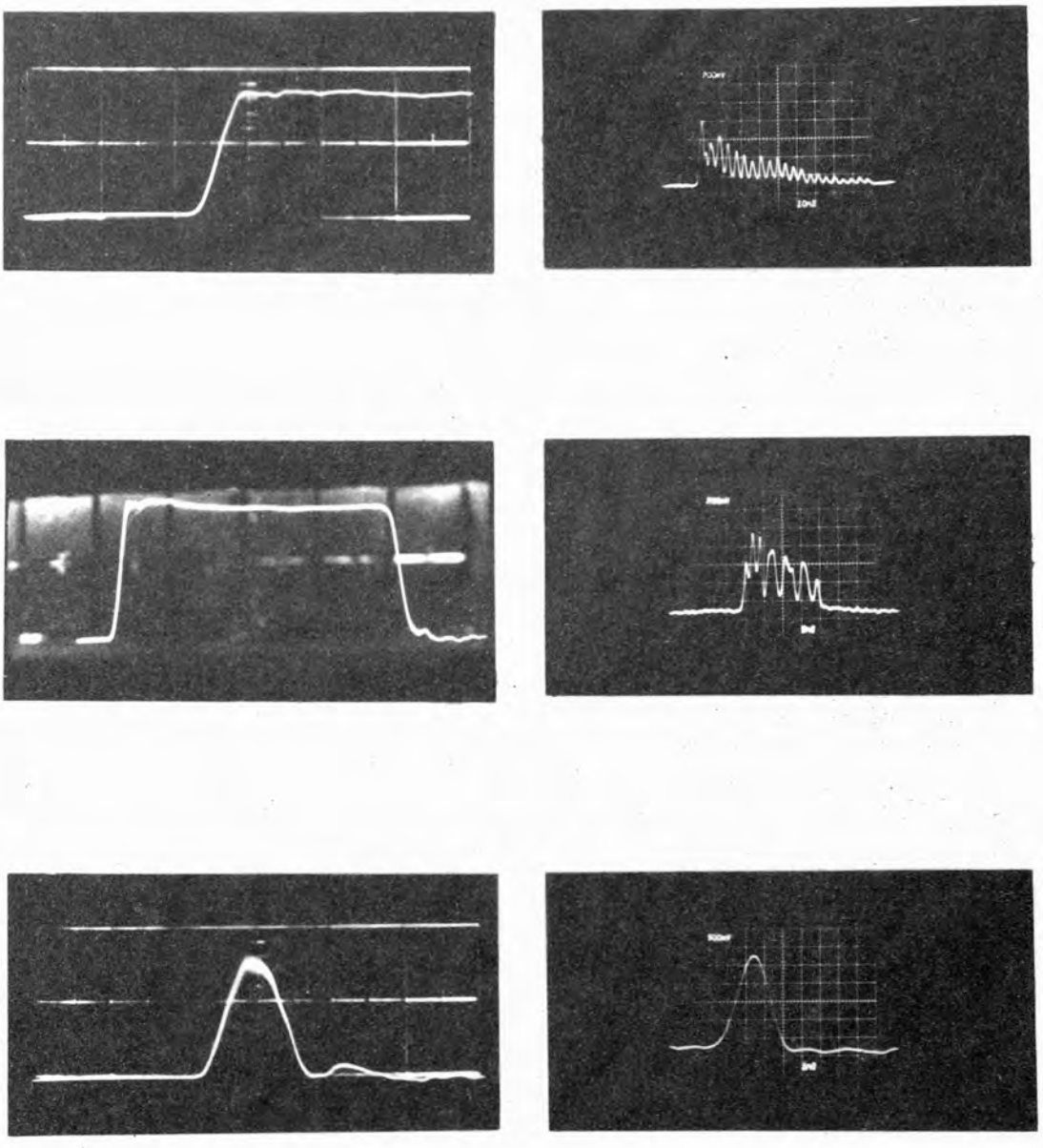

Fig.3.9
Typical examples of the generated CO_2 laser pulses - on the right - (10 ns/div; 5 ns/div; 1 ns/div, from top to bottom) together with the corresponding electrical pulses which activate the Pockels cell - on the left - (2 ns/div; 5 ns/div; 2 ns/div, from top to bottom)

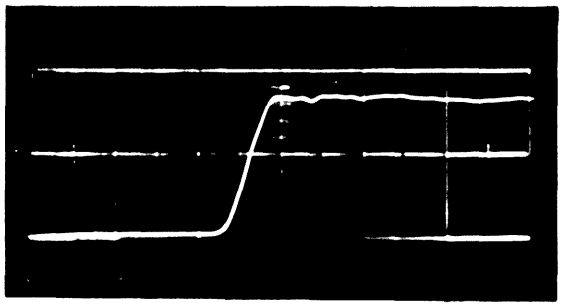

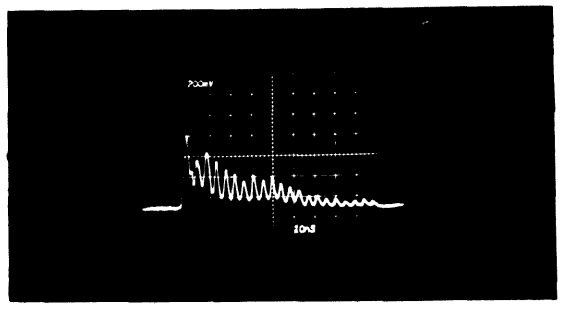

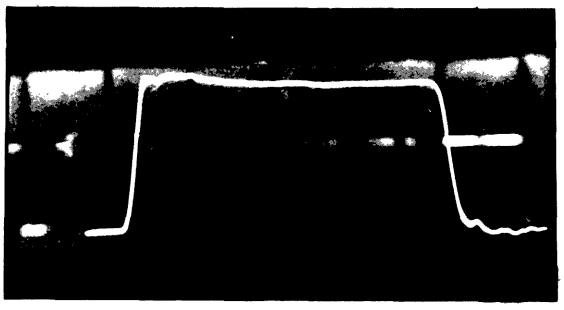

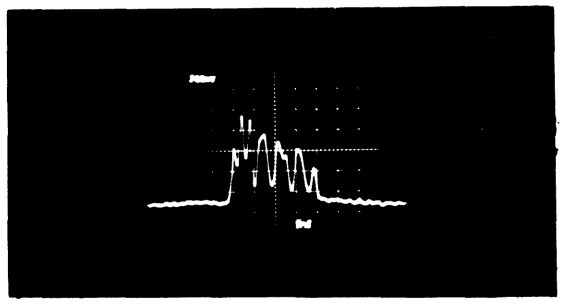

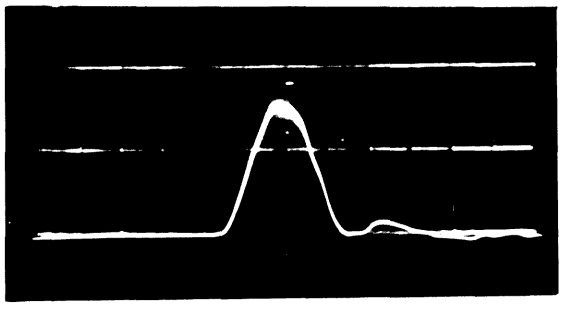

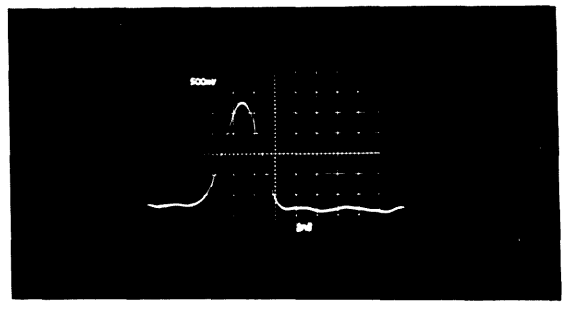

Here, N_0 is the number of electrons emitted from the electrode and α is the first Townsend ionization coefficient (i.e. the number of ionizing collisions per centimetre made by one electron travelling in the electric field direction). This process continues until the entire gap is bridged with an ionized conducting path. The velocity of the avalanche v_a is considered as equal to the electron drift velocity ($v_a \sim 10^7$ cm/sec). This mechanism, however, fails when the measured delay time is shorter than the time required for the avalanche to travel a distance equal to the gap length d. In such a situation the more rapid 'streamer' mechanism is required to account for the temporal behaviour of the breakdown. In this process according to RAETHER[170], the electron multiplication follows the avalanche process until the number of electrons reaches a critical value $N_c \simeq 10^8$ after a distance of travel x_c. At this stage the avalanche is transformed into a plasma streamer advancing rapidly with a velocity $v_s \sim 10^8$ to 10^9 cm/sec. The total formative time, which can be defined as the period of time that elapses between the creation of the electrons on the target electrode and the appearance of the high voltage on the opposite electrode, may therefore be expressed as:

$$t_f = \frac{x_c}{v_a} + \frac{d - x_c}{v_s}$$

or using equation (3.20)

$$t_f = \frac{\ell n(N_c/N_o)}{\alpha v_a} + \frac{d - x_c}{v_s} . \qquad \ldots (3.21)$$

3.11 DELAY TIME AND JITTER

Although the self-mode-locked pulse of the Double-Rogowski module was normally used to trigger the gap, it was necessary to use the 70 ns single longitudinal pulse from the laser described in Chapter VI in order to measure accurately the delay time, jitter and threshold power for breakdown of the gap. The peak power of the pulse transmitted through the Ge lens; ranging from 0 - 2 MW, was indirectly measured with the aid of a beam-splitter located in front of the lens and a calibrated photon drag detector. The

spontaneous mode-beating that normally occurs in a TEA CO_2 laser, and the difficulty of its removal, might account for the paucity of data on delay time and jitter measurements in the literature, by contrast with the numerous measurements pertaining to ruby, dye, YAG and Nd glass lasers.

The delay time, t_d, of a LTSG - defined as the period of time between the arrival of the laser pulse on the target electrode and the appearance of the electrical pulse on the opposite electrode - may be considered as the sum of two smaller periods of time:

(a) the time, t_e, needed for the laser to heat the target material to its melting point T_m (i.e. the time needed for the emission of the N_0 electrons); and

(b) the formative time, t_f, which has already been defined.

In the present case where the CO_2 laser pulse has a slow rise time ($\sim$70 ns) the value of t_e can be readily shown to be comparable with - or even greater than - the value of t_f and cannot therefore be overlooked as it can with laser pulses of a few picoseconds[171] or a few nanoseconds[165] duration.

As shown later,

$$t_e = \frac{K}{P_\ell^2}$$

where

$$K = \frac{T_m^2 \pi \rho ck}{4A^2}$$

is a thermal constant of the target material, and P_ℓ is the incident laser power density. Thus, using equation (3.21), the delay time $t_d = t_e + t_f$ is:

$$t_d = \frac{T_m^2 \pi \rho ck}{4A^2} \frac{1}{P_\ell^2} + \frac{\ell n\, N_c - \ell n\, N_0}{\alpha v_a} + \frac{d - x_c}{v_s} . \qquad \ldots (3.22)$$

Equation (3.22) theoretically predicts the effect on the delay time of the laser pulse, voltage, gap spacing and pressure, and the experimental behaviour qualitatively agreed with its predictions.

As a result of an increase in laser power, shorter values of t_d were recorded, presumably because of the smaller value of t_e. Fig.3.10 indicates

the effect of the charging voltage of the gap, V, on the delay time. The observed increase in the delay time with decreasing V is clearly due to the fact that both α and v_a decrease with the decreasing field.

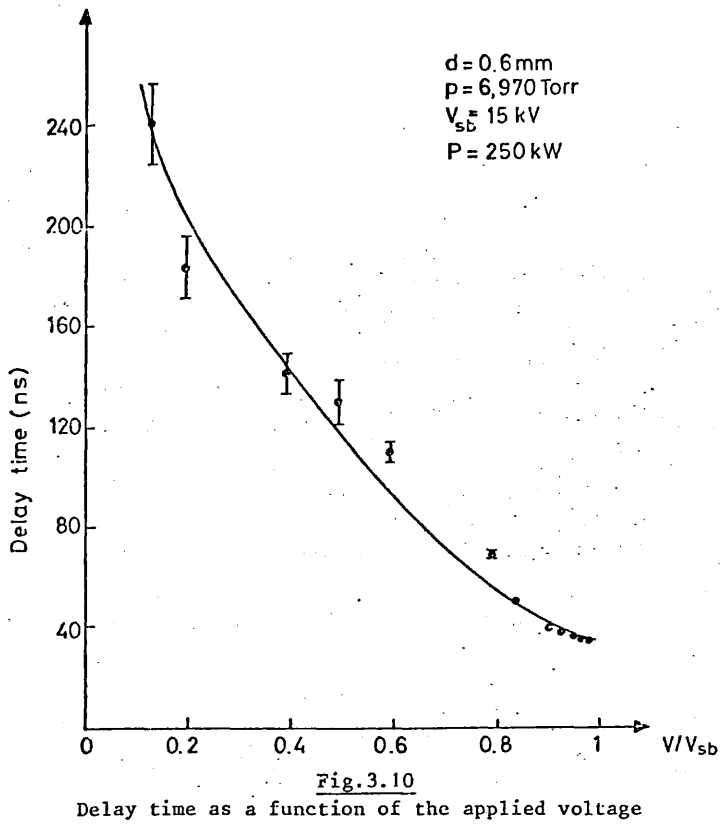

Fig.3.10
Delay time as a function of the applied voltage

When the pressure P was increased simultaneously with a decrease in the gap spacing, keeping the ratio E/P constant, a decrease in the value of t_d was observed. This result is in agreement with equation (3.22) since the Townsend coefficient α is proportional to the pressure P for constant E/P.

It thus follows that in order to minimise the delay time of a CO_2 LTSG, the highest permissible values of laser power and pressure should be used in conjunction with a charging voltage as near to the self-breakdown value as possible.

The error bars in Fig.3.10 indicate the maximum jitter of the delay time. Subnanosecond jitter is observed for $V \geq 0.8\,V_{sb}$. It should be noted here however, that the jitter remains low only if the power of the incident laser pulse does not change from shot-to-shot. Any variation of the laser power results in a considerable increase of the jitter even when $V \geq 0.8\,V_{sb}$. This is apparently caused by changes in the value of t_e, which is dependent on laser power. The peak power of the laser beam which entered

the gap when the measurements in Fig.3.10 were taken was 250 kW. The minimum power required to trigger the gap when the charging voltage $V \simeq 0.95\, V_{sb}$ was found to be ~ 20 kW, corresponding to a threshold energy of 1.5 mJ.

3.12 ELECTRODE MATERIAL

Since the electron emission from the target electrode is regarded as thermionic[172-174,177], attention must be given to the choice of target material to achieve the lowest possible delay time, t_d. When the target electrode is irradiated by a 'triangular' laser pulse of duration τ, the temperature T at the surface, as a function of time $t(t \leq \tau)$ is given by the relation[175]:

$$T = \frac{2 A P_\ell}{\sqrt{\pi \rho c k}}\, t^{\frac{1}{2}} \qquad \ldots (3.23)$$

where A is the absorbed fraction of the incident radiation, P_ℓ the laser power density and ρ, c, k, the density, specific heat and thermal conductivity of the electrode material respectively.

Tungsten has been claimed as the best material for spark gaps triggered by laser radiation of up to 1 μm wavelength[174,175] with aluminium, brass and stainless steel in descending order of desirability. However, the longer wavelength of the CO_2 laser (10 μm) requires the resistivity of the material to be taken into account, for this determines the value of the absorption A[176], i.e.

$$A = 3.65 \times 10^{-3}\, (R/\lambda)^{\frac{1}{2}} \qquad \ldots (3.24)$$

where λ is the wavelength in μm and R is the resistivity in Ω.μm. Using the relations (3.23) and (3.24) to ascertain the comparative rates of laser heating, the different electrode materials can be listed in order of desirability for $\lambda \sim 10$ μm as: stainless steel, tungsten, brass, aluminium and copper.

Although brass electrodes were used in the present case, they were found to be quite satisfactory for the generation of nanosecond pulses

because for any value of the charging voltage $V \geq 0.7\,V_{sb}$ the electrical pulse appears on the output of the L T S G before the laser pulse reaches its peak (see Fig.3.10). By suitably delaying the electrical pulse, its arrival on the Pockels cell can be arranged to coincide with the peak of the laser pulse.

3.13 RISE TIME DEPENDENCE ON GAS TYPE, PRESSURE GAP SPACING AND CHARGING VOLTAGE

While there has been thorough investigation of the delay time and jitter in L T S G operation - notably the articles by GUENTHER et al[167,175] proposing how these parameters can be optimized - there is very limited experimental data[177] on the effect of spark gap parameters - such as gas pressure and operating voltage - upon the rise time of the electrical pulse.

Since the rise time of the transmitted laser pulse is determined by that of the electrical pulse, it is essential to ascertain the operating conditions for the minimum rise time.

Figures 3.11 and 3.12 illustrate the effect of the gap spacing and the gas pressure respectively, on the rise time of the electrical pulse. The gas pressure was held constant for the former and the gap spacing for the latter. The ratio V/V_{sb} was maintained at a constant value in both cases.

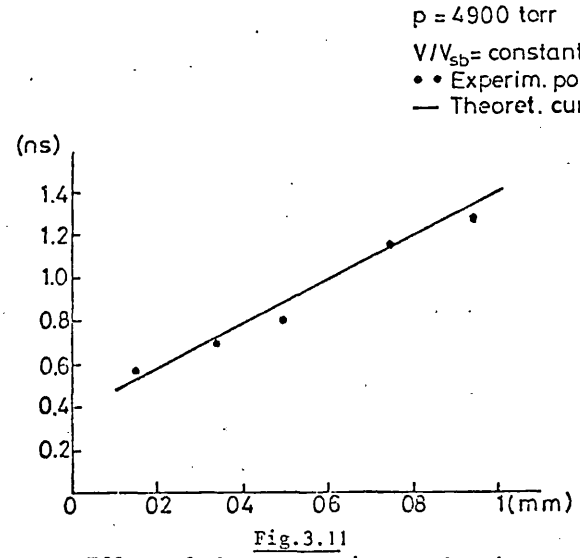

Fig.3.11
Effect of the gap spacing on the rise time of the electrical pulse

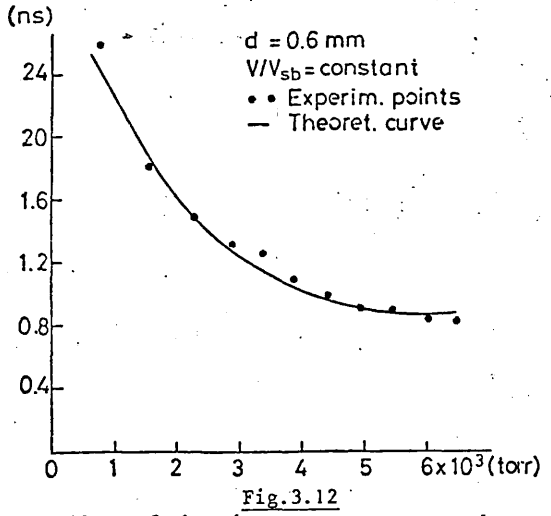

Fig.3.12
Effect of the nitrogen pressure on the rise time of the electrical pulse

The solid lines are theoretical curves based on the relation[177]

$$t_r = 3.5\, P\, d^2/SV^2 \qquad \ldots (3.25)$$

which gives the rise time as a function of the gap spacing d, the gas pressure P and the applied voltage V. The best fit to the experimental points gives a value for the constant S of 440 torr cm^2 V^{-2} s^{-1}. The close agreement (a) between this value of S and those of 450 torr cm^2 V^{-2} s^{-1} [177] and 418 ± 10% torr cm^2 V^{-2} s^{-1} [178] obtained in other investigations, and (b) between the measured and the predicted values of the rise time, full endorses the validity of equation (3.25).

Nitrogen was chosen as the insulating gas because of its high dielectric strength. It has often been suggested[162,179] that a mixture of nitrogen and argon (which has a lower dielectric strength) should be used in order to achieve shorter delay times. However the addition of argon was avoided, in the present case, for two reasons:

(a) because there is no need for any further reduction in the delay time while the maintenance of as short a rise time as possible is essential.

(b) because this will necessitate longer gap spacings to hold off the same voltage, which, in turn, will increase the rise time of the electrical pulse.

Should the need arise in future applications of the CO_2 L T S G for even shorter delay time, this could be achieved - without any adverse effect on the rise time of the electrical pulse - by replacing the brass electrodes with those of stainless steel, rather than by adding argon to the nitrogen.

Equation (3.25) indicates how any change in the voltage applied across the gap affects the rise time of the electrical pulse (i.e. for constant pressure and gap spacing: $t_r \propto \frac{1}{V^2}$). Thus, operation as near self-breakdown as possible, is essential not only to obtain shorter delay time but, more importantly, to achieve faster-rising electrical pulses.

3.14 CONCLUDING REMARKS

The electro-optical shutter, whose operational characteristics have been fully analysed here, has been used to generate single subnanosecond CO_2 laser pulses from the output of the Double-Rogowski oscillator[94].

Figure 3.9 shows three laser pulses (on the right) of duration 100, 20 and ~1.5 nsec transmitted by the shutter, together with the corresponding electrical pulses (on the left) that activated the GaAs crystal. The performance of the device has shown no signs of deterioration after two years of use. However, there are some improvements which could be made in the existing arrangement:

(1) The main limitation on its performance is the finite contrast ratio (signal/background noise) of the switched-out laser pulses due to the intrinsic birefringence of the GaAs crystal. The upper limit of this ratio (i.e. the extinction ratio of the crystal) is attained when the voltage of the electrical pulse is made equal to the half-wave retardation voltage $V_{\frac{1}{2}}$ (in the present case $V_{\frac{1}{2}} = 21$ kV). Up to now the voltage used has been $V \simeq \frac{1}{3} V_{\frac{1}{2}}$, and therefore increasing this would significantly improve the present contrast ratio. However, this should be followed by an appropriate increase in the pressure of the nitrogen in the spark gap in order to maintain the fast rise time of the electrical pulse (see equation (3.25)).

(2) As a further step to improve the contrast ratio, a second GaAs crystal could be used together with an additional polarizer[180]. This should greatly improve the contrast ratio because the upper limit in this case will be determined by the product of the extinction ratio of the two crystals: $E_c = E_c^{(1)} \times E_c^{(2)} \sim 10^7$.

CHAPTER IV

AMPLIFICATION OF NANOSECOND PULSES: TELESCOPIC AMPLIFIER

4.1 INTRODUCTION

The low optical damage threshold inherent in GaAs ($0.2\,J/cm^2$) and CdTe ($0.13\,J/cm^2$) [181] which are the two electro-optical materials most widely used with CO_2 lasers restricted the energy of the generated ns pulses, in the present investigation, to 1 mJ. Comparably low energies (1 - 2 mJ) have also been noted elsewhere[92,96,97]. An attempt to generate more powerful pulses resulted in the damage of the GaAs crystal (section 3.7). The detection of such low intensity pulses is difficult in the presence of the large radio frequency noise usually associated with pulsed lasers and the application of such pulses to any laser plasma experiment is impractical. The Double-Discharge module was used to amplify these pulses and to examine their capability for extracting the optical energy stored in the active medium.

The attachment to this module of a specially-designed optical cavity converted it into a telescopic amplifier by means of which the innate inefficiency of the pre-amplification stages of the ns pulses was effectively eliminated. The design and performance of this telescopic amplifier are analysed and the obtained results compared with those which were achieved when more conventional means of amplification were used.

4.2 GAIN SATURATION MEASUREMENTS OF ns PULSES

Gain saturation measurements in the Double-Discharge module for pulses of 70 ns duration were presented in section 2.5.4. In this section, the gain saturation properties of this module are examined under 1.1 ns (FWHM) pulse-illumination. The experimental arrangement is schematically shown in Fig.4.1. The low energy of the switched-out pulse accounted for the double-pass amplification illustrated in this figure. Gain measurements were taken by monitoring the energy of the ns pulse before and after its second

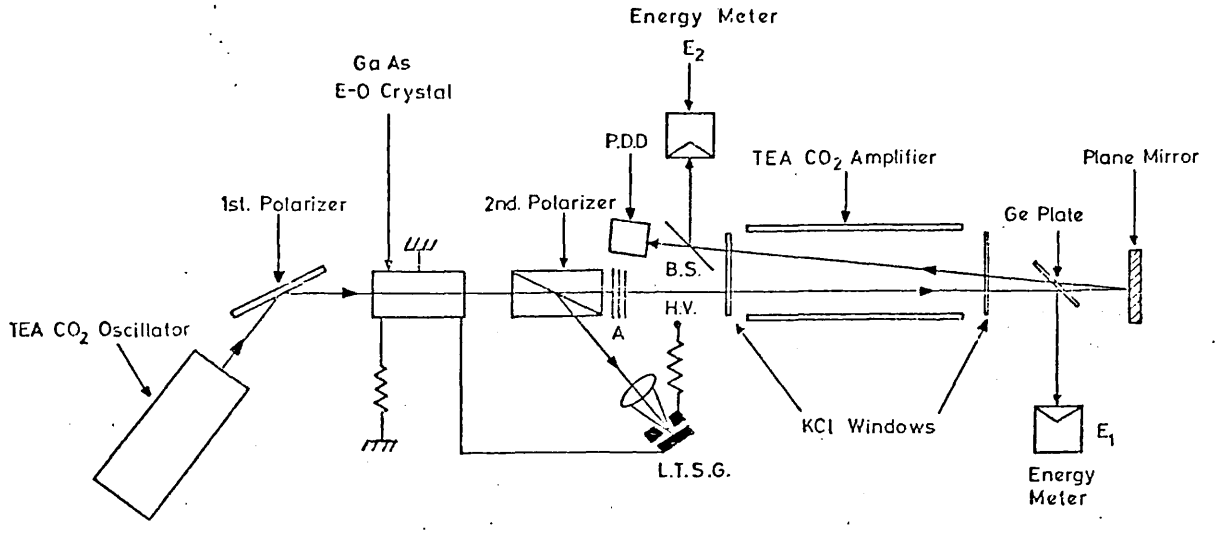

Fig.4.1
Experimental arrangement for gain saturation measurements of ns pulses

traverse of the amplifier. The intensity of the pulse entering the amplifier was adjusted - by rotating the germanium beam splitter - so as to equal the intensity of the pulse incident on the first energy meter. Thus the input energy E_i was given directly by this meter while the output energy E_0 was given by: $E_0 = \frac{E_2}{T_1 T_2}$, E_2 being the energy measured by the second meter and $T_1 = 0.92$, $T_2 = 0.86$ being the transmission coefficients of the KCl plate and beam splitter respectively. The value of E_i was varied by positioning thin polyethylene attenuators after the second polarizer. The ns pulse shape, monitored by a photon drag detector, was displayed on a fast oscilloscope (Tek. 7904).

The measured values of E_i, E_0 are shown in Fig.4.2, where the solid line theoretical curve is plotted using the two-level amplifier equation (5.2). The optimum fit to the experimental points was obtained when the saturation energy intensity took the value of 30 mJ/cm^2.

Gain measurements for the 70 ns pulse are replotted from Fig.2.16 for purposes of comparison. The spectral content (P20 line of the 10.4 μm band)

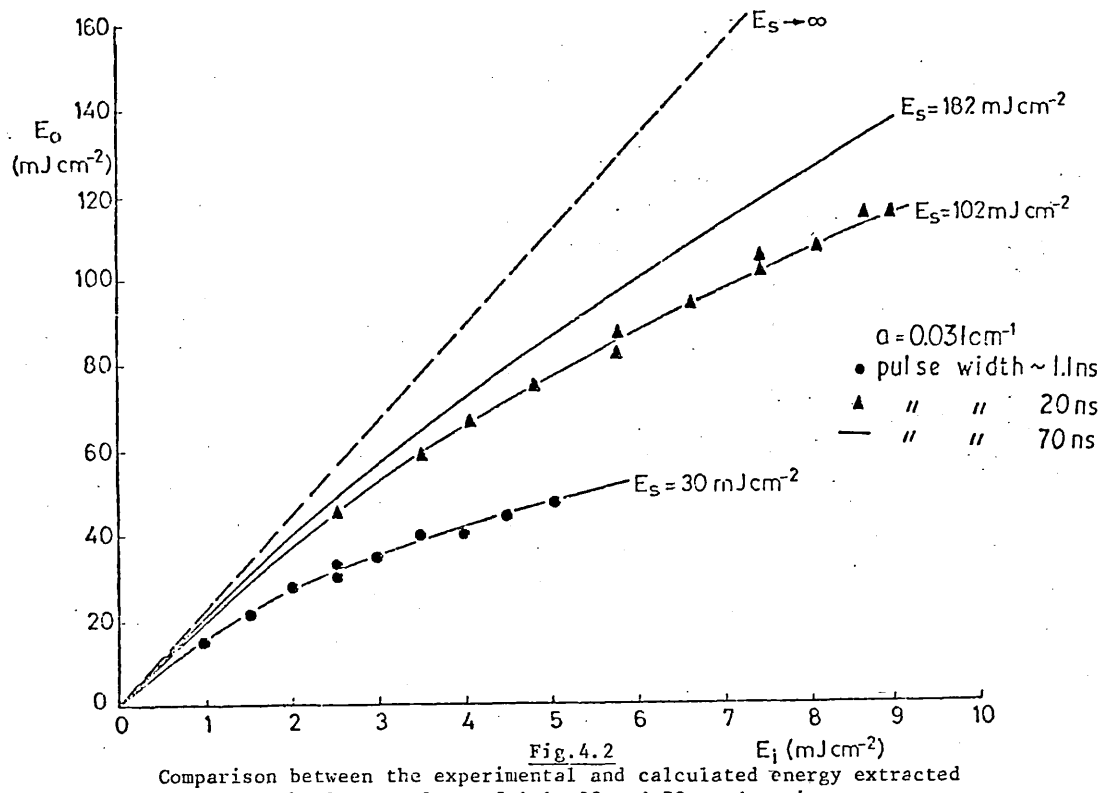

Fig.4.2

Comparison between the experimental and calculated energy extracted by laser pulses of 1.1, 20 and 70 ns duration

and the small signal gain ($\alpha_0 = 0.031\ cm^{-1}$) were the same in both cases.

These measurements indicate that the maximum optical energy that could be extracted from this amplifier by a 1.1 ns single line pulse is:

$$E_{ext} = E_s \cdot \alpha_0 = 0.93\ J/\ell$$

and this is only one sixth of the energy

$$E_{ext} = E'_s \cdot \alpha_0 = 5.64\ J/\ell$$

available to a 70 ns pulse. Similar measurements using a 20 ns pulse also shown in Fig.4.2, indicate that a 20 ns pulse is three and a half times more efficient in extracting the optical stored energy than the 1.1 ns pulse ($E_s = 102\ mJ/cm^2$).

This pulse duration dependence of the value of E_s and the subsequent limitation on the efficiency of the ns pulse amplification are due to the finite relaxation rate of the rotational sub-levels within the upper laser level 00°1. Discussion of these aspects is presented in the next chapter (section 5.1).

The maximum energy extracted by the 1.1 ns pulse in its double pass was 92 mJ. To increase this output the KCl beam splitter in Fig.4.1 was replaced by a fully reflecting plane mirror and the pulse was directed for a third time through the amplifier. The extracted energy in this case was almost doubled at 180 mJ. The cross-section of the output beam was 1.5 cm^2 which accounted for the poor efficiency in extracting the energy potentially available to ns pulses from this module which has an effective circular cross-section of $A = 19.6\ cm^2$. This constitutes only 10% of the energy, $E_{ext} = E_s \cdot \alpha_0 \cdot A \cdot L_a = 1.82\ J$ (where $L_a = 100$ cm is the length of the amplifier), extractable by a 1 ns pulse having such a cross-section.

4.3 PULSE BROADENING

The finite rate of the rotational energy transfer between the numerous sublevels within the 00°1 vibrational level, as well as accounting for the low efficiency of the ns pulse amplification, is also responsible for an undesirable effect upon the temporal profile of such pulses. Theoretical studies[63,64,182,183] have indicated pulse-broadening for a saturated amplification by contrast with the pulse-narrowing associated with a two-level amplifying system without rotational energy transfer (as, for example, a ruby laser). The leading edge of an intense ns pulse rapidly extracts the optical energy stored in the active rotational level, as well as all the energy transferred into this level via collisions during the rise-time of the pulse. The trailing edge of the pulse, on the other hand, experiences a gain which increases with time, as the rate at which the energy is transferred into the active level gradually exceeds the rate at which the energy is extracted - the latter being proportional to the intensity of the pulse which, in this case, decreases with time. The result is an increase in the pulse-width as the pulse propagates through the amplifier.

FELDMAN[184] has theoretically shown that this pulse-broadening can be minimized by using a multiline input pulse. The theoretically predicted

pulse-broadening and its elimination were experimentally investigated using triple-pass amplification to achieve gain saturation. The pulse shape was monitored after the first and third pass, using two identical photon drag detectors and was displayed on the same oscilloscope (Tektronix 7904) using cables of equal length. Fig.4.3(a) shows the recorded shapes of the input pulse (on the left) and output pulse (on the right); the resultant pulse-broadening is clearly evident. When the laser oscillator was forced to emit the P(16), P(18) and P(20) lines simultaneously (see next chapter) the pulse broadening was considerably reduced as Fig.4.3(b) illustrates.

It is believed that this is the only experimental evidence reported to date of the elimination of pulse-broadening using a multi-line ns input pulse.

4.4 TELESCOPIC AMPLIFIER

The development, in the course of this research, of the telescopic CO_2 laser amplifier[94] provided a much more efficient method for extracting the stored energy. By this means, the weak input pulse was simultaneously expanded and amplified while preserving its transverse mode structure. With a reflecting telescope arrangement, full use of the amplifying medium could be made because the design combines adequate beam expansion with high overall gain (triple-pass). The system is ideal for raising weak signals to higher power in a single stage and can be adapted for use in large amplifier systems to match a wide range of weak sources.

The optical cavity of the telescopic amplifier, shown in Fig.4.4, is effectively an unstable confocal resonator belonging to the positive branch, with a central hole on the concave mirror. The confocality of the resonator ensured a collimated output with diffraction-limited divergence. The common focal point of the two mirrors comprising the resonator lies outside the latter, thereby precluding the risk of optical breakdown associated with the

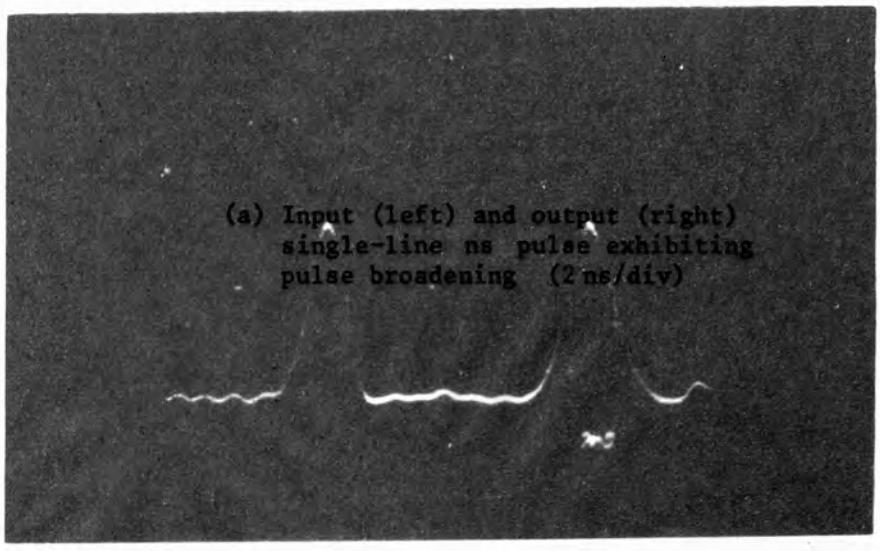

(a) Input (left) and output (right) single-line ns pulse exhibiting pulse broadening (2 ns/div)

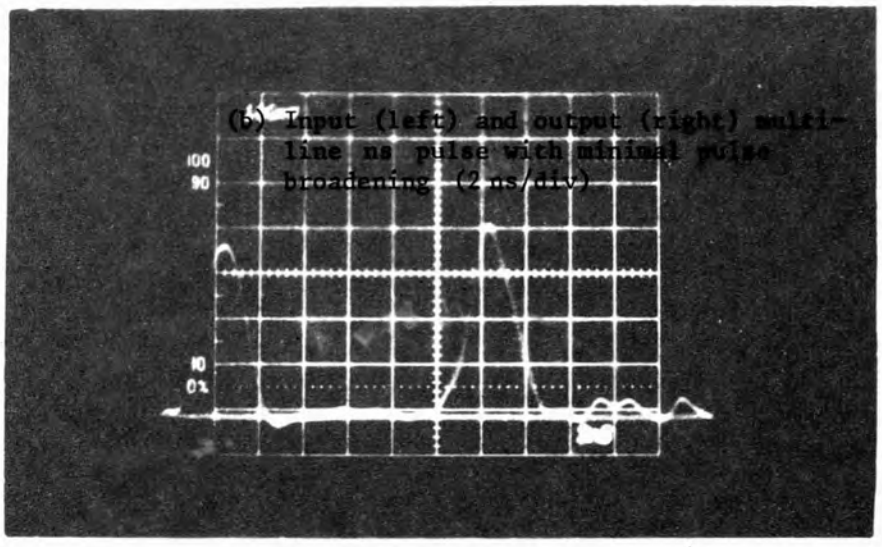

(b) Input (left) and output (right) multi-line ns pulse with minimal pulse broadening (2 ns/div)

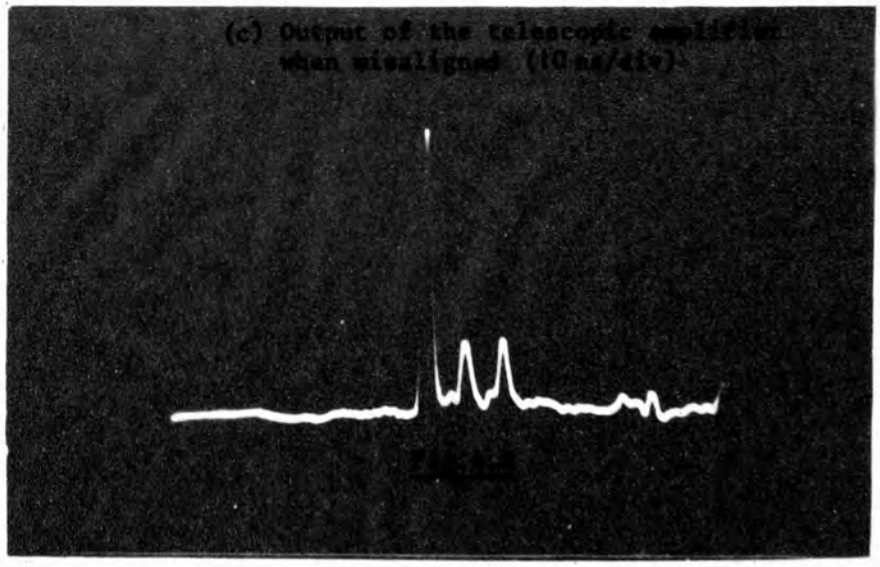

(c) Output of the telescopic amplifier when misaligned (10 ns/div)

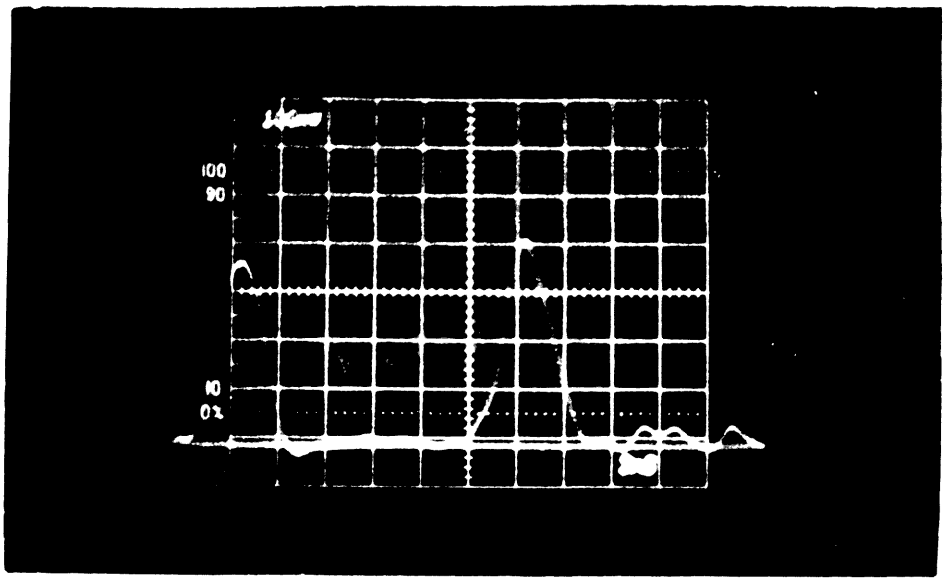
100
90
10
0%

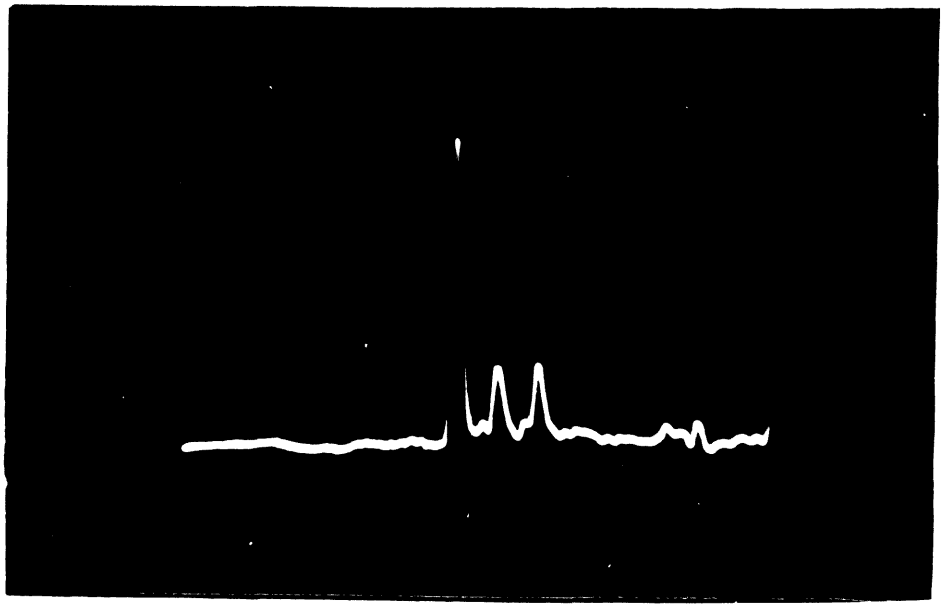

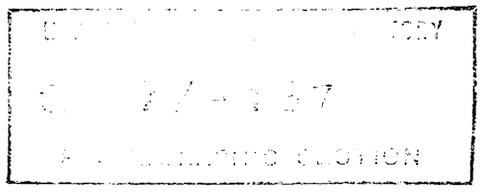

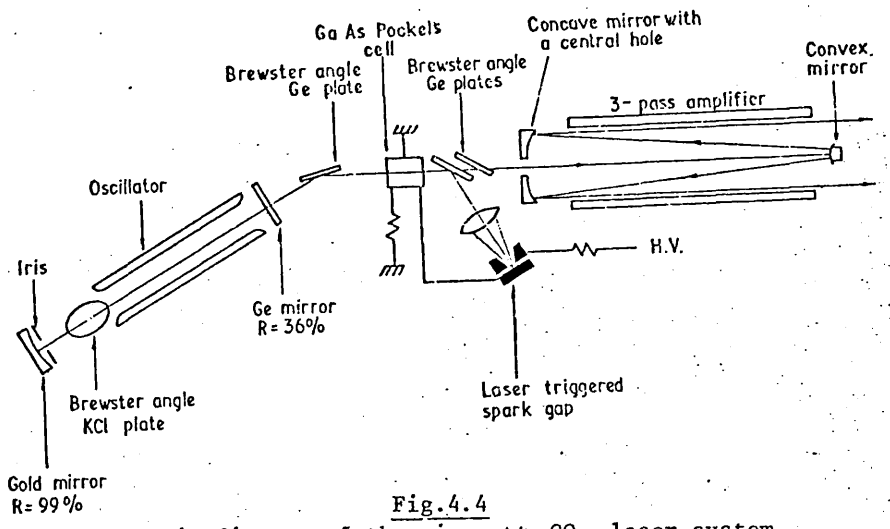

Fig.4.4

Schematic diagram of the gigawatt CO_2 laser system

negative branch of confocal resonators. Parallel light entering from the left through the hole in the concave mirror traverses the central part of the amplifying medium to strike the convex mirror. After reflection, the light returns as a diverging beam to the concave mirror, where it is reflected as an expanded parallel beam for its third and final traverse of the amplifying medium. This arrangement also achieves optical matching of the output to subsequent amplifying stages of larger aperture than the input beam, without the severe loss of intensity normally associated with a passive beam expander.

Particular care was taken to ensure that parallel beams in the amplifier were restricted to only three passes of the amplifying medium in order to diminish the possibility of self-oscillation occurring from resonant feedback in the cavity. Although this restriction was observed, strong self-oscillation initiated by optical feed-back, was detected as a result of light diffraction at the mirror apertures.

4.4.1 Amplifier Design

Two main sets of criteria have to be fulfilled in order to achieve a stable three-pass amplifier. First, self-oscillation must be prevented and in a normally-adjusted system, this means that diffraction losses have to be controlled by a suitable choice of cavity apertures and optical magnification. Secondly, the efficient extraction of energy depends upon the entrance aperture 2x being greater than or equal to the diameter of the convex mirror $2a_1$. If D is the electrode spacing and M the linear magnification of the system, we have the following relations: $2x \geq 2a_1$, and $M = \frac{D}{2a_1}$ for normal adjustment; hence $x \geq \frac{D}{2M}$.

A further factor must be taken into account as a result of the geometry. The output beam has an annular cross-section with an inner diameter controlled by 2x: hence, the smaller the value of x, the greater the percentage of stored energy that can be extracted. For $x \leq \frac{D}{7}$ it can be easily shown that a sufficiently high fraction of the stored energy (> 90%) could - in principle - be extracted. The aboveconsiderations impose the following limits on the design:

$$\frac{D}{2M} \leq x \leq \frac{D}{7} . \qquad \ldots (4.1)$$

Finally, a practical limit to the magnification is set by the ratio of the electrode spacing to the diameter of the input beam: $M \leq 10$.

4.4.2 Diffraction Loss versus Self-Oscillation

According to ANAN'EV and SHERSTOBITOV[185] the quantity $|\gamma|$ which determines the double-pass diffraction loss δ in an unstable resonator with a central hole is given by:

$$\ell n|\gamma| = \frac{\ell n\, M\, \ell n \dfrac{M}{2\pi N_{eq}(M^2-1)}}{\ell n \dfrac{4N_{eq}}{N^0_{eq}}} \qquad \ldots (4.2)$$

where $\delta = 1 - |\gamma|^2$ and N_{eq} and N^0_{eq} are the equivalent Fresnel numbers of

the resonator and of the entrance aperture respectively. For a telescopic resonator, N_{eq} according to SIEGMAN[186] is given by

$$N_{eq} = \frac{a_1^2}{2\lambda L}(M-1) \qquad \ldots (4.3)$$

where λ is the wavelength of the cavity radiation and L the length of the cavity. ANAN'EV and SHERSTOBITOV[185] give:

$$N_{eq}^0 = \frac{x^2}{2\lambda L}\,\frac{M-1}{M}\,. \qquad \ldots (4.4)$$

Using equations (4.3) and (4.4), equation (4.2) becomes:

$$\ell n|\gamma| = \frac{\ell n\, M\, \ell n\, \dfrac{\lambda L}{\pi a_1^2}\,\dfrac{M}{(M^2-1)(M-1)}}{\ell n\, \dfrac{4a_1^2}{x^2}\,M}\,. \qquad \ldots (4.5)$$

The quantity γ at which no self-oscillation occurred was first determined experimentally for an existing telescopic resonator with $M = 2.875$, $L = 1.25\,m$ and $a_1 = 8.35\,mm$ for a discharge region with dimensions $1m \times 49\,mm \times 49\,mm$.

The input aperture radius x for which self-oscillation ceased was determined by placing a non-reflecting carbon disk cover on the pole of the concave mirror, to simulate a circular aperture the diameter of which could be readily adjusted. The diameter was increased until the system reached a point where oscillation ceased with the amplifier fully energized. The effective value of x was thus found to be 16 mm.

In Fig.4.5, the normalized oscillator output energy is shown as a function of the ratio $\frac{x}{a_2}$, where a_2 is the radius of the concave mirror. Such an optical cavity, however, although below the self-oscillation threshold, would have been inappropriate since it does not satisfy the condition given by the relation (4.1). Using equation (4.5) and the confocal condition : $a_2 = M a_1$, substitution of the appropriate values of L, a_1, x and M for $\lambda = 10.6\,\mu m$ gives $\ell n|\gamma| = -3.78$. On the basis that the double pass gain should be equal to the double pass diffraction loss when the value of x is

such that the oscillation ceases, the expected value of $\ell n|\gamma|$ is:

$$\ell n|\gamma| = -\alpha_0 L_a = -3.1$$

where $\alpha_0 = 0.031\ cm^{-1}$ is the small signal gain in the amplifier and $L_a = 100$ cm is the length of the active medium. Although this agrees only approximately with the value given by equation (4.5), the practical significance of this equation lies in the fact that it enables the parameters of a number of other similar cavities - having the same diffraction loss - to be calculated, thereby allowing more convenient values of M and x to be determined. When the approximate values of the diffraction loss of two cavities are equal, it is reasonable to assume that the exact values should also be equal and therefore no cavity for which $\ell n|\gamma| = -3.78$ should oscillate.

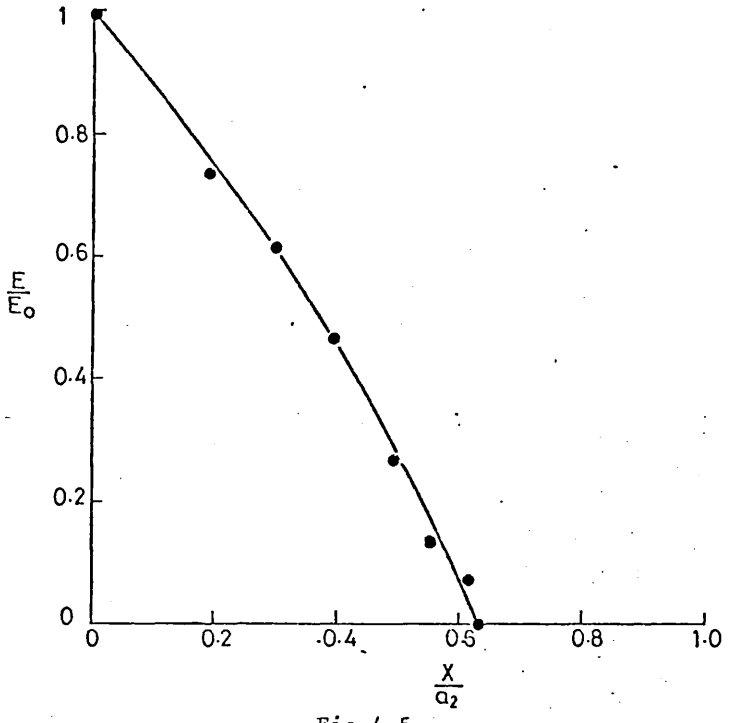

Fig.4.5
Graph of relative self-oscillation energy vs hole size

A combination of M and x that satisfied both the condition $M < 10$ and the inequality $\frac{D}{2M} \leq x \leq \frac{D}{7}$, and at the same time gave a value for $\ell n|\gamma| = -3.78$, was found to be $M = 7$ and $x = 5.4$ mm. For optimum power output, $2a_2 = D = 49$ mm, determined by the electrode separation in TEA geometry. Thus, $a_2 = \frac{a_2}{M} = 3.5$ mm. The radius of curvature of the concave mirror was ascertained from simple telescope theory to be 2917 mm and that of the convex mirror was 417 mm, requiring a cavity length $L = 1.25$ m. As was expected, a cavity constructed with the above parameters showed no signs of self-oscillation.

4.4.3 Parasitic Oscillation

Although self-oscillation in the amplifier had been eliminated, persistent parasitic oscillation was observed - independent of the cavity mirrors - and continued even when the mirrors were removed. The effect of this parasitic radiation was particularly severe when the switching system which isolated the oscillator from the amplifier was removed and the subsequent parasitic radiation from the amplifier caused a reduction of up to six times in the peak power of the oscillator according to measurements taken from a photon-drag detector. It was found that this reduction in power was approximately proportional to the intensity of the parasitic oscillation in the amplifier, measured when only the amplifier was energized.

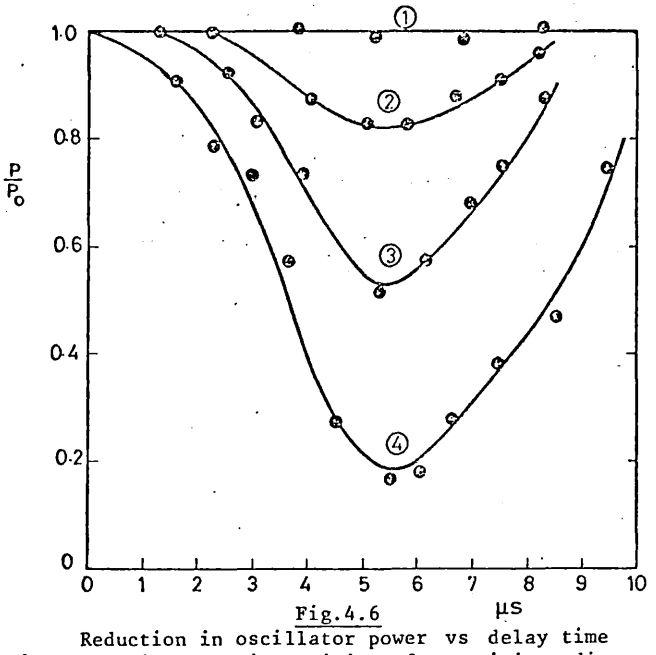

Fig.4.6
Reduction in oscillator power vs delay time for different intensities of parasitic radiation from the amplifier. Curve 1, no feedback; Curves 2 - 4 increasing feedback

Figure 4.6 shows the normalized peak power of the oscillator plotted against t, the delay time between the firing of the amplifier and the oscillator, for four different intensities of parasitic oscillation, effectd by the introduction of thin attenuators. It was realized that this parasitic oscillation was due to the reflection caused by the mirror mounts and once the mounts had been covered with carbon paper the oscillation ceased. With the elimination of the parasitic oscillation, the amplifier's presence did not affect the oscillator's performance in any way. An energy meter capable of measuring integrated energy densities down to 0.05 mJ/cm^2 was used to confirm that the parasitic and self-oscillations of the amplifier had been completely eliminated and the operation of this device as a 'true' amplifier was thereby accomplished.

4.4.4 Performance of the Telescopic Amplifier

The fast electro-optic shutter described in Chapter III was used to switch-out a nanosecond pulse from the self-mode-locked output (Fig.4.7(a)) of the oscillator described in Chapter II. The generated pulse was directed into the amplifier where three passes were made in the active medium via the Cassegrain telescope system. A photograph of the complete laser system for the generation and amplification of ns pulses is shown in Fig.4.8. The output of the amplifier was monitored with a calibrated photon drag detector (Rofin model 7415) and the pulse intensity profile displayed on a 7904 oscilloscope (Fig.4.7(c). The recorded width of 1.3 ns FWHM included the rise times of the detector (0.6 ns) and of the oscilloscope (0.8 ns). Assuming a Gaussian temporal profile, the actual pulse width calculated from these values was 830 ps FWHM. Pulses of this duration were the shortest recorded using this system. The pulse energy was measured using a Gen-Tec pyroelectric energy meter. Because of the finite extinction ratio (signal/background noise), the measured energy contained two components: the energy in the short pulse and the amplified noise. The latter was measured by disconnecting the trigger of the electro-optical shutter, thereby making it inactive, and firing both oscillator and amplifier. This energy was then subtracted from the total to give an output pulse energy of 1 J. Similarly, the energy of the input pulse was found to be 1 mJ. Thus the telescopic amplifier had an energy gain of 1000. This is more than five times greater than the energy gain of 180 for the conventional triple-pass amplification described earlier in this chapter and sixty-five times greater than the single-pass energy gain of ~15. The peak power of the amplified pulse was estimated from the response of the photon drag detector and was found to be ~1 GW. Comparison with the input of ~1 MW shows the close agreement between the energy and power measurements of the gain for a ns pulse.

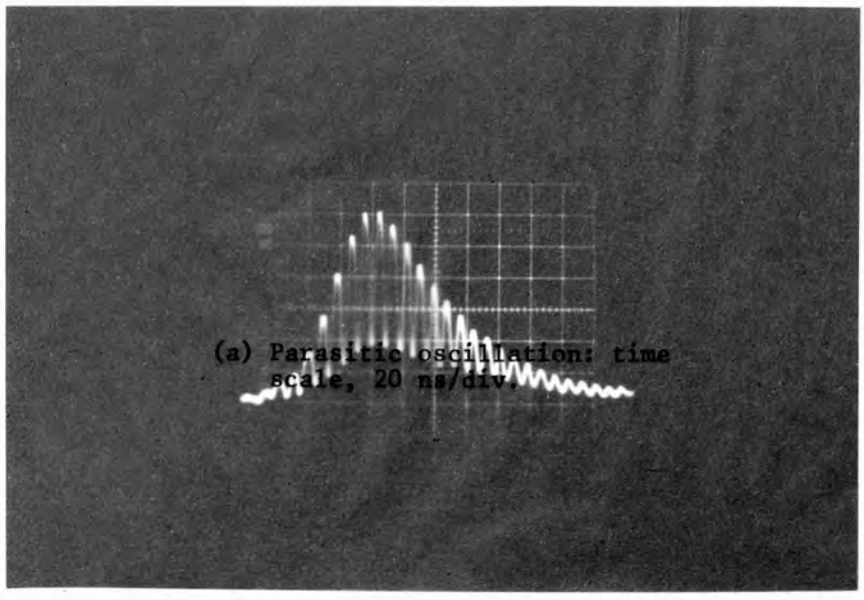

(a) Parasitic oscillation: time scale, 20 ns/div.

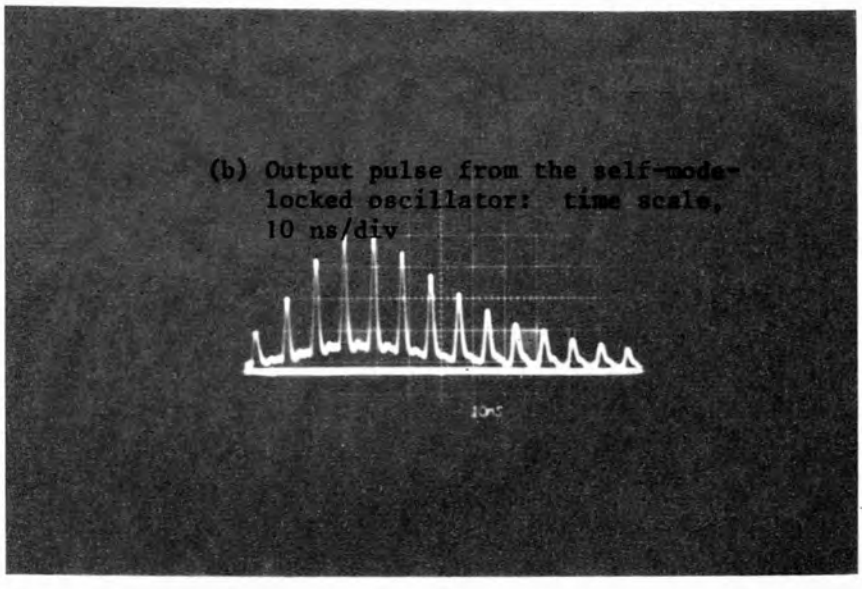

(b) Output pulse from the self-mode-locked oscillator: time scale, 10 ns/div.

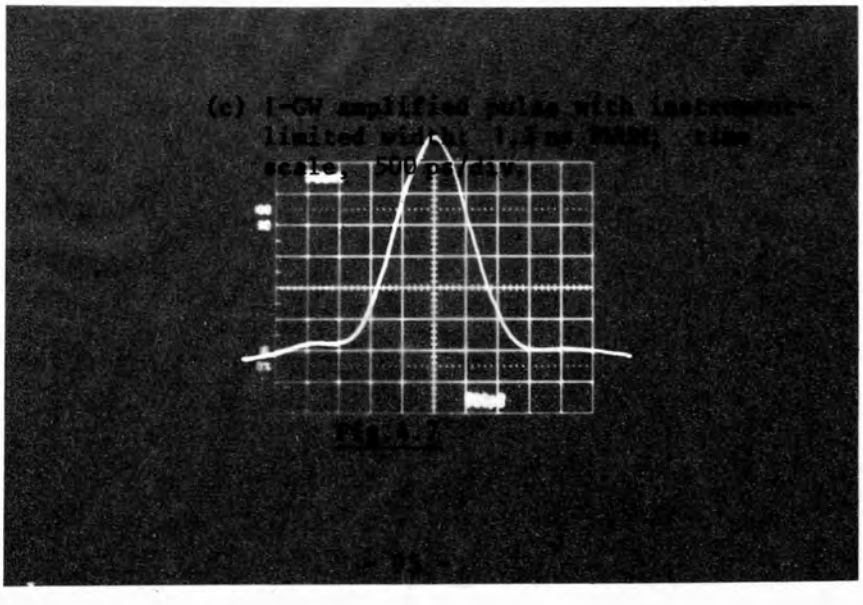

(c) [illegible]-GW amplified pulse with instrument-limited width; [illegible] ns FWHM; time scale, [illegible] ns/div.

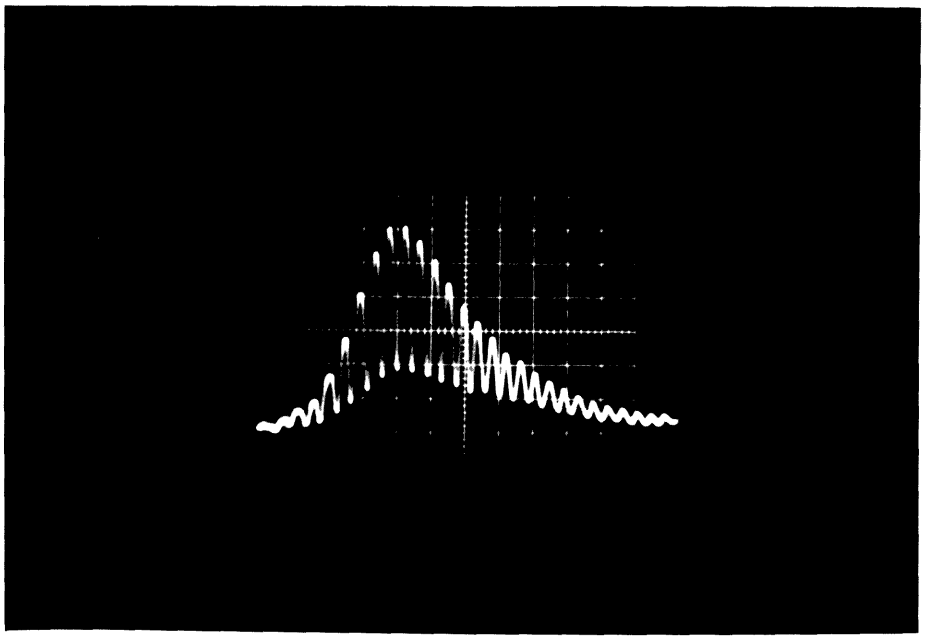

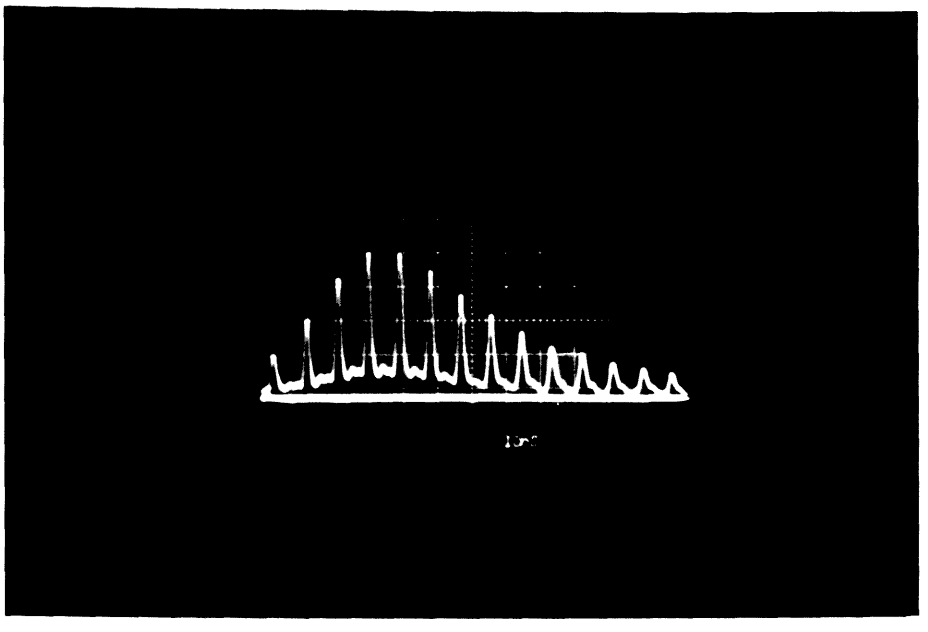

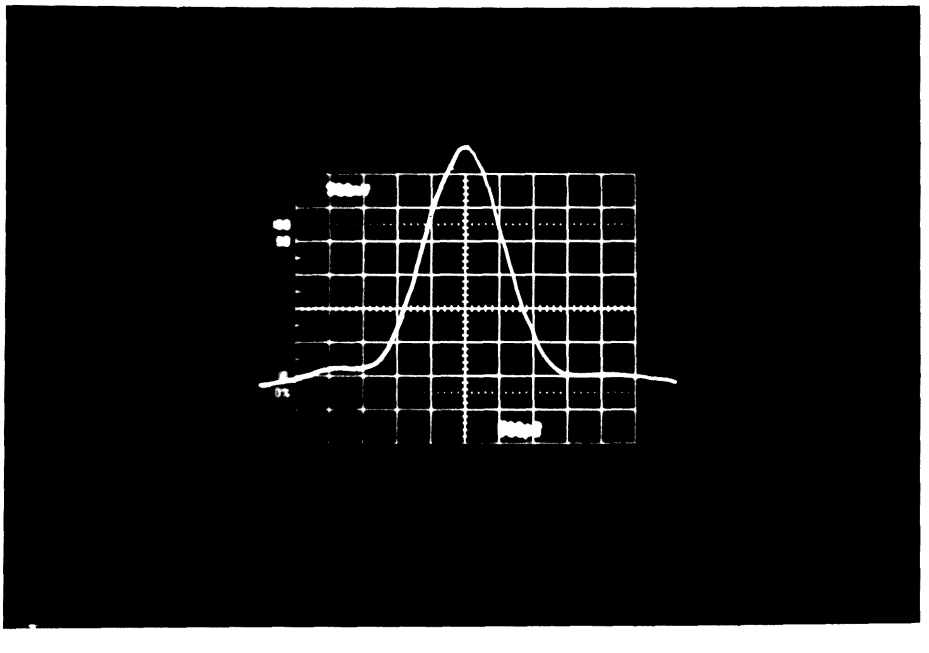

Fig.4.8
The Gigawatt CO_2 Laser System


WARNING
HIGH VOLTAGE
WARNING
Culham

Using this telescopic amplifier, ~55% of the energy available to an infinitely strong pulse (E_{ext} = 1.82 J, section 4.2) was extracted by a very weak pulse (1 mJ). This offers a major advantage over the methods employed at other laboratories[96-98] where the gigawatt level is obtained by using two to four laser modules having an active medium of 2 - 2.5 metres long.

Although telescopic amplification benefits weak input pulses in particular, it can even be used to advantage with fully saturating ns pulses. This is because ~ 40% of the active medium is twice traversed by the pulse (which cannot - as has been shown - normally extract all the energy stored in the (00°1) vibrational level, regardless of its intensity). Consequently, extra energy is extracted due to the rotational repopulation which takes place before the pulse makes its final pass through the amplifier.

It should be noted, however, that unless care is taken to ensure that the input beam is travelling sufficiently parallel to the laser axis, and the two mirrors are adequately aligned, the output will contain subsidiary pulses (Fig.4.3(c)). These apparently result from a feed-back into the amplifier - by the convex mirror - of part of the annular beam in its third pass.

Telescopic amplification of the kind described in this chapter could be used to advantage in larger high-power laser systems. In particular, electron-beam-controlled CO_2 and glass disc amplifiers - might well profit from exploiting this technique.

CHAPTER V

MULTI-LINE PULSE AMPLIFICATION

5.1 INTRODUCTION

It has been shown in the previous chapter (section 4.2) that the saturation energy parameter E_s of a TEA CO_2 laser amplifier - and, as a result, the maximum extractable energy - is greatly reduced when the duration of the input pulse is shortened. In particular it was found that a 1.1 ns single line pulse was capable of extracting no more than $\frac{1}{6}$ of the optical energy extractable by a 70 ns pulse. This substantial limitation on the efficiency of nanosecond pulse amplification originates from the fact that the optical energy stored in the upper laser level, i.e. the (00°1) vibrational level, is distributed over a large number of rotational sublevels. These sublevels are coupled via collisions with a relatively slow rotational relaxation time $t_R = 0.154$ ns atm. in a $CO_2 : N : He$, $1 : \frac{1}{6} : 2$ mixture (section 1.4.4).

A single line laser pulse - e.g. the P(20) of the 10.4 μm band - traversing a CO_2 amplifier extracts energy from only one of the rotational sublevels (J = 19) having a partition fraction K(19) = 0.064 at 400°K (equation (1.2). Therefore a pulse with duration shorter than the rotational relaxation time can extract, at most, only $\frac{K(19)}{2} = 3.2\%$ of the optical energy stored in the 00°1 vibrational level since neither repopulation of this sublevel nor relaxation of the corresponding lower level can take place during the pulse. Clearly, the longer the pulse the greater the extractable energy.

The influence of intramode vibrational-vibrational energy transfer can be ignored for pulses of duration $t_p < 100\ t_R$ [187]. On this assumption the amplification of a single line laser pulse is determined by the following rate equations[63,64]:

$$\frac{\partial n}{\partial t} + c\,\frac{\partial n}{\partial z} = \sigma c n \delta$$

$$\frac{\partial \delta}{\partial t} = -2\sigma c n \delta - \frac{\delta - K(J)\Delta}{t_R} \qquad \ldots (5.1)$$

$$\frac{\partial \Delta}{\partial t} = -2\sigma c n \delta$$

where $n = n(z,t)$ is the photon number density at position z and time t; δ, Δ are the inversion densities between the upper and lower rotational and vibrational levels respectively; and σ is the stimulated emission cross section.

The limiting solutions of these equations results in the well-known two-level amplifier equation derived by FRANTZ and NODVIK[148]:

$$E_{out} = E_s \ln\left\{1 + \exp(a_0 L)\left[\exp(E_{in}/E_s) - 1\right]\right\} \qquad \ldots (5.2)$$

where the value of the saturation energy parameter E_s ranges from $\frac{\hbar\omega}{2\sigma}$ to $\frac{\hbar\omega}{2K(J)\sigma}$ depending on pulse duration. This equation is also applicable to the amplification of a multi-line/multi-band pulse provided that an effective value $(E_s)_{ef}$ of the saturation parameter is used to correspond to the spectral content and pulse duration. This value is given approximately by[188]:

$$(E_s)_{ef} = f \cdot \frac{\hbar\omega}{K(J)\sigma}\left[1 - (1 - K)\exp(-Kt_p/t_r)\right] \qquad \ldots (5.3)$$

where f equals $\frac{1}{2}$ or $\frac{2}{3}$ for a single or double band pulse respectively and $K = \Sigma K(J)$ is the sum of the partition fractions of all the non-common upper levels of the rotational lines contained in the spectrum of the amplified pulse.

The stimulated emission cross section:

$$\sigma = \frac{\lambda^2 A_{u\ell}}{4\pi^2 \Delta\nu_H}$$

where $A_{u\ell} = 0.187\ s^{-1}$ (see section 1.4.1) and the homogeneous line width $\Delta\nu_H$[189]:

$$\Delta\nu_H = 7.58\left(\psi_{CO_2} + 0.73\,\psi_{N_2} + 0.64\,\psi_{He}\right)P.\left(\frac{300}{T}\right)^{\frac{1}{2}} \qquad \ldots (5.4)$$

was calculated to be $\Delta\nu_H = 4.37\ GHz$ for the pressure and gas mixture used.

Three methods have been proposed by means of which the energy extraction efficiency of nanosecond pulses can be improved[60,63]. In one of these methods, currently under investigation at Les Laboratoires de Marcoussis in France[190], the laser pulse traverses the amplifying medium eight times with an appropriately selected time delay between the consecutive passes so that not only rotational but also vibrational repumping and relaxation can take place. Another way to improve the efficiency is to reduce the value of the rotational relaxation time t_R by operating the amplifier at higher than atmospheric pressures. Finally the use of multiline pulses will increase the value of K and thus the extracted energy. The potentialities of this last approach were investigated experimentally and the results obtained are presented later in this chapter, following a description of the multi-line oscillator developed for the purpose.

5.2 THE MULTI-LINE OSCILLATOR

For multi-line operation, equalization of the net gain of several lines is required to prevent any single line from being dominant. The use of intracavity etalons[191], gaseous absorption cells[192,193], or ammonia mixed with the laser gas[194] have all resulted in multi-line oscillation. The wavelength-dependence of the transmission - in the case of the etalon - and of the absorption - in the other two cases - accounted for the gain equalization.

The normalized gain coefficients of the six strongest CO_2 laser transitions, measured by adopting the same procedure as in section 2.5.1, are shown in Fig.5.1. The anomalously high gain ($\sim$ 10%) of the P(20) line is attributed to stimulated emision from the so-called 'hot band' ($01^11 \rightarrow 11^10$) [145]. The wave-number difference between the P(20) and one of the hot band transitions, R(23), is less than a line-width[206] and this results in an increase in the gain coefficient of the P(20) line by an amount determined by the population inversion of the hot band.

The small signal gain of the P(20) line in the laser module used could be adjusted in the range of $0.015\,cm^{-1}$ to $0.025\,cm^{-1}$ approximately by changing the gas mixture and the electrical input energy. Thus, in order to equalize the gain per pass (active medium: 70 cm) of this line with one (or more) of the other five lines, a loss ranging from 10% to 23% had to be introduced on the P(20) line.

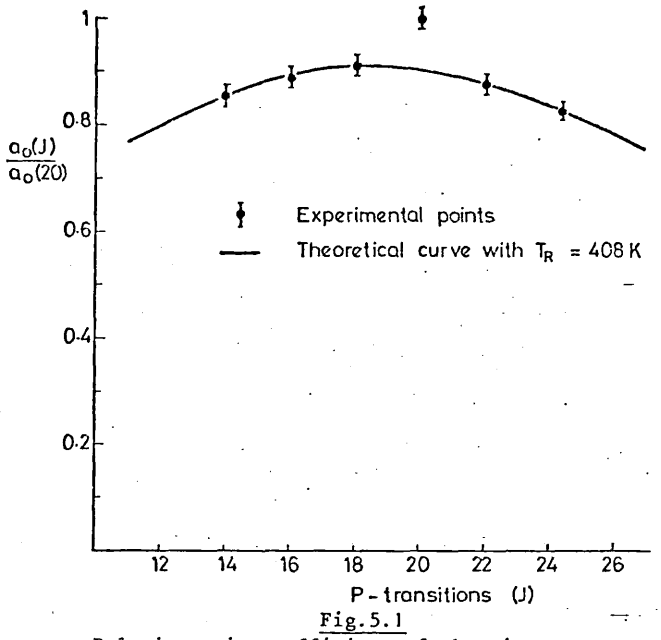

Fig.5.1
Relative gain coefficient of the six strongest transitions of the 10.4 µm band

An intracavity etalon in the form of a plane-parallel KCl plate provided the wavelength-dependent loss. The plate was mounted in such a way that it could be finely rotated around an axis perpendicular to the laser axis (Fig.5.2). For small angles of incidence θ, the transmittance of this etalon is given by[153, pp.323-9]:

$$T = \left[1 + \left[\left(\frac{\eta^2-1}{2\eta}\right)\sin\frac{2\pi\eta d\cos(\theta/\eta)}{\lambda}\right]^2\right]^{-1} \qquad \ldots (5.5)$$

where $\eta = 1.454$ is the refractive index of KCl and d is the thickness of the plate. Equation (5.5) represents an approximate sine-squared modulation of the transmission function with amplitude 13%.

Tuning of a single etalon resulted in reliable two-line operation. It was found however, that in order to obtain three-line emission using one etalon it was necessary to reduce the small signal gain. Nevertheless, reliable three-line emission at full pumping was obtained by combining two uncoupled intracavity etalons.

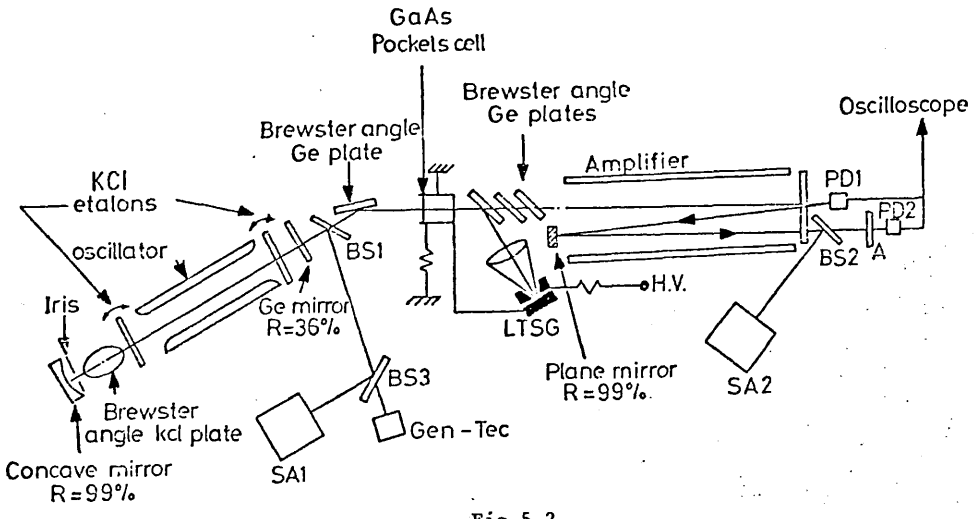

Fig.5.2
Experimental arrangement for multi-line pulse amplification

The equalization of the intensities of the emitted lines was also possible - unlike in the case of a single etalon - with careful tuning. Reproducible operation on any three of the P(16) - P(22), as well as any two of the P(14) - P(22), lines was readily achieved.

The importance of the parallelism of the KCl etalons should be emphasized. Plates with wedge angles $\phi \geq 1.4 \times 10^{-4}$ rad had no effect on the spectral properties of the oscillator because, as can be easily shown, in order to introduce the minimum required 10% loss in the P(20) line, the wedge angle must be $\phi \leq \frac{1.1}{D} \times 10^{-4}$ rad where D, in cm, is the diameter of the laser beam.

The spectral characteristics of this oscillator were examined using a CO_2 laser spectrum analyser (Optical Engin. Model 16 - A). The various lines of the laser beam were spatially separated by the diffraction grating of this device, and displayed on a calibrated graphite screen. The relative intensity of the different lines was ascertained by observing the intensity of the incandescence induced by each line on the graphite.

The total energy output measured by a Gen-Tec calorimeter was constant for either single or multiline operation. This represents an advantage

offered by the use of KCL etalons - as opposed to gaseous absorbers - for multiline oscillation where the output energy suffers a 50 - 75% reduction[193].

5.3 MULTI-LINE NANOSECOND PULSE GENERATION

The same procedure as that adopted for the generation of single-line nano-second pulses was also applied to the generation of multiline pulses. However, a simultaneous spectral analysis of both the long and the nano-second pulse (see Fig.5.2) revealed that, in most cases, not all the lines contained in the long pulse were present in the spectrum of the nanosecond pulse. The recording of the fine structure of the long pulse shape on a fast oscilloscope using a photon drag detector offered a possible explanation of this discrepancy.

It was observed that when the long pulse shape was similar to the one shown in Fig.5.3(a), the spectrum of both pulses contained three lines. Conversely, the nanosecond pulse contained two or - more often - only one line when the pulse shape was similar to the one shown in Fig.5.3(b). On the basis of this observation, it could be reasonably argued that the recorded output pulse is the superposition of three independently oscillating pulses, each one emitting only one line. Because the oscillation is restricted to the fundamental transverse mode, the output pulse of each line is nearly 100% self-mode-locked with a shape similar to the one shown in Fig.5.3(a), i.e. a train of ~ 2 ns pulses at intervals of ~ 9 ns.

Therefore, a three-line nanosecond pulse should be expected only when the individual pulses of the three independent oscillations coincide. The small probability ($\sim$ 5%) for such a coincidence necessitates multi-transverse mode operation in which the self-modulation is $\sim 20\%$ (Fig.5.3(c)). This operation, achieved by the removal of the mode-limiting aperture (iris), resulted in reliable three-line nanosecond pulse generation.

Finally, as will be seen in the next chapter, the approximately equal intensity of each line must be ensured by careful etalon tuning because - in

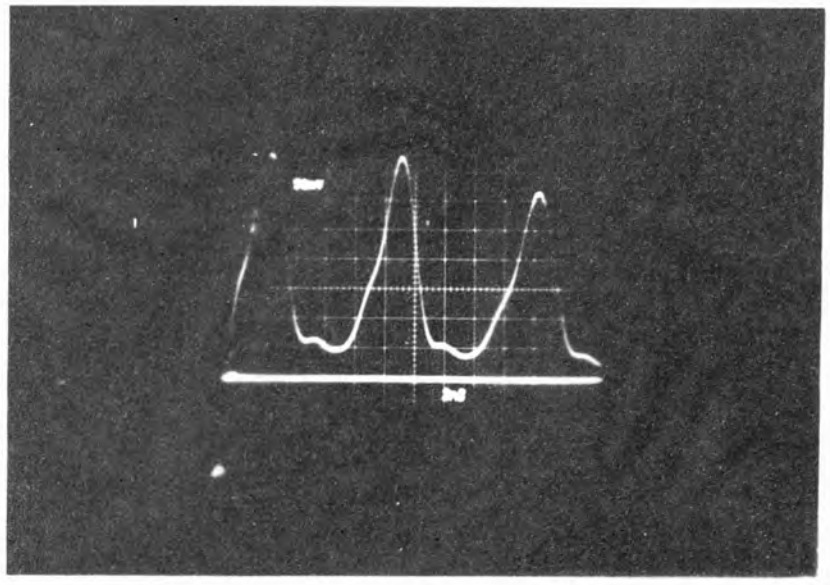

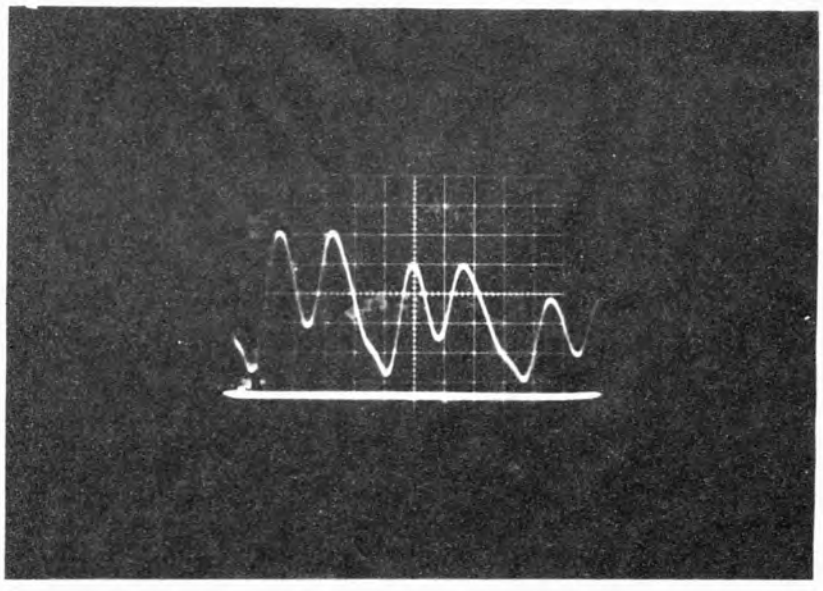

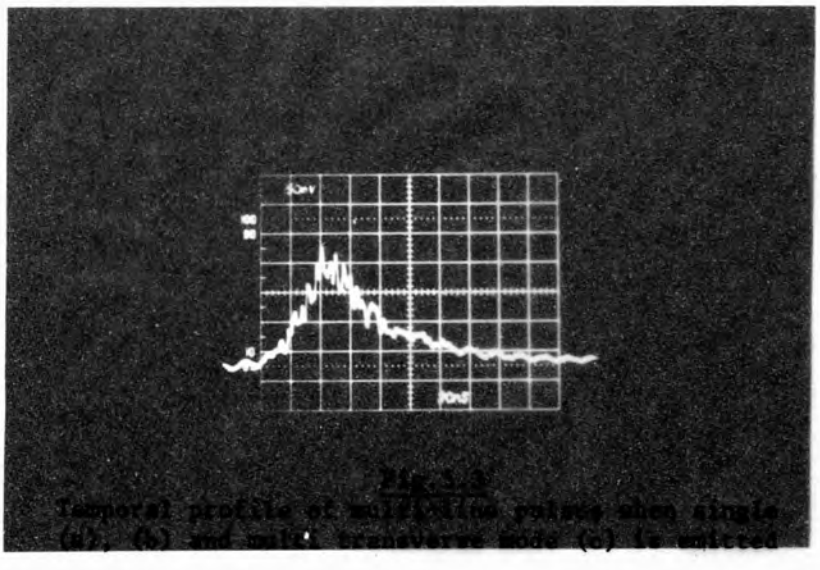

Fig. 3.3
Temporal profile of multipulse pulses when single (a), (b) and multi transverse mode (c) is emitted

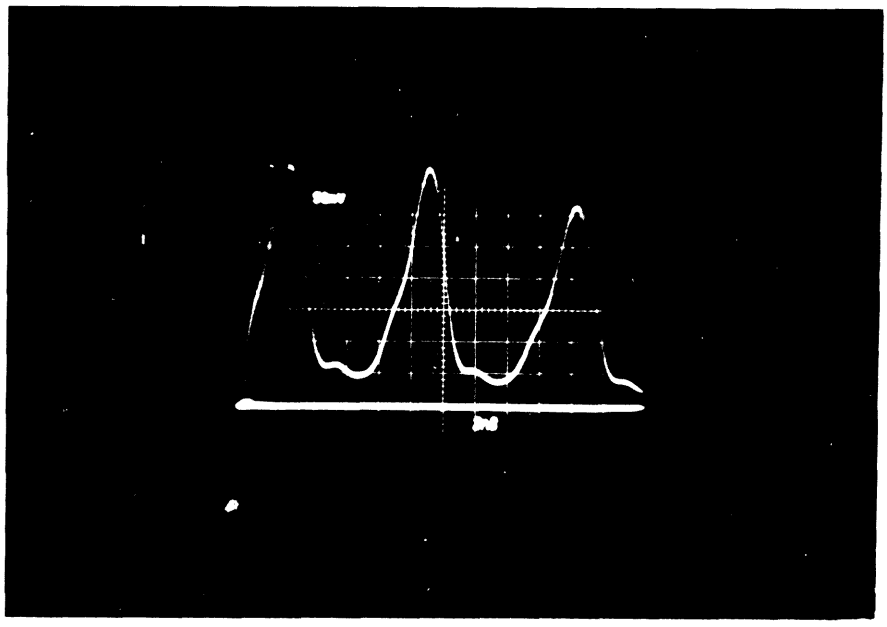

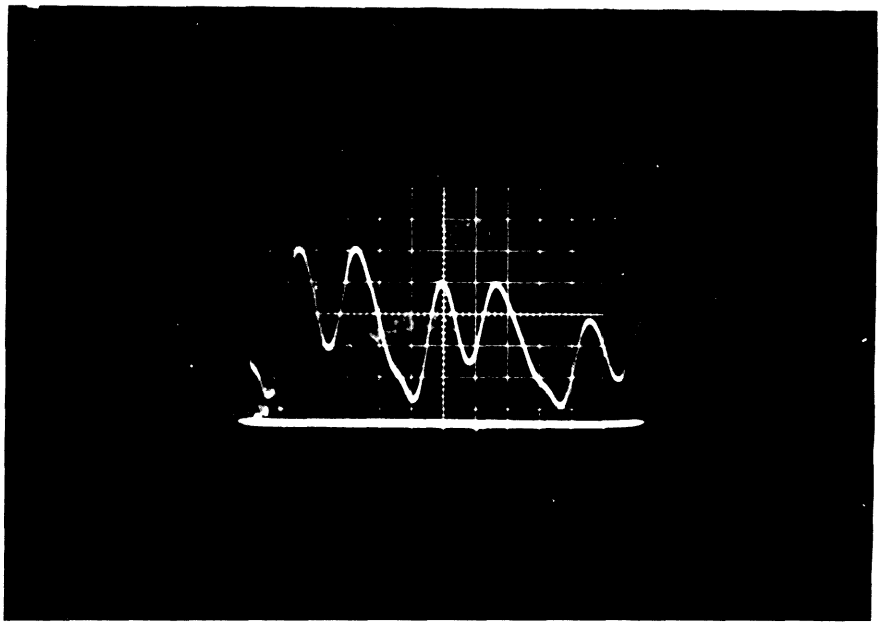

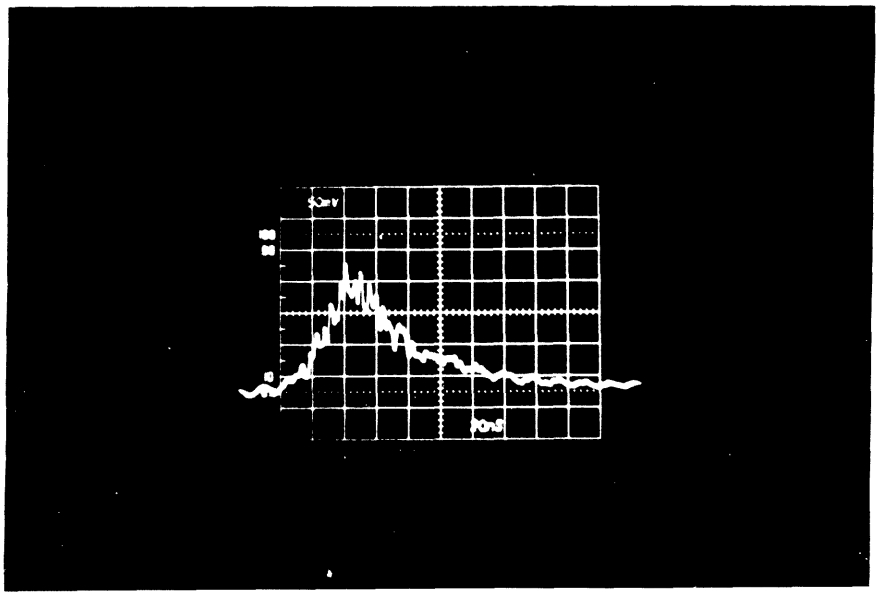

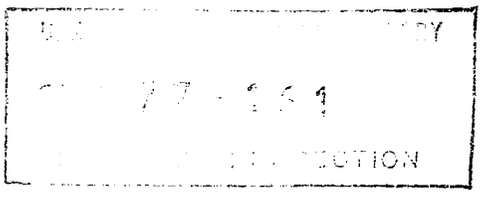

the case of unequal intensities - the long pulses, as a whole, could be considerably displaced in time and this again will result in a nanosecond pulse of fewer than three lines.

5.4 AMPLIFICATION OF MULTI-LINE NANOSECOND PULSES

In order to amplify the low power nanosecond pulses emitted from the multiline oscillator - electro-optical shutter system - and, at the same time, to measure the input energy, the experimental arrangement shown in Fig.5.2 was used.

The generated multiline nanosecond pulse was monitored after its first pass through the amplifier, using the photon drag detector PD1. The reflected beam from the polished plane surface of this detector traversed the amplifier where - after its second pass - it was directed by a fully reflecting plane mirror for its third and final pass through the active medium. The fraction of the output reflected by the beam splitter, BS2, was directed to the spectrum analyser, SA2, while the fraction transmitted by the beam splitter and a calibrated attenuator, A, was monitored on a second photon drag detector, PD2. The output of the two detectors was displayed on a Tektronix 7904 oscilloscope.

Figures 5.4(a) and 5.4(b) show the oscilloscope records of the input pulse (on the left) and the output pulse (on the right) for one and three lines respectively. It can be clearly seen that an approximately equal input power results in a different output for the two cases.

The known degree of attenuation of A, as well as the known reflectivities of: the PD1; the KCl output window of the amplifier: and the BS2, allowed the calculation of the input and output intensities for a series of single-, double- and triple-line pulses to be made. The results of these energy extraction measurements are shown in Fig.5.5 where the output energy density is plotted against the input. The theoretical curves in this figure

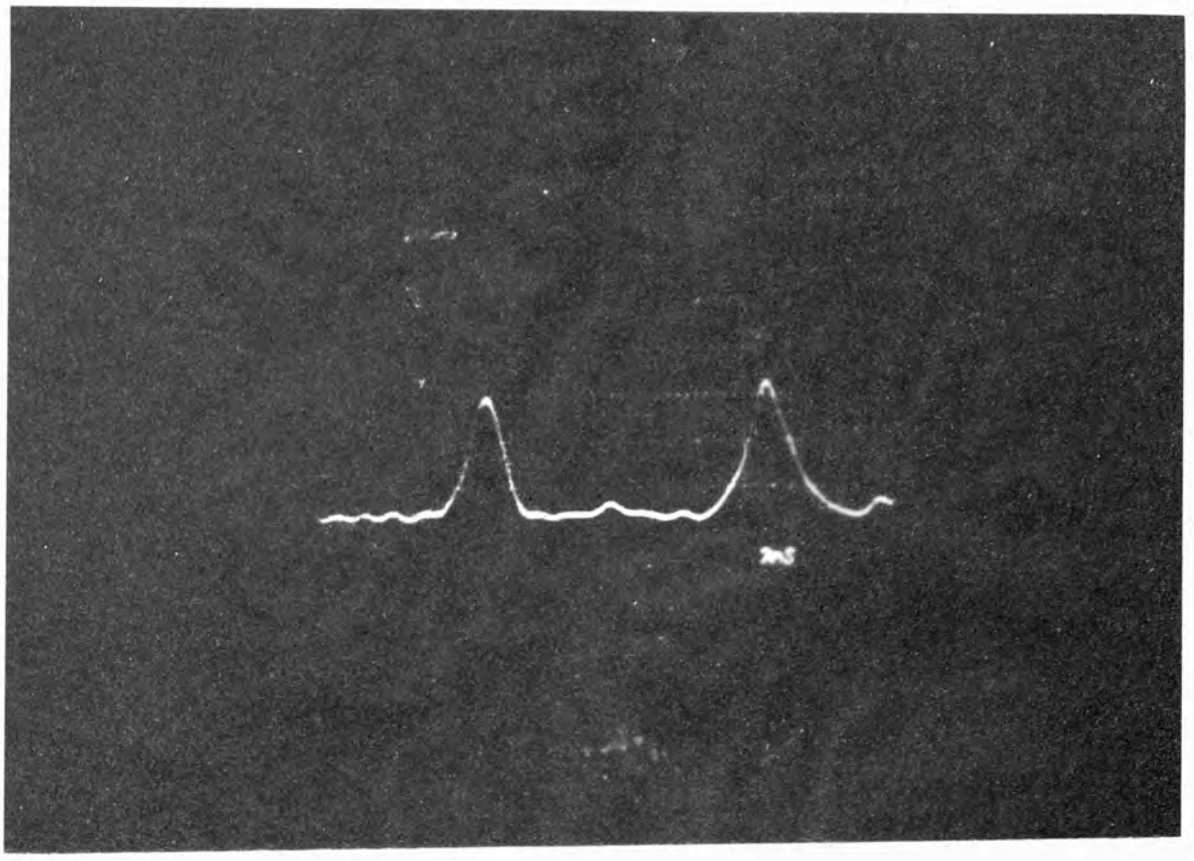

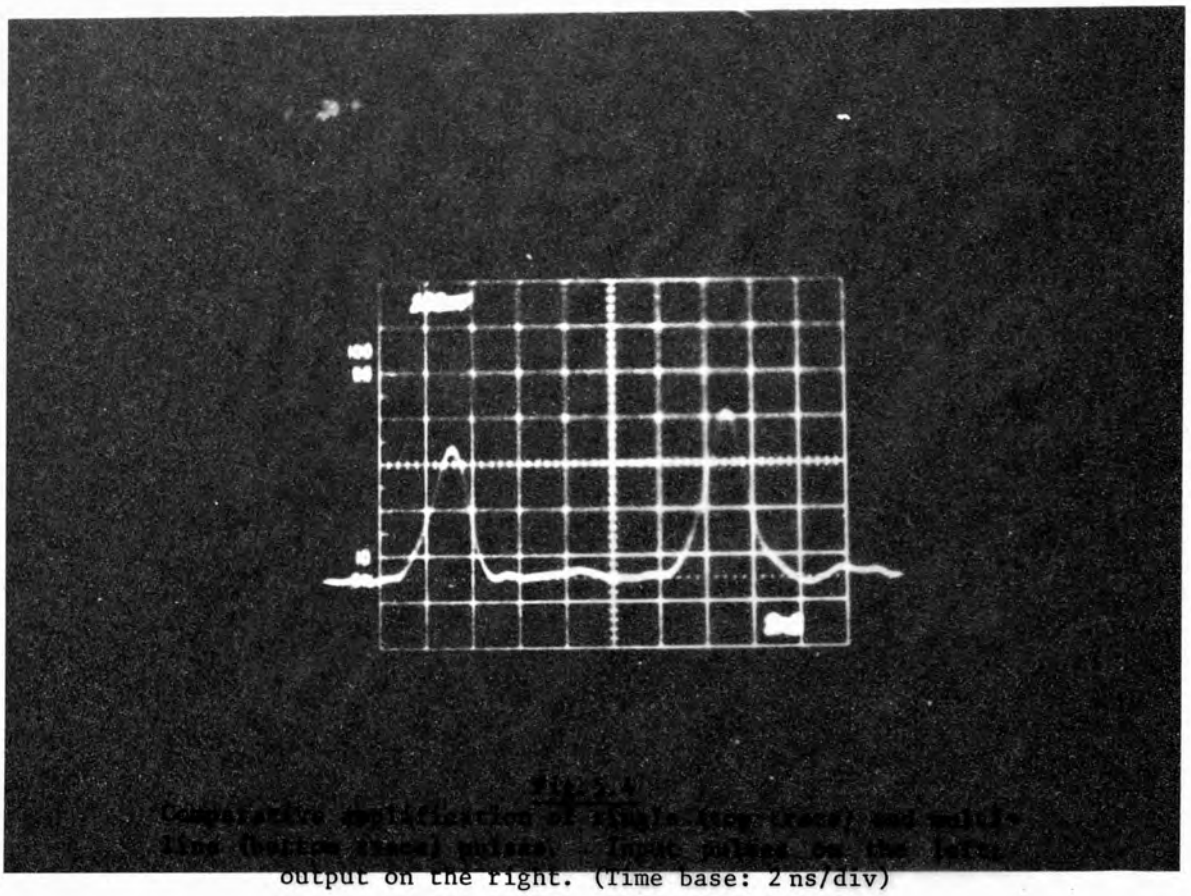

Fig. 2.4
Comparative amplification of single-ring (top trace) and multi-ring (bottom trace) pulses. Input pulses on the left, output on the right. (Time base: 2 ns/div)

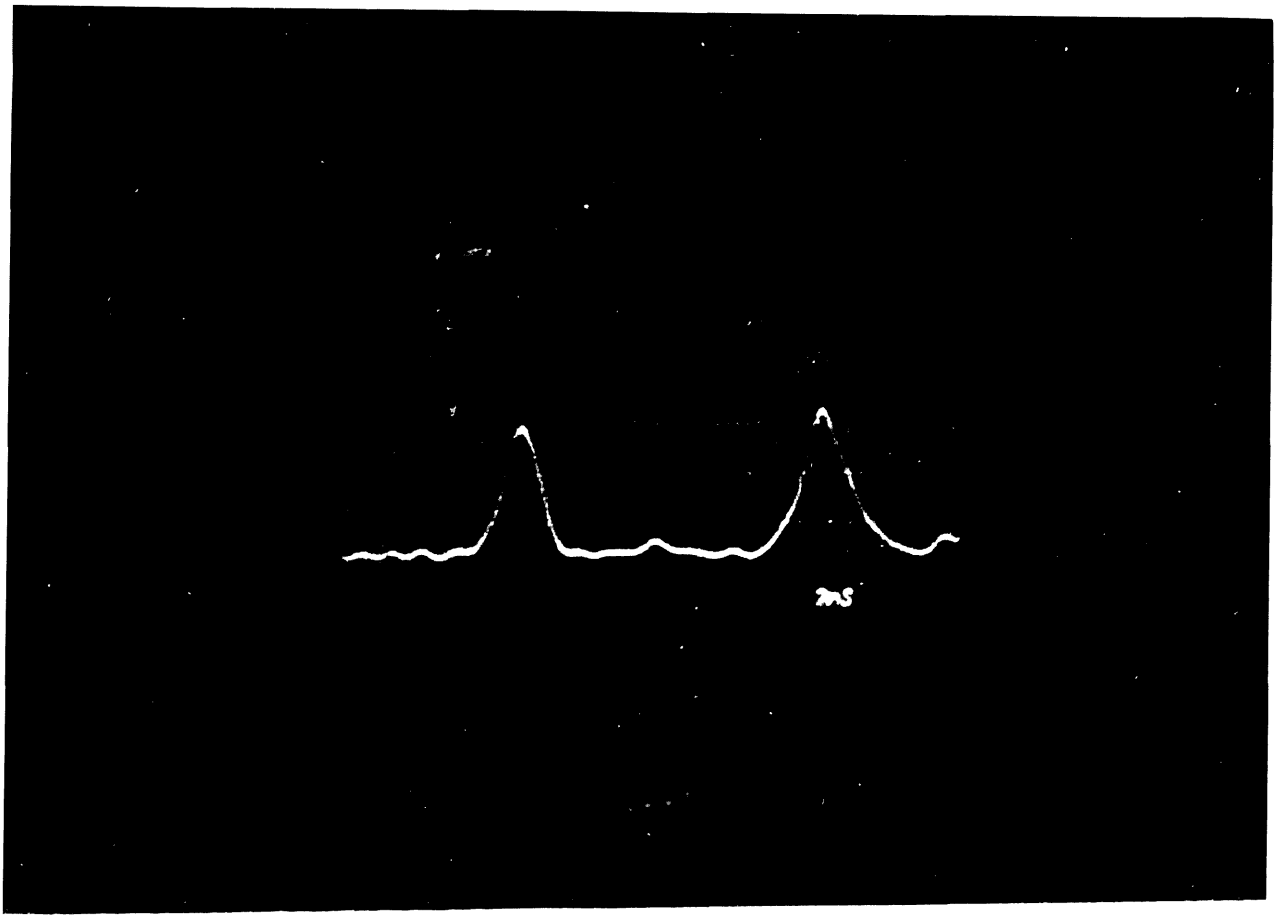

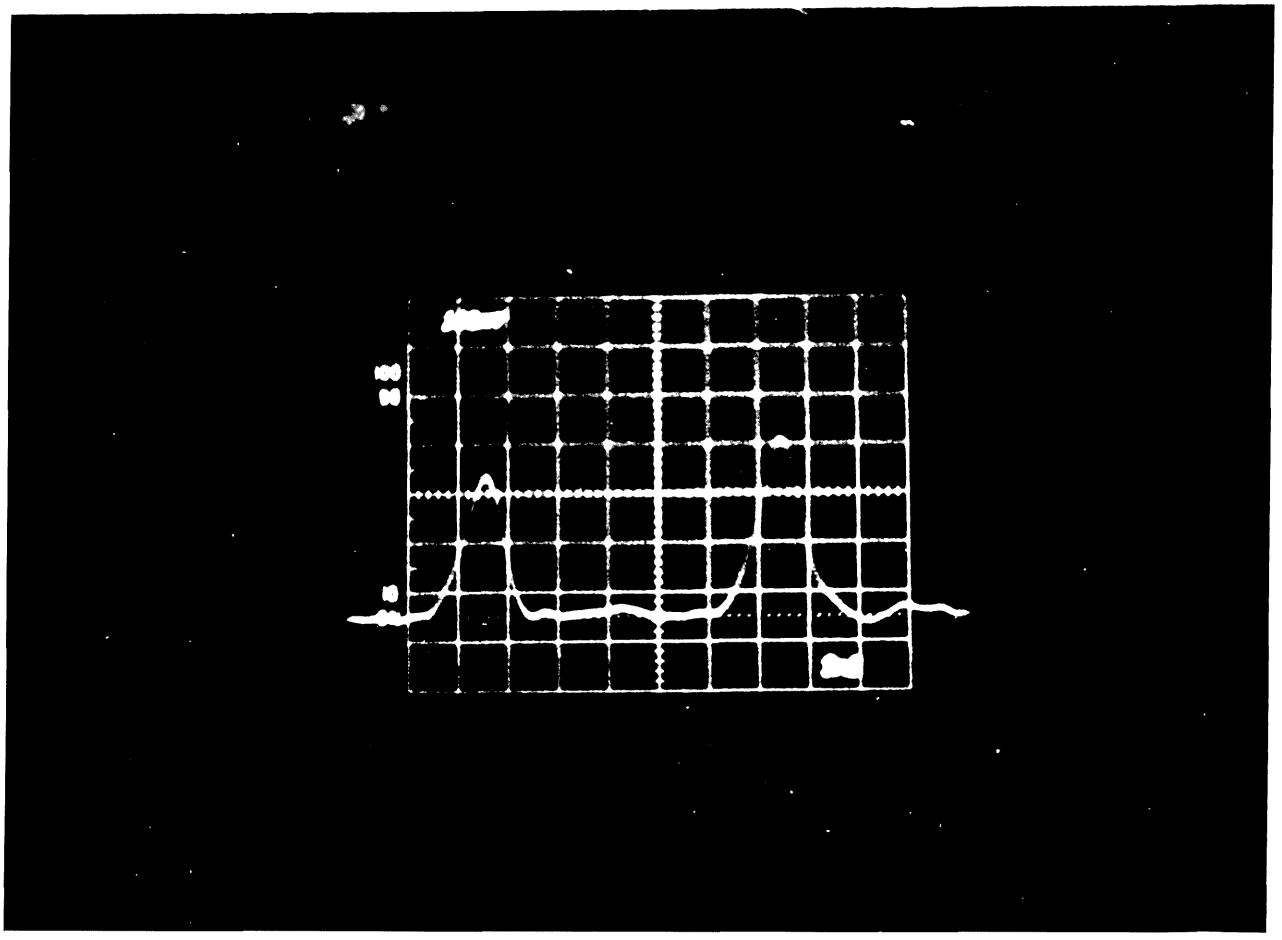

5.4

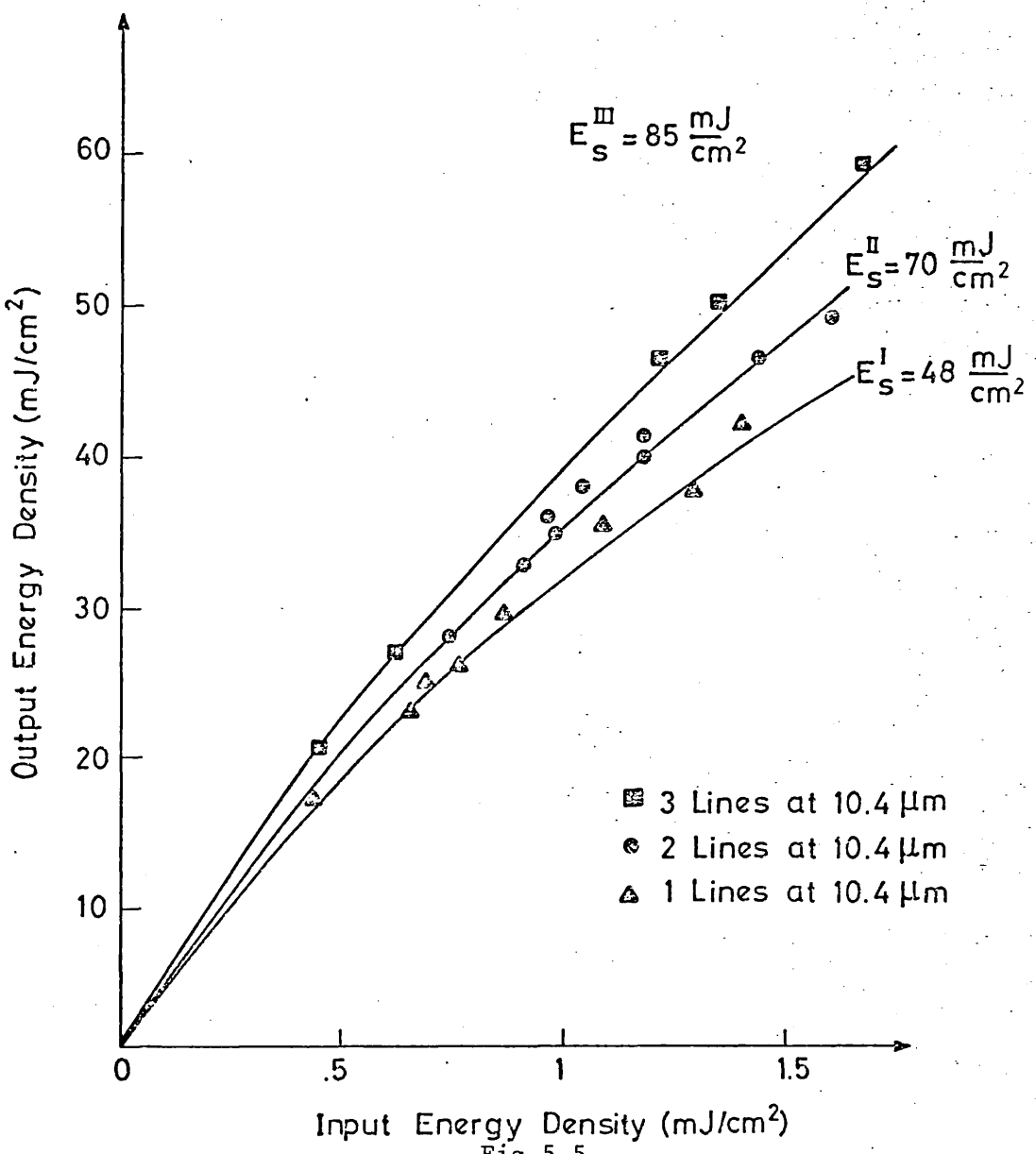

Fig.5.5

Comparison between the experimental and calculated energy extracted by single-, double- and triple-line pulses

were calculated using equation (5.2). The optimum fit to the experimental points is obtained when the saturation energy takes the values

$$E_s^I = 48 \text{ mJ/cm}^2 \text{ , } E_s^{II} = 70 \text{ mJ/cm}^2 \text{ and } E_s^{III} = 85 \text{ mJ/cm}^2$$

for one, two and three lines respectively.

These results indicate that the energy extractable by a ~ 1.7 ns pulse from a TEA CO_2 amplifier can be increased by $\sim 46\%$ or by 77% when a two or three line pulse is amplified instead of a single-line pulse. Using $t_p = 1.7$ ns and $t_R = 0.154$ ns the increase in the extractable energy predicted by equation (5.3) is found to be 44% in the case of two lines ($K = 0.127$) and 64% for three lines ($K = 0.189$). The agreement between the theoretical and experimental results is highly acceptable. This advantageous use of multi-line nanosecond pulses has also been supported by experiments carried out at Los Alamos Scientific Laboratory[195] and by the Marcoussis group in France[190].

5.5 CONCLUSIONS

The theoretically predicted improvement in energy extraction in nanosecond pulse amplification using multi-line pulses was experimentally verified. Although the use of KCl etalons could not provide double-band multi-line operation, it has the advantage of simplicity and does not adversely affect the oscillator output.

The amplification of multi-line pulses remains the only proven method - to date - for obtaining higher amplifier efficiency, for the efficacy of the multi-pass method has yet to be validated. Judging from the problems associated with the suppression of parasitic and self-oscillation, already experienced with the three-pass telescopic amplifier described in the previous chapter, it can be assumed that the same problems will present some difficulty in the realization of this - otherwise - excellent approach.

The more distant prospect of large-volume, high-pressure (> 5 atm) amplifiers will eventually diminish the importance of multi-line amplification as far as efficient extraction of the stored energy is concerned. However, as has been shown in the previous chapter (section 4.3), multi-line input pulses eliminate the pulse-broadening associated with the single-line CO_2 amplifier which might otherwise distort the shape of the input pulse to a degree unacceptable for laser fusion experiments.

Finally, a different - though less serious - pulse distortion effect, detected by SCHAPPERT and HERBST[196] deserves mention here. They have shown that the velocity of a short pulse is reduced when it is propagated through a CO_2 laser amplifier rather than through a zero gain medium. This delay, which is proportional to the gain coefficient, is particularly important for the amplification of multi-line pulses. In such a case, the pulse is broadened as a result of the gain coefficient difference between its spectral components effecting an unequal delay during amplification. If $\Delta\alpha_0$ is the gain coefficient difference of two lines, an active medium of length L_a will produce a separation of the two components by[196]:

$$\Delta t = \frac{L_a \Delta\alpha_0}{2\pi\Delta\nu_H} . \qquad \ldots (5.6)$$

In a typical chain of CO_2 laser amplifiers - such as that presently under construction at Culham (OPALS - TROJAN) - $\alpha_0 L_a \simeq 20$ and, as equation (5.6) implies, the P(20) line, at atmospheric pressure, will be delayed by ~ 100 ps more than the adjacent lines over which it has a 10% higher gain, and by an even wider margin over the more distant lines where the gain difference is still greater. This undesirable pulse broadening can, however, be minimized by operating the amplifiers at higher than atmospheric pressure since (a) $\Delta t \propto \frac{1}{\Delta\nu_H} \propto \frac{1}{P}$, and (b) at pressures $P > 2$ atm all P-branch lines in the 10.4 μm band are overlapped by the hot band lines[197] thereby reducing the gain difference $\Delta\alpha_0$ between the P(20) and other P-lines of this band.

CHAPTER VI

LONGITUDINAL MODE SELECTION : THREE MIRROR RESONATOR

6.1 INTRODUCTION

To generate nanosecond CO_2 laser pulses by gating the output of a single longitudinal mode oscillator, rather than by switching out a single pulse from the pulse train of a mode-locked laser, is more advantageous since it allows resonant gaseous absorbers to be used to improve the signal-to-background noise ratio[198,199]. Hot CO_2 ($\sim 725^{\circ}K$) at a pressure of $\sim$ 30 torr could act as a narrow-band absorber to selectively absorb the background pulse which has an equally narrow spectral width while the broad-band pulse is transmitted with negligible attenuation.

A novel method for single longitudinal mode operation was devised during the present research[89] whereby a three-mirror resonator (TMR) was used in a coupled unstable resonator arrangement as shown in Fig.6.1. The active medium of the Double-Discharge module described in Chapter II was utilized resulting in the attainment of peak powers in the range 30-100 MW.

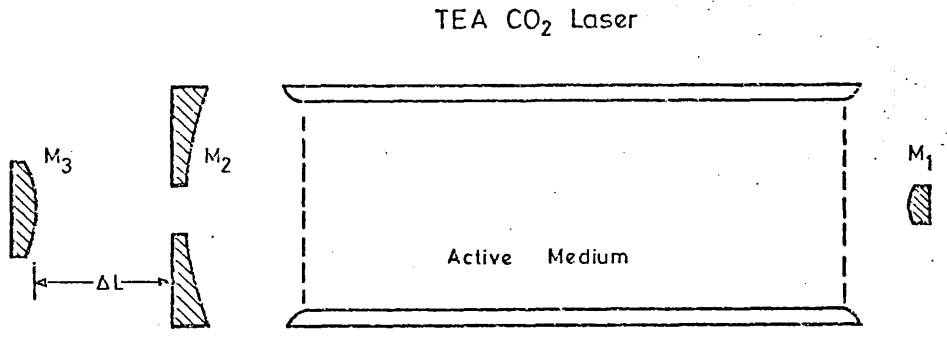

Fig.6.1
Schematic Diagram of the TMR

The optical system consisted of two unstable resonators coupled by the common convex mirror M1 and sharing the active medium. The basic principle of the operation of this single frequency oscillator can be

outlined as follows. Each resonator has been designed to have a diffraction loss slightly exceeding the maximum available gain (i.e. the net round trip gain $g \leqslant 1$) and therefore neither can oscillate independently.

However, modes which are resonant in both cavities will experience a smaller diffraction loss and therefore could, in principle, oscillate. The frequency spacing between these modes - which will henceforth be referred to as TMR modes - is:

$$\Delta \nu = \frac{c}{2\Delta L} \qquad \ldots (6.1)$$

where ΔL is the difference in length of the two cavities. Therefore, for a sufficiently small ΔL the value of $\Delta \nu$ can be made approximately equal to the frequency range over which the gain exceeds the loss of the three-mirror resonator. In this way, oscillation on a single longitudinal mode in the P(20) line of the 10.4 μm band can be ensured.

6.2 MECHANISM OF THE SINGLE FREQUENCY OPERATION OF THE THREE-MIRROR RESONATOR

A possible interpretation of the single longitudinal mode operation will be offered here, based on SOOY's[200] analysis where the mode selection is attributed to the different build-up time of the various modes on which oscillation is possible. A pre-requisite of such an analysis is the estimation of the diffraction loss of the three-mirror resonator and of the number of round trips required for the build-up of the emitted power.

6.2.1 Diffraction Loss and Threshold Condition of the TMR

If it is assumed that the two resonators formed by the mirrors $M_1 M_2$ and $M_1 M_3$, when separately considered, have equal diffraction loss per round trip, δ, and are both just below the oscillation level, the following relation applies:

$$|\gamma|^2 = M^{-2} \simeq e^{-2\alpha_0 L_a} \qquad \ldots (6.2)$$

where $M^{-2} = |\gamma|^2 = 1 - \delta$ is the fractional power feed-back per round trip in each resonator, M is the magnification of the $M_1 M_3$ resonator, α_0 is the

small signal gain and L_a is the length of the active medium. Thus, the power feed-back for a TMR mode is approximately:

$$M^{-2} + |\gamma|^2 \simeq 2e^{-2\alpha_0 L_a} \qquad \ldots (6.3)$$

and the oscillation threshold condition for such a mode becomes:

$$2 \exp\left[2 L_a (\alpha - \alpha_0)\right] > 1 \qquad \ldots (6.4)$$

where α is the small signal gain which corresponds to the frequency of this mode.

In the present case, $L_a = 100\,\text{cm}$ and $\alpha_0 = 0.031\,\text{cm}^{-1}$ and so the above relation is equivalent to:

$$\alpha > 0.888\,\alpha_0 \,. \qquad \ldots (6.5)$$

This relation indicates that oscillation is possible on the frequency range over which the gain is greater than 88.8% of that at the line centre. For TEA CO_2 lasers the line is pressure-broadened and the small signal gain is given as a function of frequency ν by[196]:

$$\alpha(\nu) = \alpha_0 (\tfrac{1}{2}\Delta\nu_H)^2 \left[(\nu - \nu_0)^2 + (\tfrac{1}{2}\Delta\nu_H)^2 \right]^{-1} \qquad \ldots (6.6)$$

where ν_0 is the frequency at the line centre and $\Delta\nu_H$ is the line width (FWHM). For the mixture used ($CO_2 : N_2 : He$, $1 : \frac{1}{6} : 2$) the value of $\Delta\nu_H$ can be calculated[189] to be $\Delta\nu_H = 4.37\,\text{GHz}$. Thus using the relations (6.5) and (6.6), it can be ascertained that oscillation is possible on a range which extends only 765 MHz either side of the line centre. Therefore, by making the difference in length of the two resonators $\Delta L < 9.8\,\text{cm}$, the inter-mode frequency spacing given by equation (6.1) becomes greater than the frequency over which oscillation is permitted.

6.2.2 Experimental Observations

For values of $\Delta L < 25\,\text{cm}$ however, it was found that the TMR had a multi-mode output similar to that of the two-mirror resonator with the familiar mode beating, despite keeping both resonators below the oscillation threshold. Pulse shape records taken using a photon drag detector[112] and

a fast oscilloscope (Tektronix 7904) revealed that the frequency spacing of the emitted modes was, to a high approximation, given by $\Delta\nu = \frac{c}{L_1 + L_2}$ where L_1 , L_2 are the lengths of the $M_1 M_2$ and $M_1 M_3$ resonators respectively. When $\Delta L > 25$ cm, pulses with a smooth temporal profile - with peak power ~ 30 MW - were obtained, a typical example of which is shown in Fig. 6.2(a).

Such pulse shapes could be conclusive evidence of single longitudinal mode operation if it could be shown that the detection system had a sufficiently fast response to resolve the ~ 600 MHz modulation which would result when more than one mode was emitted. The only other case in which smooth pulse shapes could occur is the emission of a large number of modes, and this condition can be safely ruled out here on account of the narrow frequency range over which oscillation can occur.

When the frequencies of the TMR modes are symmetrically placed about the line centre (a condition which can be achieved by a fine adjustment of ΔL) the two modes on either side of the line-centre experience the same gain and should, therefore, both be emitted. Interaction of these two modes should result in a sinusoidal waveform - such as that shown in Fig.6.3(c) - with frequency equal to $\Delta\nu = \frac{c}{2\Delta L}$.

The 580 MHz recorded modulation frequency closely corresponds to the calculated value when $\Delta L = 26$ cm as was the present case.

Thus the waveform of Fig.6.3 not only strongly supports the single longitudinal mode nature of the pulses in Figs.6.2, 6.4, 6.5, but also substantiates the assumption made earlier that the intermode frequency spacing in the TMR is given by equation (6.1).

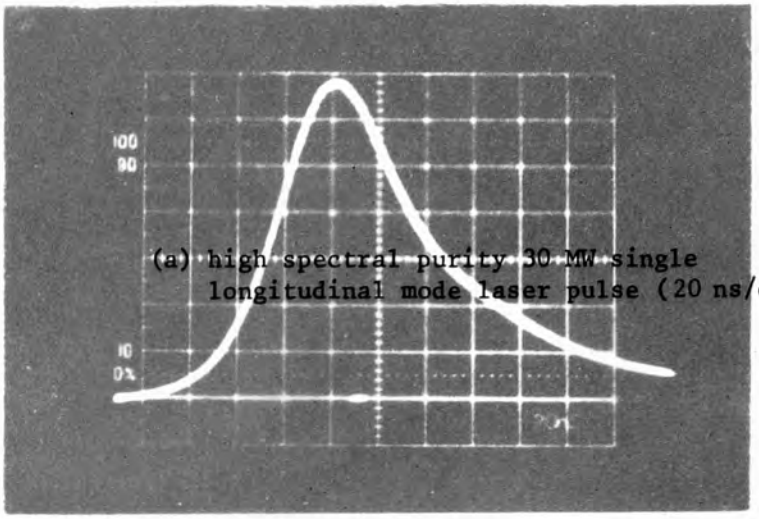

(a) high spectral purity 30 MW single longitudinal mode laser pulse (20 ns/div)

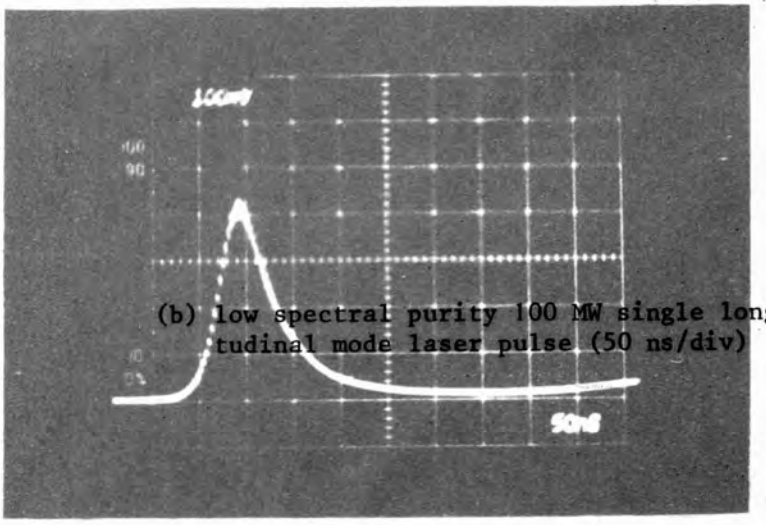

(b) low spectral purity 100 MW single longitudinal mode laser pulse (50 ns/div)

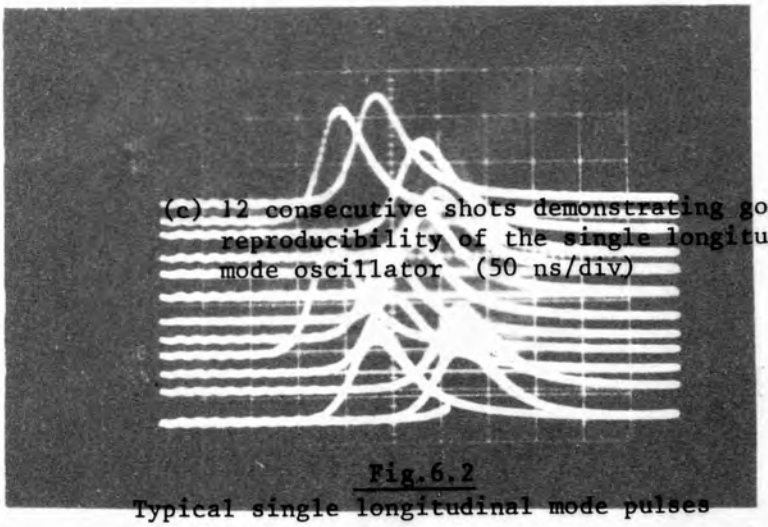

(c) 12 consecutive shots demonstrating good reproducibility of the single longitudinal mode oscillator (50 ns/div)

Fig.6.2
Typical single longitudinal mode pulses

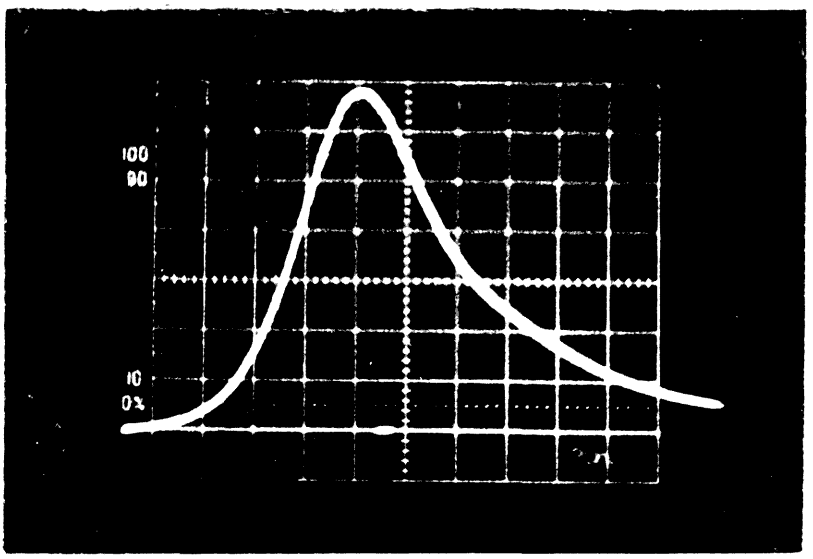
100
90
10
0%

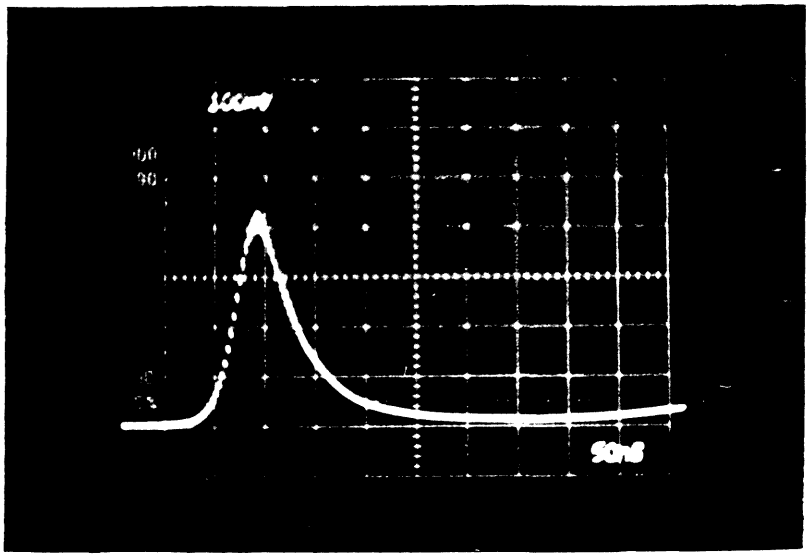

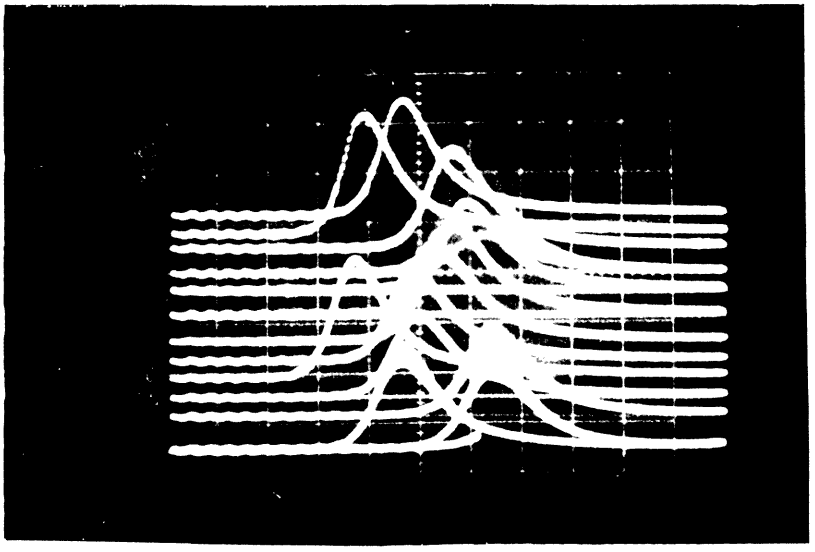

76/141

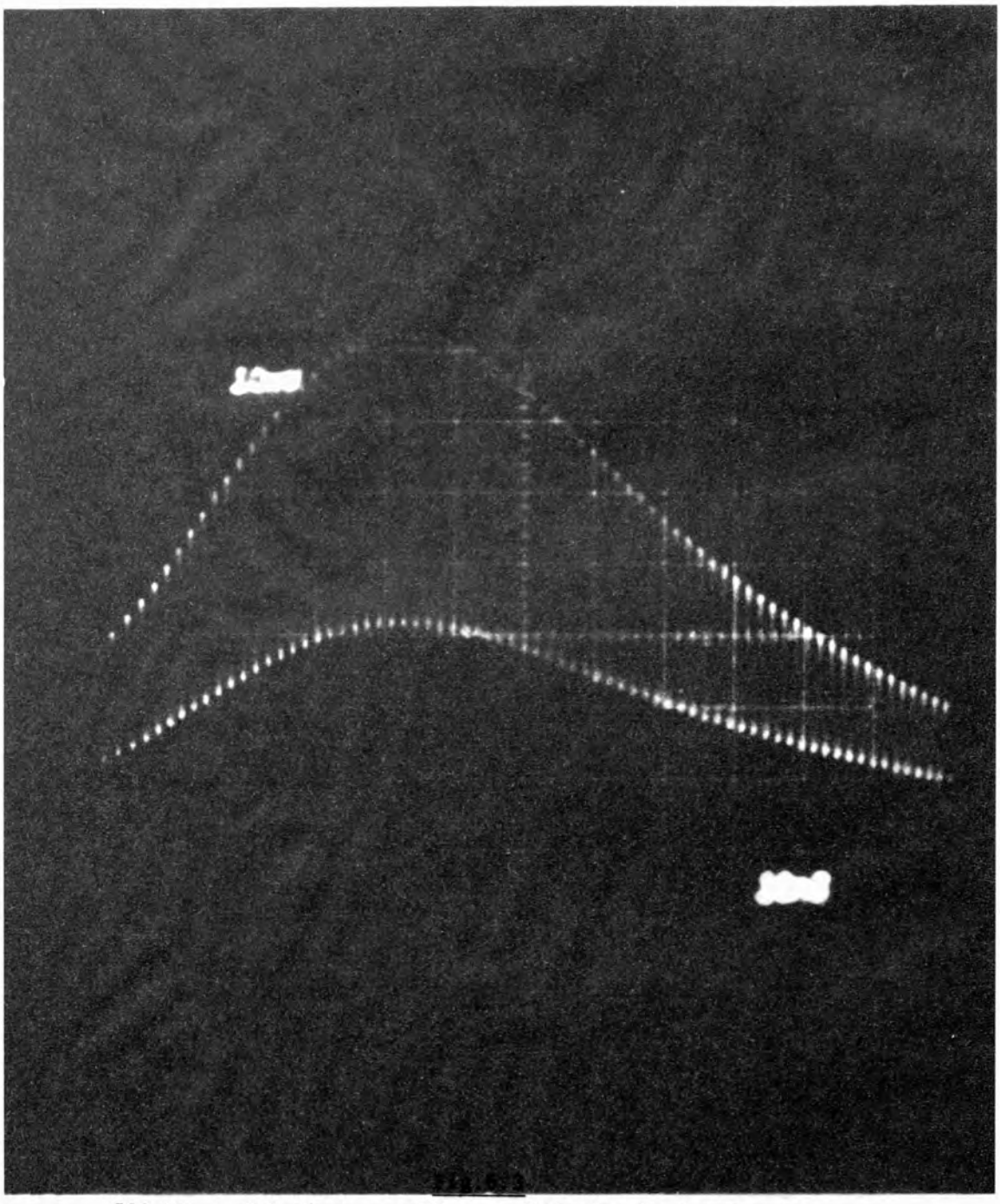

580 MHz modulation revealing oscillation in 2 TMR modes

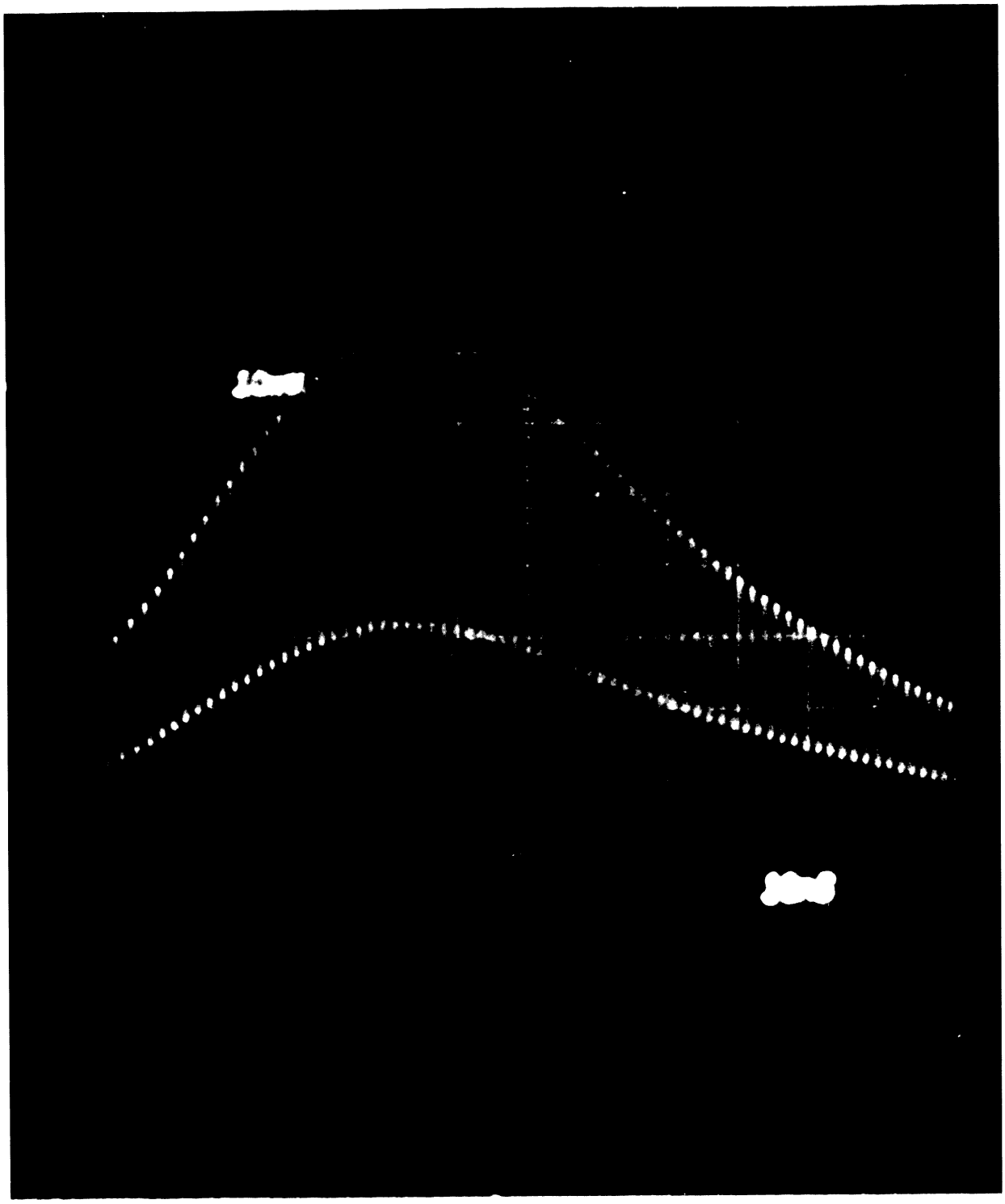

6.2.3 TMR Mode Selection: Pulse Monochromaticity

Using the equations (6.3) and (6.6), it can be shown that the peak net round trip gain $g(\nu)$ experienced by a TMR mode having frequency ν is given by:

$$g(\nu) = 2 \exp\left\{-2\alpha_0 L_a(\nu - \nu_0)^2 \left[(\nu-\nu_0)^2 + (\tfrac{1}{2}\Delta\nu_H)^2\right]^{-1}\right\} \quad \ldots (6.7)$$

The maximum value of $g(\nu_0) = 2$ is experienced by the TMR mode lying at the line centre. In this case the gain of the two adjacent modes having the frequency $\nu = \nu_0 \pm 580$ MHz is $g(\nu) = 1.315$. As a result of this difference in the round trip gain, these modes will develop a progressively increasing difference in their intensities as they grow independently away from the same level of spontaneous emission (10^{-12} W [201]).

To build up to the observed peak powers of the order of 10^7 W a signal augmentation of $G \simeq 10^{19}$ is required. The number of round trips, q, through the active medium necessary for such an augmentation cannot be easily estimated because the value of $g(\nu_0)$ varies with time in the range $1 < g(\nu_0) < 2$ during the intensity build-up. Nevertheless the lower limit in the value of q can be estimated as: $q = \frac{\ell n\, G}{\ell n\, 2} = 63$. On this basis, the lower limit in the ratio of the intensities of the central to the adjacent TMR mode - referred to as the monochromaticity factor - is given by:

$$M_F = \left[\frac{g(\nu_0)}{g(\nu)}\right]^q \simeq 2.9 \times 10^{11}.$$

Therefore, it has been shown that the single longitudinal mode operation can be explained as the result of the relatively large number of round trips required for the build-up of the emitted powers, in conjunction with the substantial gain difference between the central and adjacent TMR modes.

It should be noted, however, that no attempt was made to measure the monochromaticity of the emitted pulse. Such measurements have been undertaken for the hybrid CO_2 laser [202] where the expected values of $M_F = 10^8$ have been confirmed.

The above analysis can also justify the multi-mode nature of a TEA CO_2 laser using a two mirror resonator (e.g. those described in Chapter II). Here, the small net gain difference (1 to 2%) between the closely-spaced modes ($\Delta\nu = 120\,MHz$) as well as the smaller number of round trips required for the intensity build-up (due to the smaller loss) result in the emission of 7 to 9 modes with intensities of the same order of magnitude.

6.3 DESIGN OF THE TMR

The design of the M_1, M_2 resonator has already been described in section 4.4.2, and it only remains to ensure that the $M_1 M_3$ resonator is incapable of oscillating to complete the design of the TMR. This non-oscillation condition is satisfied when:

$$M^{-2}\, e^{2\alpha_0 L_a} \leq 1 \qquad \ldots (6.8)$$

Using the expression[186]:

$$M = 2g_1g_2 + 2\sqrt{g_1g_2(g_1g_2 - 1)} - 1 \qquad \ldots (6.9)$$

(where $g_1 = 1 - \frac{L_2}{R_1}$, $g_2 = 1 - \frac{L_2}{R_3}$) and the known values of L_2, R_1 and α_0, it can be easily shown that the condition in point is satisfied when M_3 is a convex mirror with radius of curvature $|R_3| \leq 3\,m$.

6.4 POWER MEASUREMENTS: PULSE WIDTH

When an existing convex mirror of 1.3 m radius of curvature was used as the M_3 mirror, the power of the emitted pulse was measured to be of the order of 30 MW. The energy of the pulse ($\sim$ 2J) measured using a Gen-Tec joule-meter confirmed the power measurements made with the aid of a calibrated photon drag detector.

The high reproducibility of the single longitudinal mode operation at these power levels can be gauged from the results of 100 consecutive shots in one run, where no more than 10% showed detectable modulation. A typical example of the reproducibility is shown in Fig.6.2(c) where two out

of twelve consecutive shots showed mode beating. The laser pulse width was determined by the ratio of partial pressures of nitrogen and carbon dioxide in the gas mixture. It could be adjusted in the range 60-200 ns by varying the ratio P_{N_2}/P_{CO_2} from $\frac{1}{6}$ for the lower value (Fig.6.2(a)) to $\frac{4}{3}$ for the longer pulse (Fig.6.4(b)). The absence of any pulse tail (Fig.6.4(c)) for all the gas mixtures used - by contrast with the findings in the case of the stable resonator described in section 2.4.7-should be noted. When the M_3 was replaced by a flat fully reflecting mirror, the emitted power increased three-fold (~100 MW) but at the expense of a slight modulation (Fig.6.2(b)) indicating a decrease in the pulse monochromaticity.

6.5 MULTI-LINE SINGLE LONGITUDINAL MODE PULSES

The previous chapter indicated that for increased efficiency in the amplification of nanosecond CO_2 laser pulses, multi-line emission is required. In order to assess the possibility of achieving single longitudinal mode multi-line pulses, a 5 mm thick KCl etalon was inserted between the M_2 and M_3 mirrors. It was found that by tuning the KCl etalon, double- or, occasionally, triple- rotational line emission could be obtained, while the TMR maintained oscillation on a single longitudinal mode on each line. A similar arrangement has been used by ANAN'EV et al[203] to restrict the number of oscillating modes on a neodymium-glass laser.

Using this arrangement, oscillation was found to be possible on only the three strongest lines of the 10.4 μm band - the P(20), P(18) and P(16). This, however, was to be expected since the small signal gain of only these three lines (see Fig.5.1) satisfied the oscillation condition (equation (6.5)) due to the very high loss of the TMR.

A CO_2 laser spectrum analyser (Optical Engin. Model 16-A) was used to resolve the spectral content of the emitted pulses. It was observed that when the intensities of the emitted lines were unequal (a situation indicated

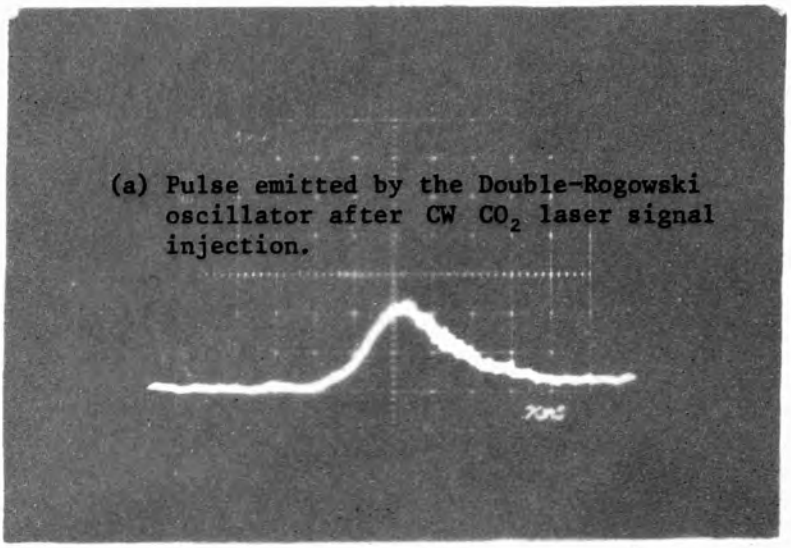

(a) Pulse emitted by the Double-Rogowski oscillator after CW CO_2 laser signal injection.

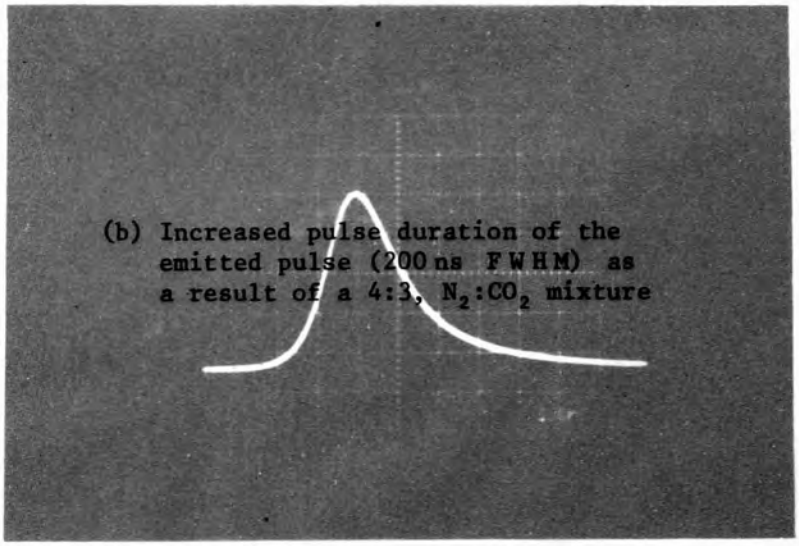

(b) Increased pulse duration of the emitted pulse (200 ns FWHM) as a result of a 4:3, N_2:CO_2 mixture

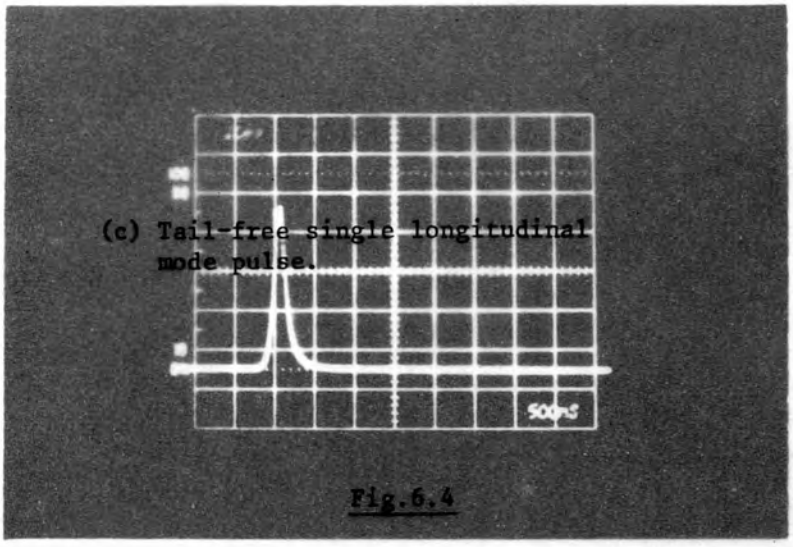

(c) Tail-free single longitudinal mode pulse.

Fig.6.4

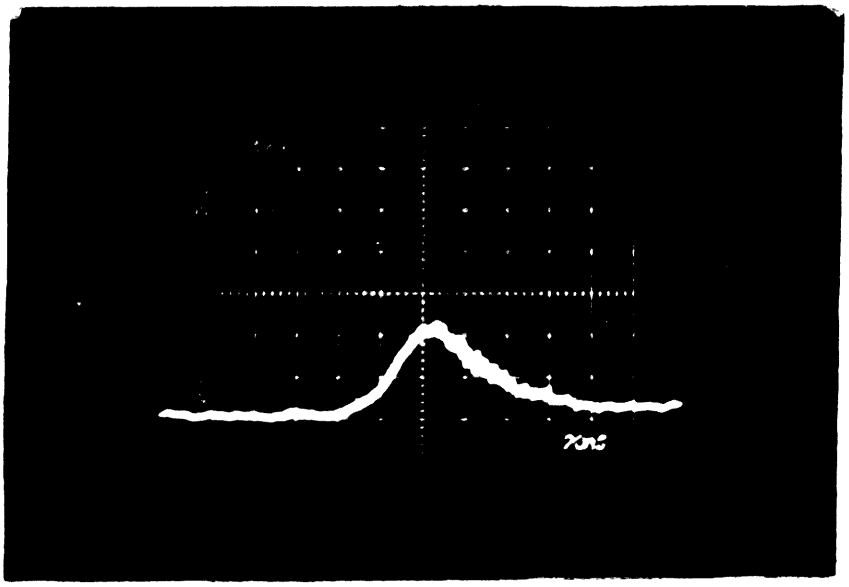
20nS

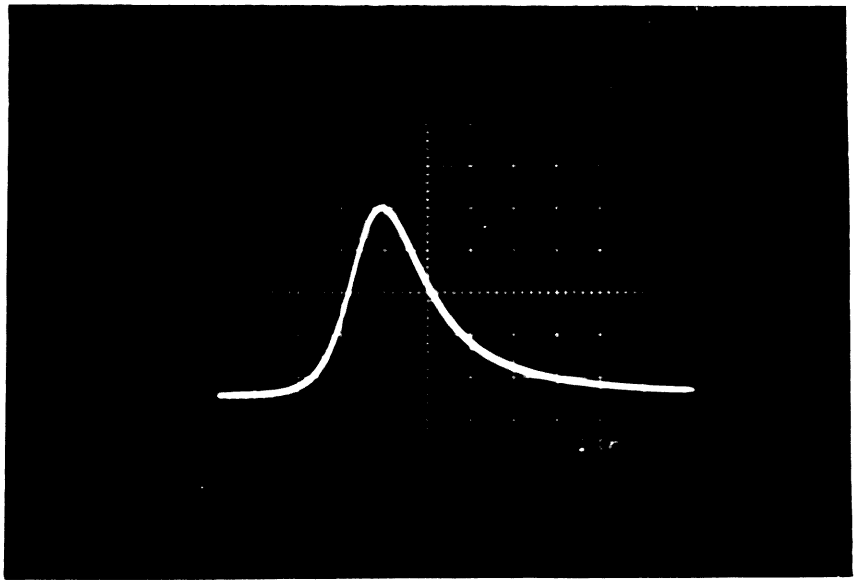

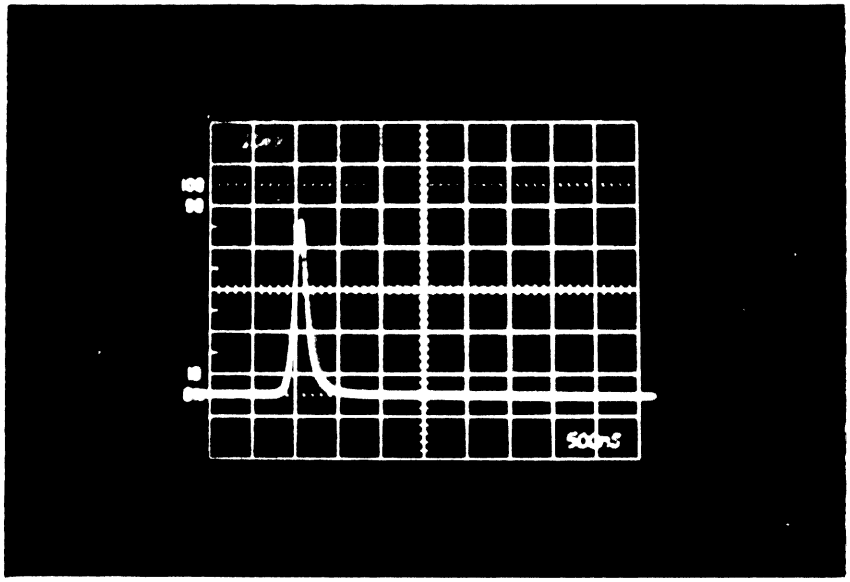
500nS

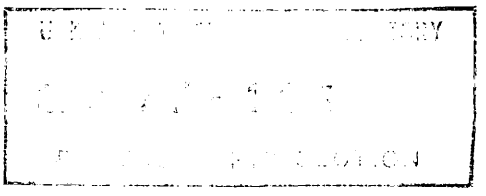

by the relative intensities of the incandescence induced by each line on the graphite screen) the temporal profile of the laser pulse showed two - and occasionally three - distinct peaks separated by as much as 900 ns (Fig.6.5(d) upper trace). In order to confirm that the observed pulse was the superposition of two - or three - independent pulses, each one corresponding to a different line, the spectrum analyser was converted into a monochromator. This was effected by allowing the radiation of only one line - P(18) - to be transmitted through a slit made on the appropriate position on the calibrated screen . The photon drag detector, PD1, monitored the total pulse; the PD2 only the P(18) line. The outputs of both detectors were displayed on a double beam oscilloscope (Tektronix 7884).

It can be seen that, depending on the extra loss introduced by the etalon on the P(20) line, it can be made to appear simultaneously with Fig.6.5(a), before Figs.6.5(b), 6.5(c) or after Fig.6.5(d), the P(18) line; in every case, the more powerful line was the first to be emitted.

Therefore, it is clear that in order to achieve any beneficial effect from multi-line single longitudinal mode operation in the amplification of nanosecond CO_2 laser pulses, it is essential that equalisation of the intensities of the emitted lines be ensured since this entails their temporal overlapping.

Although, for the present arrangement of the TMR, oscillation was confined to only the three strongest lines, it could - in principle - be extended to other lines of this band, or even the 9.4 μm band, by substituting a diffraction grating for the M_3 mirror and the etalon.

6.6 SMOOTHING THE TEMPORAL PROFILE OF THE DOUBLE-ROGOWSKI MODULE OUTPUT

It has been reported[103] that the modulation of the emitted pulse can be minimized by injecting radiation from a CW CO_2 laser into a TEA laser

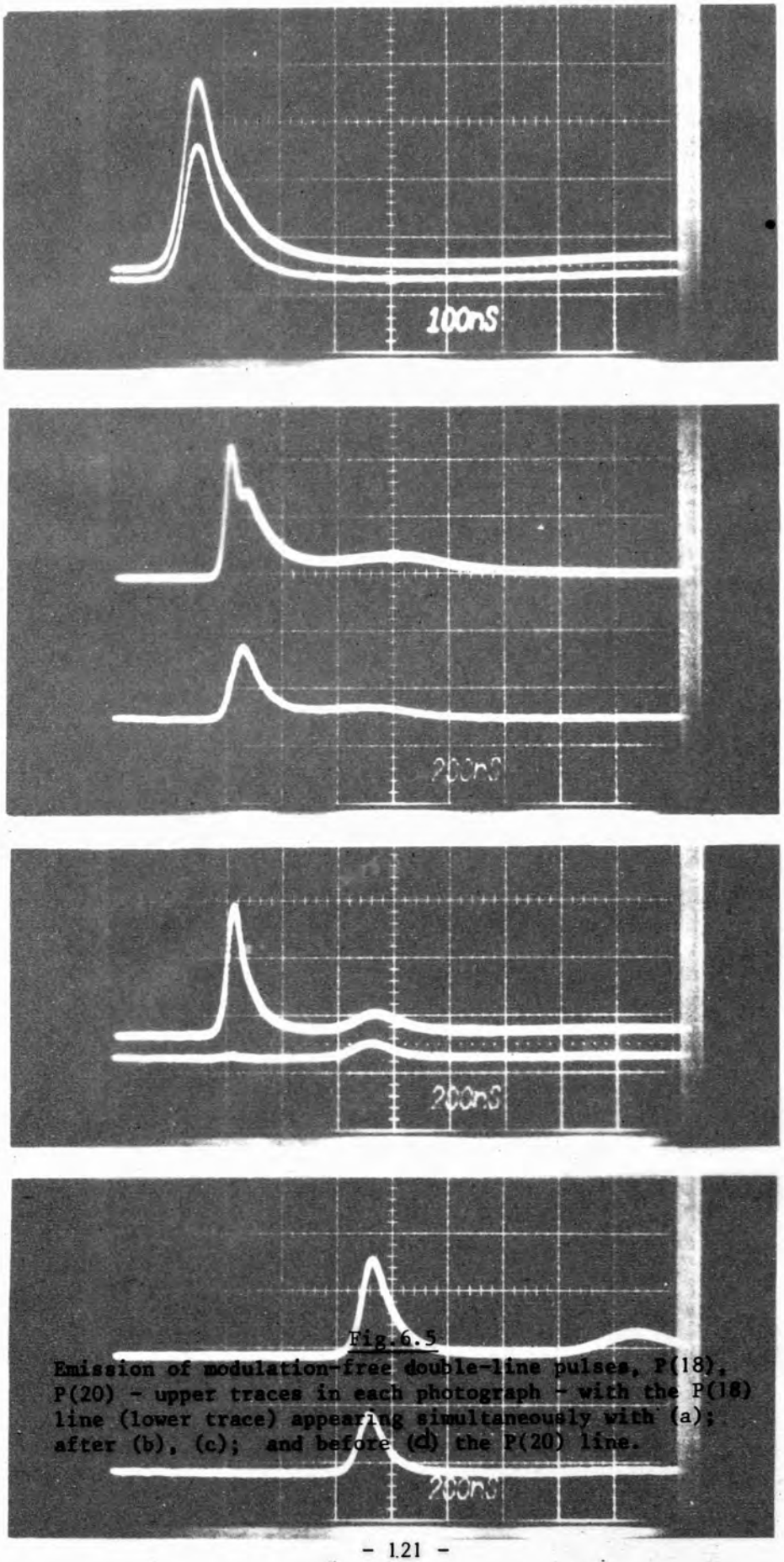

Fig.6.5
Emission of modulation-free double-line pulses, P(18), P(20) - upper traces in each photograph - with the P(18) line (lower trace) appearing simultaneously with (a); after (b), (c); and before (d) the P(20) line.

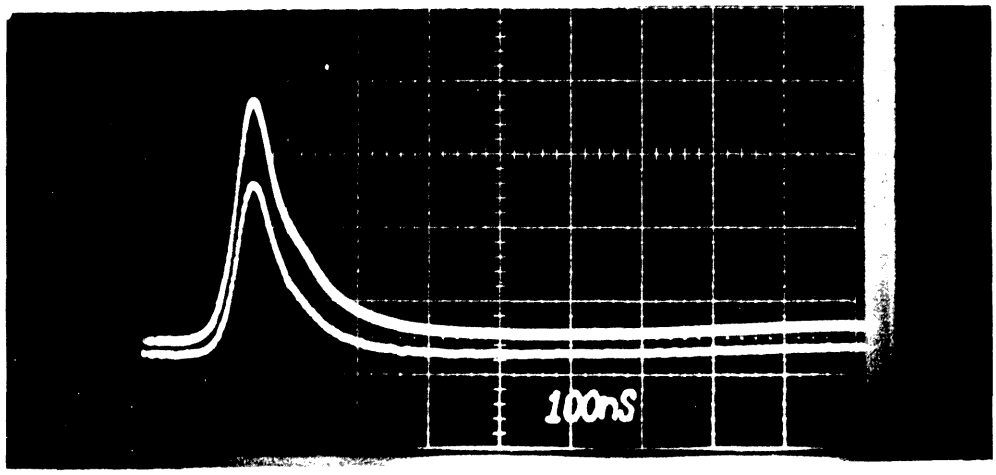
100nS

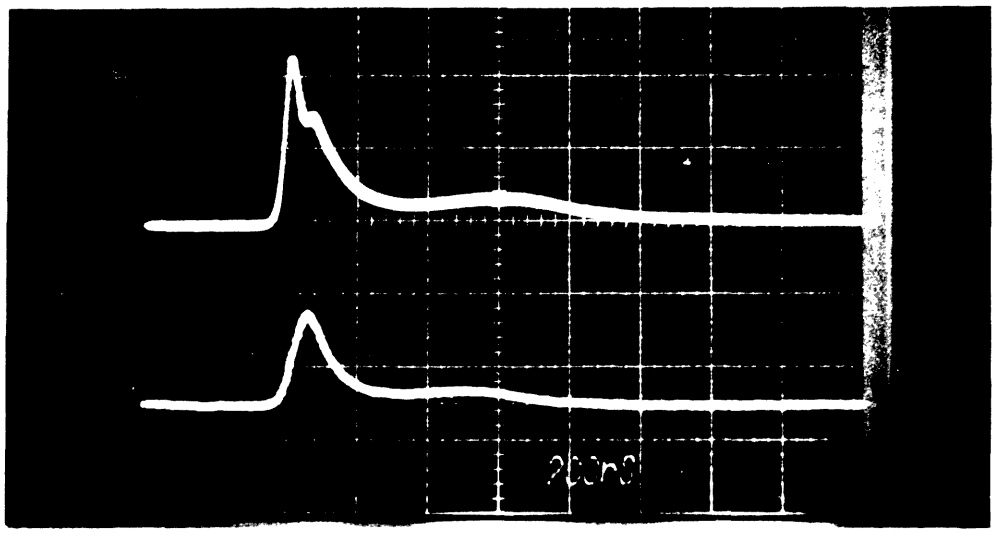
200nS

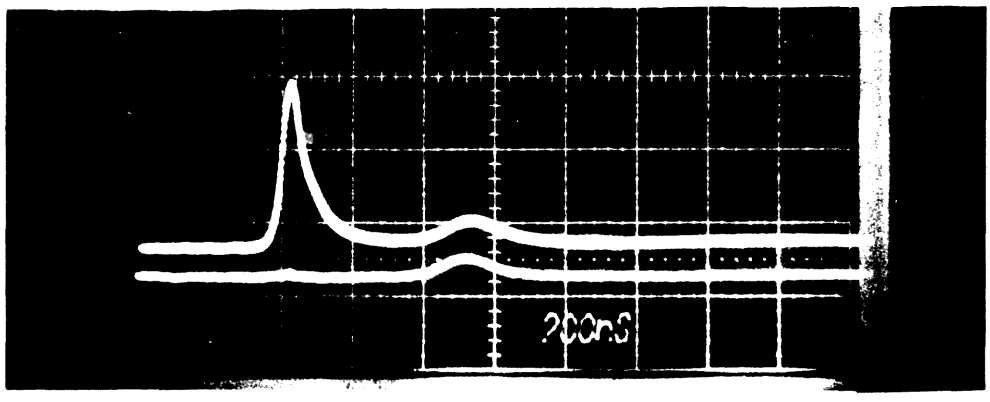
200nS

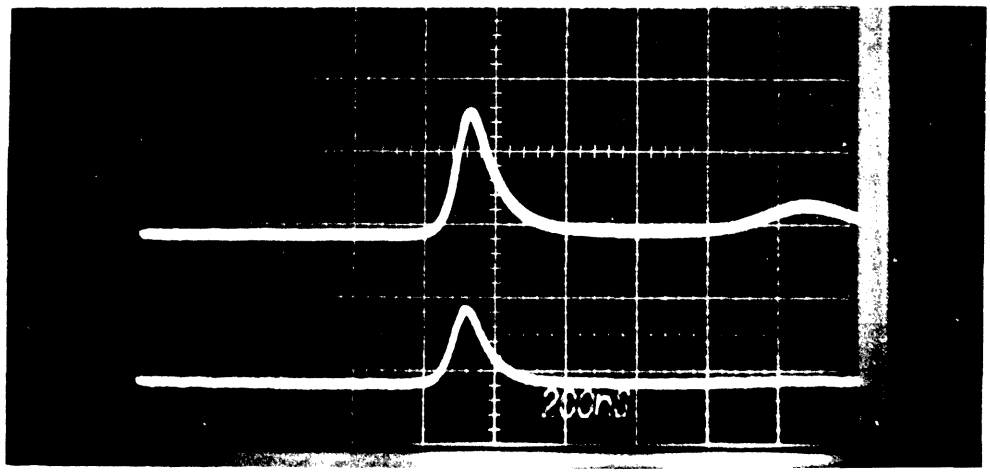
200nS

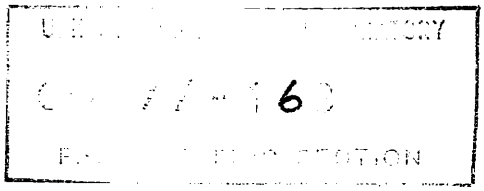

77-114

using a stable resonator. An attempt was made to apply this technique to the Double-Rogowski module described in section 2.4. For this purpose, a fraction (~0.2 W) of the radiation emitted from a commercial CW CO_2 laser (Apollo-XB) was injected into this module and the emitted TEA pulse - the time profile of which is shown in Fig.6.4(a) - was monitored using a Ge photon drag detector.

It can be seen that the strong modulation normally observed in the output of this module (see Fig.2.8) has been significantly reduced at the expense, however, of a substantial decrease in the emitted power. The reason for this reduction is that it was found necessary to reduce the electrical input energy in this module if the CW laser was to have any significant effect upon the temporal profile of the TEA pulse. It was also found that unless the CW laser emitted the P(20) line, the injected radiation had no effect whatsoever on the Double-Rogowski module. Overall, therefore, this technique clearly lacks most of the advantages inherent in the TMR.

6.7 FURTHER APPLICATIONS OF THE TMR

A single longitudinal mode operation is essential for the generation of nanosecond CO_2 laser pulses in the so-called optical free-induction decay method[100]. The large cross-section and the high power emitted from the TMR would be found highly desirable in this method.

An application requiring smooth temporal profile is the generation of nanosecond CO_2 pulses using a method reported by ALCOCK et al[103] in which fast switching can be obtained by reflection of the CO_2 laser radiation from optically-induced carriers in a polycrystalline Ge plate. The CO_2 laser pulses used in this method had been smoothed by the earlier-mentioned CW injection technique. It is believed that the advantage offered by the TMR single longitudinal mode laser over the CW injection technique could

benefit the application. The required plane polarized pulses can be easily obtained through the introduction of intra-cavity Brewster angle windows.

As has been seen in section 3.11, the smoothness of the laser pulse emitted by this oscillator was crucial to the accurate measurement of the delay time, the jitter and the threshold energy for gap breakdown in the LTSG.

This device may also be applied to laser-plasma interaction studies, where the smooth temporal envelope of the incident pulse provides a reference for interpreting amplitude modulations imposed on the reflected pulse[204]. In fact, the single longitudinal mode laser, described in this chapter, has already been used in such an application at Culham Laboratory[205].

6.8 CONCLUDING REMARKS

In conclusion, it has been shown experimentally that by the addition of a third reflector, a TEA CO_2 telescopic laser amplifier can be converted into a high power oscillator operating on a single longitudinal mode. The output power was found to be more than one order of magnitude higher than that obtained from laser oscillators employing a stable resonator[70,82-85]. This considerable improvement is accounted for by the fact that the fundamental transverse mode can be arranged to occupy the whole volume of active medium in an unstable resonator, whereas the mode volume of a stable resonator - used in the other methods - is strictly limited, resulting in a substantial reduction of output power.

Temporally smooth pulses with peak powers of 14 MW have been observed using an unstable resonator with an SF_6 cell in a grating-tuned cavity[72].

A further important feature of the three-mirror resonator is the low divergence $\sim 5 \times 10^{-4}$ rad of the output beam, which equals the diffraction-limited divergence of the conventional telescopic resonator. As has also

been noted by ANAN'EV[203] the angular divergence remained close to the diffraction limit whether the M_3 was a convex, plane or concave mirror.

The simplicity of the described method as well as the anticipated high spectral purity and reproducibility of the emitted pulse should also be recognized as advantages of this method over others currently in existence.

CHAPTER VII

GENERAL CONCLUSIONS

7.1 INTRODUCTION

The principal findings of the research undertaken are collectively summarised in this chapter, although they have already been separately discussed in more detail in the relevant sections.

The application of these findings to a larger system — TROJAN — OPALS — is also discussed and a brief outline of the system's design and assessment of the main problems which need to be resolved in order to achieve the intended performance are presented.

7.2 SYNOPSIS OF MAIN RESULTS

Experimental investigation of the operational characteristics of the laser modules used has shown that both the emitted power of the TEA CO_2 oscillator and the small signal gain of the amplifier are optimised when two conditions are fulfilled:

(a) a 6 : 1, $CO_2 : N_2$ mixture is used; and

(b) the helium concentration is kept as low as possible while still sustaining an arc-free discharge.

The introduction of organic vapours (triethylamine, tripropylamine) into the discharge permitted smaller concentrations of helium to be used, as a result of which greater peak power and gain were recorded. Furthermore, the introduction of the seedant substantially improved the normally poor spatial uniformity of the active medium of the Double-Discharge module (sections 2.4.7, 2.4.8, 2.5.3).

A single longitudinal mode oscillator was developed with an output power in the range of 30 - 100 MW. The single longitudinal mode operation is the result of coupling two unstable resonators sharing the active medium

whose individual diffraction loss exceeds the available gain preventing them from oscillating independently.

CO_2 laser pulses of sub-nanosecond duration were achieved using the self-mode-locked output of the Double-Rogowski module and an electro-optical shutter. In order to attain sub-nanosecond rise time the laser-triggered spark gap had to be pressurized to 9 atm. and to be charged to a voltage as near the self-breakdown as possible. The signal-background noise ratio of these pulses was limited by the residual birefringence of the electro-optical crystal. Although extinction ratios of the order of 3×10^3 were obtained, pulses with higher extinction ratio ($> 10^6$) are required for amplification in the enlarged system (OPALS - TROJAN) currently under construction. This requirement necessitated the introduction of an additional crystal and polarizer in the electro-optical shutter of this system. An improved version of the laser-triggered spark gap has also been developed which is capable of operating at higher voltage (30 kV) and pressure (15 atm.) while its stainless steel target electrode should contribute to a shorter delay time (section 3.13).

The saturation energy density for single-line pulses of duration 1.1, 20 and 70 ns was measured to be 30 mJ/cm^2, 100 mJ/cm^2 and 180 mJ/cm^2. Using a telescopic amplifier, 0.5 J/litre were extracted by 1 mJ, 1 ns single line input pulses. This represents more than 50% of the energy available to an infinitely strong pulse $E_{ext} = E_s \cdot \alpha_0 = 0.93$ J/litre. The electrical input energy density was 100 J/litre and therefore the amplification efficiency of nanosecond single-line pulses was $\eta = 0.5\%$.

Multi-line input pulses resulted in improved amplification efficiency. The output of the telescopic amplifier was increased by $\sim$ 30% and $\sim$ 50% for input pulses containing two and three lines respectively. It is therefore evident, that, even with multi-line input pulses, the nanosecond pulse

amplification efficiency using double-discharge, TEA CO_2 lasers is less that 1%. However, higher efficiency ($\sim$ 2%) is expected in the OPALS - TROJAN system (see section 7.3). Finally, it was shown that the use of multi-line input pulses minimized the pulse-broadening experienced by single-line pulses.

7.3 FUTURE WORK

The central concern of the work reported in this thesis has been the reliable generation of nanosecond CO_2 laser pulses and their efficient amplification to gigawatt power levels. The further amplification of these pulses to intensities appropriate for laser-induced fusion studies, suggests itself as the logical progression of this work. Although the findings of this research can be directly applied to the larger system, the question of optical isolation, which could easily be circumvented in the original system, will demand solution before satisfactory operation can proceed.

THE OPALS - TROJAN system whose construction is almost complete at Culham Laboratory, has been designed to register an output of 200 - 400 GW and consists of:

(a) a single longitudinal mode U.V. preionized oscillator;

(b) a double electro-optical shutter;

(c) two U.V. preionized atmospheric pressure pre-amplifiers, each with an active medium of $5 \times 5 \times 100\ cm^3$ and one of which takes the telescopic form described in Chapter IV;

(d) a $20 \times 25 \times 200\ cm^3$ e-beam sustained amplifier capable of operating at a pressure of two atmospheres.

The expectation of higher efficiency in this ~~module~~ system is based upon the following premises:

(a) in the U.V. preionized (OPALS) and e-beam sustained (TROJAN) CO_2 laser modules, a higher percentage of excitation energy is stored in the upper vibrational level (section 1.3);

(b) the main laser amplifier (TROJAN) operating at 2 atm. reduces the rotational-relaxation time, t_R; and

(c) a helium-free mixture which has been found to be compatible with this module[207] further reduces the value of t_R (see section 1.4.4).

Simple calculations using equations (5.2), (5.3) and (5.4), which were found to be in good agreement with the experimental results (see section 5.4), and the typical value of $\alpha_0 = 0.04\ cm^{-1}$ indicate that a 1 ns, 10 mJ/cm^2, three-line pulse can extract 6.6 J/litre from TROJAN operating at 2 atm. and filled with a 4 : 1, $CO_2 : N_2$ mixture. The typical electrical excitation energy for this device is ~ 150 J/litre·atm. and, therefore, a ~ 2% ns-pulse amplification efficiency is possible, provided the optical isolation problems — discussed in the next section — are overcome without a significant reduction in the energy output of the OPALS - TROJAN system. The input beam in this amplifier will extract from 60 litres of its active medium, thus indicating a potential output of up to 400 J in pulses of 1 ns duration.

7.4 OPTICAL ISOLATION

The incorporation of an effective saturable optical isolator into a high-gain oscillator-amplifier CO_2 laser system is essential to overcome the problems of pre-pulse amplification and parasitic oscillations which can result in premature target-disintegration and partial depletion of the population-inversion before the arrival of the nanosecond pulse. Furthermore, an optical isolator is required to minimize the amplification of target reflections. Approximately 5% of the energy of the pulse incident on the target is returned by the focusing optics into the laser system[207] and can be amplified — due to the collisional re-population of the upper laser level — to intensities far beyond the damage threshold of the optical components.

In the OPALS - TROJAN system, nanosecond pulses will traverse the 6m — long active medium which has an overall small signal gain of 5×10^8. It can be easily shown that in order to avoid target damage (damage threshold 50 μJ [208]) by the prepulse radiation, the signal-to-background ratio of the unamplified nanosecond pulse (with typical energy of ~1 mJ) must be of the order of 10^{11}. However, it has been indicated in Chapter III, that the extinction ratio of the double electro-optical shutter can be, at best, ~ 10^7. Clearly a 4 orders of magnitude suppression in the small signal gain is required to avoid destruction of the target by the background radiation prior to the main pulse, which can attain energy of the order of 1 J, by undergoing exponential amplification.

A variety of saturable absorbers — including p-type germanium [74,102], deuterated ammonia [209]; a mixture of N_2F_4 and C_2H_5OH [210] — have been used with CO_2 laser systems in an attempt to eliminate the above-mentioned problems. Additionally hot CO_2, acting as a narrow-band gaseous absorber has been employed to reduce the prepulse transmission [102,199] while electrically-driven plasmas, triggered after the passage of the main pulse, have been shown to provide a considerable attenuation of target reflections [211].

The ideal saturable absorber would be a gas added to the laser discharge which was capable of suppressing the small signal gain without appreciably reducing the energy otherwise extractable by the main laser pulse. A preliminary investigation of the effect of 2.5 torr triethylamine added to the laser gas had the result of reducing the gain coefficient of the Double-Discharge module by 25%, although, when it was operated as an oscillator, the laser output energy was reduced by no more than 5% [211]. The spectral content of the emitted pulse, was the same — P(20) — in both cases. The reasons for the small signal gain suppression are not as yet understood, since absorption of the 10.6 μm radiation by the triethylamine

itself is negligible; the possibility of new compounds forming during the discharge cannot be excluded however.

Assuming that the triethylamine will have a similar effect on the OPALS — TROJAN system, its small signal gain will be reduced by a factor of more than 200, although the effectiveness of this additive will depend upon whether a comparably low (5%) reduction in the energy of the output pulse can be sustained.

In order to further suppress the small signal gain, it is suggested that the convex metal mirror of the telescopic amplifier could be replaced by an equivalent mirror made of an appropriately thick p-type Ge disc, the front and back surfaces of which have anti-reflection and high-reflectivity coatings respectively.

In conclusion, it is hoped that the present work may have made some contribution to short pulse laser technology, and may have gone some way towards elucidating those physical processes which determine the efficient amplification of nanosecond CO_2 laser pulses.

APPENDIX 'A'

LIGHT PROPAGATION IN CRYSTALS

An understanding of the operation of the electro-optical shutter can be facilitated by a brief summary of the main features of light propagation in both (a) isotropic and (b) anisotropic media.

(a) Isotropic Media

The optical isotropy of a medium is the result of its dielectric properties which could be described in a linear relation between an electric field $\bar{E}$ (e.g. the $\bar{E}$ field of the electro-magnetic radiation incident on the crystal) and the resultant electric displacement $\bar{D}$:

$$\bar{D} = \varepsilon \varepsilon_0 \bar{E} \ . \qquad \ldots (A.1)$$

The scalar quantity ε is the dielectric constant, or the relative permittivity of the medium, while ε_0 is the permittivity of the free space. Using Maxwell's equations, it can be shown that electro-magnetic radiation of any state of polarization is propagated unchanged through media for which equation (A.1) applies with phase velocity $U = c/\sqrt{\varepsilon} = c/\eta$, irrespective of the direction of propagation.

(b) Anisotropic Media

Equation (A.1) cannot describe the dielectric properties of either an isotropic electro-optic material, when an electric field is present, or any natural anisotropic medium. To describe the dielectric properties in either case, a new relation between $\bar{D}$ and $\bar{E}$ is required in which each component of $\bar{D} = [D_1 , D_2 , D_3]$ is linearly related to all three components of $\bar{E} = [E_1 , E_2 , E_3]$

$$\begin{aligned} D_1 &= \varepsilon_0(\varepsilon_{11}E_1 + \varepsilon_{12}E_2 + \varepsilon_{13}E_3) \\ D_2 &= \varepsilon_0(\varepsilon_{21}E_1 + \varepsilon_{22}E_2 + \varepsilon_{23}E_3) \qquad \ldots (A.2) \\ D_3 &= \varepsilon_0(\varepsilon_{31}E_1 + \varepsilon_{32}E_2 + \varepsilon_{33}E_3) \end{aligned}$$

The nine quantities ε_{ij} are constants of the medium. In order to describe the dielectric properties of an anisotropic medium, it is necessary to specify the nine coefficients $\varepsilon_{11}, \varepsilon_{12}, \ldots,$ which can be conveniently written in the form:

$$[\varepsilon_{ij}] \quad \begin{bmatrix} \varepsilon_{11} & \varepsilon_{12} & \varepsilon_{13} \\ \varepsilon_{21} & \varepsilon_{22} & \varepsilon_{23} \\ \varepsilon_{31} & \varepsilon_{32} & \varepsilon_{33} \end{bmatrix} .$$

The quantity $[\varepsilon_{ij}]$ is the dielectric tensor of the medium.

When equation (A.2) instead of (A.1) is used in conjunction with Maxwell's equations, it can be shown (reference (153) p.671) that the structure of the anisotropic medium permits two linearly polarized plane electromagnetic waves, with their directions of vibration mutually perpendicular, to travel with two different phase velocities in any given direction of propagation. The directions of the two permitted linear polarizations are determined by (a) the structure of the medium, (b) the direction of propagation, and (c) the direction of the external electric field. Plane electromagnetic waves, linearly polarized along either of these directions, will emerge from the medium unchanged - just as if they had traversed an isotropic medium - and, for this reason, they are often termed the privileged directions. If x and y denote the privileged directions for propagation along an axis z, then, x, y, z form a Cartesian system of coordinates.

Plane electro-magnetic waves linearly polarized along an arbitrary direction in the x, y plane, will, in general, emerge from the medium elliptically polarized. This could be visualized if it were assumed that the electro-magnetic wave was resolved into two linearly-polarized components with their directions of vibration along x and y. The two components which travel with velocities U_1 and U_2, being in phase initially, will develop a continuously growing phase difference as they traverse the medium. These

components emerging from the anisotropic medium, will retain their phase difference as they propagate in the surrounding isotropic medium and, therefore, the electro-magnetic wave that results from the recombining of the two out-of-phase components is elliptically polarized.

APPENDIX 'B'

LIST OF SYMBOLS

A_{ul}	Einstein coefficient for spontaneous emission
A	absorbed fraction of incident radiation; also laser beam cross section
a_1 a_2	mirror radius
B	rotational constant
C	capacitance
c	velocity of light; also specific heat of target electrode
D	centrifugal distortion constant; also electrode spacing in the telescopic amplifier; and diameter of laser beam
$\bar{D}$	electric displacement
$D_{\infty h}$	a point group
d	fringe spacing; also spark gap spacing; and etalon thickness
E	laser energy; also electric field
E_c	extinction ratio of Pockels cell
E_p	extinction ratio of electro-optical shutter; also saturation energy parameter
E_{ext}	extractable optical energy from amplifier
E_r	rotational energy
$(E_s)_{eff}$	effective saturation energy parameter
F	total flow rate (ℓ/min) of the laser gas
$g(\nu)$	net round trip gain
g	resonator g-parameter
h	Planck's constant
I, I_0	intensity of CW laser
J	rotational quantum number
k	thermal conductivity of target electrode
k_i	roots of the secular equation
K	thermal constant of the target electrode
K_e , K'_e	resonant exchange rate constant
K_i	vibrational relaxation-rate constant
K(J)	Boltzmann partition fraction
K_R	rotational relaxation-rate constant
L	laser cavity length; also length of electro-optical crystal; also inductance
L_a	length of active medium

ℓ	angular momentum quantum number
M	collisional partner M; also magnification of the unstable resonator; also molecular weight
M_F	monochromaticity factor
m	number of plates comprising the polarizer
N	vibrational population
N_J	rotational population
N, N_0	number of electrons in the L T S G
N_{eq}	equivalent Fresnel number
n	photon number density
P	gas pressure; also degree of polarisation
P_ℓ	laser power
P(J)	P-branch vibrational-rotational transition
P_s	partial pressure of additive
q	number of round trips for oscillation build-up
R	resistivity of target electrode
R_i	mirror radius of curvature
R(J)	R-branch vibrational-rotational transition
$R_\perp$, $R_\parallel$	reflectivities of linearly polarized radiation
r_{41}	GaAs electro-optical coefficient
$[r_{ijk}]$	electro-optical tensor
S	L T S G constant
T	translational temperature of gas; also transmittance of an electro-optical shutter or etalon
T_m	melting point of target electrode
T_R	rotational temperature
t	time
t_d	delay time
t_e	time required for heating target electrode to its melting point
t_f	formative time
t_p	laser pulse duration
t_r	rise time of electrical pulse
t_R	rotational relaxation time
U	phase velocity
V	voltage
V_{sb}	self-breakdown voltage
$V_{\frac{1}{2}}$	half-wave retardation voltage
V	vibrational quantum number of N_2

v_a	avalanche velocity
v_s	streamer velocity
Z_0	characteristic impedance of transmission line
α	Townsend first coefficient
α_0	small signal gain coefficient
γ	Eigenvalue determining the power loss, δ, per round trip ($\delta = 1 - \|\gamma\|^2$)
Δ	vibrational inversion population density
$\Delta\nu_H$	pulse-broadened line width
δ	rotational inversion population density; also round trip output coupling; and phase difference between two orthogonally polarized waves
ε	dielectric constant
ε_i	principal dielectric constants
η_i	quantum number of the three CO_2 normal modes of vibration; also principal refractive indices
η	laser efficiency, also refractive index
θ	angle of divergence; also angle of incidence
κ	Boltzmann constant
λ	wavelength
ν, ν_0	optical frequency
ν_i	frequency of the three fundamental modes of vibration
ρ	density; also reflection coefficient in a transmission-line
σ	stimulated emission cross-section
τ_1, τ_2	lifetimes of upper and lower vibrational laser levels
ϕ	angle between the transmission axis and one of the privileged directions; also wedge angle
ψ	mole fraction of component in a gas mixture
ω	angular frequency
ω_0	lowest transverse mode spot size

REFERENCES

(1) BASOV, N.G. and KROKHIN, O.N., Proc. Third Int. Quant. Electron. Conf., Paris, 1963, vol.2, 0.1373, Dunod, Paris and Columbia Univ. Press, New York, (1964).

(2) DAWSON, M., Phys. Fluids, 7, 981 (1964).

(3) NUCKOLLS, J., WOOD, L., THIESSEN, A. and ZIMMERMAN, G., Nature, 239, 139 (1972).

(4) LASER FOCUS, 13, 32 May 1977.

(5)a. PATEL, C.K.N., FAUST, W.L. and McFARLANE, R.A., Bull. Amer. Soc., 9, 500 (1964).

b. PATEL, C.K.N., Phys. Rev., 136, A1187 (1964).

(6) STARK, E., Laser Fusion Program, LA-6616-PR, LASL, Univ. of California, Los Alamos, (1977).

(7) TYCHINSKII, V.P., Soc. Phys. Uspekhi, 10, 131 (1967).

(8) TYTE, D.C., 'Carbon Dioxide Lasers', Advances in Quantum Electronics, Academic Press, London (1970).

(9) CHEO, P.K., 'CO_2 Lasers' In Lasers, vol.3, (Edited by A.K. Levine and A.J. Demaria), Dekker, New York, 1971.

(10) WOOD, O.R., Proc. IEEE, 62. 355 (1974).

(11) DENNISON, D.M., Rev. Mod. Phys., 12, 175 (1940).

(12) HERZBERG, G., 'Infrared and Raman Spectra of Polyatomic Molecules'. D. Van Nostrand, New York, (1945).

(13) COURTOY, C.P., Can. J. Phys., 35, 608 (1957).

(14) FERMI, E., Z. Physik, 71, 250 (1931).

(15) AMAT, G. and PIMBERT, M., J. Mol. Spectrosc., 16, 278 (1965).

(16) GORDON, H.R. and McCUBBIN, T.K., J. Mol. Spectrosc., 19, 137 (1966).

(17) CHACKERIAN, C. and EGGERS, D.F., J. Mol. Spectrosc., 27. 59 (1968).

(18) HOWARD-LOCK, H.E. and STOICHEFF, B.P., J. Mol. Spectrosc., 37, 321 (1971).

(19) PETERSEN, F.R., McDONALD, D.G., CUPP, J.D. and DIANELSON, B.L., 'Laser Spectroscopy', (Edited by R.G. Brewer and A. Mooradian), Plenum Press, New York, p.562 (1974).

(20) HERZBERG, G., 'Spectra of Diatomic Molecules', D. Van Nostrand, New York (1950).

(21) WILLETT, C.S., 'An Introduction to Gas Lasers: Population Inversion Mechanisms', Pergamon Press, p.266 (1974).

(22) BECK, R., ENGLISH, W., GÜRS, K., 'Table of Laser Lines in Gases and Vapours', Springer-Verlag, Berlin (1976).

(23) BONESS, M.J.W. and SCHULZ, G.J., Phys. Rev. Lett., 21, 1031 (1968).

(24) ANDRICK, A., DANNER, D. and EHRHARDT, H., Phys. Lett., 29A. 346 (1969).

(25) CLAYDON, C.R., SEGAL, G.A. and TAYLOR, H.S., J. Chem. Phys., 52, 3387 (1970).

(26) SOBELEV, N.N. and SOKOVIKOV, V.V., Sov. Phys. Uspekhi, 10, 153 (1967).

(27) SHARMA, R.D. and BRAU, C.A., J. Chem. Phys., 50, 924 (1969).

(28) LINDER, F., Endeavour, 120, 124 (1974).

(29) SCHULZ, G.J., Phys. Rev., 135, A988 (1964).

(30) NIGHAN, W.L., Phys. Rev. A, 2, 1989 (1970).

(31) NIGHAN, W.L., 11th Int. Conf. on Phenomena in Ionized Gases, 1973 (Invited papers), Prague, Sept. 10-14, 1973 (Edited by L. Pekárek, L. Láska).

(32) MOORE, C.B., WOOD, R.E., HU, B.L. and YARDLEY, J.T., J. Chem. Phys., 46, 4222 (1967).

(33) STATZ, H., TANG, C.L. and KOSTER, G.F., J. Appl. Phys., 37, 4278 (1966).

(34) ELETSKII, A.V. and SHLYAPNIKOV, G.V., Sov. Phys. Doklady, 19, 222 (1974).

(35) GERRY, E.T. and LEONARD, D.A., Appl. Phys. Lett., 8, 227 (1966).

(36) McCUBBIN, T.K. Jr. and MOONEY, T.R., J. Quant. Spect. Radiat. Transfer, 8, 1255 (1968).

(37) COUSIN, C., ROSSETTI, C. and MEYER, C., C.R. Acad. Sci. Paris, series B268, 1640 (1969).

(38) MURRAY, E.R., KRUGER, C. and MITCHNER, M., Appl. Phys. Lett., 24, 180 (1974).

(39) BIRYUKOV, A.S., VOLKOV, A.Yu., KUDRYAVTSEV, E.M. and SERIKOV, R.I., Sov. J. Quantum Electron., 6, 946 (1976).

(40) TAYLOR, R.L. and BITTERMAN, S., Rev. Mod. Phys., 41, 26 (1969).

(41) LEWIS, P.L. and TRAINOR, D.W., AVCO Everett Research Lab., AMP 422 (Nov. 1974).

(42) HUETZ-AUBERT, M. and LEPOUTRE, F. (and cited references), Physica, 78, 435 (1974).

(43) SEPUCHA, R.C., Chem. Phys. Lett., 131, 75 (1975).

(44) REID, J., GARSIDE, B.K. and BALLIK, E.A., IEEE J. Quantum Electron., QE-9, 602 (1973).

(45) ROSSER, W.A., WOOD, A.D. and GERRY, E.T., J. Chem. Phys., 50, 4996 (1969).

(46) CANNEMEIJER, F. and DeVRIES, A.E., Physica, 70, 135 (1973).

(47) STEPHENSON, J.C., WOOD, R.E. and MOORE, C.B., J. Chem. Phys., 54, 3097 (1971).

(48) VARGIN, A.N., GOGOKHIYA, V.V., KONYUKHOV, V.K. and PASYNKOVA, L.M., Sov. J. Quant. Electron., 6, 119 (1976).

(49) ROSSER, W.A. and GERRY, E.T., J. Chem. Phys., 51, 4222 (1967).

(50) CHEO, P.K., J. Appl. Phys., 38, 3563 (1967).

(51) REID, J., BALLIK, E.A. and GARSIDE, B.K., Optics Commun., 13, 126 (1975).

(52) GARSIDE, B.K., REID, J. and BALLIK, E.A., IEEE J. Quant. Electron. QE-11, 583 (1975).

(53) SIMPSON, C.J.S.M. and CHANDLER, T.R.D., Proc. Roy. Soc., London, A., 317, 265 (1970).

(54) MERRILL, K.M. and AMME, R.C., J. Chem. Phys., 51, 844 (1969).

(55) CANNEMEIJER, F. and DeVRIES, A.E., Physica, 64, 123 (1973).

(56) BASS, H.E., J. Chem. Phys., 58, 4783 (1973).

(57) JUDD, O.P., Los Alamos Sci. Lab., LA-5892-MS, UC-34a, (March 1975).

(58) MURRAY, E.R., KRUGER, C.H. and MITCHNER, M., J. Chem. Phys., 62, 388 (1975).

(59) JACOBS, R.R., PETTIPIECE, K.J. and THOMAS, S.J., Phys. Rev. A., 11, 54 (1975).

(60) CRAFER, R.C., GIBSON, A.F. and KIMMITT, M.F., J. Phys. D., series 2, 2, 1135 (1969).

(61)a. CHEO, P.K. and ABRAMS, R.L., Appl. Phys. Lett., 14, 47 (1969).
b. ABRAMS, R.L. and CHEO, P.K., Appl. Phys. Lett., 15, 177 (1969).

(62) JACOBS, R.R., PETTIPIECE, K.J. and THOMAS, S.J., Appl. Phys. Lett., 24, 375 (1974).

(63) FELDMAN, B.J., I E E E J. Quant. Electron., QE-9, 1070 (1973).

(64) SCHAPPERT, G.T., Appl. Phys. Lett., 23, 219 (1973).

(65) WOOD, O.R., ABRAMS, R.L. and BRIDGES, T.J., Appl. Phys. Lett., 17, 376 (1970).

(66) FIGUEIRA, J.F., REICHELT, W.H. and SINGER, S., Rev. Sci. Instrum., 44, 1481 (1973).

(67) RICHARDSON, M.C., Appl. Phys. Lett., 25, 31 (1974).

(68) SAKANE, T., Optics Commun., 12, 21 (1974).

(69) GIBSON, A.F., KIMMITT, M.F. and ROSITO, C.A., Appl. Phys. Lett., 18, 546 (1971).

(70) NURMIKKO, A., DeTEMPLE, T.A. and SCHWARZ, S.E., Appl. Phys. Lett., 18, 130 (1971).

(71) FORTIN, R., RHEAULT, F., GILBERT, J., BLANCHARD, M. and LACHAMBRE, J.L., Can. J. Phys., 51, 414 (1973).

(72) DYER, P.E. and JAMES, D.J., Appl. Phys. Lett., 26, 331 (1975).

(73) GIBSON, A.F., KIMMITT, M.F., and NORRIS, B., Appl. Phys. Lett., 24, 306 (1974).

(74) GIBSON, A.F., ROSITO, C.A., RAFFO, C.A. and KIMMITT, M.F., Appl. Phys. Lett., 8, 356 (1972).

(75) FELDMAN, B.J. and FIGUEIRA, J.F., Appl. Phys. Lett., 25, 301 (1974).

(76) WALKER, A.C. and ALCOCK, A.J., Optics Commun., 12, 430 (1974).

(77) ALCOCK, A.J. and WALKER, A.C., Appl. Phys. Lett., 25, 299 (1974).

(78) BELANGER, P.A. and BOIVIN, J., Can. J. Phys., 54, 720 (1976).

(79) ALCOCK, A.J., CORKUM, P.B., JAMES, D.J. and LEOPOLD, K.E., I E E E J. Quant. Electron., 13, 89 (1977).

(80) ALCOCK, A.J., CORKUM, P.B. and JAMES, D.J., Appl. Phys. Lett., 30, 148 (1977).

(81) HILL, G.A., JAMES, D.S. and RAMSDEN, S.A., Optics. Commun., 9, 237 (1973).

(82) WEISS, J.A. and GOLDBERG, L.S., IEEE J. Quant. Electron., QE-8, 757 (1972).

(83) HAMMOND, C.R., JUYAL, D.P., THOMAS, G.C. and ZEMBROD, A., J. Phys. E: Scient. Instrum., 7, 45 (1974).

(84) GONDHALEKAR, A., HOLZHAUER, E. and HECKENBERG, N.R., Phys. Lett., 46A, 229 (1973).

(85) GIRARD, A., Optics Commun., 11, 346 (1974).

(86) LOY, M.M.T. and RONALD, P.A., Rev. Sci. Instrum., 48, 554 (1977).

(87) LACHAMBRE, J-L., LAVIGNE, P., OTIS, G. and NOËL, M., IEEE J. Quant. Electron., QE-12, 576 (1976).

(88) CASON, C., WERKHEISER, A.H., OTTO, W.F. and JONES, R.W., J. Appl. Phys., 48, 2531 (1977).

(89) STAMATAKIS, T. and SELDEN, A.C., Phys. Lett., 58A, 221 (1976).

(90) RICHARDSON, M.C., Optics Commun., 10, 302 (1974).

(91) FIGUEIRA, J.F. and SUTPHIN, H.D., Appl. Phys. Lett., 25, 661 (1974).

(92) DAVIS, D.T., SMITH, D.L. and KOVAL, J.S., IEEE J. Quant. Electron, QE-8, 816 (1972).

(93) RHEAULT, F., LACHAMBRE, J-L., LAVIGNE, P., PEPIN, H. and BALDIS, H.A., Rev. Sci. Instrum., 46, 1244 (1975).

(94) LITTLE, V.I., SELDEN, A.C. and STAMATAKIS, T., J. Appl. Phys., 47, 1295 (1976).

(95) PAN, Y-L, SIMPSON, J.R., BERNHARDT, A.F. and KIERGAN, S.E., IEEE J. Quantum. Electron., QE-10, 44 (1974).

(96) STARK, E.E., REICHELT, W.H., SCHAPPERT, G.T. and STRATTON, T.F., Appl. Phys. Lett., 23, 322 (1973).

(97) MANES, K.R., LINDQUIST, W.B., RENARD, P.A., EDDLEMAN, H.E., SMITH, D.L., GLAROS, S.S., STEWART, T.C. and HAAS, R.A., IEEE J. Quantum. Electron., QE-12, 265 (1976).

(98) CHAMPAGNE, L.F., HARRIS, N.W., O'NEILL, F. and WHITNEY, W.T., IEEE J. Quantum Electron., QE-10, 681 (1974).

(99) MATOBA, N., NISHIMURA, H., TOYA, H., FUJITA, H., IBA, K., NAKAI, S. and YAMANAKA, C., Tech. Reports of the Osaka Univ., vol.26. No.1287, Osaka University, Osaka, Japan, (1976).

(100) YABLONOVITCH, E. and GOLDHAR, J., Appl. Phys. Lett., 25, 580 (1974).

(101) KWOK, H.S. and YABLONOVITCH, E., Appl. Phys. Lett., 30, 158 (1977).

(102) STARK, E., 'Laser Fusion Program', LA-6510-PR, LASL, University of California, Los Alamos, (1976).

(103) ALCOCK, A.J., CORKUM, P.B. and JAMES, D.J., Appl. Phys. Lett., 27, 680 (1975).

(104)a DUMANCHIN, R., LAVARINI, B., MICHON, M., NEUBAUER, M. and ROCCA-SERRA, J., IEEE J. Quantum. Electron. QE-6, 4 (1970).

b. DUMANCHIN, R., FARCY, J.C., MICHON, M. and ROCCA-SERRA, J., Paper presented at the 1970 Int. Quant. Electr. Conf., Kyoto, Japan.

c. DUMANCHIN, R., FARCY, J.C., BOUDINET, G. and ROCCA-SERRA, J., IEEE J. Quantum. Electron., QE-8, 163 (1972).

(105) PAN, Y-L, BERNHARDT, A.F. and SIMPSON, J.R., Rev. Sci. Instrum., 43, 662 (1972).

(106) LAMBERTON, H.M. and PEARSON, P.R., Electron. Lett., 7, 141 (1971).

(107) PEARSON, P.R. and LAMBERTON, H.M., I E E E J. Quantum Electron., QE-8, 145 (1972).

(108) DYER, P.E. and JAMES, D.J., J. Appl. Phys., 46, 1679 (1975).

(109) BUSHNELL, A.H., GUNDERSEN, M. and BURKES, T.R., I E E E J. Quantum. Electron., QE-12, 447 (1976).

(110) BYCHKOV, Y.I., OSIPOV, V.V. and TARASENKO, V.F., Sov. J. Quant. Electron., 3, 262 (1973).

(111) BYCHKOV, Y.I., KUDRYASHOV, V.V. and OSIPOV, V.V., Sov. J. Quant. Electron., 4, 695 (1974).

(112) GIBSON, A.F., KIMMITT, M.F. and WALKER, A.C., Appl. Phys. Lett., 17, 75 (1970).

(113) SIEGMAN, A.E., "An Introduction to Lasers and Masers', McGraw-Hill Inc., New York, pp.321-8 (1971).

(114) KRUPKE, W.F. and SOOY, W.R., I E E E J. Quantum. Electron., QE-5, 575 (1969).

(115) DATSKEVICH, N.P., KARLOVA, E.K., KARLOV, N.V., KOVAL'CHUK, B.M., KONEV, Yu.B., KONONOV, N.N., KOCHETOV, I.V., KUZ'MIN, G.P., MESYATS, G.A., NIKIFOROV, S.M., PEVGOV, V.G. and PROKHOROV, A.M., Sov. J. Quant. Electron., 7, 258 (1977).

(116) FREIBERG, R.J., CHENAUSKY, P.P. and BUCZEK, C.J., I E E E J. Quantum. Electron., QE-8, 882 (1972).

(117) REILLY, J.P., I E E E J. Quantum. Electron. QE-8, 136 (1972).

(118) DYER, P.E., JAMES, D.J. and RAMSDEN, S.A., Optics. Commun., 5, 236 (1972).

(119) SIEGMAN, A.E., Appl. Optics., 13, 353 (1974).

(120) ANAN'EV, Y.A., Sov. J. Quant. Electron., 1, 565 (1972).

(121) GILBERT, J., LACHAMBRE, J-L., RHEAULT, F. and FORTIN, R., Can. J. Phys., 50, 2523 (1972).

(122) KOGELNIK, H., 'Modes in Optical Resonators', In Lasers, vol.1, (Edited by A.K. Levine), Marcel Dekker, New York, p.317 (1966).

(123) BLOOM, A.L., 'Gas Lasers', John Wiley & Sons Inc., New York, pp.82-85 (1968).

(124) FREIBERG, R.J. and HALSTED, A.S., Laser Focus, 4, 21 (1968).

(125) LYON, D.L., GEORGE, E.V. and HAUSS, H.A., Appl. Phys. Lett., 17, 474 (1970).

(126) GILBERT, J. and LACHAMBRE, J-L., Appl. Phys. Lett., 18, 187 (1971).

(127) CROCKER, A. and LAMBERTON, H.M., Electron. Lett., 7, 272 (1971).

(128) NAKATSUKA, M., YAMABE, C., YOKOYAMA, M. and YAMANAKA, C., Japan J. Appl. Phys., 11, 114 (1972).

(129) CHANG, T.Y. and WOOD, O.R., I E E E J. Quantum Electron., QE-8, 721 (1972).

(130) SMITH, P.W., DUGUAY, M.A. and IPPER, E.P., 'Mode-Locking of Lasers', Progress in Quant. Electron., 3, part 2, Pergamon (1974).

(131) KLINE, L.E., DENES, L.J. and PECHERSKY, M.J., Appl. Phys. Lett., 29, 574 (1976).

(132) McKEN, D.C., SEGUIN, H.J. and TULIP, J., IEEE J. Quant. Electron., QE-12, 470 (1976).

(133) LEVINE, J.S. and JAVAN, A., Appl. Phys. Lett., 22, 55 (1973).

(134) JUDD, O.P. and WADA, J.Y., IEEE J. Quantum Electron., QE-10, 12 (1974).

(135) WILLET, C.S. and GLEASON, T.J., Laser Focus, 7, 30 (June 1971).

(136) FOSTER, H., Optics and Laser Tech., 4, 121 (1972).

(137) DULEY, W.W., 'CO_2 Lasers, Effects and Applications', Academic Press, New York (1976).

(138) MAZURENKO, Y.T. and RUBINOV, Y.A., Sov. J. Quant. Electron., 6, 328 (1976).

(139) REITS, B.J. and OLBERTZ, A.H.M., Appl. Phys. Lett., 26, 335 (1975).

(140) REITS, B.J. and OLBERTZ, A.H.M., Appl. Phys. Lett., 27, 24 (1975).

(141) NAKATSUKA, M. and KUBO, U., Japan J. Appl. Phys., 15, 1175 (1976).

(142) ROBINSON, A.M., Can. J. Phys., 50, 2471 (1972).

(143) GIRARD, G., HUGUET, M. and MICHON, M., IEEE J. Quant. Electron., QE-9, 426 (1973).

(144) BRINKSCHULTE, H. and LANG, R., Phys. Lett., 47A, 455 (1974).

(145) SINGER, S., IEEE J. Quant. Electron., QE-10, 829 (1974).

(146) LELAND, W.T., KIRCHER, M.J., NUTTER, M.J. and SCHAPPERT, G.T., J. Appl. Phys., 46, 2174 (1975).

(147) SMITH, D.C., DeMARIA, A.J., J. Appl. Phys., 41, 5212 (1970).

(148) FRANTZ, L.M., NODVIK, J.S., J. Appl. Phys., 34, 2346 (1963).

(149) GIRARD, A. and PEPIN, H., Optics. Commun., 8, 68 (1973).

(150) LACHAMBRE, J., GILBERT, J., RHEAULT, F., FORTIN, R. and BLANCHARD, M., IEEE J. Quant. Electron., QE-9, 459 (1973).

(151) FIGUEIRA, J.F., REICHELT, W.H., SCHAPPERT, G.T., STRATTON, T.F. and FENSTERMACHER, C.A., Appl. Phys. Lett., 22, 216 (1973).

(152) DOMEY, J., Rev. Sci. Instrum., 46, 811, (1975).

(153) BORN, M. and WOLF, E., 'Principles of Optics', Pergamon, 4th ed. (1970).

(154) RAMACHANDRAN, G.N. and RAMESESHAN, S., 'Crystal Optics', In Handbuch der Physik, vol. 25/1, Berlin: Springer-Verlag, p.192 (1961).

(155) NYE, J.F., 'Physical Properties of Crystals', Oxford: Clarendon Press, pp.41-42 (1957).

(156) FIGUEIRA, J.F., IEEE J. Quantum. Electron., QE-10, 572 (1974).

(157) LITTLE, V.I., SELDEN, A.C. and STAMATAKIS, T., J. Phys. E: Scient. Instrum., 7, 962 (1974).

(158) CRISP, M.D., BOLING, N.L. and DUBÉ, G., Appl. Phys. Lett., 21, 364 (1972).

(159) CRISP, M.D., IEEE J. Quant. Electron., QE-10, 57 (1974).

(160) KINOSITA, K., J. Phys. Soc. Japan, 8, 219 (1953).

(161) PENDLETON, W.K. and GUENTHER, A.H., Rev. Sci. Instr., 36, 1546 (1965).

(162) BETTIS, J.R. and GUENTHER, A.H., I E E E J. Quant. Electron., QE-6, 483 (1970).

(163) ALCOCK, A.J., RICHARDSON, M.C. and LEOPOLD, K., Rev, Sci. Instr., 41, 1028 (1970).

(164) FLETCHER, R.C., Rev. Sci. Instr., 20, 861 (1949).

(165) BEWLEY, L.V., 'Travelling Waves on Transmission Lines', John Wiley & Sons Inc., New York, p.318 (1951).

(166) POTTER, J.L. and FICH, S.J., 'Theory of Networks and Lines', Prentice-Hall Inc., New Jersey, p.398 (1963).

(167) GUENTHER, A.H. and BETTIS, J.R., I E E E J. Quant. Electron., QE-3, 584 (1967)

(168) NOGUCHI, T., YANO, M., SHIMOMURA, T. and HORII, K., Electr. Eng. in Japan, 92-A, 27 (1972).

(169) PINNEKAMP, F., HIMMEL, G. and BERGSTEDT, K., Opt. Commun., 11, 225 (1974).

(170) RAETHER, H., 'Electron Avalanche and Breakdown in Gases', Butterworth, Washington D.C. (1964).

(171) DEWHURST, R.J., PERT, G.J. and RAMSDEN, S.A., J. Phys. D: Appl. Phys., 5, 97 (1972).

(172) STEINMETZ, L.L., Rev. Sci. Instr., 39, 904 (1965).

(173) NURMIKKO, A.V., I E E E J. Quant. Electron., QE-7, 470 (1971).

(174) KHAN, S.H. and WALSH, D., J. Phys. D: Appl. Phys., 4, 344 (1971).

(175) GUENTHER, A.H. and BETTIS, J.R., Proc. I E E E , 59, 689 (1971)

(176) KIMMITT, M.F., 'Far Infrared Techniques', Pion Ltd., p.12 (1970).

(177) IRELAND, C.L.M., J. Phys. E: Sci. Instr., 8, 1007 (1975).

(178) HESS, H. and DEPARADE, W., Proc. 3rd Int. Conf. on Gas Discharges, London, I E E Conference Publication No.118, 136 (1974).

(179) DEUTSCH, F., J. Phys. D: Appl. Phys., 1, 1711-9 (1968).

(180) MANES, K.R., SMITH, D.L., HAAS, R.A. and GLAROS, S.S. I E E E J. Quant. Electron., QE-11, 635 (1975).

(181) SKOBERNE, F., 'Laser Fusion Program', LA-6050-PR, L A S L, Univ. of California, Los Alamos, (1976).

(182) HOPF, F.A. and RHODES, C.K., Phys. Rev. A., 8, 912 (1973).

(183) ARMANDILLO, E. and SPALDING, I.J., J. Phys. D: Appl. Phys., 46, 1322 (1975).

(184) FELDMAN, B.J., Optics Commun. 14, 13 (1975)

(185) ANAN'EV, Y.A., SHERSTOBITOV, V.E., Sov. Phys. - Tech. Phys., 18, 640 (1973).

(186) SIEGMAN, A.E., Laser Focus, 7, 42 (May 1971).

(187) HARRACH, R.J., I E E E J. Quant. Electron., QE-11, 349 (1975).

(188) STRATTON, T.F., 'High-Power Gas Lasers 1975' (Edited by E.R. Pike) Inst. Phys. Conf., Ser. No.29, 294 (1976).

(189) ABRAMS, R.L., Appl. Phys. Lett., 25, 609 (1974),
In Eq.(5.4) cited from this reference, ψ is the fractional content of each gas in the mixture; P is the total pressure in torr and T is the absolute temperature; $\Delta\nu_H$ is given in MHz

(190) FARCY, J.C., FERTAL, A., HUGNET, M., GIRARD, G. and MICHON, M., Post-deadline Paper 18.12, CLEA, Washington D.C. (1975).

(191) PILTCH, M., Optics Commun., 7, 397 (1973).

(192) BAUMHACKER, H. and LANG, R.S., Phys. Lett., 47A, 429 (1974).

(193) SCHAPPERT, G.T. and FIGUEIRA, J.F., Optics Commun., 13, 104 (1975).

(194) BAUMHACKER, H., BRINKSCHULTE, H., FILL, E. and LANG, R.S., IPP 4/121 Max-Planck-Institut fur Plasmaphysik, Garching-Bei-Munchen, (August 1974).

(195) FIGUEIRA, J.F., LADISH, J.S., SCHAPPERT, G.T. and THOMAS, S.J., Appl. Phys. Lett., 27, 591 (1975).

(196) SCHAPPERT, G.T. and HERBST, M.J., Appl. Phys. Lett., 26, 314 (1975).

(197) MILLER, J.L., ROSS, A.H.M. and GEORGE, E.V., Appl. Phys. Lett., 26, 523 (1975).

(198) SKOBERNE, F. 'Laser Fusion Program', LA-6245-PR, LASL, University of California, Los Alamos, p.26 (1975).

(199) FELDMAN, B.J., FISHER, R.A. and McLELLAN, E.J., Appl. Phys. Lett., 31, 189 (1977).

(200) SOOY, W.R., Appl. Phys. Lett., 7, 36 (1965).

(201) BEAULIEU, J.A., Proc. IEEE, 59, 667 (1971).

(202) HECKENBERG, N.R. and MEYER, J., Optics Communications, 16, 54 (1976).

(203) ANAN'EV, Y.A., GRISHMANOVA, N.I., PETROVA, I.M. and SVETSITSKAYA, N.A., Sov. J. Quant. Electron., 5, 408 (1975).

(204) BASOV, N.G., KROKHIN, O.N., PUSTOVALOV, V.V., RUPANSOV, A., SILIN, V.P., SKLIZKOV, G.V., TIKHONCHUK, V.T. and SHIKANOV, A.S. Sov. Phys. JETP, 40, 61 (1975).

(205) DONALDSON, T.P., HUBBARD, M. and SPALDING, I.J., Phys. Rev. Lett., 37, 1348 (1976).

(206) McCUBBIN, T.K., 'Research in the Field of High Resolution Infrared Spectroscopy', AFCRL-67-0437, Air Force Cambridge Research Laboratories, Bedford, Mass., p.45 (1967).

(207) WALKER, A.C., McGEOCH, M.W., STAMATAKIS, T., WARD, S., WILLIS, B.L. and SPALDING, I.J., Culham Laboratory Preprint CLM-P 488, (1977).

(208) LEONARD, T., MONCUR, N.K. and SULLIVAN, D., J. Appl. Phys., 47, 4021 (1976).

(209) SCHAPPERT, G.T. and STARK, E.E. Jnr., Appl. Phys. Lett., 25, 602 (1974).

(210) LAVIGNE, P., LACHAMBRE, J.L. and GILBERT, J., Appl. Phys. Lett., 28, 265 (1976).

(211) BURNETT, N.H. and RICHARDSON, M.C., Rev. Sci. Instrum., 47, 241 (1976).

(212) STAMATAKIS, T. and WALKER, A.C., 3rd Nat. Quant. Electron Conf., University of Southampton, 14-16 September (1977).

PUBLICATIONS

CO_2 LASER WITH 30 MW SINGLE MODE OUTPUT

T. STAMATAKIS * and A.C. SELDEN
Culham Laboratory, Abingdon, Oxon, OX14 3DB, UK
(Euratom/UKAEA Fusion Association)

Received 12 July 1976

The operating principles and performance of a simple three mirror telescopic resonator for generating *temporally smooth* laser pulses of at least 30 MW peak power and controlled duration in the range 60 to 200 ns are discussed.

We describe the reliable generation in a *single longitudinal mode* of smooth CO_2 laser pulses with >30 MW peak power, which is believed to be the highest reported output for a single mode oscillator to date. A simple three-mirror system is used in a coupled unstable cavity arrangement (see fig. 1); this has the advantage of a large aperture for potential scaling to higher powers and is of very simple construction [1]. One application of this device is to laser-plasma interaction studies, where the smooth temporal envelope of the incident pulse provides a reference for interpreting amplitude modulations imposed on the reflected pulse [2].

The optical system is shown in fig. 1, and consists of two unstable cavities coupled by the small convex mirror M_1 and sharing the same active medium. Each cavity has a loss which slightly exceeds the available gain and therefore neither can oscillate independently. The design of the cavity defined by the mirrors M_1, M_2 has already been described in a telescopic amplifier application [3]. The radius of curvature of the third mirror M_3 was so chosen that the cavities M_1, M_2 and M_1, M_3 have the same diffraction losses. Some of the radiation leaving M_1, M_2 is returned by M_3, and vice versa, so that the nett loss for a resonant mode of the combined cavities is less than that of the independent modes (resonant feedback) and oscillation can take place. The frequencies of the longitudinal modes differ by

$$\Delta\nu = c/2\Delta L$$

where ΔL is the difference in length of the two cavities, determined by the position of M_3. By adjusting ΔL to make $\Delta\nu$ equal to the frequency range over which the gain exceeds the loss of the three-mirror cavity, we can ensure oscillation on a single mode within a given rotational line of the 10.4 μm band. The optimum setting for reliable single mode operation of our system was found to be $\Delta L \approx 25$ cm, giving a mode spacing $\Delta\nu \approx 600$ MHz in a cavity of maximum length 1.5 m.

Examples of generated pulse shapes are given in fig. 2, recorded with a Rofin 7415 photon drag detector and Tektronix 7904 oscilloscope combination, whose frequency response was checked with M_3 repositioned to give beating between two adjacent modes, for which a maximum modulation depth of $\sim 60\%$ was observed at 600 MHz. Operation on a single rotational line was confirmed using a laser spectrum analyzer (Optical Engineering Model 16-A). The figures shows: (i) a smooth pulse of 30 MW peak power and 70 ns FWHM with a measured energy of 2 joules, and (ii) a 100 MW pulse with slight modulation, reflecting the generation of two or more modes at the higher pump energies involved. The high reproducibility of smooth pulse generation at 30 MW can be judged from the results of 100 consecutive shots in

* On attachment from Royal Holloway College (University of London), Egham, Surrey, TW20 OEX, UK.

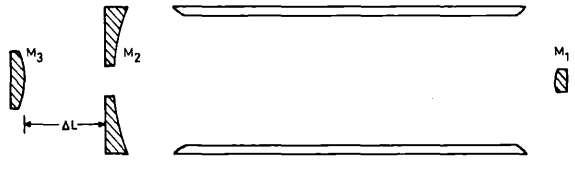

Fig. 1. Optical configuration for generating a single longitudinal mode (not to scale).

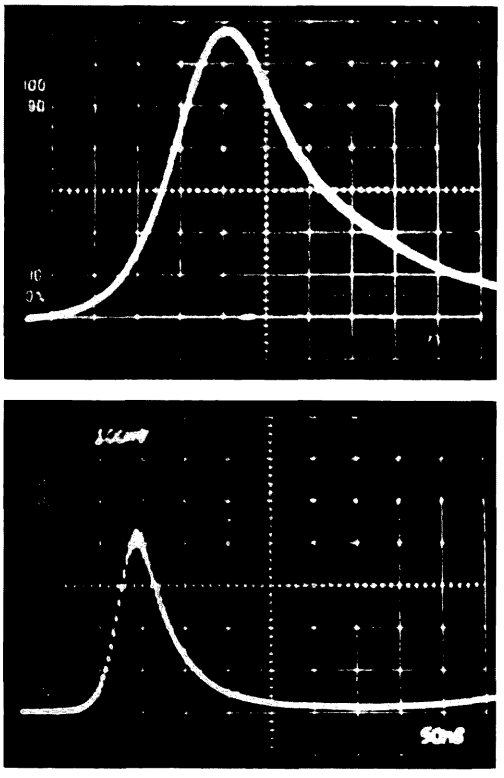

Fig. 2. Output pulses from the telescopic resonator: (i) 30 MW with smooth envelope (20 ns/div); (ii) 100 MW pulse with some modulation (50 ns/div).

one run, of which no more than 10% showed detectable modulation.

The laser pulse width is determined by the ratio of the partial pressures of nitrogen and carbon dioxide in the gas mixture, and can be adjusted in the range 60 to 200 ns by varying the ratio $P_{N_2} : P_{CO_2}$ from 1 : 6 for the lower value to 4 : 3 for the longer pulse.

In conclusion it has been shown experimentally that by addition of a third reflector, a TEA CO_2 telescopic laser amplifier can be converted to a high power unstable cavity oscillator operating on a single longitudinal mode. The output power was found to be more than an order of magnitude higher than that obtained from laser oscillators employing a stable resonator [4–6]. This considerable improvement reflects the fact that the fundamental transverse mode can be arranged to occupy the whole volume of active medium in an unstable cavity, whereas the mode volume of a stable resonator is strictly limited, resulting in a large reduction of output power. A further important feature of the three-mirror cavity is the low divergence $\sim 5 \times 10^{-4}$ rad of the output beam, which equals the diffraction limited divergence of the conventional telescopic resonator [1].

Temporally smooth pulses with peak powers of 14 MW have been observed using an unstable resonator with SF_6 cell in a grating-tuned cavity [7]; however, no information was given on the reproducibility of smooth pulse generation in this case.

We wish to record our appreciation of the keen interest taken in this work by Dr. V.I. Little, especially the many fruitful discussions we had about it; our thanks to Drs. T.K. Allen and I.J. Spalding for their support.

References

[1] Yu.A. Anan'ev, N.I. Grishmanova, I.M. Petrova and N.A. Sventsitskaya, Soviet J. Quant. Electron. 5 (1975) 408.
[2] N.G. Basov et al., Soviet Phys. JETP 40 (1975) 61.
[3] V.I. Little, A.C. Selden and T. Stamatakis, J. Appl. Phys. 47 (1976) 1295.
[4] A. Nurmikko, T.A. deTemple and S.E. Schwartz, Appl. Phys. Lett. 18 (1971) 130.
[5] J.A. Weiss and L.S. Goldberg IEEE J. Quant. Electron. QE-8 (1972) 757.
[6] A. Gondhalekar, E. Holzhauer and N.R. Heckenberg, Phys. Lett. 46A (1973) 229.
[7] P.E. Dyer and D.J. James, Appl. Phys. Lett. 26 (1975) 331.

A gigawatt CO_2 laser with telescopic amplifier

V. I. Little,* A. C. Selden, and T. Stamatakis†

Culham Laboratory, Abingdon, Oxon, OX14 3DB, United Kingdom
(Received 16 December 1975)

The first production of gigawatt pulses from a 1-m CO_2 telescopic amplifier with megawatt input is reported. This device has been used to generate 1-J pulses of 830 ps FWHM from a suitably gated source.

PACS numbers: 42.60.Lh, 42.60.Cz

I. INTRODUCTION

The power output of a gated CO_2 laser oscillator for generating pulses 1 ns in duration is typically about 1 MW. To increase this to the gigawatt region for pulse injection to a typical amplifier chain, a preamplifier with a power gain of $\sim 10^3$ is required. This, in turn, needs up to 3 m of active path in CO_2,[1-3] using either a one-pass multistage system or else arranging 2—3 passes with partially overlapping beams in a single-stage amplifier.[4,5] In each case the result is inefficient extraction of the total stored energy, and attendant problems of beam divergence and mode control. These limitations on the preamplification of nanosecond pulses to gigawatt powers can be overcome, in principle, by the telescopic amplifier,[6] in which the weak input beam is simultaneously expanded and amplified while preserving its mode structure. With a *reflecting* telescope arrangement full use of the stored energy can be achieved, because the design combines adequate beam expansion (magnification $M \sim 10$) with high overall gain (triple pass). The system is ideal for raising weak signals to high power in a single stage, and can be adapted to match a wide range of weak sources (oscillators) to large laser amplifier systems. It has previously been employed on neodymium lasers for generating millisecond pulses with energies of several hundred joules.[7] In this paper the design and performance of a 1-m TEA CO_2 laser telescopic amplifier for producing gigawatt pulses of nanosecond duration is described.

The use of unstable resonators in high-power oscillators was first described by Siegman.[8] Of the various possible configurations, a confocal system, i.e., telescopic resonator, has the advantage that it provides a collimated output. Furthermore, in high-power systems it is clearly good design to arrange for the common focal point to lie outside the cavity so that the risk of optical breakdown is minimized. For this reason an unstable configuration on the positive branch of the stability diagram was chosen for the present work. The optical cavity (see Fig. 1) is effectively a Cassegrain telescope in normal adjustment. Parallel light, entering from the left through a hole in the concave mirror, traverses the central part of the active medium to strike the convex mirror. After reflection the light returns as a diverging beam to the concave mirror, where it is reflected as an expanded parallel beam for its third and final traverse of the active medium. This arrangement also achieves optical matching of the output to subsequent amplifying stages of larger aperture than the input beam, without the severe loss of intensity normally associated with a passive beam expander.

In the present work, care was taken to ensure that only three passes of the active medium were possible for parallel beams in the amplifier, in order to prevent the onset of self-oscillation by resonant feedback in the modified cavity. Even with this restriction it was possible for self-oscillation to be initiated by optical feedback arising from light diffraction at the various apertures.[6]

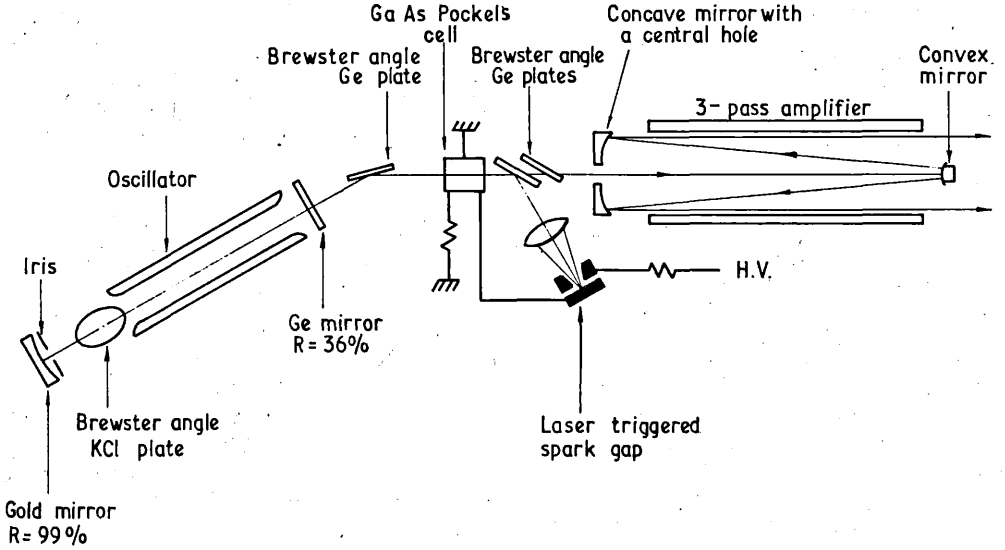

FIG. 1. Experimental arrangement

II. AMPLIFIER DESIGN

A. Preliminary considerations

To achieve a stable three-pass amplifier, two main sets of criteria have to be satisfied. First, self-oscillation must be prevented, and in a normally adjusted system this means that diffraction losses have to be controlled by a suitable choice of cavity apertures and optical magnification. Second, the efficient extraction of energy imposes the condition that the entrance aperture $2x$ should be greater than or equal to the diameter of the convex mirror, $2a_1$. If D is the electrode spacing and M is the linear magnification of the system, we have the following relations: $2x \geq 2a_1$ and $M = D/2a_1$ for normal adjustment, hence $x \geq D/2M$.

A further factor enters as a result of the geometry. The output beam has an annular cross section with an inner diameter controlled by $2x$. Hence, the smaller x, the greater the availability of the stored energy. If 90% of the stored energy is to be usefully employed, the above considerations impose the following limits on the design:

$$D/2M \leq x \leq \tfrac{1}{7}D.$$

Finally, a practical limit to the magnification is set by the ratio of the electrode spacing to the diameter of the input beam: $M \leq 10$.

B. Diffraction loss vs self-oscillation

According to Anan'ev *et al.*,[9] the quantity $|\gamma|$ which determines the diffraction loss δ, where $\delta = 1 - |\gamma|^2$, is given by

$$\ln|\gamma| = \frac{\ln(M)\ln[M/2\pi N_{eq}(M^2-1)]}{\ln(4N_{eq}/N_{eq}^0)}, \tag{1}$$

where N_{eq} and N_{eq}^0 are the equivalent Fresnel numbers of the resonator and of the entrance aperture, respectively.

For a telescopic resonator, N_{eq} according to Siegman[10] is given by

$$N_{eq} = (a_1^2/2\lambda L)(M-1), \tag{2}$$

where λ is the wavelength of the cavity radiation and L is the length of the cavity. Anan'ev *et al.*[9] gives

$$N_{eq}^0 = \frac{x^2}{2\lambda L}\,\frac{M-1}{M}. \tag{3}$$

Using Eqs. (2) and (3), Eq. (1) becomes

$$\ln|\gamma| = \left[\ln(M)\ln\left(\frac{\lambda L}{\pi a_1^2}\right)\frac{M}{(M^2-1)(M-1)}\right] \times \left[\ln\left(\frac{4a_1^2}{x^2}\right)M\right]^{-1}. \tag{4}$$

The quantity γ was first determined experimentally for an existing telescopic resonator with $M = 2.875$, $L = 1.25$ m, and $a_1 = 8.35$ mm, for a discharge region with dimensions 1 m×49 mm×49 mm.

The input aperture radius x for which self-oscillation ceased was determined by placing a nonreflecting carbon disk cover the pole of the concave mirror to simulate a circular aperture whose diameter could readily be adjusted. The diameter was increased until the system just stopped oscillating with the amplifier fully energized. The effective value of x was thus found to be 16 mm.

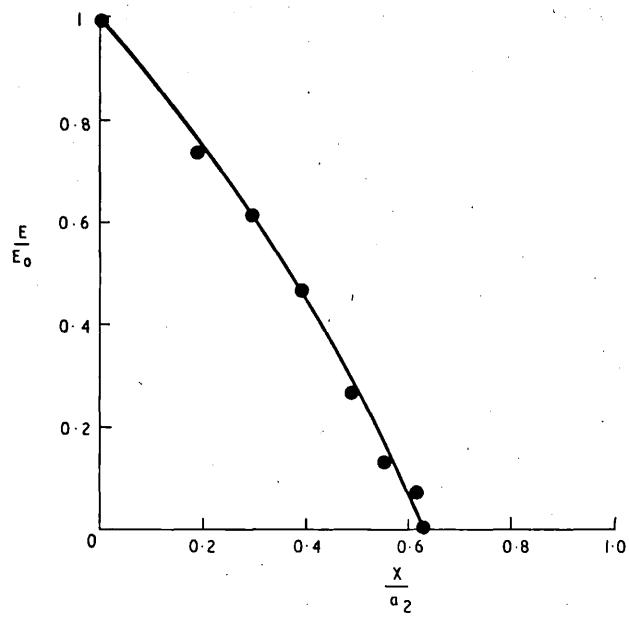

FIG. 2. Graph of relative self-oscillation energy vs hole size.

In Fig. 2, the normalized oscillator output energy is shown as a function of the ratio x/a_2, where a_2 is the radius of the concave mirror. Using Eq. (4) and the confocal condition $a_2 = Ma_1$, substitution of the appropriate values of L, a_1, x, and M for $\lambda = 10.6$ μm gives $\ln|\gamma| = -3.78$. This figure specified the diffraction loss of the cavity used and enabled the parameters of any other similar cavity having the same diffraction loss to be calculated, thus allowing more convenient values of M and x to be determined. A combination of M and x that satisfied both the condition $M < 10$ and the inequality $D/2M \leq x \leq \frac{1}{7}D$, and at the same time gave a value for $\ln|\gamma| = -3.78$, was found to be $M = 7$ and $x = 5.4$ mm. For optimum power output, $2a_2 = D = 49$ mm, determined by the electrode separation in TEA geometry. Thus, $a_2 = 24.5$ mm and $a_1 = a_2/M = 3.5$ mm. Simple telescope theory then gave 2917 mm for the radius of curvature of the concave mirror and 417 mm for that of the convex mirror, requiring a cavity length $L = 1.25$ m.

C. Parasitic oscillation

Having eliminated self-oscillation in the amplifier, a parasitic oscillation was observed which was independent of the cavity mirrors [Figs. 4(a)]; in fact, it persisted when the latter were removed. This oscillation was traced to the reflection introduced by the mirror mounts. A covering of carbon paper over the mounts effectively eliminated it. When the switching system isolating the oscillator from the amplifier was removed, the parasitic radiation from the amplifier section resulted in a reduction of up to six times in the peak power of the oscillator, as measured using a photon-drag detector. This reduction in power was found to be roughly proportional to the intensity of the parasitic oscilla-

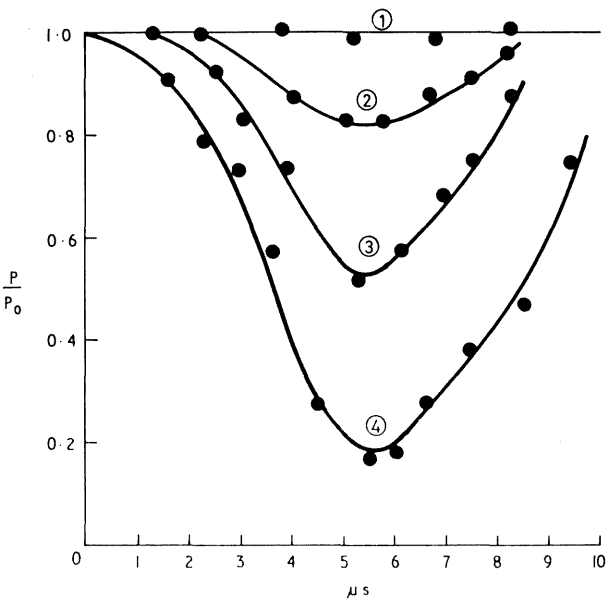

FIG. 3. Reduction in oscillator power vs delay time for different intensities of parasitic radiation from the amplifier. Curve 1 , no feedback; curves 2 – 4 increasing feedback.

tion in the amplifier, measured when the amplifier alone was energized. However, when this parasitic oscillation was completely suppressed, as described above, the presence of the amplifier had no effect upon the performance of the oscillator. In Fig. 3, the normalized peak power of the oscillator is plotted against T, the delay time between the firing of the amplifier and the oscillator, for four arbitrarily chosen values of the intensity of the parasitic oscillation.

The final elimination of both the parasitic and self-oscillations of the amplifier was checked using a General Technology calorimeter capable of measuring integrated energy densities down to 0.05 mJ/cm^2.

III. EXPERIMENT

The experimental arrangement for generating and amplifying a nanosecond laser pulse is shown schematically in Fig. 1. A fast electro-optic switch was used to select a single pulse from the oscillator output and transmit it to the amplifier, where three passes were made in the active medium via the Cassegrain telescope system. The oscillator was of the Lamberton-Pearson type[11] with two Rogowski profile electrodes of length 700 mm and spacing 25 mm. The optical cavity was formed by a 99% reflecting concave mirror with a radius of curvature of 10 m and a Ge flat antireflection coated on one face. These were arranged to give a cavity length of 1.35 m. A KCl plate set at the Brewster angle was placed inside the cavity of polarize the output and increase the power reflected from the first Ge polarizer. An intracavity diaphragm of diameter 9 mm restricted oscillation to a single transverse mode. Using this arrangement a self-mode locked pulse train was generated, with individual pulses of ~2 ns duration [Fig. 4(b)]. The modulation depth ranged from 85 to 100%, and the shape of individual pulses was not reproducible from shot to shot, reflecting the fact that no mode-locking element was present in the cavity. The GaAs electro-optic crystal for selecting a single pulse was energized by a ~2-ns high-voltage pulse derived from a pressurized laser-triggered spark gap.[12] By adjusting the gas pressure and the length of the delay line the arrival of the electrical pulse in the GaAs crystal was synchronized with the arrival of one of the strongest laser pulses in the train, thereby reducing the noise level (interpulse energy) of the transmitted signal. The selected pulse then entered the triple-pass amplifier, whose output beam was monitored with a

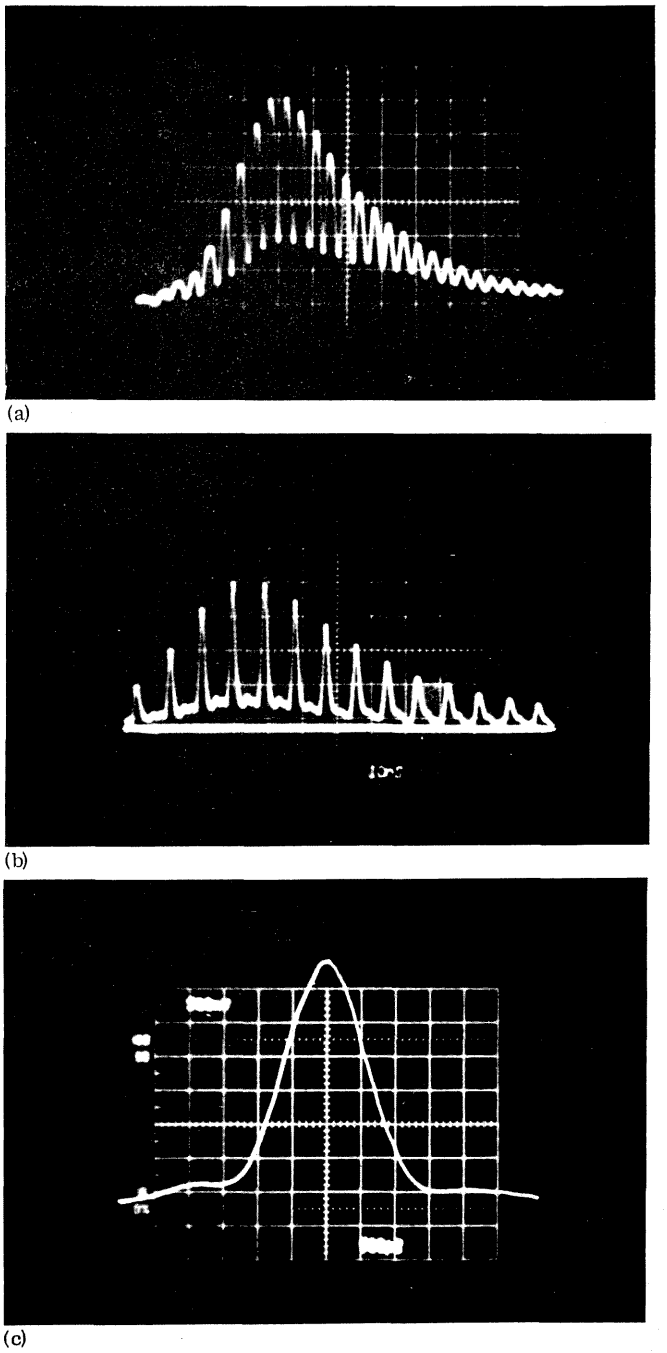

(a)

(b)

(c)

FIG. 4. (a) Parasitic oscillation: time scale, 20 ns/div. (b) Output pulse from the self-mode-locked oscillator: time scale, 10 ns/div. (c) 1-GW amplified pulse with instrument-limited width: 1.3 ns FWHM; time scale, 500 ps/div.

photon-drag detector (Rofin, model 7415) and the pulse intensity profile displayed on a Tektronix 7904 oscilloscope [Fig. 4(c)]. The recorded width of 1.3 ns FWHM included the rise time of the detector (0.6 ns) and of the oscilloscope (0.8 ns). Assuming a Gaussian profile, the actual pulse width calculated from these values was $t = 830$ ps FWHM. The pulse energy was measured using a General Technology pyroelectric calorimeter. Because of the finite contrast ratio (signal/background noise), the measured energy contained two components: the energy in the short pulse and that of the amplified noise. The latter was measured by disconnecting the trigger of the electro-optic switch, thereby making it inactive, and firing both oscillator and amplifier. This energy was then subtracted from the total to give an output pulse energy of 1 J. Similarly, the energy of the input pulse was found to be 1 mJ. Thus, the triple-pass amplifier had an energy gain of 1000. The peak power of the amplified pulse was estimated from the response of the photon-drag detector and found to be ~1 GW. Comparison with the input of ~1 MW (1 mJ, 1 ns) shows the close agreement between the energy and power measurements of the gain for a nanosecond pulse.

IV. CONCLUSIONS

A triple-pass TEA CO_2 telescopic laser amplifier has been developed with an energy gain of 1000 for millijoule laser pulses of ~1 ns in duration, compared with a gain of 20 for the same device operated as a single-pass amplifier. Pulses with ≥ 0.8 ns width and 1 GW peak power (total energy 1 J) were obtained from an active length of only 1 m for an input power of 1 MW.

The design of the amplifier both ensured optimum energy extraction and eliminated the problem of self-oscillation caused by optical feedback from diffraction at the edges of the telescope apertures. The problem of parasitic oscillation in the amplifier, which initially caused a large reduction of the oscillator output, was overcome by minimizing the specular and diffuse reflection from the window and mirror mounts.

Triple-pass amplification of the kind described in this paper could well be used to advantage in larger high-power laser systems; in particular, electron-beam–controlled CO_2 [13] and glass disk amplifiers, which have active media with respectively higher and lower gain than that of the medium used in the present work.

*Present address: Physics Department, Royal Holloway College, University of London, Egham, Surrey, England.
†On attachement from Royal Holloway College, University of London, Egham, Surrey, England.

[1] L. F. Champagne, N. W. Harris, F. O'Neill, and W. T. Whitney, IEEE J. Quantum Electron. QE-10, 681 (1974).
[2] F. Rheault, J. L. Lachambre, J. Gilbert, R. Fortin, and M. Blanchard, Opt. Commun. 8, 132 (1973).
[3] E. E. Stark, W. H. Reichelt, G. T. Shappert, and T. F. Stratton, Appl. Phys. Lett. 23, 322 (1973).
[4] H-S. Kowk and E. Yablouovitch, Rev. Sci. Instrum. 46, 814 (1975).
[5] Yu-Li Pan, J. R. Simpson, A. F. Bernhardt, and S. E. Kiergan, IEEE J. Quantum Electron. QE-10, 44 (1974).
[6] Yu. A. Anan'ev, Sov. J. Quantum Electron. 1, 565 (1972).
[7] Yu. A. Anan'ev, N. I. Grishmanova, L. V. Koval'chuk, N. A. Sventsitskaya, and V. E. Sherstobitov, Sov. J. Quantum Electron. 2, 157 (1972).
[8] A. E. Siegman, Proc. IEEE 53, 277 (1965).
[9] Yu. A. Anan'ev and V. E. Sherstobitov, Sov. Phys.-Tech. Phys. 18, 640 (1973).
[10] A. E. Siegman, Laser Focus 7, 42 (May 1971).
[11] H. M. Lamberton and P. R. Pearson, Electron. Lett. 7, 141 (1971).
[12] A. J. Alcock, M. C. Richardson, and K. Leopold, Rev. Sci. Instrum. 41, 1028 (1970).
[13] Laser Focus 11, 22 (Sept. 1975).

APPARATUS AND TECHNIQUES

Observation of wedge fringes on CO_2 laser optical components

V I Little,† A C Selden‡§ and T Stamatakis‡§
† Physics Department, Royal Holloway College, University of London, Egham, Surrey
‡ UKAEA Research Group, Culham Laboratory, Abingdon, Oxon
§ On attachment from Royal Holloway College, University of London, Egham, Surrey

Received 6 June 1974

Abstract During the operation of a high power pulsed CO_2 laser system, damage was observed to a GaAs modulator crystal. The cause of the damage was possibly the creation of wedge fringes within the crystal. Wedge fringes were also formed in the system by a Ge polarizing plate. This note describes how the formation of such fringes can be avoided and also how they can be used to measure small wedge angles over long path differences.

Since damaged components in a laser system limit the performance of high power lasers, it is of critical concern to make the optical element of the laser less susceptible to such damage.

The use of optical components made of material with a high refractive index—like Ge or GaAs—as beam splitters, windows, polarizers and electro-optical modulators of the laser beam usually results in the formation of undesirable sharp fringes.

Usually these fringes are of equal thickness (straight line wedge fringes) which occur when the two surfaces of the component are inclined. Generally in such components the locus of the points of equal thickness, which represents the edge of the wedge, forms an angle with the geometrical edge of the component i.e. a rectangular plate. As a result of this, the fringes which are produced on transmission or reflection appear to rotate when the angle of incidence is changed, that is the angle between the plane of incidence and the straight line fringes appears to change (figure 1(*a*)).

Using these fringes the generally very small angle ϕ of the inclined surfaces can be calculated by measuring the fringe spacing d. For normal incidence ϕ is given by:

$$\phi = \lambda/2nd \qquad (1)$$

where λ is the wavelength and n the refractive index.

Recently this method was used (McLeod 1974) to check the parallelism of glass blocks with a He–Ne laser.

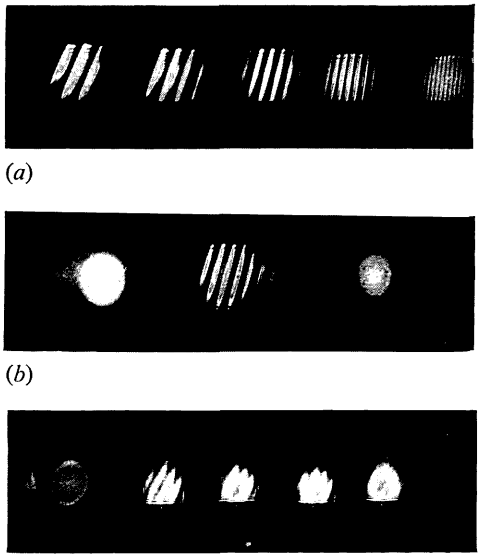

(*a*)

(*b*)

(*c*)

Figure 1 Wedge fringes on CO_2 laser components
(*a*) Rotation of fringes with varying angle of incidence; (*b*) Effect of back surface finish of Germanium plate on fringe visibility: from left to right, incident beam, reflected fringes (both faces polished), and smooth reflected beam with matt back surface; (*c*) Effect of applied voltage on fringes produced in GaAs electro-optic crystal—voltage increasing left to right from zero to quarter wave value (12 kV cm^{-1}). Incident beam on far left

In a TEA (transversely excited atmospheric pressure) CO_2 10·6 μm laser system for producing short laser pulses by electro-optical means, a germanium plate was used to produce linearly polarized light by reflection. This light was then incident upon a gallium arsenide crystal.

However, both the Ge plate and the GaAs crystal produced wedge fringes and surface damage occurred to the 50 mm long crystal. The exit surface of the crystal was damaged whilst the entrance surface suffered no damage. It has been proposed that this is due to the effect of Fresnel reflection (Crisp *et al.* 1972). In the case of GaAs, which has refractive index $n = 3{\cdot}3$, the light intensity inside the GaAs at the exit surface is $4n^2/(n+1)^2 = 2{\cdot}35$ times greater than the intensity inside the GaAs at the entrance surface.

Since the fringes arise as a consequence of multiple reflection, the transmitted fringe maxima have intensity I_{max} equal to that of the incident light I_0. On the other hand when these fringes do not occur, the intensity at the exit surface equals

$I = TI_0$ (where $T = 2n/(n^2+1) = 1/1{\cdot}8$ is the transmissivity of the whole GaAs crystal).

Therefore when the incident radiation has intensity I_0 within the range $I_{th} < I_0 < 1{\cdot}8\ I_{th}$, ($I_{th}$ being the damage-threshold intensity for the exit surface) the formation of the fringes causes the damage to the crystal and this is what is likely to have happened in the present case. Thus it is important to avoid forming fringes in systems operating near the damage threshold, for example where the maximum signal is required.

In order to avoid the fringes produced by the Ge plate, its back surface was given a matt finish using wet emery cloth. Consequently, the fringes disappeared as is shown in figure 1(*b*) and a uniform beam of linearly polarized light was reflected from the plate.

The fringes which are produced by the crystal can be excluded by applying a bias DC voltage. With increasing voltage the fringes gradually diminish. When the applied DC voltage equals the quarter wave value the fringes almost disappear (figure 1(*c*)). Consequently the disappearance of the fringes can be used to measure the quarter wave voltage and the electro-optic coefficient r_{41} of the GaAs.

The inclination of the two faces of the GaAs crystal was found from equation (1) using the observed fringe spacing d, and the known values of refractive index n and wavelength λ. This agreed within 4% with the values deduced from the displacement of the reflected and transmitted beams caused by refraction in the wedge. This is a valuable method of measuring small wedge angles on infrared components over relatively long path differences—50 mm in the present case.

References

Crisp M D, Boling N L and Dubé G 1972 *Appl. Phys. Lett.* **21** 364–6

McLeod J 1974 *Optics and Laser Techn.* **6** 57–60

Journal of Physics E: Scientific Instruments 1974 Volume 7
Printed in Great Britain

CLM - P 483

UKAEA

Preprint

MULTIKILOJOULE CO_2 LASER HEATING OF POLYTHENE PELLETS

A C WALKER
M W McGEOCH
T STAMATAKIS
S WARD
B LAVILLIS
I J SPALDING

CLM-P 488

MULTIKILOJOULE CO_2 LASER HEATING OF POLYTHENE PELLETS

A.C. Walker, M.W. McGeoch, T. Stamatakis, S. Ward, B.L. Willis and I.J. Spalding

Euratom-UKAEA Fusion Association, Culham Laboratory, Abingdon, OX14 3DB, United Kingdom.

ABSTRACT

A multikilojoule CO_2 laser ('TROJAN') has been used to heat $\frac{1}{2}$-1 mm polyethylene cubes at incident intensities $\lesssim 4 \times 10^{12}$ Wcm^{-2}, in preliminary assessments for a laser plasma stellarator-filling experiment. Measurements of transmission through the resulting laser-plasma, and of refraction and back-reflection, indicate energy losses of $\lesssim$ 1, 10 and 5% respectively. These and other measurements will be discussed.

To be presented at VIII European Conference on Controlled Fusion and Plasma Physics, Prague, September 1977.

May, 1977.

1. INTRODUCTION

Ohmic-heating typically generates a plasma having an energy content of $\sim$ 300J in CLEO Stellarator.[1] This paper examines the efficiency with which multikilojoule CO_2 lasers may be used to create laser-plasmas, as an alternative means of filling CLEO and other toroidal traps.[2] Earlier measurements of reflection from plane carbon targets[3] have indicated that back-reflection can be small, since absorption is significantly stronger than that attributable to inverse-bremmstrahlung alone;[4,5] the present work extends such observations by investigating transmission and refraction losses when finite targets are irradiated. It is hoped to use free-falling cryogenic deuterium targets[6] for this cooperative Euratom programme, but for these preliminary assessments the targets were (suspended) polythene cubes.

2. EXPERIMENTAL TECHNIQUE

The experimental arrangement is illustrated in Fig.1. The electrical characteristics of the electron beam preionized laser ('TROJAN') have been described previously.[5] For the present experiments the system was filled with gas at one standard atmosphere, with a $He:N_2:CO_2$ ratio of 0:1:2; its active volume was $\sim$ 180 cm x 20 cm x 25 cm. An unstable confocal optical resonator having a magnification of 2.8 was used to ensure low-order transverse mode, gain-switched, output pulses. The initial spike typically had a peak power of $\gtrsim$ 30 GW and exhibited mode beating; its envelope had a duration of 50 ns (FWHM) and a tail lasting some 2 μs. The energy contained in this tail could be conveniently controlled by adjusting the duration of the electron-gun pulse; Fig.2 illustrates typical pulse shapes generated for the present experiments. The incident power and energy were monitored by the photon-drag (P1) and large area pyroelectric (E1) detectors illustrated in Fig.1; similarly P2 and E2 measured the power and energy back-reflected from the target. The effective (17 x 20 cm^2) cross section of the laser beam was focused by a 4.5m focal length spherical mirror on to the target; the focal spot size,

determined by a grating technique,[7] was 750 μm (FWHM). The polythene targets were hand cut from sheet, and stuck with a minimum of epoxy resin to 10 μm diameter glass fibres supported on a micromanipulator within the target chamber at a vacuum pressure of 10^{-4}-10^{-5} torr.

3. EXPERIMENTAL RESULTS

Energy balance measurements have been made in which 0.6 - 1.6 kJ laser pulses, of duration 50 ns to 2 μs respectively (cf Fig.2), have been focused centrally on to both 1 mm and $\frac{1}{2}$ mm polythene cubes. These have given reproducible results showing, for all cases, high coupling of the laser energy into the pellet plasma.

Detector E2, sampling light directed back through the focusing optics with an effective aperture of f/17, indicated $\lesssim$ 5% direct energy reflection. A cone calorimeter, E3, placed behind the target and matched in size to the beam diameter gave a response typically < 8% of that recorded with no pellet in position. Such a device, however, considerably underestimates the magnitude of high energy (unattenuated) pulses, because of plasma formation at its entrance aperture. To investigate further, calibrated film was placed behind the pellet to give a spatial measure of the energy density of both transmitted and refracted CO_2 laser radiation. (The calibration was obtained by directing various known intensities of 10 μm radiation on to the film, in vacuum, and observing the colour of the resulting burn.) Fig.3 illustrates typical energy density contours, derived in this way, for CO_2 radiation transmitted and refracted through the plasma. It indicates that the direct transmission is < 1% of the incident energy, but that refraction, confined to a cone of (full) angle $\lesssim 60^{o}$ contributes the major energy loss, of $\lesssim$ 10%. Film placed at other positions within the target chamber gave no detectable response except when close to the laser beam direction, indicating that additional back-scattered light not reaching the focusing optics amounted to no more than 1% of the incident energy.

Detector P2, sampling the reflected intensity, showed enhanced back-reflection of the long μs tail of the pulse, relative to the intense (50 ns) initial spike (Fig.4).

4. CONCLUSION

These energy balance measurements demonstrate that small, submillimetre,

$(CH_2)_n$ targets can be efficiently heated using (relatively slow) kilojoule CO_2 laser pulses. Measurements of total charge, using ion probes, etc., are in hand to establish whether pre-pulses of the type discussed in ~ 100J Nd laser heating experiments[6,8] will be necessary to ensure full ionization in the present higher energy, microsecond duration experiments. (A highly simplified model suggests that this practical complication may be avoided,[5] or perhaps restricted to the use of only a 10.6 μm prepulse.[9])

REFERENCES

1. ATKINSON, D.W. ET AL - 'Plasma Physics and Controlled Nuclear Fusion Research 1976' Nucl.Fusion Suppl.1977, IAEA-CN-35/D1.
2. Culham Study Group on Heating and Injection (1970); and SPALDING, I.J. - Kvantovaya Elektron 4, 40 (1972)
3. DONALDSON, T.P. ET AL - Phys.Rev.Lett.37, 1348 (1976)
4. DONALDSON, T.P., SPALDING, I.J. - Phys.Rev.Lett.36, 467 (1976)
5. SPALDING I.J. ET AL - 'Plasma Physics and Controlled Nuclear Fusion Research 1976', Nucl.Fusion Suppl.1977, IAEA-CN-35/G3-3.
6. BAUMHACKER, H. ET AL - Appl.Phys.Lett.30, 461 (1977)
7. MARQUET, L.C. - Appl.Opt.10, 960 (1971)
8. GREIG, J.R., PECHACEK, R.E. - Appl.Phys.Lett.29, 798 (1976) and J.Appl. Phys.48, 596 (1977)
9. cf DONALDSON, T.P. ET AL - Culham preprint CLM-P480 (1977)

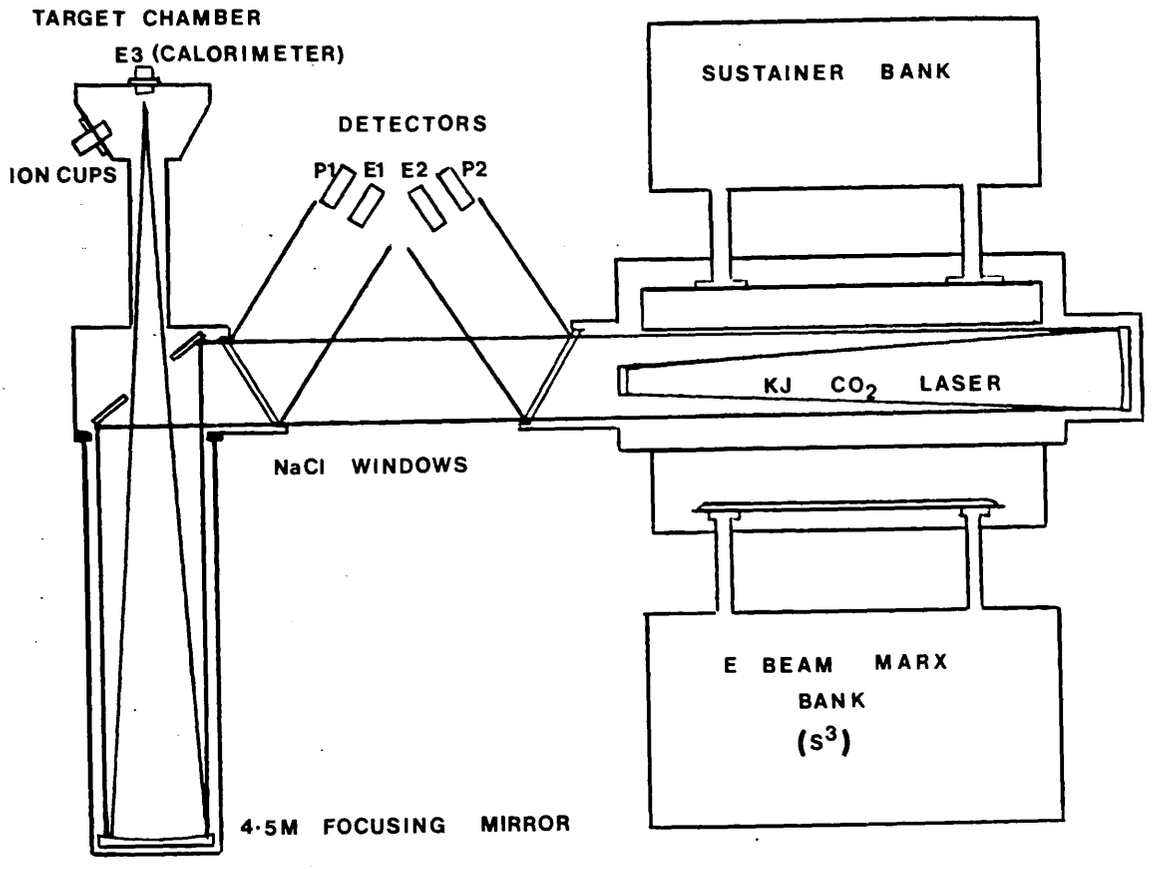

FIGURE 1 Plan-view of experimental arrangement

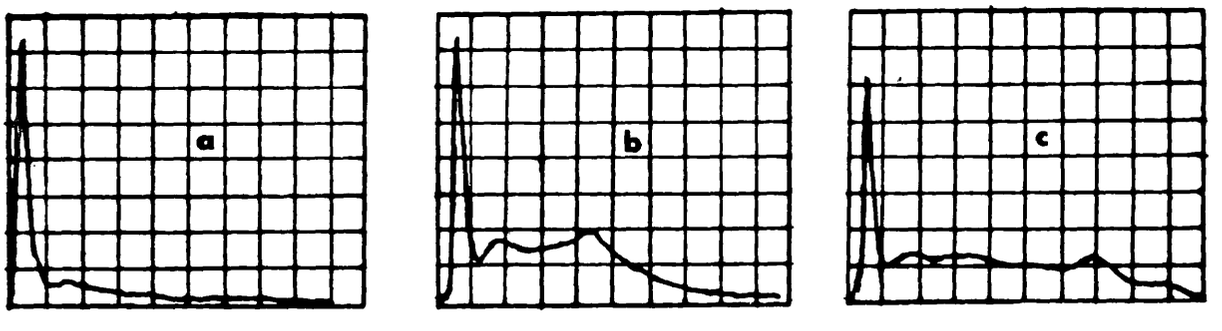

FIGURE 2 Time variation of 'TROJAN' output power, using an electron beam of (a) 0.8, (b) 1.6 and (c) 2 μs duration. (Vertical: ~ 3 GW/div., horizontal: 200 ns/div.)

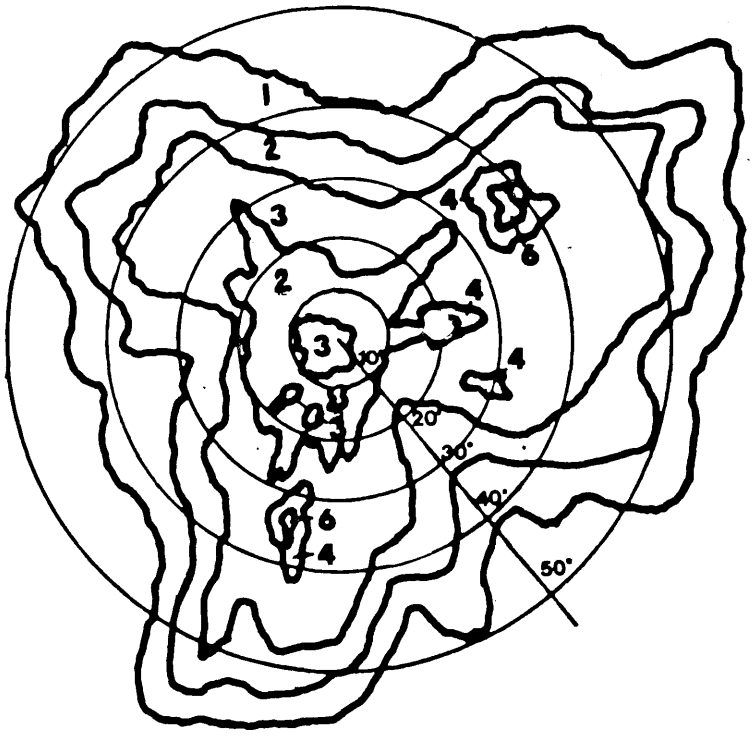

FIGURE 3 Distribution of transmitted and refracted laser radiation on a plane 7.5 cm behind a $\frac{1}{2}$ mm polythene cube irradiated by a 1.5 kJ (2 μs) pulse. Numbers indicate average energy density in joules/cm^2 between contours. Circles show cone (full) angles relative to pellet position.

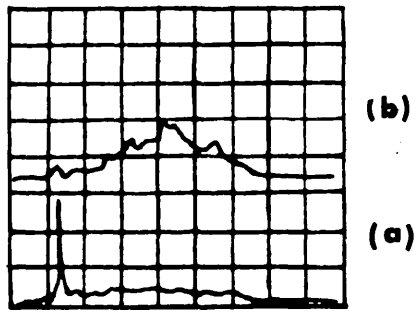

FIGURE 4 Incident (a) and back-reflected (b) pulse shapes for experiment of Fig.3 (500 ns/div).